



Transplantation and Inflammation: Role of Chemokines, microRNA and Extracellular Vesicles

Chong Yun Pang

Thesis submitted in partial fulfilment of the requirements for the degree of Doctor of
Philosophy

Translational and Clinical Research Institute

Newcastle University

August 2023

Abstract

Ischemia reperfusion injury (IRI) is an inevitable occurrence during the process of organ transplantation. The biphasic nature of IRI subjects the allografts to two distinct inflammatory insults which can affect the short-term and long-term outcomes of the allografts post transplantation. This thesis aimed to address the implications of several dysfunctional cellular processes as a result of ischemia.

Firstly, I show that the excessive presence of reactive nitrogen species can result in protein post translational nitration. In particular, I focused on CXCL8 and showed that nitration impaired its capability to orchestrate neutrophil migration during reperfusion injury. Furthermore, this modified CXCL8 was identified in bronchoalveolar lavage samples from patients with ventilator associated pneumonia using a novel antibody and validated with mass spectrometry. Secondly, transcriptional profiling of renal glomerular endothelium showed upregulation of miR-210 when subjected to hypoxia. This was accompanied by a perturbation in cellular metabolism. Our work showed that overexpression of miR-210 upregulates renal glomerular endothelium glycolysis but mitochondrial function remained unaltered. Finally, I examined surface marker expression on extracellular vesicles (EVs) derived from renal allografts microvasculature. EVs derived from deceased allograft donors showed higher expression of class II major histocompatibility molecules (MHC class II) as well as signatures associated with endothelial activation. This high expression of MHC class II was also recapitulated in vitro, suggesting that endothelial derived EVs might play an essential role in potentiating allorecognition. This mechanism could be responsible for maintaining long-term response of alloreactive T cells against allografts.

Collectively, I have shown several cellular processes that are regulated in response to ischemic damage to either function as a priming or a resolution mechanism within the allograft to elicit a secondary inflammatory response during the reperfusion phase of organ transplantation.

COVID-19 Impact

The declaration of the COVID-19 pandemic in March 2020 resulted in university wide shut down for 6 months. Following the university reopening, enforcement of social distancing measures resulted in further limited access to the university. As the nature of the project was entirely laboratory based, this resulted in extensive disruption for an entire year. Furthermore, the supply chain disruption brought on by the pandemic extended beyond 2021, with long waiting time on reagents and delayed shipments of samples to collaborators around the world. In turn, exacerbating the delay in the progress of the research.

In the instance for the mass spectrometry data on the bronchoalveolar lavages, uncertainty in the shipping routes and disruption in collaborator's access to the laboratory meant a two-year delay in acquisition of the data. This also resulted in deviation from the original research plan to ensure sufficient data generation for a PhD thesis. Hence a second project with strong emphasis on bioinformatics analysis was conceptualised, which allowed for flexible working during periods of time when lab access is restricted.

Acknowledgements

This PhD would not have been possible without the generous funding from Engineering and Physical Sciences Research Council Molecular Sciences for Medicine Centre for Doctoral Training (EPSRC MosMed CDT), Kidney Research UK (KRUK), Northern Accelerator and National Institute for Health and Research Blood and Transplant Research Unit (NIHR BTRU).

I would also like to express my deepest gratitude to my Supervisors Professor Simi Ali, Professor Neil Sheerin, and Professor John Kirby for the continuous support throughout the whole journey. Particularly, Professor Simi Ali for giving me the opportunity during a time when funding for international students was not the norm and giving me the opportunity to carry out the research independently.

Work done in this thesis would not have been possible without the input of many, including collaborators and peers. I am grateful for the opportunity for the collaboration with Professor Paul Proost, Professor Krishna Rajarathnam and Professor John Simpson. I would also like to thank Professor Jeremy Lakey for his expertise in biophysical assays, Dr Chelsea Griffiths for guiding me through the process of EV isolation, Dr Hannah Fuller for assisting me in setting up the Seahorse assays, Dr Jeremy Palmer for being always helpful and Dr Rachel Crossland for assistance with Nanostring and everything EV related. Additionally, I am also grateful to the Trost lab for giving me access to their ultracentrifuge.

I would not have made it through the PhD without the support from members from the Kirby/Ali group, dealing with my facial expressions and comments during group meetings as well as all the daily banter in the office. In particular, Anne for being a motherly figure for everyone in the group and Jenny, who started this PhD journey together with me, supporting me through thick and thin.

Finally, I would like to thank my family and Han Teng for their continuous support throughout this journey and allowing me to indulge in 4 additional years in education.

Table of Contents

Acknowledgements	v
Table of Contents	vi
Table of Figures	xii
Table of Tables	xiv
Abbreviations	xv
1. Introduction	1
1.1. Transplantation	1
1.2. Cellular and Molecular Mechanisms of IRI	2
1.2.1. Oxidative and Nitrosative Stresses in IRI	4
1.3. Chemokines	6
1.3.1. <i>Chemokine-GAG Interaction</i>	8
1.3.2. <i>Chemokine-Receptor Interaction</i>	9
1.3.3. <i>Chemokine Regulation</i>	10
1.3.4. <i>Clinical Targeting of Chemokine System</i>	13
1.4. miRNAs	15
1.4.1. <i>miRNA Biogenesis and Function</i>	15
1.4.1.1. <i>Canonical Pathway</i>	15
1.4.1.2. <i>Non-Canonical Pathway</i>	16
1.4.2. <i>Regulation of Gene Expression</i>	16
1.4.3. <i>Circulating miRNA</i>	19
1.4.4. <i>Role of miRNA in IRI</i>	19
1.4.4.1. <i>miR17~92 Cluster</i>	20
1.4.4.2. <i>miR-21</i>	20
1.4.4.3. <i>miR-210</i>	21
1.5. Extracellular Vesicles.....	22
1.5.1. <i>Biogenesis</i>	23
1.5.1.1. <i>ESCRT-Dependent Pathway</i>	24
1.5.1.2. <i>ESCRT-Independent Pathway</i>	24
1.5.2. <i>Cargo Sorting and Loading</i>	25
1.5.2.1. <i>Protein Cargo</i>	25

1.5.2.2.	<i>RNA Cargo</i>	25
1.5.3.	<i>EVs in Transplantation</i>	26
1.5.3.1.	<i>Pre-Transplantation</i>	26
1.5.3.2.	<i>IRI</i>	26
1.5.3.3.	<i>Immune Regulation</i>	27
1.5.4.	<i>Therapeutic Potentials of EVs</i>	28
2.	Hypothesis	30
3.	Aims	30
4.	Methods	31
4.1.	Laboratory Procedure	31
4.2.	Cell Culture.....	31
4.2.1.	Cell Maintenance.....	31
4.2.2.	<i>Cryopreservation of Cells</i>	32
4.2.3.	<i>Human Microvascular Endothelial Cells (HMEC-1)</i>	32
4.2.4.	<i>Human Microvascular Endothelial Cells transduced with HLA-DR (HMEC-1 HLADR+)</i> 32	
4.2.5.	<i>Conditionally Immortalised Glomerular Endothelial Cells (CiGEnCs)</i>	32
4.2.6.	<i>Primary Human Glomerular Endothelial Cells (HGENCs)</i>	33
4.2.7.	<i>Primary Human Renal Proximal Tubular Epithelial Cells (PTEC)</i>	33
4.2.8.	<i>Primary Neutrophils</i>	33
4.3.	Quantitative Gene Expression	34
4.3.1.	<i>Standard RNA Isolation</i>	34
4.3.2.	<i>Total RNA Isolation</i>	35
4.3.3.	<i>RNA Quantification</i>	36
4.3.4.	<i>mRNA Reverse Transcription</i>	36
4.3.5.	<i>miRNA Reverse Transcription</i>	36
4.3.6.	<i>mRNA Quantitative Real-time Polymerase Chain Reaction (qPCR)</i>	37
4.3.7.	<i>miRNA Quantitative Real-time Polymerase Chain Reaction (qPCR)</i>	38
4.4.	Protein Quantification	38
4.4.1.	<i>Cell Preparation</i>	38
4.4.2.	<i>Protein Quantification</i>	38
4.4.3.	<i>Denaturing Protein Samples</i>	39

4.4.4.	<i>Sodium Dodecyl Sulfate Polyacrylamide Gel Electrophoresis (SDS-PAGE)</i>	39
4.4.5.	<i>Protein Transfer</i>	39
4.4.6.	<i>Immunoblotting</i>	40
4.5.	<i>Immunostaining</i>	42
4.5.1.	<i>Tissue staining</i>	42
4.6.	<i>Flow cytometry</i>	43
4.7.	<i>Statistical analysis</i>	44
5.	Regulation of CXCL8 activity by nitration	45
5.1.	<i>Introduction</i>	45
5.2.	<i>Specific Aims</i>	46
5.3.	<i>Specific Materials and Methods</i>	46
5.3.1.	<i>Patient Samples</i>	46
5.3.2.	<i>Cell Culture and Treatment</i>	46
5.3.3.	<i>Cell Viability Assessment</i>	47
5.3.4.	<i>ELISA (Enzyme-Linked Immunosorbent Assay)</i>	47
5.3.5.	<i>Trichloroacetic Acid (TCA) Precipitation of Proteins</i>	48
5.3.6.	<i>Circular Dichroism</i>	48
5.3.7.	<i>Fluorescence Spectroscopy</i>	49
5.3.8.	<i>Chemotaxis Assays</i>	49
5.3.8.1.	<i>Trans-filter Chemotaxis</i>	49
5.3.8.2.	<i>Trans-endothelial Chemotaxis</i>	50
5.3.9.	<i>Glycosaminoglycan (GAG) Binding Assay</i>	50
5.3.10.	<i>β-arrestin Recruitment Assay</i>	50
5.3.11.	<i>Immunoprecipitation</i>	51
5.3.12.	<i>Immunosorbent Sample Preparation and Nano-Scale Liquid Chromatography-Tandem Mass Spectrometry for Proteoform Analysis (ISTAMPA)</i>	51
5.3.12.1.	<i>Sample Preparation</i>	52
5.3.12.2.	<i>Mass Spectrometer Settings</i>	52
5.4.	<i>Results</i>	53
5.4.1.	<i>Generation of Nitrated CXCL8</i>	53
5.4.2.	<i>Nitration Impedes Neutrophil Chemotaxis</i>	53
5.4.3.	<i>Nitration of CXCL8 Attenuate GAG Binding and Cognate Receptors Signaling</i>	55

5.4.4.	<i>Nitration Did Not Alter CXCL8 Structure</i>	57
5.4.5.	<i>In Vitro Model of CXCL8 Nitration</i>	58
5.4.6.	<i>Detection of Nitrated CXCL8 in Lung Ischemia Reperfusion Injury.</i>	62
5.4.7.	<i>Detection of Nitrated CXCL8 In Vivo</i>	63
5.4.8.	<i>Mass spectrometry detection of nitrated CXCL8</i>	65
5.4.9.	<i>Detection of CXCL8 proteoforms in bronchoalveolar lavage by mass spectrometry</i> 67	
5.5.	Discussion.....	69
6.	miRNA Regulation in Glomerular Endothelium	73
6.1.	Introduction	73
6.2.	Specific Aims	74
6.3.	Specific Materials and Methods	74
6.3.1.	<i>Hypoxia and Re-oxygenation</i>	74
6.3.2.	<i>XTT Assay</i>	74
6.3.3.	<i>miRNA-Sequencing</i>	75
6.3.3.1.	<i>Library Preparation</i>	75
6.3.3.2.	<i>Read Mapping, Quantification and Gene Expression</i>	75
6.3.4.	<i>mRNA Sequencing</i>	76
6.3.4.1.	<i>Library Preparation</i>	76
6.3.4.2.	<i>Read Mapping, Quantification and Gene Expression</i>	77
6.3.5.	<i>Gene-Set Enrichment Analysis (GSEA)</i>	77
6.3.6.	<i>Over-representation Analysis</i>	77
6.3.7.	<i>Transfection</i>	77
6.3.7.1.	<i>Efficiency Assessment</i>	78
6.3.7.2.	<i>miR-210-3p Transfection</i>	78
6.3.8.	<i>Transferrin Receptor 1 (TfR1) Surface Expression</i>	79
6.3.9.	<i>Mitochondria Ultrastructure Visualisation</i>	79
6.3.10.	<i>Real-time Cell Metabolic Assays</i>	80
6.3.10.1.	<i>Mitostress Test</i>	81
6.3.10.2.	<i>Glycolysis Stress Test</i>	81
6.3.10.3.	<i>Normalisation</i>	82
6.4.	Results.....	82

6.4.1.	<i>Viability of HGENC Remains Unchanged in Hypoxia</i>	82
6.4.2.	<i>miRNA Expression Clustered by Biological Replicates</i>	83
6.4.3.	<i>Hypoxia Induced only miR-210-3p Upregulation</i>	83
6.4.4.	<i>miR-210-3p Remained Upregulated Post-Hypoxia</i>	86
6.4.5.	<i>mRNA Expression Clustered by Biological Replicates</i>	87
6.4.6.	<i>Hypoxia Exposure Induced Transcriptomic Changes</i>	88
6.4.7.	<i>Gene Expression of HGENC Post 4 Hours Hypoxia</i>	91
6.4.8.	<i>Gene Expression of HGENC Post 12 Hours Hypoxia</i>	93
6.4.9.	<i>Gene Expression of HGENC Post 24 Hours Hypoxia</i>	93
6.4.10.	<i>Validation of Gene Expression</i>	96
6.4.11.	<i>Integrated Analysis Identified 22 miR-210-3p Regulated mRNA Targets</i>	96
6.4.12.	<i>CiGENCs is a Valid Model of HGENCs</i>	96
6.4.13.	<i>Differential Regulation Between ciGENCs and PTECs in Hypoxia</i>	99
6.4.14.	<i>Transfection Efficiency of ciGENCs</i>	100
6.4.15.	<i>mRNA Targeting by miR-210-3p</i>	102
6.4.16.	<i>TfR1 is Targeted by miR-210-3p</i>	103
6.4.17.	<i>Overexpression of miR-210-3p Increased Glycolysis but not Mitochondria Function</i>	104
6.4.18.	<i>Mitochondrial Morphology unaltered by miR-210-3p Overexpression</i>	107
6.5.	<i>Discussion</i>	108
7.	<i>Characterisation of Renal Allograft Derived Extracellular Vesicles</i>	112
7.1.	<i>Introduction</i>	112
7.2.	<i>Specific Aims</i>	113
7.3.	<i>Specific Materials and Methods</i>	113
7.3.1.	<i>Kidney Effluent Collection</i>	113
7.3.2.	<i>Cell Culture and Treatment</i>	113
7.3.3.	<i>Generation of EVs from In Vitro Culture</i>	114
7.3.4.	<i>Extracellular Vesicle Isolation</i>	114
7.3.4.1.	<i>Differential Centrifugation</i>	114
7.3.4.2.	<i>Size Exclusion Chromatography</i>	115
7.3.5.	<i>Nanoparticle Tracking Analysis (NTA)</i>	115
7.3.6.	<i>Electron Microscopy</i>	115

7.3.7.	<i>EV Surface Proteome Analysis</i>	116
7.3.8.	<i>Total RNA Extraction from EVs</i>	117
7.3.9.	<i>RNA Quantification</i>	117
7.3.10.	<i>Nanostring®</i>	118
7.3.10.1.	<i>Sample preparation</i>	118
7.3.10.2.	<i>Codeset Hybridisation</i>	118
7.3.10.3.	<i>Sample Loading and Data Acquisition</i>	119
7.3.10.4.	<i>Data analysis</i>	119
7.4.	Results	120
7.4.1.	<i>Characterisation of EVs</i>	120
7.4.2.	<i>Total EVs Isolated Correlated with Allograft Cold Ischemic Time (CIT)</i>	122
7.4.3.	<i>Surface Proteome of Kidney Effluent EVs</i>	123
7.4.4.	<i>Deceased Donors Associated with Increased EV MHC Class II Expression</i>	124
7.4.5.	<i>Deceased Donors Clustered Independently from Living Donors</i>	125
7.4.6.	<i>MHC Class II and CD105 Contributes to Distinct Clustering in DCD samples.</i>	125
7.4.7.	<i>RNA Isolation from Kidney Effluent EVs</i>	127
7.4.8.	<i>No Distinct miRNA Signature was Identified from Kidney Effluent EVs</i>	127
7.4.9.	<i>Induction of Endothelial MHC Class II Expression In Vitro</i>	127
7.4.10.	<i>EV Generation from HMEC-1 In Vitro</i>	132
7.4.11.	<i>IFN-γ Stimulation Resulted in Co-isolation of Lipoprotein</i>	132
7.4.12.	<i>EVs Isolated from HLA-DR Transduced HMEC-1 did not Show Contaminating Lipoprotein</i>	134
7.4.13.	<i>HLA-DR is present on EVs derived from HLA-DR transduced HMEC-1</i>	137
7.5.	Discussion	138
8.	Discussion, Limitations and Future Directions	142
8.1.	General Discussion	142
8.2.	Limitations of Study and Future Directions	146
9.	References	148
10.	Publications and Presentations	183
10.1.	Publications	183
10.2.	Presentations	184

Table of Figures

Figure 1.1 10 years transplant statistics from NHS Blood and Transplant.	2
Figure 1.2. Overview of the main molecular mechanisms of ischemia reperfusion injury.	4
Figure 1.3 Schematic for chemokine glycosaminoglycan and receptor signaling.	7
Figure 1.4 Schematic of chemokine regulation.	11
Figure 1.5 Visualisation of nitrated chemokine peptide sequence and modified residues.	12
Figure 1.6 Overview of miRNA biogenesis and function.	17
Figure 1.7 Schematic of canonical exosome biogenesis.	23
Figure 4.1 Purity assessment of isolated neutrophils from human whole blood.	34
Figure 5.1 HPLC chromatogram and mass spectra of nitrated CXCL8.	54
Figure 5.2 Assessment of the migratory potential of nitrated CXCL8 <i>in vitro</i>	54
Figure 5.3 Comparisons of CXCL8 variants for glycosaminoglycan binding.	56
Figure 5.4 Differential signaling between CXCL8 variants with receptors.	56
Figure 5.5 Secondary structure assessment of CXCL8 variants.	57
Figure 5.6 SIN-1 nitrates CXCL8 <i>in vitro</i>	58
Figure 5.7 HMEC-1 viability in response to SIN-1.	60
Figure 5.8 CXCL8 gene and protein expression in response to nitrosative stress.	61
Figure 5.9 Lung immunofluorescence staining for the presence of nitrated CXCL8.	62
Figure 5.10 CXCL8 levels in bronchoalveolar lavage samples.	64
Figure 5.11 Detection of nitrated CXCL8 in Bronchoalveolar lavage samples.	64
Figure 5.12 Fragmentation of CXCL8 and theoretical mass to charge (m/z) of CXCL8.	65
Figure 5.13 Detection of nitrated CXCL8 using the ISTAMPA workflow.	66
Figure 5.14 Nitrated CXCL8 detection post immuno-isolation.	67
Figure 5.15 Nitrated CXCL8 detection within BAL samples by mass spectrometry.	68
Figure 5.16 Total CXCL8 proteoforms detected within the BAL samples by mass spectrometry.	68
Figure 5.17 CXCL8 peptide sequence.	70
Figure 6.1 Gating strategy for transfection efficiency determination.	78
Figure 6.2 Gating strategy for CD71 expression on ciGenCs.	79
Figure 6.3 Viability assessment of HGenC in hypoxia.	82
Figure 6.4 miRNA-sequencing of hypoxia treated HGenCs.	84
Figure 6.5 Differentially regulated miRNA between hypoxia and normoxia treated HGenC.	85
Figure 6.6 miR-210-3p upregulation across HGenCs and PTECs.	86
Figure 6.7 Elevated miR-210-3p levels detected post-hypoxia.	87
Figure 6.8 mRNA-sequencing of hypoxia treated HGenCs.	88
Figure 6.9 Clustering of the DEGs.	89
Figure 6.10 Gene ontology analysis for individual clusters.	90
Figure 6.11 GSEA of hypoxia time-course in HGenCs.	91
Figure 6.12 mRNA expression of HGenC post 4 hours exposure to hypoxia.	92
Figure 6.13 mRNA expression of HGenC post 12 hours exposure to hypoxia.	94
Figure 6.14 mRNA expression of HGenC post 24 hours exposure to hypoxia.	95

Figure 6.15 RNA-seq validation.	97
Figure 6.16 Co-analysis of the DEGs from mRNA sequencing with miR-210-3p targets.	98
Figure 6.17 miRNA and mRNA expression of ciGenCs in hypoxia.	99
Figure 6.18 PTECs mRNA regulation in hypoxia.	100
Figure 6.19 Transfection efficiency assessment of ciGenCs for small RNA uptake.	101
Figure 6.20 miR-210-3p targeting in ciGenCs.	102
Figure 6.21 miR-210-3p targeting in ciGenCs 24 hours post-transfection.	103
Figure 6.22 TfR1 expression post miR-210-3p transfection.	104
Figure 6.23 Assessment of ciGenCs glycolytic function post miR-210-3p transfection.	105
Figure 6.24 Assessment of ciGenCs mitochondria function post miR-210-3p transfection.	106
Figure 6.25 Mitochondria ultrastructure of ciGenCs post miR-210-3p transfection.	107
Figure 7.1 Gating strategy for HMEC-1.	114
Figure 7.2 Gating strategy for MACSPlex Human Exosome kit.	116
Figure 7.3 Characterisation of EVs isolated from kidney effluents.	121
Figure 7.4 Correlation between total particles released with allograft cold ischemic time.	122
Figure 7.5 Normalised MFI of kidney effluent EVs.	123
Figure 7.6 Significant differentially expressed surface markers.	125
Figure 7.7 Data clustering by surface marker expression on kidney effluent.	126
Figure 7.8 PCA loading driving separation of samples.	126
Figure 7.9 RNA quantification from kidney effluent EVs.	128
Figure 7.10 miRNA signature in kidney effluent EVs.	129
Figure 7.11 Activated endothelial phenotype post-IFN- γ stimulation.	130
Figure 7.12 MHC class II expression in activated endothelial cells.	131
Figure 7.13 Characterisation of HMEC-1 EVs.	133
Figure 7.14 Comparisons of EVs isolated under basal or IFN- γ stimulation.	135
Figure 7.15 Characterisation of EVs isolated from HLA-DR transduced HMEC-1.	136
Figure 7.16 Surface marker characterisation of EVs.	137

Table of Tables

Table 1.1 Summary of Amino Acids Modified During Nitrosative Stress.	14
Table 1.2. Recent literature on the role of EVs in IRI.....	27
Table 1.3 Recent literatures on the role of EVs in solid organ transplantation	29
Table 4.1 Centrifugation speed for various cell types.	31
Table 4.2 Primer list for small-RNA species used for target specific reverse transcription and PCR.	36
Table 4.3 Primer list for mRNA qPCR.	37
Table 4.4 Components for SDS-PAGE gel.....	39
Table 4.5 Antibody list and incubation conditions for western blot.	41
Table 4.6 Antibody list and incubation condition for tissue staining.	42
Table 4.7 Antibodies used for conventional flow cytometry.	43
Table 5.1 Phosphate buffer composition.....	48
Table 7.1 Donor allograft parameters and 1 year kidney function.	122
Table 7.2 Pooled kidney effluent EVs and final particle count.	123

Abbreviations

ACKR	Atypical Chemokine Receptor
Ago	Argonaute Protein
AKI	Acute Kidney Injury
APC	Antigen Presenting Cells
ATCC	American Type Culture Collection
ATP	Adenosine Triphosphate
BAL	Bronchoalveolar Lavage
BioCOSHH	Biological Control of Substances Hazardous to Health
BSA	Bovine Serum Albumin
CCR4-NOT	Carbon Catabolite Repression—Negative On TATA-less
CD	Cluster of Differentiation
cDNA	Complementary Deoxyribonucleic Acid
CID	Collision Induced Dissociation
ciGENCs	Conditionally Immortalised Glomerular Endothelial Cells
CIITA	Class II Transactivator
CIT	Cold Ischemic Time
CO ₂	Carbon Dioxide
COSHH	Control of Substances Hazardous to Health
cryo-EM	Cryo-electron Microscopy
DAMPs	Damage Associated Molecular Patterns
DBD	Donation after Brain Death
DCD	Donation after Circulatory Death
DEG	Differentially Expressed Genes
DGCR8	DiGeorge Syndrome Critical Region 8
DGF	Delayed Graft Function
DMSO	Dimethylsulfoxide
DNA	Deoxyribonucleic acid
ECD	Extended Criteria Donor
EDTA	Ethylenediaminetetraacetic Acid
ELISA	Enzyme-Linked Immunosorbent Assay
ELR	Glutamic acid-Leucine-Arginine
ESCRT	Endosomal Sorting Complex Required for Transport
ESI-microTOF	Electrospray Ionisation Time of Flight Mass Spectrometry
ETC	Electron Transport Chain
EVLP	<i>Ex Vivo</i> Lung Perfusion
EVs	Extracellular Vesicles
FBS	Foetal Bovine Serum
FCCP	Carbonyl Cyanide-p-trifluoromethoxyphenylhydrazone
FFPE	Formalin Fixed, Paraffin Embedded
GAG	Glycosaminoglycan
GPCRs	G-protein Coupled Receptors
GSEA	Gene Set Enrichment Analysis
GW182	Glycine-Tryptophan-182

H ₂ SO ₄	Sulfuric Acid
hAECs	Human Amniotic Epithelial Cells
HGEnCs	Primary Human Glomerular Endothelial Cells
HIF	Hypoxia Inducible Factor
HIF-1 α	Hypoxia Inducible Factor 1 Alpha
HIF-1 β	Hypoxia Inducible Factor 1 Beta
HIF-2 α	Hypoxia Inducible Factor 2 Alpha
HLA	Human Leukocyte Antigen
HMEC-1	Human Microvascular Endothelial Cells
HMEC-1 HLA-DR+	Human Microvascular Endothelial Cells transduced with HLA-DR
HRE	Hypoxia Response Element
HRS	Hepatocyte Growth Factor-Regulated Tyrosine Kinase Substrate
IFN- γ	Interferon Gamma
ILV	Intraluminal Vesicles
IP	Immunoprecipitation
IRI	Ischemia Reperfusion Injury
ISTAMPA	Immunosorbent Sample Preparation and Nano-Scale Liquid Chromatography-Tandem Mass Spectrometry for Proteoform Analysis
LAMP2	Lysosomal Associated Membrane Protein 2
MFI	Median Fluorescence Intensity
MHC	Major Histocompatibility Complex
miRISC	miRNA associated Ribonucleic acid Silencing Complex
miRNA	Micro Ribonucleic Acid
MISEV2018	Minimal Information for Studies of Extracellular Vesicles 2018
MRM	Multiple Reaction Monitoring
mRNA	Messenger Ribonucleic Acid
MsigDB	Molecular Signature Database
MVB	Multi-Vesicular Body
NADH	Nicotinamide Adenine Dinucleotide
NADPH	Nicotinamide Adenine Dinucleotide Phosphate
nano-LC-MS/MS	Nano-Liquid Chromatography coupled to Tandem Mass Spectrometry
ncRNA	Non-Coding Ribonucleic Acid
NOS	Nitric Oxide Synthase
NOX	NADPH oxidase
PAZ	Piwi Argonaute Zwillig
PBS	Phosphate Buffered Saline
PFA	Paraformaldehyde
pri-miRNA	Primary Micro ribonucleic Acid
PTECs	Primary Human Renal Proximal Tubular Epithelial Cells
qPCR	Reverse Transcription Quantitative Polymerase Chain Reaction
RCF	Relative Centrifugal Force
RIPA	Radioimmunoprecipitation
RNA	Ribonucleic acid
RNS	Reactive Nitrogen Species

ROS	Reactive Oxygen Species
RP-HPLC	Reverse Phase High Performance Liquid Chromatography
SCD	Standard Criteria Donor
SDS-PAGE	Sodium Dodecyl-Sulfate Polyacrylamide Gel Electrophoresis
SIN-1	3-morpholinopyridone
siRNA	Silencing RNA
STAM	Signal Transducing Adapter Molecule
TBST	Tris-buffered Saline with Tween 20
TCA	Trichloroacetic Acid
TCA	Tricarboxylic Acid
TEM	Transmission Electron Microscopy
TFA	Trifluoroacetic Acid
TfR1	Transferrin Receptor 1
TGF- β	Transforming Growth Factor Beta
TMB	3,3',5,5'-Tetramethylbenzidine
TNF- α	Tumour Necrosis Factor- α
TRBP	Transactivation Response Element Ribonucleic Acid-Binding Protein
UMI	Unique Molecular Identifier
UV	Ultraviolet
UW [®]	University of Washington
VAP	Ventilator Associated Pneumonia
w/v	Weight/Volume
XTT	2,3-Bis-(2-Methoxy-4-Nitro-5-Sulfophenyl)-2 <i>H</i> -Tetrazolium-5-Carboxanilide
YBX1	Y-Box Binding Protein 1

1. Introduction

1.1. Transplantation

Within the span of 70 years since the first reported successful organ transplant (Merrill et al., 1956) to the current the gold standard of care for patients with end stage organ failure, the progress in the field of solid organ transplantation have been made possible by advancement in both the surgical procedures as well as our understanding of the complex cellular processes during and post-transplantation.

However, there are several challenges that still prohibit the widespread utilisation of transplantation as a therapeutic intervention. Firstly, there is a disproportionately higher number of patients on the transplant waiting list compared to the number of organ donors (Figure 1.1). To address this disparity, there is an increase in the utilisation of extended criteria donor (ECD). However, ECD graft survival from ECD tend to perform poorer than standard criteria donor (SCD) (Merion et al., 2005, Lund et al., 2017, Amin et al., 2004). Therefore, novel platforms for organ preservation and functional assessment *ex situ* have been developed with the aims of improving the overall graft quality from ECD (Richards et al., 2023, Hosgood et al., 2023, Nilsson et al., 2020, Divithotawela et al., 2019).

Secondly, the occurrence of ischemia reperfusion injury (IRI) is unavoidable during the process of transplantation. Currently, clinical interventions to circumvent the injuries associated with IRI have very limited success, in part due to the complexity of IRI pathophysiology.

Finally, allograft rejection remains the primary cause of transplant failure. Transplant rejection can be classified under three broad categories: hyperacute, acute and chronic rejection (Moreau et al., 2013). The occurrence of hyperacute rejection is limited due to the current standard practice of blood group testing and screening of pre-existing donor specific human leukocyte antigen (HLA) antibodies during donor and recipient cross matching (Moreau et al., 2013). Acute rejection can also be controlled using a variety of immunosuppressants, which dampens the recipient immune system to prevent targeting of allografts. However, there is limited success in the clinic to prevent the occurrence of chronic rejection. This is in part due to limited understanding on the molecular mechanisms driving the process as well as the difficulty in clinical diagnosis (Moreau et al., 2013).

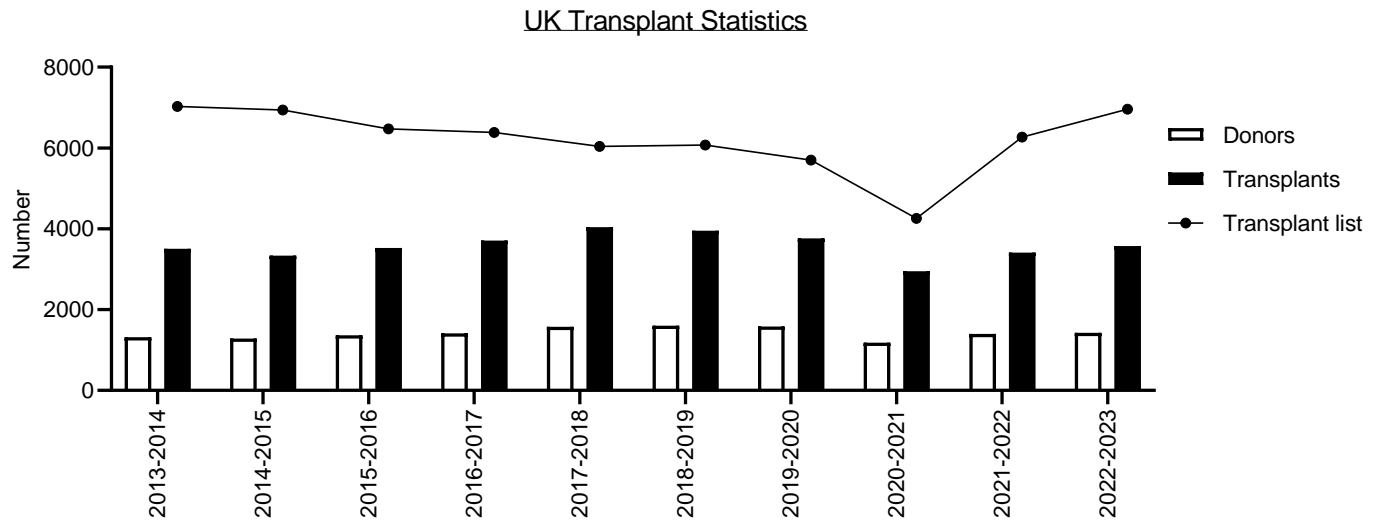


Figure 1.1 10 years transplant statistics from NHS Blood and Transplant.

UK transplant statistics indicating the annual transplant activity from April 2013 to March 2023. A steady number of transplants (black bar) was carried out annually with a reduction of number of patients on the transplant waitlist (line graph) from 2013 to the beginning of 2020. A decline in numbers of patients on the waitlist was observed in the 2020-2021 before a sharp increase in the following year of 2021-2022 and 2022-2023. Adapted from NHSBT Transplant Statistics 2023.

1.2. Cellular and Molecular Mechanisms of IRI

IRI occurs in a wide range of clinical scenarios including myocardial infarction, stroke, and organ transplantation. The biphasic nature of IRI includes the initial restriction of blood supply, resulting in a hypoxic and nutrient deficient environment. In turn, this disrupts normal cellular metabolism and function. Subsequently, reperfusion reinstates the flow of blood which provides the oxygen and metabolites necessary to restore cellular metabolism and normal function. However, tissue oxygenation brings about a paradoxical increase in cellular dysfunction and tissue injury.

This cascade of events is first initiated by tissue or organ hypoperfusion. Hypoxia induces the stabilisation of hypoxia inducible factor-1 α (HIF-1 α) (Ong et al., 2014, Koeppen et al., 2018) and hypoxia inducible factor-2 α (HIF-2 α) (Koeppen et al., 2018). This allows the dimerisation to hypoxia inducible factor-1 β (HIF1- β) and translocation to the nucleus, inducing metabolic shift towards anaerobic metabolism (Kim et al., 2006). In turn, this results in cytosolic acidosis and leads to an overall decrease in adenosine triphosphate (ATP) (Figure 1.2). The disruption of cellular homeostasis is further aggravated by the ionic imbalance within the cells, triggering endoplasmic reticulum dysfunction (Shen et al., 2021), cell swelling and cell death (Eltzschig and Eckle, 2011). Interruption to the electron transport chain (ETC) due to the low intracellular ATP

coupled with increased intracellular calcium ion concentration leads to mitochondrial dysfunction and succinate accumulation within the mitochondria (Chouchani et al., 2014).

In addition to the loss of oxygen and nutrient supply, endothelial cells lining the vessel lumen lose the mechano-transduction brought about by the blood flow. Mechano-sensors including the glycocalyx (Baeyens et al., 2014) and ion channels (Ranade et al., 2014) lining the luminal surface of endothelial cells provide constitutive signaling and maintain overall cellular function. Loss of these signaling in turn activates the inflammatory signaling, thereby promoting endothelial dysfunction and upregulation of surface adhesion molecules priming the endothelium for immune cell adhesion.

In parallel, the change to cellular metabolism causes oxidative and nitrosative stresses as well as free radical formation (Chouchani et al., 2014). These free radicals damage cellular components that act as damage associated molecular patterns (DAMPs). DAMP sensing mechanisms expressed on both stromal and tissue resident immune cells (Wu et al., 2007) subsequently trigger an inflammatory signaling cascade, causing the release of inflammatory cytokines and pre-formed inflammatory mediators from within the Weibel-Palade bodies of endothelial cells (Utgaard et al., 1998).

Paradoxically, while timely reperfusion is pivotal to limit ischemic damage, re-establishment of blood supply is associated with further tissue damage. Firstly, reperfusion exacerbates the oxidative and nitrosative stresses that are initiated during ischemia (Eltzschig and Eckle, 2011). Secondly, immune cells are recruited into ischemic tissue by chemokines and other chemotactic molecules such as complement fragments and products of the cyclooxygenase pathway, further exacerbating tissue injury. Leukocytes are not only mediators of tissue injury. A second phase involving the infiltration of reparative leukocytes, in particular macrophages, occurs later during the resolution phase and is critical for tissue repair (Eltzschig and Eckle, 2011).

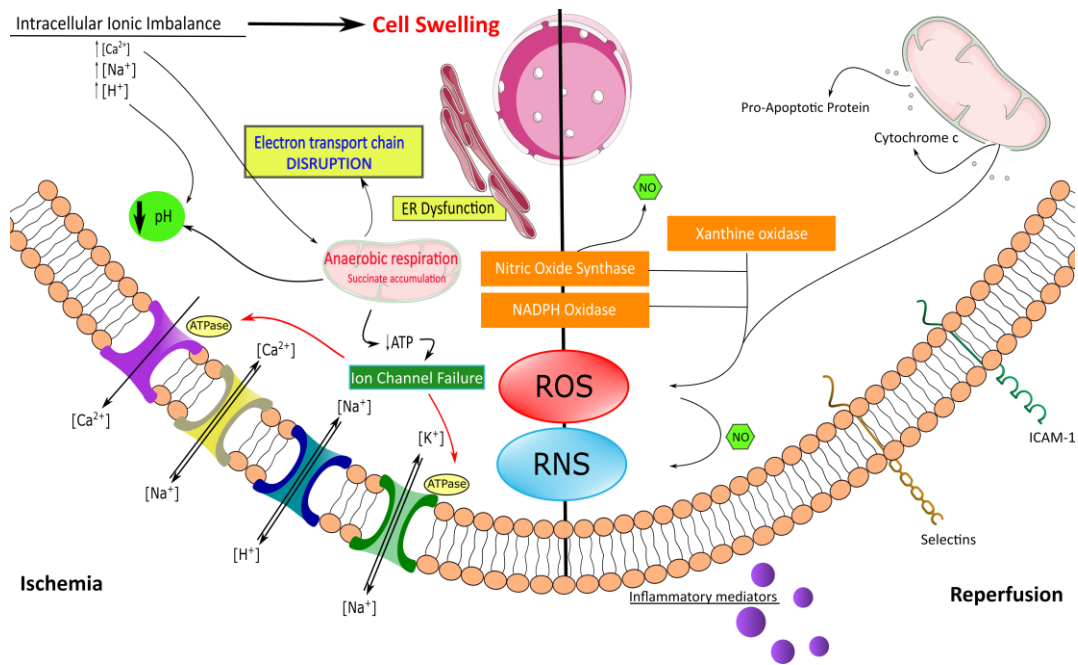


Figure 1.2. Overview of the main molecular mechanisms of ischemia reperfusion injury.

This ischemic state induces anaerobic metabolism which results in decreased cellular pH, disruption to electron transport chain and in turn ionic imbalance. As a result, cell swelling, and impaired enzymatic activity leads to the production of reactive oxygen species including nitric oxide synthase and NADPH oxidase. During reperfusion, further ROS is produced by xanthine oxidase. These excess ROS in turn interact with the abundant nitric oxide forming RNS. In response to the damage brought by the ROS and RNS, release of inflammatory mediators and expression of adhesion molecules recruit immune cells and promotes the extravasation into the parenchyma.

1.2.1. Oxidative and Nitrosative Stresses in IRI

Although reactive oxygen species (ROS) are integral to cellular signaling (Irani et al., 1997, Arnold et al., 2001, Joneson and Bar-Sagi, 1998) and function, redox imbalance results in the development of pathological oxidative stress. During IRI, sources of ROS can be broadly categorised into enzymatic and non-enzymatic sources. Mitochondria are the predominant non-enzymatic source of ROS. Together with the switch from aerobic to anaerobic respiration during ischemia (M.Kosieradzki and Rowinski, 2008), cytoplasmic calcium ion overload leads to mitochondrial swelling and uncoupling of oxidative phosphorylation (Liu et al., 2018, Kuznetsov et al., 2019, Zorov et al., 2014). At the same time, the accumulation of succinate during ischemia drives the reverse electron transfer during reperfusion at mitochondrial complex I (Murphy, 2009, Chouchani et al., 2014) and opening of the permeability transition pore leads to an exacerbation in mitochondrial dysfunction.

Nitric oxide synthase (NOS), NADPH oxidase (NOX) and xanthine oxidase are the three main enzymatic sources of ROS during IRI. As a result of the dysfunctional endothelium and increased oxidative stress, the constitutive dimeric NOS are uncoupled due to essential co-factor oxidation (Vásquez-Vivar et al., 1998, Pascali et al., 2014) and S-glutathionylation (Pascali et al., 2014, Chen et al., 2010, Chen et al., 2011) which produces ROS in place of nitric oxide (Vásquez-Vivar et al., 1998, Pascali et al., 2014). Additionally, hypoxanthine, the breakdown product of ATP is produced during ischemia (Berne, 1963, Farthing et al., 2015). Xanthine oxidase dependent metabolism of hypoxanthine to xanthine and then uric acid on re-oxygenation is a major source of superoxide ions (Wu et al., 2018).

At reperfusion, leukocytes are recruited into areas of tissue injury. Neutrophils (Vinten-Johansen, 2004) and macrophages (Caldwell-Kenkel et al., 1990, Zhao et al., 2017) both possess lytic granules containing key enzymes such as myeloperoxidase and NOX capable of generating bursts of free radicals (Vinten-Johansen, 2004). This process, termed oxidative burst, is used to kill pathogens but during reperfusion, it functions as an additional source of ROS. Interestingly, NOX activation not only occurs in immune cells, but has also been described in the brain (A. Miller et al., 2006, Tang et al., 2012), heart (Matsushima et al., 2015) and liver (Mark et al., 2003) during IRI where it may play a role in both ischemic and reperfusion injury.

Similar to ROS, nitric oxide is important in physiological cellular processes (Pacher et al., 2007). Yet during IRI, nitric oxide becomes a double-edged sword. On one hand, it has been shown to be protective and attenuates the damage brought about by IRI (Kanno et al., 2003, Park et al., 2003, Phillips et al., 2009, Brunner et al., 2003, N. Panahian et al., 1996, Kurose et al., 1994); indeed, nitric oxide has been used to limit ischemic injury with varying success (Botha et al., 2007, Terpolilli et al., 2012, John D. Lang et al., 2007). On the other hand, the potential for nitric oxide to react with ROS and generate reactive nitrogen species (RNS) is increased by an elevation in nitric oxide concentration during ischemia (Zweier et al., 1995, Salom et al., 2005).

Detection of ROS and RNS is difficult due to their extremely short half-life, but their capacity to modify deoxyribonucleic acid (DNA) (Pinlaor et al., 2003, Pacher et al., 2007) and protein (Pacher et al., 2007, Ischiropoulos, 1998) generates unique signatures that can be detected *in vivo*. In particular, the formation of the cytotoxic metabolite peroxynitrite via the rapid reaction between superoxide anion and nitric oxide (Pacher et al., 2007) has been associated with IRI.

1.3. Chemokines

Chemokines are small chemotactic proteins (8-14kDa) that play an integral role in modulating cellular migration during both homeostasis and inflammation. These proteins are classified based on the conserved cysteine residues in their N-terminus: C, CC, CXC, CX3C and XC where X represents additional amino acids juxtaposed between conserved cysteines. Structurally, all chemokines share a similar monomeric structure consisting of an N-terminus irregular strand that leads to an α -helix and a subsequent anti-parallel three stranded β -sheet (Zlotnik and Yoshie, 2012) despite having a sequence homology across chemokines ranging from 20-90%. Apart from CX3CL1 (Bazan et al., 1997) and CXCL16 (Matloubian et al., 2000), the other 44 human chemokines identified are released as soluble factors (Zlotnik and Yoshie, 2012).

In order for chemokines to exert their biological functions, two key interactions are critical, namely with tissue glycosaminoglycans and cognate receptors expressed on the target cell surface (Figure 1.3) with the exception of CXCL4 (Gray et al., 2023). The interaction between chemokines and glycosaminoglycan (GAG) results in the formation of a haptotactic gradient that provides directional cue for chemotaxis. Besides directing cellular migration, signaling through chemokine receptors also results in an array of biological responses that results in cellular activation, proliferation, and migration (Figure 1.3).

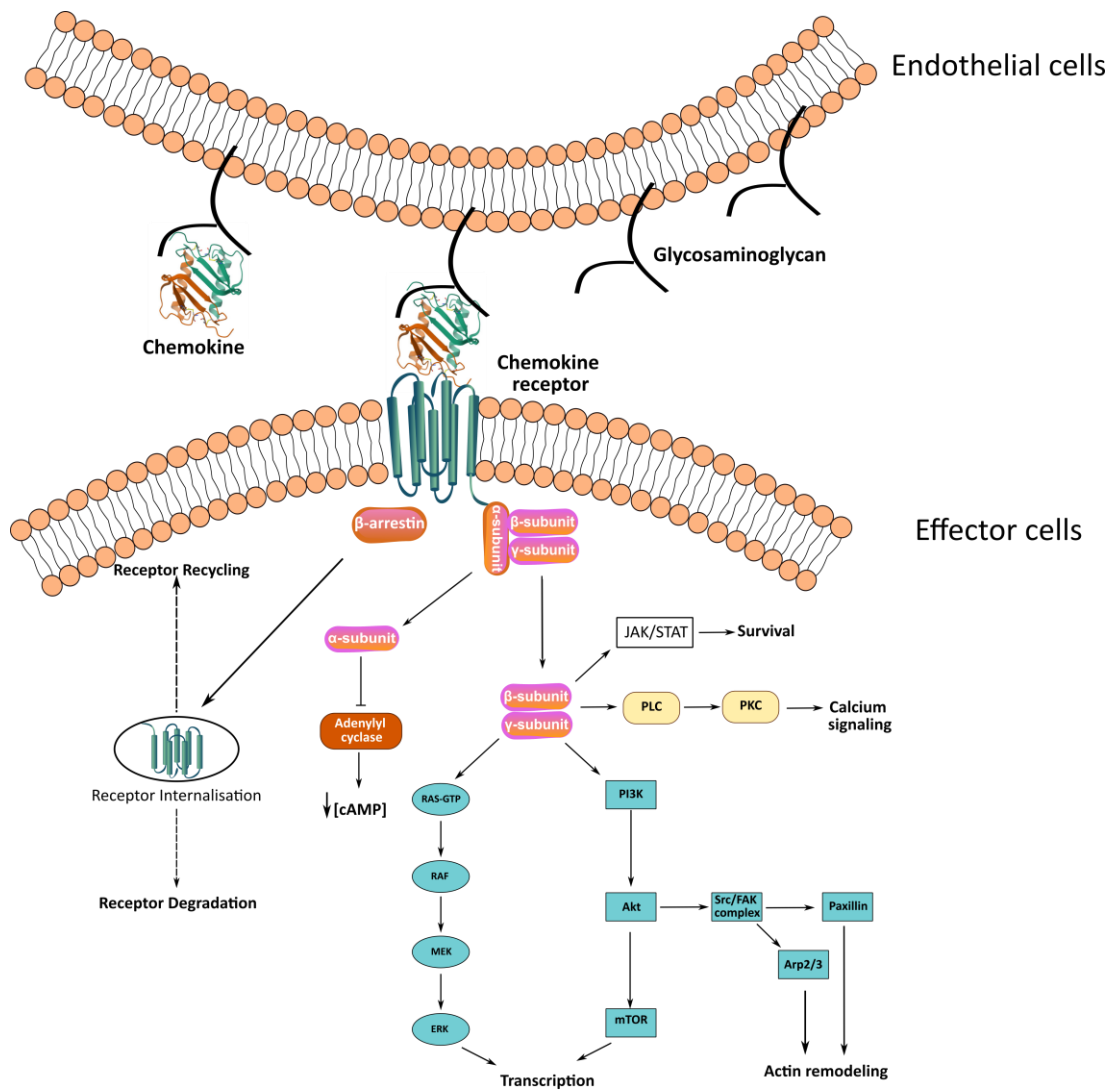


Figure 1.3 Schematic for chemokine glycosaminoglycan and receptor signaling.

Chemokines interact with the glycosaminoglycan which results in the formation of a chemotactic gradient, providing a direction cue for the effector cell to migrate towards. Upon binding with the chemokine cognate receptors, chemokines trigger downstream signaling via either the G-protein subunits or β -arrestins to elicit a variety of cellular response ranging from receptor regulation, cellular activation, cytoskeletal remodeling, and migration.

1.3.1. Chemokine-GAG Interaction

GAGs are long linear polysaccharides constituted by the repeating disaccharide subunits of an uronic acid and a hexosamine (Pomin and Mulloy, 2018). These GAGs are ubiquitously present on the cell surface as proteoglycans and higher order glyocalyx, dissipating fluid shear stress, functioning as key mechanosensors and allow binding by soluble factors in circulation. While they can be commonly categorised into 4 main groups: heparan sulfate, dermatan/ chondroitin sulfate, keratan sulfate and soluble hyaluronic acid, the non-templated and regio-selectivity of its modifications gives rise to an extremely complex and variable structures (Pomin and Mulloy, 2018). Furthermore, these chemical modifications also confer different physiochemical properties to the GAG. In particular, sulfation of the repeating subunits results in a net negative charge which are essential in the interaction with chemokines (Gray et al., 2023).

Since chemokines are small positively charged proteins, regional concentrations in the blood and tissue are augmented by the laminar blood flow. Electrostatic forces and hydrogen bonding between chemokines and GAG allows localisation of the chemokines onto the surface of the cells, resulting in the formation of a chemotactic gradient. This interaction is regulated by the **BBXB** or the **(B)Bxx(x/B)BxxB(B)** motif on the chemokines, where B refers to a basic amino acid residue and X refers to any amino acid residue (Proudfoot et al., 2003, Thompson et al., 2017). Furthermore, this was identified to be quintessential for chemokine activity as non-GAG binding mutants were unable to elicit cellular migration *in vivo* (Ali et al., 2005, Proudfoot et al., 2003). However, whether the GAG bound chemokines can trigger receptor signaling remains contentious with conflicting data across different chemokines (Schwarz et al., 2016, Bonvin et al., 2017). This led to the current proposal that within the glyocalyx, chemokines are present in an equilibrium between two forms; glycosaminoglycan bound and in solution. GAG binding concentrates chemokines at the production site to prevent displacement by blood flow. Subsequently, the reversible interaction with GAG occurs to allow for its release to bind receptors expressed on the effector cells (Graham et al., 2019).

1.3.2. Chemokine-Receptor Interaction

Chemokine receptors are G-protein coupled receptors (GPCRs) that result in signal transduction through $G\alpha_i$ protein and β -arrestin upon chemokine binding (Figure 1.3). The expression of the 18 signaling and 4 non-signaling human chemokine receptors has been identified across a wide range of cell types, most notably on immune cells (Hughes and Nibbs, 2018) with peptide homology ranges from 45-70%.

Interactions between chemokines and their cognate receptors are mediated through a 2-step binding model initially identified via site directed mutagenesis. The first step involves the interaction of the receptor N terminus with the chemokine core-domain (termed chemokine recognition site 1) followed by the insertion of the chemokine N-terminus into the receptor binding pocket (chemokine recognition site 2) to stabilise the binding (Pease et al., 1998, Monteclaro and Charo, 1996, Rajagopalan and Rajarathnam, 2009). This model was subsequently confirmed recently by various high-resolution chemokine-receptor crystal and cryo-electron microscopy (cryo-EM) structures (Liu et al., 2020, Shao et al., 2021, Zhang et al., 2021a, Wu et al., 2010).

In the instances of the non-signaling receptors (atypical chemokine receptors-ACKR), the lack of the Asp-Arg-Tyr-Leu-Ala-Iso-Val (DRYLAIV) motif within their second intracellular loop prevents the association with G-proteins (Nibbs et al., 2003). As a result, these receptors are unable to induce canonical downstream signaling associated with cell activation. Furthermore, mutagenesis in an attempt to reconstitute the motif back into the ACKR did not result in G-protein recruitment (Hoffmann et al., 2012), suggesting the presence of other residues playing a fundamental role in G-protein signaling.

One key challenge with research in chemokines is the promiscuity of interactions between the various ligands and receptors. In many instances, a chemokine can bind to multiple receptors and similarly, one receptor can recognise multiple chemokines. Initial idea for this promiscuous interaction between chemokine ligands and receptors was thought to be nature's way of building in redundancy but now are thought as a means to fine tune cellular location. Additionally, this already complex interaction was further complicated by the concept of bias agonism. Binding of different ligands to the same receptor can elicit divergent downstream signaling. This in turn meant a different cellular response can be obtained (Rajagopal et al., 2013, Zheng et al., 2022). This also holds true for the same ligand binding various different receptors (Wang et al., 2011).

1.3.3. Chemokine Regulation

Due to the importance of timely cellular recruitment, various regulatory mechanisms are present to prevent aberrant activation and migration of cells (Figure 1.4). This ranges from polymorphisms in the gene encoding both chemokine ligands (Winkler et al., 1998) and their receptors (Huang et al., 1996). Subsequently, post transcriptional regulation can also be mediated by non-coding ribonucleic acid (RNA) (Amrouche et al., 2017, Fanucchi et al., 2019). Upon their release, ACKRs regulates local concentrations by either scavenging or functioning as chemokine sinks (Darbonne et al., 1991) to maintain optimal gradient formation. This is particularly important as the potential of chemokines to exist as monomers or homo/hetero-oligomers (Hundelshausen et al., 2017) is spatiotemporally dependent. In turn, this can alter the capacity to induce signaling and GAG binding.

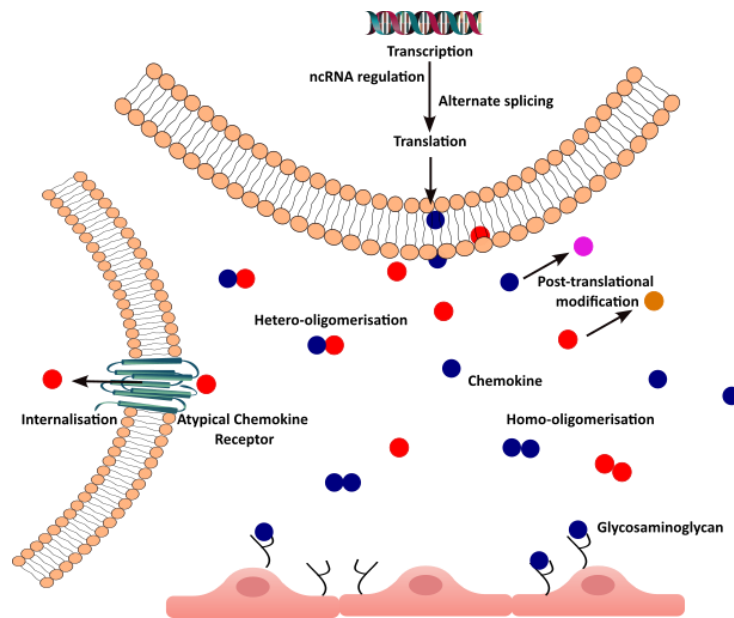


Figure 1.4 Schematic of chemokine regulation.

Chemokines regulation occurs at every stage of transcription down to post-translation. Within a cell, polymorphisms in genes encoding chemokine have been identified and alternate splicing can occur, generating variants upon translation. Subsequently, fine-tuning of these can also be controlled by non-coding RNA (ncRNA) before being secreted. Upon release, the local concentration of chemokines can be controlled by cells expressing ACKRs and in turn, affect its capability to oligomerise with either similar chemokines or other chemokines within the environment. Post-translational modification can also potentiate chemokine function, either to increase their activity or function as a mechanism to dampen inflammation.

Chemokines can also undergo a variety of post-translational modifications. The majority of these modifications occur in the context of inflammation. The most prominent modification is mediated by enzymatic truncation at either the N- terminus or C-terminus end (Cambier et al., 2023, Metzemaekers et al., 2016). Truncation at the N-terminus of many chemokines lead to an increased potency to induce cellular activation and migration (Cambier et al., 2023) whereas C-terminus truncation often result in functional loss (Zinkernagel et al., 2008, Dillemans et al., 2023, Shao et al., 2021), reflecting the importance of chemokine recognition site 1 in the interaction with cognate receptors. Additionally, another enzyme mediated modification includes citrullination by peptidyl arginine deiminase (Loos et al., 2009, Struyf et al., 2009), converting the arginine to citrulline.

Furthermore, non-enzymatic post-translational modification involves nitration by an RNS species, peroxynitrite. Peroxynitrite can react with multiple amino acids and results in many different modifications (**Table 1.1**). Amongst these modifications, 3-nitrotyrosine is the most studied and has been identified in several pathologies, including IRI (Barker et al., 2017). To date, 6 chemokines has been reported: CCL2 (Barker et al., 2017, Molon et al., 2011), CCL3 (Sato et al., 2000b), CCL5 (Sato et al., 1999), CCL11 (Sato et al., 2000a), CXCL8 (Sato et al., 2000c, Thompson et al., 2023) and CXCL12 (Janssens et al., 2016) (**Figure 1.5**).

The available literature, although limited to only 6 chemokines, suggests that nitration leads to impaired chemokine function. Different residues can be nitrated, and the nitration profile appears to determine the effect on function. Whether the function of other chemokines is similarly affected by nitration is unknown, nor do we know the types of modification that will occur *in vivo* during an inflammatory response. It is also evident that once nitrated, chemokines may no longer be detected using standard antibody-based assay methods and this potentially limits our understanding of chemokine biology during disease.

<u>Chemokine</u>	<u>Peptide sequence</u>
CCL2	MKVSAALLCLLIAATFIPQGLA QPDAINAPVTCCY* [*] NFTNRKISVQRLASY* [*] RRITSSKCPKEAVIFKTIVAKEICADPKQKW* [*] VQDSMDHLDKQTQTPKT
CCL3	MQVSTAALAVLLCTMALCNQFSA SLAADTPTACCFYSYTSRQIPQNFADYFETSSQCSKPGVIFLTKRSRQVCADPSEEWVQKYVSDLELSA
CCL5	MKVSAALAVILIAALCAPASA SPYSSDTPCCFAYIARPLPRAHIKEYFYTSGKCSNPAVVFVTRKNRQVCANPEKKWVREYINSLEMS
CCL11	MKVSAALLWLLIAAAFSPQGLA GPASVPTTCCFNLANRKIPLQRLESYRRITSGKCPQKAVIFKTKLAKDICADPKKKWVQDSMKYLDQKSPTPKP
CXCL8	MTSKLAVALLAFLISAALCEG AVLPRAKELRCQCIKY* [*] SKPFHPKFIKELRVIESGPHCANTEIIVKLSDGRELCLDPKENWVQRVVEKFLKRAENS
CXCL12	MNAKVVVVVLVLTALCLSDG KPVLSY* [*] RCPCRFFESHVARANVKHLKILNTPNCALQIVARLKNNNRQVCIDPKLKWIQEYLEKALNKRFKM

Figure 1.5 Visualisation of nitrated chemokine peptide sequence and modified residues.

Chemokines are first produced as a pro-peptide and during the secretion, cleavage of the signal peptides on the N-terminus (green) results in the release of matured chemokines that are functional. Among the 6 known nitrated chemokines, only CCL2 and CXCL12 have been subjected to mass spectrometry to identify nitrated residues (*). CCL11 and CXCL8 nitration on the sole tyrosine residue was determined using immunological detection with 3-nitrotyrosine antibody. While similar immunological detection identified 3-nitrotyrosine in CCL3, CCL5, the exact residue modified cannot be determined with current literature due to the presence of multiple tyrosine residues in the peptide sequence.

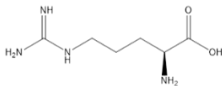
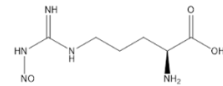
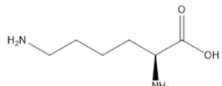
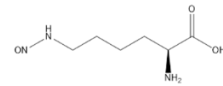
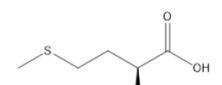
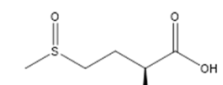
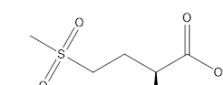
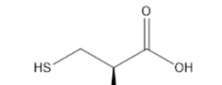
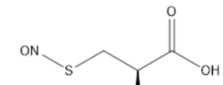
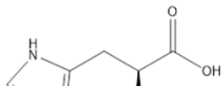
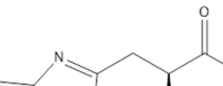
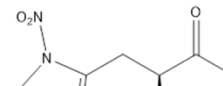
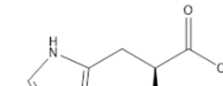
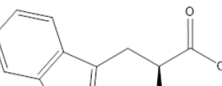
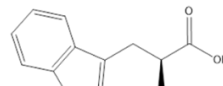
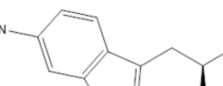
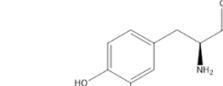
1.3.4. Clinical Targeting of Chemokine System

Attempts to target the chemokine systems have been met with limited success over the past 30 years. To date, there are only three chemokine antagonists approved for use in clinic: Plerixafor (CXCR4), Maraviroc (CCR5) and Mogamulizumab (CCR4). This is in part due to complex ligand-receptor interaction, as well as the requirement for timely therapeutic administration of therapeutics to prevent propagation of the inflammatory response.

In the context of transplantation, many clinical studies have demonstrated that increased expression of chemokines can occur in several waves. Immediately after transplantation, levels of CCL2 (Shah et al., 2012) and CXCL8 (Fisher et al., 2000) are released in high concentrations to recruit monocytes, macrophages and neutrophils. Several days after transplantation, several other chemokines, including CCL4, CCL5 (Yun et al., 20002), CXCL9, CXCL10 and CXCL11 (Shino et al., 2022) are released to mobilise the adaptive immune cells to modulate overall inflammatory response to the allografts. Knockouts of these chemokine receptors (Gerard and Rollins, 2001, Gelman et al., 2010) in pre-clinical studies confirmed the importance of these chemokines in regulating allograft rejection and overall outcomes post transplantation.

Alternative strategies to target these chemokines have led researchers to look to mechanisms evolved by other species in order to evade immune responses. For example, some viral and parasite protein derivations have the capability to perturb ligand-receptor interactions with very high potency, thereby providing a potential therapeutic avenue for clinical intervention for chemokine-related diseases (Kuo et al., 2014, Devkota et al., 2023, Darlot et al., 2020).

Table 1.1 Summary of Amino Acids Modified During Nitrosative Stress.

Native amino acid structure	Modified amino acid structure		
Arginine 	N-nitroso arginine 	-	-
Lysine 	N-nitroso lysine 	-	-
Methionine 	Methionine sulfoxide 	Methionine sulfone 	-
Cysteine 	S-nitroso cysteine 	Oxidised cysteine 	-
Histidine 	2-oxo histidine 	N-nitroso histidine 	4-nitro histidine 
Tryptophan 	N- nitroso tryptophan 	6-nitro tryptophan 	-
Tyrosine 	3-nitro tyrosine 	3-hydroxy tyrosine 	3,3'-dityrosine 
Phenylalanine 	<i>o</i>-tyrosine/ <i>m</i>-tyrosine/ <i>p</i>-tyrosine 		4-nitrophenylalanine 

1.4. miRNAs

Besides, chemokines, other mediators are dysregulation of other mediators are also known to play a role in mediator IRI pathogenesis. miRNAs are small non-coding RNAs first discovered in *Caenorhabditis elegans* (Lee et al., 1993) and subsequent identification of their regulatory role in *Drosophila* (Lai and Posankony, 1997). Only during the early 2000s were they acknowledged as part of a novel class of RNAs (Lagos-Quintana et al., 2001). With estimates that more than 60% of protein coding genes have conserved miRNA binding sites predominantly at the 3' untranslated region (UTR)(Friedman et al., 2009), these ~22 nucleotide sequence functions as a guide which base pairs with the target mRNA. Subsequently, the miRNA loaded Argonaute (Ago) protein along with other co-factors forms the miRNA induced silencing complex (miRISC) to induce translational repression, mRNA deadenylation, mRNA decay or storage (Figure 1.6).

1.4.1. miRNA Biogenesis and Function

The importance of these evolutionarily conserved miRNA to regulate gene and protein expression are essential for the homeostatic functions of the organisms. Unsurprisingly, dysregulation of miRNA can result in a variety of diseases (Yanaihara et al., 2006, Kato et al., 2007). Therefore, cellular machineries are present to regulate every process of miRNA biogenesis from initial transcription down to the loading into the miRISC and execution of their function (Ha and Kim, 2014).

1.4.1.1. Canonical Pathway

Majority of the mammalian miRNAs are encoded in the intronic regions of non-coding transcripts (Rodriguez et al., 2004), but miRNAs do exist within intronic regions and exonic regions of protein transcripts (Kim and Kim, 2007, Baskerville and Bartel, 2005). This transcription is driven by RNA polymerase II (Lee et al., 2004) and in some instances RNA polymerase III (Borchert et al., 2006). The initially transcribed primary miRNA (pri-miRNA) exists as a long RNA hairpin that requires processing by Microprocessors, which consist of Drosha and DiGeorge Syndrome Critical Region 8 (DGCR8). This heterotrimeric protein functions as a molecular scissors which recognise the conserved motifs on the pri-miRNA (Partin et al., 2020) and cleaves the basal segments to generate pre-miRNA (Kwon et al., 2016) (Figure 1.6).

The pre-miRNA is subsequently exported from nucleus by interacting with the basic residues present within Exportin-5 with its 3' overhang (Okada et al., 2009, Yamazawa et al., 2018). In the final maturation step, the exported pre-miRNA interacts with Dicer, which in conjunction with transactivation response element RNA-binding protein (TRBP) (Fareh et al., 2016) selectively induce a cleavage to result in mature miRNA. This mechanism is driven by the hydrophobic interaction between both the 3' and 5' end of the pre-miRNA with the hydrophobic PAZ domains to provide an accurate determinant of the mature miRNA length (Tian et al., 2014). A conserved motif was also identified on the pre-miRNA to accurately pinpoint the exact site for Dicer cleavage (Lee et al., 2023).

1.4.1.2. Non-Canonical Pathway

Alternative pathways for the generation of miRNAs have been reported. This includes miRNA derived from intronic splicing and subsequent dicing termed "mirtrons" (Figure 1.6) (Berezikov et al., 2007), Dicer independent maturation for miR-451 (Figure 1.6) (Cheloufi et al., 2010), small nucleolar RNA derived miRNA (Ender et al., 2008) and transfer RNA derived miRNA (Babiarz et al., 2010). While these alternate pathways highlight the diverse mechanisms that can result in the generation of miRNAs, they represent only a small subset of the total miRNA generation. Hence the survival advantage conferred by these alternative pathways remains to be investigated (Ha and Kim, 2014).

1.4.2. Regulation of Gene Expression

In order for miRNA to function as a transcription regulator, the post-Dicer processed miRNA duplex requires loading into the Ago along with other essential components of the miRISC. This loading is mediated by the intermediate complex termed RISC loading complex (MacRae et al., 2008), where Dicer and TRBP interacts with Ago to hand the RNA duplex. Following the loading of the miRNA duplex, Ago unwinds the double stranded RNA before selecting a single strand to retain in the complex, while removing the complementary strand which are commonly targeted for degradation. This selection process is mediated by an asymmetry rule where the less energetically stable end is selected for loading. Subsequently, the recruitment of the other core component of RISC, Glycine-Tryptophan-182 (GW182) (Eulalio et al., 2008) which can initiate recruitment of other factors to mediate gene silencing like CCR4-NOT for polydeadenylation (Chekulaeva et al., 2011).

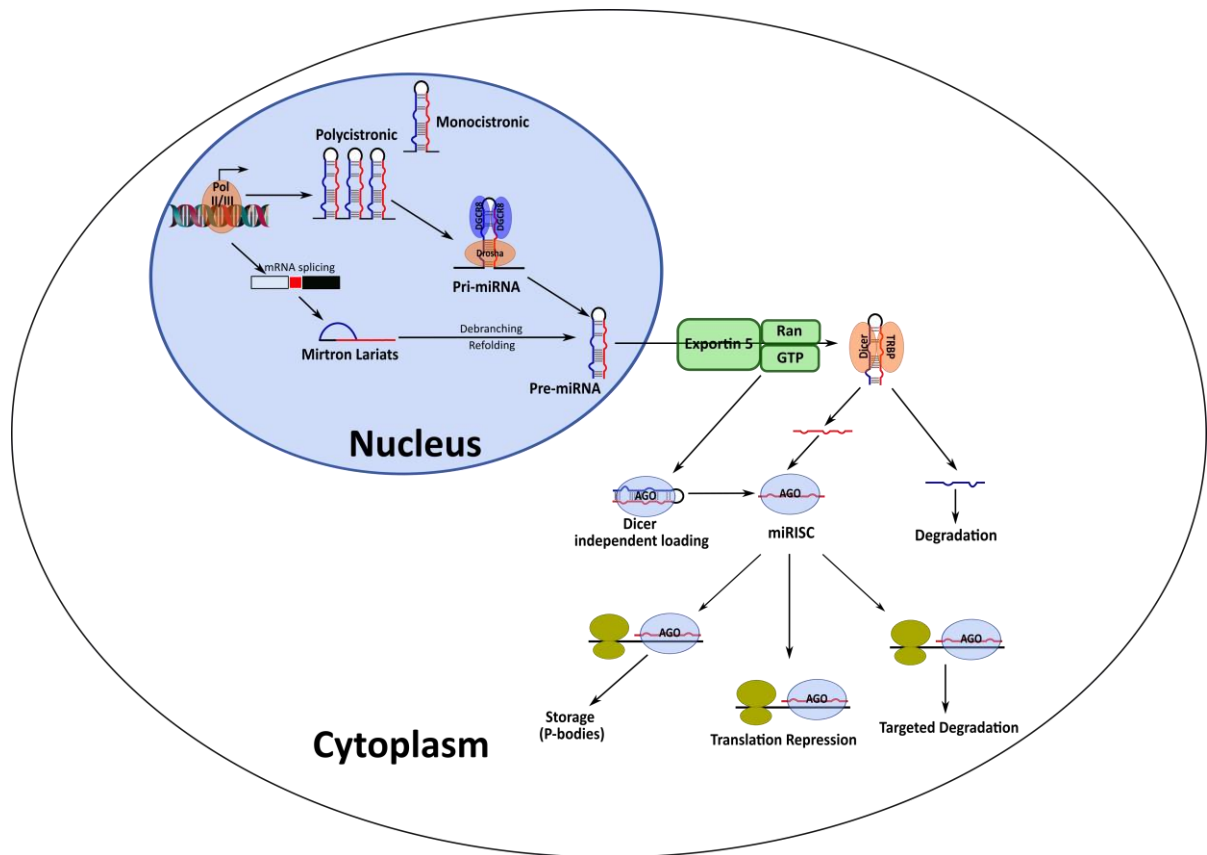


Figure 1.6 Overview of miRNA biogenesis and function.

Transcription of the intronic or exonic region of the loci encoding miRNA can give rise to either a monocistronic or polycistronic primary miRNA hairpin. This pri-miRNA undergo processing by the Microprocessor heterotrimeric protein to form pre-miRNA, which are subsequently exported out of the nucleus to the cytoplasm. An example of non-canonical pre-miRNA generation is shown with the formation of mirtron lariats during alternate splicing. The exported pre-miRNA undergoes another round of processing by Dicer to give rise to the mature miRNA, which is then loaded onto Ago2 to form the miRISC complex to regulate target mRNA expression. Alternatively, there are also Dicer independent mechanisms for the generation of mature miRNA and loading into the miRISC.

Recognition of miRNA is heavily mediated by the complementary base pairing between the seed region of the miRNA (nucleotide 2-8) with the target mRNA and has since been computationally and experimentally validated. The higher complementarity results in a more favorable binding affinity and in turn, a more likely target (McGeary et al., 2019, Agarwal et al., 2015). The fate of the target mRNA however relies on several factors. Firstly, 4 human Ago protein paralogs are associated with the formation of miRISC but only Ago2 are known to have the capability to cleave RNAs (Meister et al., 2004). Secondly, complementarity and in turn binding affinity affects the outcomes of the interaction between the miRISC and the mRNA targets. For mRNA degradation induced by miRISC, this would require the complete complementarity between the miRNA and the mRNA targets on an Ago2 complex. In high order eukaryotes, this complete complementarity is rare.

Instead, the fate of the mRNA and protein expression post miRISC engagement remains controversial. Some studies show the interaction of miRISC with the mRNA represses overall protein expression whilst maintaining the RNA stability (Pillai et al., 2005, Baek et al., 2008). Furthermore, the in vitro reporter assays show a shift in the polysomal fraction, indicating translational stalling (Bhattacharyya et al., 2006). On the flip side, studies have shown target mRNA decapping and deadenylation along with the decrease in protein expression (Eulalio et al., 2009, Selbach et al., 2008, Baek et al., 2008, Guo et al., 2010), suggesting mRNA degradation precedes translational repression. The caveats to these studies however were the focus on specific miRNA regulation in very specific cell types and context. In reality, the regulation is likely to vary across miRNA and cell types processing the target mRNA. This is further complicated by the presence of tissue specificity in certain miRNA expression (Wienholds et al., 2005). As such, more recent work indicated that whilst both repression of translation and degradation of mRNA targets are true, but it is likely that translational repression occurs before destabilisation of the target mRNA (Bazzini et al., 2012, Djuranovic et al., 2012). Additionally, stalling of the translation of the target mRNA can also be subjected to reactivation under different cellular context, providing insights to the possibility of regulating protein translation at the appropriate timing (Bhattacharyya et al., 2006).

1.4.3. Circulating miRNA

Beyond the conventional role of intracellular regulator of transcription and translation, there has been emerging evidence that these miRNAs can be secreted extracellularly to mediate paracrine and even endocrine signaling (Zhao et al., 2020). While the mechanism for miRNA release is not fully understood, it is thought to be mediated through both an active process and leakage from damaged cells. These released miRNAs can be found circulating in complex with Ago (Turchinovich et al., 2011), high-density lipoprotein or encapsulated within small extracellular vesicles (EVs) released by the cells (Valadi et al., 2007) (also discussed in further details in Section 1.5), thereby protecting them from extracellular nucleases. Importantly, in all these instances, these miRNAs are identified to be functional with the capability to exert regulatory functions on the recipient cells. Since the dysregulation of miRNA results in diseases, there are also increasing interest of miRNAs as potential biomarker for diseases (Arroyo et al., 2011).

1.4.4. Role of miRNA in IRI

Many miRNAs have been shown to participate in the pathogenesis of IRI. The roles of these miRNAs can be broadly categorised as protective or pathogenic. Some of these miRNAs have been identified to alter their regulation in response to IRI, allowing for cellular adaptation. Alternatively, other miRNAs have been shown to be prone to dysregulation in IRI, therefore partaking in the process of cellular damage. As the role of these miRNAs have been discussed extensively in several reviews (Cao et al., 2021, Mahtal et al., 2022, Kong et al., 2022), this thesis will focus on several prominent miRNAs and their roles in IRI.

1.4.4.1. *miR17~92 Cluster*

miR17~92 cluster is a polycistronic miRNA family which encodes for 6 miRNAs: miR-17, miR18a, miR-19a, miR-20a, miR-19b-1 and miR-92a-1. Predominant focus on the cluster expression have been on the angiogenic properties of this miRNA cluster due to the enrichment in the endothelium compartment. Utilising murine models, there have been conflicting data to indicate the protective and deleterious role of this miRNA cluster in supporting the overall angiogenic properties of endothelial cells post IRI. In models of myocardial ischemia, the delivery of miR-92a provides vasculo-protective role (Chiba et al., 2021) by inhibiting autophagy (Rogg et al., 2018). Furthermore, other studies have also shown the upregulation of the cluster protects the endothelial cells from ferroptosis, which can occur as a result of IRI (Xiao et al., 2019). Alternatively, the knockout models of miR17~92 clusters in heart and limb ischemia showed improved vasculogenesis and recovery post ischemia (Bonauer et al., 2009, Landskroner-Eiger et al., 2015).

1.4.4.2. *miR-21*

miR-21 is a highly expressed miRNA across a variety of different tissue and cell types. In IRI, miR-21 exhibit a bimodal role. During the onset of ischemia, the presence of hypoxia response element (HRE) upstream of the transcription start site indicates the capability to be upregulated in response to the low oxygen (Kulshreshtha et al., 2007). Transcription of miR-21 induces a strong anti-apoptotic and pro-survival phenotype that have been very well established across ischemic myocardial (Yang et al., 2018), limb (Chang et al., 2022), neuronal (Yan et al., 2021) and kidney (Song et al., 2018, Godwin et al., 2010) models. However, the sustained expression of miR-21 during reperfusion promotes a pro-fibrotic phenotype, which results in tissue remodeling (Thum et al., 2008, Chau et al., 2012). As such, there have been biomarker studies identifying miR-21 in combination with other miRNAs and cytokines to be upregulated in allografts with chronic rejection episodes (Gielis et al., 2021, Miyahara et al., 2022).

1.4.4.3. miR-210

miR-210 is the most prominent miRNA that is upregulated across all cell types in response to hypoxia (Fasanaro et al., 2008, Huang et al., 2009, Liu et al., 2017). Similar to miR-21, the presence of HRE drives the upregulation in IRI (Huang et al., 2009), particularly during ischemia. Furthermore, since HIF-1 signaling has now been identified to play a key role during inflammation (Virga et al., 2021), the scope of miR-210 have extended beyond cellular adaptation to low oxygen.

Unsurprisingly, miR-210 upregulation in IRI have been shown in a variety of tissues (Zhou et al., 2013, Liu et al., 2017, Pan et al., 2020, Song et al., 2022, Zaccagnini et al., 2017). Functionally, miR-210 has been identified to assist in metabolic transition of cells from oxidative phosphorylation to glycolysis as a main source of energy under hypoxic conditions. While knockout of miR210 did not result in embryonic lethality, these mice was however showed reduced capacity to adapt to the insult brought on by IRI and in turn, leading to excessive mitochondrial dysfunction and tissue damage (Song et al., 2022). This also links to miR-210 functioning as a negative regulator of HIF signaling, fine tuning the cellular responses to hypoxia (Costales et al., 2017) to generate adequate cellular adaptation. Additionally, the capacity of miRNA to trigger endocrine signaling was also first shown in miR-210 using parabiosis model (Zhao et al., 2020), further showcasing the stability of miR-210 in circulation.

1.5. Extracellular Vesicles

Extracellular vesicle (EV) is an umbrella term used to describe membranous structures that are ubiquitously released by all living organisms (Niel et al., 2022). These lipid nanoparticles are extremely heterogeneous and can be broadly sub-divided by either the origins (i.e. mechanism mediating biogenesis) or size range. Exosomes refer specifically to vesicles derived from the endosomal pathways (50nm-150nm), ectosomes/microvesicles referring to vesicles derived from the shedding from the plasma membrane (100-1000nm) and apoptotic bodies released in response to apoptosis transduction (100-5000nm). Historically, exosomes were thought to be a mechanism for cellular waste disposal. However, extensive literature over the past decade has highlighted the capability for EVs to mediate intercellular communication. This led to the eventual identification and discoveries of other EV subpopulations including migrasomes (Ma et al., 2014), amphisomes (Murrow et al., 2015), exomeres (Zhang et al., 2018), supermeres (Zhang et al., 2021b) and protrusion associated EVs (D'Angelo et al., 2022).

The increased interest in how EVs mediate intercellular signaling has also led to the discovery of different biomolecules expressed on the surface of these EVs as well as those encapsulated within. While there is currently limited knowledge on the overall process mediating cargo sorting, this process is highly selective and regulated. This is exemplified by the alteration in EV cargo when the parental cells are subjected to external stimuli (Jong et al., 2012). Subsequently, the acceptor cells utilise various mechanisms to mediate EV uptake to either re-express the cargo on their cell surface or released into the cytosol to exert biological functions. However, there remains a great deal of uncertainty with regards to whether this uptake by recipient cell occurs stochastically (Svensson et al., 2013) or highly specific (Fitzner et al., 2011) *in vivo*.

1.5.1. Biogenesis

The biogenesis of EVs, particularly exosomes have been the focused of most biologists within the field. Even within this subtype of EV, the full pathway has not been fully elucidated with many exceptions observed between different cargo and cell types (Niel et al., 2018). Conventionally, the most well studied pathway involves the endosomal sorting complex required for transport (ESCRT) machinery to generate intraluminal vesicles (ILV) within endosomes, forming multivesicular bodies before exporting for release (Niel et al., 2018). This, however, is non-exhaustive as there are ESCRT-independent pathways which further highlights the heterogeneity outlining the process of EV generation. Therefore, the biogenesis outlined below focuses on exosomes and the overall mechanism is non-exhaustive.

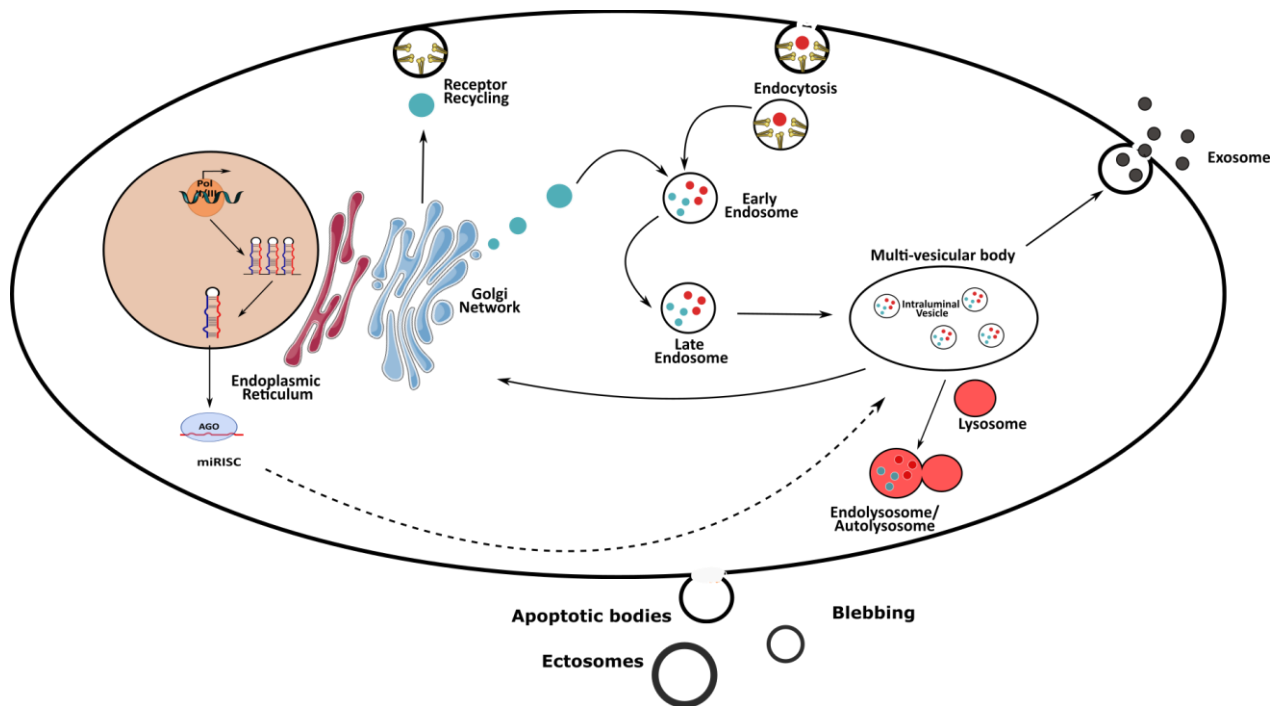


Figure 1.7 Schematic of canonical exosome biogenesis.

Exosome biogenesis begins with the transport of vesicles from either the Golgi network or derived from endocytosis. These endosomes transit through the endosomal lysosomal pathway which recruits ESCRT complex, generating intraluminal vesicles and the formation of the multivesicular body (MVB). These vesicles undergo sorting within the MVB and subsequently the vesicles are either targeting for release as exosome or driven down the route of fusion with lysosome for degradation. Ectosomes or microvesicles are formed by membrane blebbing whereas apoptotic body are derived from mechanisms associated with apoptosis transduction.

1.5.1.1. ESCRT-Dependent Pathway

As part of the first step of the cargo loading, biomolecules destined to be packaged into exosomes from the Golgi network or cell surface are transported via endosomal-lysosomal compartment (Figure 1.7), where stepwise recruitment of ESCRT-0, ESCRT-I, ESCRT-II and ESCRT-III leads to the generation of exosome. This process is initiated by the ESCRT-0 binding to the endosomes enriched with ubiquitinated proteins through the ubiquitin binding domains present on the main subunits, hepatocyte growth factor-regulated tyrosine kinase substrate (HRS) and signal transducing adapter molecule (STAM) (Mayers et al., 2011). Subsequently, this results in the recruitment of ESCRT-I (Ren and Hurley, 2011) which further recruit ESCRT-II (Gill et al., 2007). Collectively, ESCRT-I and ESCRT-II binds with a 1:1 stoichiometry to form a super complex (Boura et al., 2012) that drive bud formation through an assembly at the neck, stabilising the conformation. Finally, ESCRT-III is recruited to cleave the bud neck and generate the ILVs (Wallert and Hurley, 2010). Beyond ESCRT complex, external signaling axis including syndecan-syntenin-Alix also drives the ILV and subsequent exosome formation (Baietti et al., 2012).

1.5.1.2. ESCRT-Independent Pathway

The first discovery of ESCRT-independent pathway was triggered by a series of experiments showing persistence of MVB post- RNA interference of the ESCRT complex (Stuffers et al., 2009). Subsequently, several mechanisms have been identified. This includes a pathway requiring ceramide generation by sphingomyelinase II (Trajkovic et al., 2008). This presence of ceramide allows spontaneous formation of a membrane curvature, allowing ILVs formation (Goñi and Alonso, 2009). Ceramide can also be metabolised to sphingosine-1-phosphate, activating the cognate receptors and in turn, formation of ILVs (Kajimoto et al., 2013). Tetraspanins have also been identified to have the capability to generate exosomes independent of the ESCRT complexes, particularly CD63 but the mechanism remains to be elucidated (Niel et al., 2011).

Currently, there is no definite mechanism underpinning the release of exosomes. This reflects the recurring challenge with defining a specific sub-population utilising different cellular machinery for the transport and export of the ILVs. What is clear however is the involvement of Rab (Ostrowski et al., 2009, Baietti et al., 2012) in the trafficking of the vesicles and synaptotagmin and SNARE proteins for the fusion and release into the extracellular space (Niel et al., 2018).

1.5.2. Cargo Sorting and Loading

EVs have been reported to mediate the transfer of a wide variety of biomolecules, ranging from proteins, lipids, DNA, RNA and various metabolites. Amongst these biomolecules, proteins and RNA cargoes are the most well characterised. Yet, the mechanisms for the sorting and preferential loading of these biomolecules have yet to be fully elucidated. This is further complicated by the variety of methods for EV isolation, which is known to yield differing biomolecules (Lässer et al., 2016, Wei et al., 2017) even from the same lot of samples.

1.5.2.1. Protein Cargo

Post-translational modifications have been identified to be important for driving protein down into the MVB pathway. In particular, ubiquitination allows for recruitment of the ESCRT complexes (as described in 1.5.1.1). Indeed, ubiquitinated proteins have been identified within EVs (Smith et al., 2015) but was not identified to be essential for loading into exosomes (Huebner et al., 2016). However, deubiquitinating enzymes have been identified to remove the ubiquitin present on the proteins and the authors postulate for the functional protein within the recipient cells post release of the protein cargo (Liu et al., 2009). More recently, a pentapeptide motif was identified to be enriched in proteins preferentially loaded into exosomes via a lysosomal associated membrane protein 2 (LAMP2) dependent pathway (Ferreira et al., 2022).

1.5.2.2. RNA Cargo

EVs have been identified to encapsulate various types of RNA and understanding to date suggests that the RNA biotype distribution is not consistent between the different subtypes of EVs (Lässer et al., 2016, Wei et al., 2017). Unlike protein cargoes, multiple mechanisms for RNA, particularly miRNA have been elucidated. This includes ceramide dependent but MVB independent loading (Kosaka et al., 2010), ribonuclearprotein assisted loading by recognising specific motifs present on the miRNA (Garcia-Martin et al., 2021, Santangelo et al., 2016, Villarroja-Beltri et al., 2013). Additionally, Y-box binding protein 1 (YBX1), another ribonuclearprotein have recently been shown to drive phase-separation and sorting miRNAs into condensates, allowing packaging into exosomes (Liu et al., 2021). RNA binding protein such as Ago2 (McKenzie et al., 2016), ALIX (Iavello et al., 2016), Annexin A2 (Hagiwara et al., 2015) and major vault protein (Teng et al., 2017) have also been shown to sort miRNA specifically for loading into exosomes within the MVB. Due to their overall low abundance and the potential association with other protein complexes (as

outlined in Section 1.4.3), there still remains controversial data suggesting that these detected RNA are not present within the EVs, but instead are co-isolated contaminants (Chevillet et al., 2014).

1.5.3. EVs in Transplantation

1.5.3.1. Pre-Transplantation

As outlined in Section 1.1, several challenges have limited the widespread utilisation of solid organ transplantation for patients with end-stage organ failure. Machine perfusions have been used as a platform for functional assessments of allografts and EVs have been successfully isolated from the circulating perfusates (Woud et al., 2022, Madu et al., 2020, Eldh et al., 2014, Okamoto et al., 2016, Rutman et al., 2022). Furthermore, a time dependent increase in the total EVs isolated suggest that this process of EV released is an active process during *ex vivo* perfusion (Woud et al., 2022). Additionally, since these EVs were identified to reflect donor characteristics, there is potential for these isolated EVs to function as a molecular biomarker in conjunction with functional data to provide clinicians with better assessment matrix for the prediction of graft function.

1.5.3.2. IRI

Propagation of EVs within a biological system during pathological conditions such as IRI remains unknown and data to date have relied heavily on *in vitro* models. This is in part due to the sizes of EVs, particularly exosomes that are near or below the diffraction limit of light (200nm), making *in vivo* tracking challenging and have only been achieved in zebrafish (Verweij et al., 2019). However, the involvement of EVs in IRI remains unrefuted, as studies have highlighted both pathological and protective roles, with the single caveat being highly dependent on the donor and recipient cell of interest. Table 1.2 highlights the recent findings showing the potential of EVs to alter recipient cellular state after donor organs encountered IRI.

Table 1.2. Recent literature on the role of EVs in IRI.

Donor Cells	Recipient	Mode of Action	Outcomes	Citation
Urinary EVs of patients pre/post Txn Hypoxic human tubular epithelial cells	Hypoxic human tubular epithelial cells (HK2)	Exosomal transfer of lncRNA WAC-AS1	Propagate ferroptosis	(Li et al., 2023)
Human kidney perfusate derived EVs	Peripheral blood mononuclear cell	Exosomal transfer of miR-218-5p	Alters Th ₁ and Th ₁₇ ratio	(Rutman et al., 2022)
Exosomes from mouse kidneys RAW264.7 macrophages	Mouse renal tubular epithelial cells	Exosomal transfer of miR-155	Downregulation of SOCS1 and induce tubular injury	(Zhang et al., 2022)
Hypoxic rat renal tubular epithelial cells	Rat fibroblast	Exosomal transfer of miR-150-5p to activate fibroblast	Increased renal fibrosis	(Zhou et al., 2021)
Endothelial colony forming cells	In vivo administration in mice	Exosomal transfer of miR-486-5p	Inhibition of PTEN signaling, reduced TNF signaling	(Viñas et al., 2021)
Human Liver stem cells	In vivo administration in mice	Unknown	Reduced serum ALT, LDH, necrosis and cytokine expression	(Calleri et al., 2021)
Hypoxic human umbilical endothelial cells	Human cardiomyocyte	Overall proteome improved metabolism, redox state and calcium handling	Improved cardiomyocyte function on a chip	(Yadid et al., 2020)

1.5.3.3. Immune Regulation

The key challenge post solid organ transplantation is the management of allograft rejection. EVs have been reported to play a role in mediating allorecognition by the release of EVs expressing novel cryptic antigen that can trigger the generation of autoantibodies (Dieudé et al., 2015). In addition, allografts were also shown to release vesicles expressing high levels of major histocompatibility molecules (MHC) (Rutman et al., 2022), which in turn can result in recipient immune cell “cross-dressing”. This decoration of antigen presenting cells (APC) surface with donor allograft MHC transferred via EVs accelerates immune cell activation and allorecognition by the recipient immune cells (Marino et al., 2016, Prunevieuille et al., 2020, Hughes et al., 2019, Ono et al., 2018, Mastoridis et al., 2020, Zeng et al., 2021).

Additionally, it was recently shown that APC transfers telomeres by EVs at the immune synapse to promote long term immunological memory (Lanna et al., 2022). In the context of

transplantation, this likely results in the generation of memory immune cell that can potentiate chronic allograft rejection.

1.5.4. Therapeutic Potentials of EVs

Due to the high biocompatibility, EVs have been seen as an attractive modality both as therapeutics and means for biomolecule delivery (Usman et al., 2018, Alvarez-Erviti et al., 2011). Most prominently, stem-cell derived EVs have shown potential in pre-clinical models of IRI (Lai et al., 2010, Mackie et al., 2012). These EVs like their parental cells have been reported to be non-immunogenic, immunosuppressive, and anti-inflammatory (Kou et al., 2022, Ashcroft et al., 2022). The delivery of only the EVs also eliminate the risk of stem cell differentiation, horizontal gene transfer and vascular occlusion while boasting better biodistribution (Kou et al., 2022, Ashcroft et al., 2022). Table 1.3 highlights pre-clinical models where EVs have been utilised to recondition allografts or induction of tolerance in a whole organ context.

In addition, advances in molecular biology techniques also allow further manipulation of the parental cell. In turn, altering EV profiles to express therapeutic molecules of interest. Such methods ranges electroporating EVs with RNA of interest (Usman et al., 2018) to overexpressing protein of interest in parental cell (Kim et al., 2021, Tang et al., 2020, Wang et al., 2018). Delivery of these engineered EVs shows improved outcomes compared to controls, highlighting the efficacy and potential for biomolecule delivery. Additionally, the use of engineered constructs can also improve EV homing to specific sites, improving overall targeting and preventing off-target effects (Wang et al., 2018).

Table 1.3 Recent literatures on the role of EVs in solid organ transplantation

EV source	Organ	Additional therapeutics	Outcomes	Citation
Bone marrow derived dendritic cells	Heart	Co-administration of desoxypergualin analog	Induction of allograft tolerance	(Pêche et al., 2006)
Immature dendritic cells	Intestine	Systemic administration	Induction of allograft tolerance	(Yang et al., 2011)
Immature dendritic cells	Heart	Co-administration with rapamycin	Induction of allograft tolerance	(Li et al., 2012)
Mesenchymal stromal cells	Kidney	Administered during hypothermic machine perfusion	Reduced IRI damage	(Gregorini et al., 2017)
Mesenchymal stromal cells	Lung	Administered during machine perfusion	Reduced lung dysfunction	(Stone et al., 2017)
Mesenchymal stromal cells	Heart	Intramyocardial injection	Attenuate IRI damage via macrophage polarisation	(Zhao et al., 2019)
Human Liver Stem Cells	Liver	Administered during normothermic machine perfusion	Reduced tissue damage	(Rigo et al., 2018)

2. Hypothesis

The transplant procedure is inevitably associated with a certain degree of ischemia reperfusion injury (IRI). Clinically significant IRI manifests as primary nonfunction, delayed graft function, or acute injury in the immediate post-transplant period. Initial IRI causes the production of many reactive oxygen and nitrogen species, and subsequent recruitment and activation of inflammatory cells. Chemokines play an important role in the recruitment of leukocytes, however, oxidative stress can modify the chemokines leading to alteration in their biological activity and detectability. Additionally, endothelial dysfunction/injury compromises microcirculatory blood flow through decreased vasodilatory capacity, coagulation activation and the formation of microvascular thrombi, and increased rolling/adhesion of inflammatory cells. The regenerative capacity of endothelial cells appears limited in transplantation and microvascular damage occurring during an episode of ischemic injury can lead to permanent loss of microvasculature. This in turn favours chronic hypoxia, leading to overexpression of hypoxia inducible factor-1 α and associated downstream cellular processes that can be deleterious to allografts.

I hypothesise that “the occurrence of ischemia and reperfusion during organ transplantation can result in perturbation of many cellular processes. Developing and characterisation of these altered processes can give rise to better understanding of ischemia reperfusion injury and in turn, development of better interventions”.

3. Aims

- Identification of post-translationally modified chemokines *in vivo*.
- Profiling the response of glomerular endothelium in response to hypoxia.
- Characterisation of extracellular vesicles derived from renal allograft microvasculature.

4. Methods

4.1. Laboratory Procedure

All experiments were conducted according to the Control of Substances Hazardous to Health (COSHH) and BioCOSHH regulations as well as the University Safety Policy and Newcastle University's "Safe working with Biological Hazards" and "Safe Working with Chemicals in Laboratory" guidelines. Tissue culture was carried out in accordance with regulations for class II pathogen containment.

4.2. Cell Culture

4.2.1. Cell Maintenance

Adherent cells were sub-cultured upon reaching 80% confluence. Briefly, spent culture media was aspirated and cell monolayers were washed with sterile phosphate buffered saline (PBS). 0.05% Trypsin-EDTA (ThermoFisher) for cell lines or Accutase® (Biolegend) for primary cells was added to the flask and incubated for 5mins at 37°C. Cells were visually inspected under a light microscope to ensure complete detachment before adding equivalent volume of complete media to neutralise the trypsin. The cell suspension was transferred to a Falcon tube and pelleted by centrifugation (Table 4.1). Supernatant was discarded before resuspending the cell pellet gently in complete media before proceeding to appropriate experiments.

Table 4.1 Centrifugation speed for various cell types.

Cells	Centrifuge speed	Duration
HMEC-1	300g	5mins
HMEC-1 HLA-DR+	300g	5mins
ciGEnC	220g	3mins
HGEnC	220g	3mins
PTEC	220g	5mins

4.2.2. Cryopreservation of Cells

Immortalised cells were cryopreserved by adding 20% Dimethylsulfoxide (DMSO) foetal calf serum in a dropwise manner to cell suspension post trypsinisation in complete media to obtain a final concentration of 10% DMSO. Cell lines were passaged at a ratio of 1:4. Primary cells were pelleted by centrifugation before resuspending in Cryo-SFM (PromoCell). Cells were passaged at a ratio of 1:3. The cell suspensions containing the appropriate cryo-preserved were aliquoted into cryovials and placed into a CoolCell™ LX cell freezing container (Corning) at -80°C to cool at a rate of -1°C/min. Cells were then stored long term in the gaseous phase of liquid nitrogen tanks.

4.2.3. Human Microvascular Endothelial Cells (HMEC-1)

HMEC-1 obtained from American Type Culture Collection (ATCC®) are endothelial cells derived from human foreskin and immortalised by the transfection of PBR322-based plasmid encoding Simian Virus 40 (SV40) large tumour antigen (Ades et al., 1992). These cells were maintained in MCDB131 media (ThermoFisher) supplemented with 10% foetal calf serum, 2mM L-glutamine (ThermoFisher), 1µg/mL hydrocortisone (Sigma), 10ng/mL epidermal growth factor (ThermoFisher) and 100µg/mL penicillin/streptomycin (Sigma).

4.2.4. Human Microvascular Endothelial Cells transduced with HLA-DR (HMEC-1 HLADR+)

HMEC-1 HLADR+ cells obtained from Professor Nuala Mooney (INSERM) are HMEC-1 cells transduced with HLADRβ1*11.02 lentiviral particles (Taflin et al., 2011). These cells were maintained in MCDB131 media (ThermoFisher) supplemented with 10% foetal calf serum, 2mM L-glutamine (ThermoFisher), 1µg/mL hydrocortisone (Sigma), 10ng/mL epidermal growth factor (ThermoFisher) and 100µg/mL penicillin/streptomycin (Sigma).

4.2.5. Conditionally Immortalised Glomerular Endothelial Cells (CiGENCs).

CiGENCs obtained from Professor Simon Satchell (Bristol University) are glomerular endothelial cells transduced with temperature-sensitive SV40 large tumour antigen and telomerase using retroviral vectors (Satchell et al., 2006). CiGENCs were maintained in EGM™-2 MV Microvascular Endothelial Cell Growth Medium-2 BulletKit™ (Lonza) at 33°C. Growth arrest was induced by culturing the cells at 37°C (non-permissive temperature) for minimum of 5 days before use in experiments.

4.2.6. Primary Human Glomerular Endothelial Cells (HGENCs).

HGENCs were obtained from Cell Biologics and maintained in complete human endothelial cell medium (Cell Biologics).

4.2.7. Primary Human Renal Proximal Tubular Epithelial Cells (PTEC).

PTECs were obtained from Sciencell and maintained in complete epithelial cell medium (Sciencell).

4.2.8. Primary Neutrophils

Neutrophils were isolated from healthy donor blood with ethics from County Durham and Tees Valley Research Ethics Committee (12/NE/0121) using MACSxpress® whole blood isolation kit (Miltenyi Biotec) as per manufacturer's protocol. In brief, lyophilised isolation cocktail was reconstituted by the addition of 2mL buffer A and subsequently 2mL buffer B. Subsequently, 8mL of whole blood was added to the isolation cocktail and mixed by inversion three times and left to incubate at room temperature on MACSmix™ tube rotator (Miltenyi Biotec) on 12rpm (revolutions per minute) for 5mins. The lid of the Falcon tubes was removed and placed on the MACSxpress separator for 15mins before recovering the supernatant in a new Falcon tube. Neutrophils were pelleted by centrifugation at 300xg, 10mins at room temperature. Cell pellet was resuspended in 1x red blood cell lysis buffer (ThermoFisher) to remove residual red blood cells. The isolated neutrophils were resuspended in serum free RPMI-1640 media (Sigma) supplemented with 2mM L-glutamine (ThermoFisher), 100µg/mL penicillin/streptomycin (Sigma) and rested for 1 hour in the incubator before functional assay or purity assessment using flow cytometry. Neutrophils were identified as CD15⁺CD16⁺CD14^{low}CD193⁻ as indicated by the gating strategy in Figure 2.1a. Cells were stained as outlined in Section 2.6 without fixation. Isolated neutrophils were also cytopun and stained with haematoxylin and eosin (H&E) to assess purity based on nuclei morphology (Figure 2.1b).

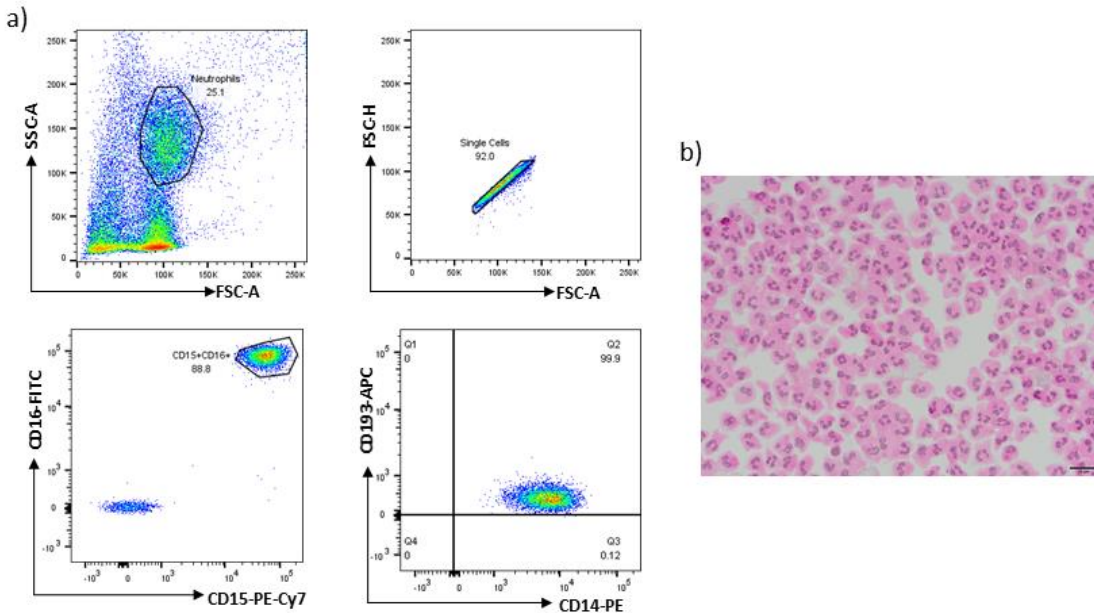


Figure 4.1 Purity assessment of isolated neutrophils from human whole blood.

Neutrophils isolated using immunomagnetic depletion strategy were subjected to a) flow cytometry and b) morphological assessment. Sample gating strategy and H&E staining showed high purity within the neutrophil isolates. Scale bar= 10µm.

4.3. Quantitative Gene Expression

Transcriptional changes in cells in response to treatment was assessment using reverse transcription quantitative polymerase chain reaction (qPCR).

4.3.1. Standard RNA Isolation

RNA isolation was carried out using RNeasy mini kit (Qiagen). Culture media was removed, and equivalent volume of PBS was added to wash the cells. PBS was then discarded and 350µL of Buffer RLT containing 1% β-mercaptoethanol (Sigma) was added to lyse the cells. Lysates were either stored at -20°C for storage or loaded directly onto QiaShredder (Qiagen). The loaded QiaShredder was spun at 17,000g for 2mins to homogenise the lysate. Flow through was collected and 350µL of 70% ethanol was added and mixed by pipetting. The total volume was transferred to an RNeasy spin column and centrifuged at 8,000g for 15secs. The mRNA at this point was retained on the silica column.

To remove any remaining cellular contaminant, flow through was discarded before the addition of 700µL of Buffer RW1. Subsequently, the RNeasy spin column was centrifuged at 8,000g for 15secs. This was followed by 2× addition of 500µL Buffer RPE and centrifuged at 8,000g for 15secs and 2mins respectively. The spin column was then transferred to a new collection tube and centrifuged at 17,000g, 1 min to dry out the silica and remove any remaining buffer. Lastly, the silica column was transferred to a 1.5mL collection tube followed by the addition of 30µL of RNase free water and the tube was centrifuged at 8,000g for 15secs to elute the RNA.

4.3.2. Total RNA Isolation

Total RNA was isolated from cells using the miRNeasy mini kit (Qiagen). Culture media was removed, and equivalent volumes of PBS were added to wash the cells. 700µL of Qiazol was added to lyse the cells before transferring the lysate to a 1.5mL RNase free tube (Sarstedt). The lysate was homogenised by 30secs vortex at room temperature before storing at -80°C or proceeded to extract the RNA.

140µL of chloroform was added to the lysate and vortexed for 15secs before resting at room temperature for 3mins. The lysate was centrifuged at 12,000g, 15 mins at 4°C. 350µL of the upper aqueous phase was transferred to a new RNase free tube before the addition of 525µL of 100% ethanol and mixed by pipetting. The total volume was transferred to an RNeasy spin column and centrifuged at 8,000g for 15secs. The total RNA at this point was retained on the silica column.

To remove any remaining cellular contaminant, the flow through was discarded before addition of 700µL of Buffer RWT. Subsequently, the RNeasy spin column was centrifuged at 8,000g for 15secs. This was followed by 2× addition of 500µL Buffer RPE and centrifuged at 8,000g for 15secs and 2mins respectively. The spin column was then transferred to a new collection tube and centrifuged at 17,000g, 1 min to dry out the silica and remove any remaining buffer. Lastly, the silica column was transferred to a 1.5mL collection tube followed by the addition of 30µL of RNase free water and the tube was centrifuged at 8,000g for 15secs to elute the RNA.

4.3.3. RNA Quantification

Extracted RNA was quantified using a Nanodrop™ spectrophotometer (ThermoFisher) unless otherwise stated. The spectrophotometer was blanked with 1μL of RNase free water before measurement of the samples. RNA purity was determined using the A260/280nm and A260/230nm ratio with values between ~1.8-2.0 indicating isolation free from contamination.

4.3.4. mRNA Reverse Transcription

500ng of isolated RNA was reverse transcribed using Tetro™ cDNA synthesis kit (Meridian BioScience). To each RNA sample, 4μL of 5× RT buffer, 1μL of 10mM dNTP mix, 1μL of Ribosafe RNase inhibitor, 1μL tetro reverse transcriptase and 1μL of oligo(dT)₁₈ primer was added. The final volume was adjusted using DPEC treated water to 20uL before centrifuging with a picofuge. The samples were transferred to a thermocycler (Bio-Rad) with the following running conditions: 25°C for 10mins, 45°C for 30mins, and 85°C for 5mins. Prepared cDNA was stored at -80°C until further use.

4.3.5. miRNA Reverse Transcription

1μL of total RNA was reverse transcribed using Taqman™ microRNA reverse transcription kit (ThermoFisher) in conjunction with Taqman™ target specific reverse transcription primer (Table 4.2, ThermoFisher). To each RNA sample, 1.5μL of 10× reverse transcription buffer, 0.15μL of 100mM dNTP (with DTTP), 0.19μL of RNase inhibitor, 1μL of MultiScribe™ reverse transcriptase, 3μL of 5× target specific RT primer and 8.16μL of nuclease-free water. The prepared samples were centrifuged and transferred to a thermocycler (Bio-Rad) with the following running conditions: 16°C for 30mins, 42°C for 30mins, and 85°C for 5mins. Prepared cDNA was stored at -80°C until further use.

Table 4.2 Primer list for small-RNA species used for target specific reverse transcription and PCR.

Gene Name	Assay ID
hsa-miR-210-3p	000512
U6	001973

4.3.6. mRNA Quantitative Real-time Polymerase Chain Reaction (qPCR)

Reverse transcribed cDNA (described in 2.3.4) was used to quantify the relative expression of the target genes. For each gene of interest, 2µL of cDNA was combined with 10µL of 2× Taqman™ Gene Expression Mastermix (ThermoFisher), 7µL of RNase-free water (Qiagen) and 1µL of gene specific Taqman™ primer (Table 4.3, ThermoFisher) in individual wells of a 96-well qPCR plate in technical duplicate. The qPCR plate was sealed and centrifuged before placing into StepOnePlus™ real-time PCR machine (ThermoFisher) with the running conditions of 50°C for 2mins, 95°C for 10mins and 40 cycles: 95°C for 15secs and 60°C for 1min. HPRT1 was used as a housekeeping gene unless otherwise stated to calculate the relative expression using the comparative Ct ($2^{-\Delta\Delta Ct}$) method.

Table 4.3 Primer list for mRNA qPCR.

Gene Name	Assay ID
<i>CXCL8</i>	Hs00174103_m1
<i>EPAS1</i>	Hs01026149_m1
<i>HIF1A</i>	Hs00153153_m1
<i>HPRT1</i>	Hs02800695_m1
<i>ISCU</i>	Hs00384510_m1
<i>NPTX1</i>	Hs00982601_m1
<i>TFRC</i>	Hs00951083_m1
<i>VEGF-A</i>	Hs00900055_m1

4.3.7. miRNA Quantitative Real-time Polymerase Chain Reaction (qPCR)

Reverse transcribed cDNA (described in 2.3.5) was used to quantify the relative expression of the target genes. For each gene of interest, 1.33µL of cDNA was combined with 10µL of Taqman™ 2× Universal Gene Expression Mastermix (ThermoFisher), 7.67µL of RNase-free water and 1µL of 20× Taqman™ small RNA assay (Table 4.2, ThermoFisher) in individual wells of a 96-well qPCR plate in technical duplicate. The qPCR plate was sealed and centrifuged before placing into StepOnePlus™ real-time PCR machine (ThermoFisher) with the running conditions of 50°C for 2mins, 95°C for 10mins and 40 cycles: 95°C for 15secs and 60°C for 1min. U6 small nuclear RNA (snRNA) was used as a housekeeping gene unless otherwise stated to calculate the relative expression using the comparative Ct ($2^{-\Delta\Delta C_t}$) method.

4.4. Protein Quantification

Protein abundance in either biological samples or cells were assessed by western blotting.

4.4.1. Cell Preparation

Following treatment of cells, culture media was removed and subsequently washed with ice-cold 1× PBS. Radioimmunoprecipitation buffer (RIPA) supplemented with protease and phosphatase inhibitor (Cell Signalling) was added to the cells and homogenised using a pipette tip. The lysates were transferred to 1.5mL tubes and agitated for 20mins at 4°C. Subsequently, lysates were spun at 12,000g, 15mins at 4°C before transferring the supernatant to a fresh 1.5mL tube and store at -20°C until use.

4.4.2. Protein Quantification

To ensure even loading, relative protein abundance was determined using Pierce™ BCA Protein Assay kit (ThermoFisher) using the microplate protocol. In brief, a protein standard was diluted according to manufacturer's instruction (Range: 2mg/ml-125µg/ml). 10µL of standards or samples were subsequently added in duplicates to a 96 well plate. 200µL of the working reagent (containing 50 parts Reagent A: 1 part Reagent B) was added to the wells before sealing the plate and incubating at 37°C for 30mins. The plate was cooled to room temperature and absorbance was measured at 562nm using a plate reader (SynergyHT, BioTek). Protein quantity in samples were determined using the standard curve established using the protein standards.

4.4.3. Denaturing Protein Samples

Sample volume corresponding to the pre-determined protein concentration required was aliquoted into a 1.5mL tube. Laemmli buffer (Bio-Rad) containing 10% β -mercaptoethanol was added at a 1:3 ratio to the samples and vortexed before heating at 95°C for 10mins. The samples were cooled before storing at -20°C or loaded onto a polyacrylamide gel to resolve the proteins.

4.4.4. Sodium Dodecyl Sulfate Polyacrylamide Gel Electrophoresis (SDS-PAGE)

Lysates were resolved through a 1.5mm thick gel consisting of both 12% or 18% resolving layer and a 5% stacking layer (Table 4.4). Samples were loaded along with a well containing molecular weight markers (10-180kDa PageRuler™ Prestained Protein Ladder, ThermoFisher). Gels were run at 150V for 90mins or until reaching desired points.

Table 4.4 Components for SDS-PAGE gel.

	18% Resolving Gel	12% Resolving Gel	5% Stacking Gel
Distilled Water	2.5mL	6.5mL	4.1mL
30% (w/v) Acrylamide: bis-Acrylamide solution (Ratio 37.5:1)	12mL	8.0mL	1.0mL
Separating gel buffer (100 mL diH ₂ O, 19.8 g Tris Base, 0.4 g SDS, pH 8.8)	5mL	5.0mL	-
Stacking Gel buffer (100 mL diH ₂ O, 6.6 g Tris Base, 0.4 g SDS) pH 6.8)	-	-	0.75mL
10 % SDS	200	200 μ L	60 μ L
10 % Ammonium persulfate (APS)	200 μ L	200 μ L	60 μ L
N,N,N',N'-Tetramethylethylenediamine (TEMED)	200 μ L	20 μ L	6 μ L

4.4.5. Protein Transfer

Resolved proteins from the SDS-PAGE gels were transferred to 0.2 μ m polyvinylidene fluoride (PVDF) unless otherwise stated using Trans-blot Turbo transfer system (Bio-Rad) using the 1.5mm gel protocol.

4.4.6. Immunoblotting

Membranes containing the transferred proteins were incubated in an appropriate blocking buffer (Table 4.5) for at least 1 hour at room temperature. Subsequently, primary antibody was added at appropriate concentration and incubated overnight at 4°C (Table 4.5). The probed membrane was washed 3 × 10mins with 0.1% Tween-20 Tris-buffered saline (0.1% TBST) before the addition of horse-radish peroxidase conjugated secondary antibody at appropriate concentration (Table 4.5) and incubated at room temperature for 1 hour. Finally, each membrane was washed 3 × 10mins with 0.1% TBST before the addition of SuperSignal™ West Pico Plus (ThermoFisher) chemiluminescent substrate and visualised either with x-ray film development or Li-Cor Odyssey Fc (Li-Cor) imaging system. Unless otherwise stated, all incubation was done with agitation on a microplate shaker.

Table 4.5 Antibody list and incubation conditions for western blot.

Block buffer	Primary antibody	Manufacturer	Dilution	Secondary antibody	Manufacturer	Dilution	Tertiary antibody	Manufacture	Dilution	Antibody buffer
5% milk in 0.1% TBST	Rabbit anti-CXCL8 polyclonal	Invitrogen, AHC0881	1:1000	Goat anti rabbit-HRP	Sigma	1:10,000	-	-	-	5% milk in 0.1% TBST
5% BSA in 0.1% TBST	Mouse anti-Nitrotyrosine monoclonal	HycultBioTech, HM5001	1:1000	Goat anti-mouse- HRP			-	-	-	5% BSA in 0.1% TBST
5% BSA in 0.1% TBST	Anti-nitrated CXCL8	Bio-Rad	1:1000	Mouse-anti-FLAG	ProteinTech	1:2000	Goat anti-mouse- HRP	Sigma	1:10,000	5% BSA in 0.1% TBST
5% milk in 0.1% TBST	Rabbit anti-CD9 monoclonal	Abcam, Ab263019	1:1000	Goat anti-rabbit-HRP	Sigma	1:2000	-	-	-	5% milk in 0.1% TBST
	Rabbit anti-TSG101 monoclonal	Abcam, Ab125011	1:1000	Goat anti-rabbit-HRP		1:2000	-	-	-	
	Rabbit anti-CD63 monoclonal	Abcam, Ab134045	1:1000	Goat anti-rabbit-HRP		1:2000	-	-	-	
	Rabbit anti-HSP70 monoclonal	Abcam, Ab181606	1:1000	Goat anti-rabbit-HRP		1:2000	-	-	-	
1% milk in 0.1% TBST	mouse anti-Calnexin monoclonal	Proteintech, 66903-1-Ig	1:1000	Goat anti-mouse-HRP			1:2000	-	-	-

4.5. Immunostaining

4.5.1. Tissue staining

4µm tissue sections were obtained from formalin fixed, paraffin embedded (FFPE) biopsies. Slides were dewaxed by immersing into xylene for 2×5mins. Tissue sections were rehydrated by immersing in 100% ethanol for 2×5mins, 90% ethanol for 5mins, 70% ethanol for 5mins and distilled water for 5mins. Antigen retrieval was immediately carried out in citric acid antigen retrieval buffer (10mM, 0.05% Tween 20, pH6.0) in a pressure cooker for 3 mins on high pressure setting. Blocking buffer (Table 4.6) was added directly on the tissue section to block for 30mins at room temperature before incubating with primary antibodies diluted in PBS at 4°C (Table 4.6) overnight. For no primary control, only PBS was added. Subsequently, slides were washed 3×5mins in PBST with agitation before the addition of appropriate secondary antibodies diluted in PBS (Table 4.6). Finally, the slides were washed with 3×5mins in the dark and mounted with mounting media containing DAPI (Vectashield). The slides were immediately imaged (AxioImager, Zeiss) or stored in the dark at 4°C. Buffer volumes for tissue staining are kept at 50µL unless otherwise stated.

Table 4.6 Antibody list and incubation condition for tissue staining.

Blocking buffer	Primary Antibody	Manufacturer	Dilution	Secondary Antibody	Manufacturer	Dilution
10% goat serum	Rabbit anti-CXCL8 polyclonal	Invitrogen, AHC0881	1:50	Goat anti-rabbit AlexaFluor488 polyclonal	Abcam, Ab150077	1:50
	Mouse anti-3-nitrotyrosine monoclonal	HycultBioTech, HM5001	1:50	Goat anti-mouse Dylight650	ImmunoReagent, GtxMu-003-F2650NHSX	1:50

4.6. Flow cytometry

Cells were cultured in 12-well plates and treated as indicated. Spent culture media was removed after treatment and washed with 1mL PBS. 500 μ L of Accutase[®] was added per well and placed in an incubator for 5mins at 37°C to detach cells. Cell suspension was transferred to flow tubes (Falcon[™]) and centrifuged at 300g, 5mins. Cells were washed twice with 1mL of ice-cold PBS with cells at the end of each round spun down at 300g, 5mins and supernatant discarded. 100 μ L of Live/Dead[™] Fixable Blue Dead Cell Stain (Invitrogen) was added to the cells and incubated on ice for 30mins according to manufacturer's protocol. Cells were washed twice with ice-cold PBS before blocking with 1 μ L Human TruStain FCX[™] (Biolegend) in 2% BSA in PBS for 15mins at room temperature. Antibodies and matching isotype controls were added to the cells and incubated for 30mins on ice (Table 4.7). Cells were then washed twice with ice-cold 2% BSA in PBS before the addition of 100 μ L 4% paraformaldehyde (PFA) and incubated at room temperature for 15mins. PFA was discarded and cells were washed twice with 1mL ice-cold PBS and was resuspended in 2% BSA PBS before data acquisition on either the Fortessa X20 or Symphony A5 flow cytometer (BD Biosciences). Data analysis was then done on FlowJo V9.

Table 4.7 Antibodies used for conventional flow cytometry.

Antibody	Volume (μ L)	Fluorophore	Clone	Manufacturer
anti-human CD14	2 μ L	PE	63D3	Biolegend
anti-human CD15		PE-Cy7	W6D3	Biolegend
anti-human CD16		FITC	3G8	Biolegend
anti-human CD193		APC	5E8	Biolegend
anti-human CD71		APC	CY1G4	Biolegend
anti-human HLA-DR		APC	L243	Biolegend
anti-human HLA-DQ		PE	HLADQ1	Biolegend
anti-human CD31		FITC	WM59	Biolegend
anti-human CD54 (ICAM-1)		FITC	HA58	Biolegend
IgG 2a, κ isotype control		APC	MOPC-173	Biolegend
IgG 2b, κ isotype control	Matching concentration	APC	27-35	Biolegend
IgG1, κ isotype control		PE	P3.6.2.8.1	eBiosciences
IgG1, κ isotype control		FITC	P3.6.2.8.1	Biolegend

4.7. Statistical analysis

Statistical analysis was performed using GraphPad Prism version 9.5. Error bars represent the standard deviation of the mean, unless otherwise stated and statistical tests are described for each experiment individually. p-values for each comparison are either shown explicitly on the graphs or otherwise depicted as follows:

* $p < 0.05$

** $p < 0.01$

*** $p < 0.001$

**** $p < 0.0001$

5. Regulation of CXCL8 activity by nitration

5.1. Introduction

CXCL8 is an inflammatory chemokine released during the onset of inflammation and acute injury to recruit circulating neutrophils. During the recruitment process, binding of CXCL8 to its cognate receptors CXCR1 and CXCR2 along with other inflammatory stimuli, primes neutrophils and allows subsequent exertion of their anti-pathogenic functions (Raghuwanshi et al., 2012). These short-lived immune cells respond to the inflammatory stimuli through a series of mechanisms ranging from phagocytosis to the delivery of noxious payloads (Németh et al., 2020). While such mechanisms are extremely potent, they are often unable to distinguish between self and non-self. In turn, surrounding tissues often suffer collateral damage.

Neutrophils trigger a transient increase in the reactive species within the inflammatory environment via an oxidative burst. Due to the lack of target specificity, the disruption of the tightly regulated redox balance not only result in excessive tissue damage, but also modifies surrounding biomolecules (Souza et al., 2008). One such species produced is peroxynitrite. In high concentrations, peroxynitrite is extremely cytotoxic and therefore effective in pathogenic clearance. However, the highly reactive nature also allows it to react with amino acids within proteins, potentially altering protein functions. Several inflammatory chemokines have been identified which can have their tyrosine or tryptophan residues nitrated by peroxynitrite (Sato et al., 1999, Sato et al., 2000b, Molon et al., 2011, Janssens et al., 2016, Barker et al., 2017).

Furthermore, previous work done in the group has identified the tyrosine residue Y13 to be the only amino acid in CXCL8 to have modifications. Consistent with published data on other nitrated chemokines, these modified CXCL8 (herein nitrated CXCL8) was also shown to lack the capability to induce neutrophil recruitment both *in vitro* and in mice.

Identification of nitrated CXCL8 in biological samples however remains a challenge with concentrations of chemokines in tissue and biological fluids in the low picomolar to nanomolar range (Schenk et al., 2001). Individual protein modification will only affect a proportion of any protein. Therefore, detection and quantification of nitrated chemokine will be challenging and require highly sensitive techniques that can distinguish between native and modified proteins.

This chapter hence focuses on the detection and identification of post-translationally modified CXCL8 in biological samples.

5.2. Specific Aims

- To assess the functional implication of tyrosine nitration in CXCL8.
- To identify the presence of nitrated CXCL8 in biological samples.
- To identify post-translational modification of CXCL8 in biological samples.

5.3. Specific Materials and Methods

5.3.1. Patient Samples

BAL samples from patients with suspected ventilator associated pneumonia and healthy controls were collected as part of study (11/NE/0242) approved by a Research Ethics committee (Hellyer et al., 2015).

Lung tissue biopsies from *ex vivo* lung perfusion (EVLP) was collected as part of NHSBT Study 66 entitled “Further Evaluation of Ex Vivo Lung Perfusion to Improve Transplantation Outcomes” (16/NE/0230). Samples taken during EVLP were then stored in the Newcastle Institute of Transplantation (IOT) Tissue Biobank (17/NE/0022).

5.3.2. Cell Culture and Treatment

Confluent HMEC-1 cells were passaged as described in Chapter 4.2. Prior to treatment, cells were seeded at a density of 200,000 cells per well in 6-well plates and cultured overnight unless otherwise stated. Cells were stimulated with tumour necrosis factor alpha (TNF- α) at a concentration of 10ng/ml for 2 hours in FBS free media. Subsequently, freshly prepared 3-morpholinosydnoimine hydrochloride (SIN-1) in sterile deionised water were added to cells at 1-5nM. Post treatment with SIN-1, culture media was collected in a 50mL Falcon tube and clarified by centrifugation at 300g, 5mins before storing at -20°C. mRNA was extracted from cells as outlined in Chapter 4.3.1 to quantify CXCL8 expression.

5.3.3. Cell Viability Assessment

A spectrophotometric assay was used to assess HMEC-1 viability post-treatment with SIN-1. In brief, 10,000 cells were seeded per well in 96 well plates and cultured overnight. Cells were treated with varying concentrations of SIN-1 over time in FBS free media. Post treatment, SIN-1 containing media was removed and cells were washed with PBS before replacing with 100µL of complete media. 50µL of XTT labelling mixture (Roche) consisting of 50 parts XTT labelling reagent: 1 part electron coupling reagent were added to each well (to obtain a final volume of 150µL) and incubated for 24 hours. Corrected absorbance corresponding to cell viability was obtained by subtracting background (650nm) signal from 450nm using a plate reader (Synergy™, BioTek).

5.3.4. ELISA (Enzyme-Linked Immunosorbent Assay)

CXCL8 levels in HMEC-1 culture media as well as bronchoalveolar lavage (BAL) samples were measured using commercial ELISA kit (DuoSet, R&D systems) according to manufacturer's protocol. 100µL of capture antibody was coated onto an ELISA plate (Immulon 4HBX, ThermoFisher) and incubated overnight. The wells were blocked for 1 hour with 300µL of 1% bovine serum albumin (BSA) in PBS. 100µL of prepared standards (2µg/ml - 31.3pg/ml) or culture media obtained from 5.3.1 was added and incubated for another 2 hours followed by an additional 2-hour incubation with the detection antibody. 100µL of streptavidin-horseradish peroxidase (HRP) was added and the plate was incubated in the dark for 20mins. 100µL of substrate solution (R&D systems) was then added and allowed to develop before quenching the reaction with 1M sulfuric acid (H₂SO₄). Absorbance of individual wells was immediately measured using a plate reader at 450nm (Synergy™, BioTek). Plates were incubated at room temperature throughout the entire assay and between each step, well contents were aspirated, and the wells were washed with 3 × 0.05% PBST before proceeding.

5.3.5. Trichloroacetic Acid (TCA) Precipitation of Proteins

5µg of insulin (ThermoFisher) was spiked into culture media from 3.3.1. 100% (w/v) TCA was added to the insulin spiked cultured media at 1:4 and incubated overnight at 4°C. Subsequently, the mixture was centrifuged at 12,000g, 5mins to pellet the protein. The supernatant was discarded, and the precipitated pellets were washed twice by resuspending in 500µL of ice-cold acetone before centrifugation at 12,000g, 5mins. Excess acetone was removed by heating the pellet to 95°C for 10mins before resuspending in 20µL of 4 x Laemmli buffer (Bio-Rad) containing β-mercaptoethanol and proceeded with sample preparation outlined in Chapter 4.4.3 to 4.4.6 for immunoblotting of CXCL8.

5.3.6. Circular Dichroism

Native CXCL8 (Peprotech) or nitrated CXCL8 (Almac) was dissolved in 50mM phosphate buffer (Table 5.1) to obtain a 1mg/ml concentration. The solution was left to sit at room temperature for 30mins before centrifugation at 12,000g for 5mins at room temperature to remove undissolved protein. The supernatant was transferred to a new microfuge tube. Circular dichroism was conducted using a spectropolarimeter (J-810, Jasco) with a 0.02cm pathlength (far UV) and a 1cm pathlength (near UV) quartz cuvette. Scans for the far UV spectrum were conducted at 180-260nm and near UV spectrum was conducted at 260-320nm. All data was collected at room temperature as an accumulation of 10 measurements (N=10), adjusted to the background spectrum (buffer only control).

Table 5.1 Phosphate buffer composition.

Reagent	Composition
1M monobasic sodium phosphate buffer	9.4ml
1M dibasic sodium phosphate buffer	40.6ml
Water	Top up to 1L
pH	7

5.3.7. Fluorescence Spectroscopy

Native CXCL8 or nitrated CXCL8 was diluted to 20µg/ml in 50mM phosphate buffer (Table 5.1). Fluorescence was measured using a fluorescence spectrophotometer (Cary Eclipse, Agilent) with a 1cm path length cuvette. Data acquisition was done with a scan rate of 120nm/min with an excitation wavelength of 280nm and emission wavelength of 300-540m. All data collected was adjusted to the background spectrum (buffer only control).

5.3.8. Chemotaxis Assays

5.3.8.1. Trans-filter Chemotaxis

24 well plates (Falcon™) were blocked with 1ml 2% BSA in PBS for 1 hour at 4°C. The blocking buffer was aspirated and replaced with 500µL FBS free RPMI-1640 or FBS free media containing CXCL8 variants. Rested neutrophils outlined in Chapter 2.2.8 were centrifuged at 300g, 10mins, and 0 break speed and placed in the top chamber of 3µm polycarbonate transwell insert (Corning) at a density of 200,000 cells/well in 500µL before incubating at 37°C for 90mins. Media in the top chamber was aspirated and discarded while media in the lower chamber was collected into labelled flow cytometry tubes. 500µL of Accutase® was added to the lower chamber and incubated at 37°C for 5mins to detached adhered neutrophils and transferred to the corresponding flow cytometry tubes. Cells were pelleted by centrifugation at 300g, 10mins and 0 break speed before resuspending in 100µL of FBS free RPMI-1640 media. 15µL of CountBright™ beads (ThermoFisher) were added to each flow cytometry tube and cell count was obtained by Fortessa X20 flow cytometer using the following formula:

$$\text{Absolute count} \left(\frac{\text{cell}}{\mu\text{L}} \right) = \frac{(\text{Cell count} \times \text{Counting beads volume})}{(\text{Counting beads count} \times \text{Cell volume})} \times \text{Counting beads concentration} \left(\frac{\text{beads}}{\mu\text{L}} \right)$$

Experimental controls include no chemokine and chemokinesis control. Results were expressed as neutrophil chemotactic index calculated using the following formula:

$$\text{Chemotactic Index} = \frac{(\text{Migrated cells in treatment} - \text{Background migration})}{\text{Chemokinesis control}}$$

5.3.8.2. *Trans-endothelial Chemotaxis*

200,000 HMEC-1 cells were seeded into the top chamber of 3µm polycarbonate transwell insert (Corning) 72 hours prior to chemotaxis assay. 24 hours before the experiment, HMEC-1 was activated with 100ng/ml of IFN-γ (Peprotech). The transwell insert was then transferred to a pre-blocked 24 well plates and assay was conducted as per outlined in the transfilter chemotaxis assay. Additionally, unstimulated HMEC-1 cells were added as an additional control.

5.3.9. *Glycosaminoglycan (GAG) Binding Assay*

GAG binding plates (BD Biosciences) were coated with 100µL of 25µg/ml heparan sulfate (Iduron) or heparin (Iduron) and left to incubate overnight. Subsequently, 300µL of 1% BSA in PBS was added to block the plate for 1 hour at room temperature. Native and nitrated CXCL8 diluted in the block buffer were added at 100µL per well and incubated for 2 hours at room temperature. 100µL of rabbit anti-human CXCL8 antibody (Invitrogen) was added at 1µg/ml and incubated for 1 hour at room temperature. Following which, goat anti-rabbit HRP antibody (Sigma) was added at 1:5000 dilution and incubated for another 1 hour. 100µL of 3,3',5,5'-Tetramethylbenzidine (TMB) substrate was added and left to develop before quenching the reaction with 50µL of 1M sulfuric acid (H₂SO₄). Absorbance of individual wells were immediately measured using a plate reader at 450nm (Synergy™, BioTek). Plates were incubated at room temperature throughout the entire assay and between each step, contents were aspirated, and wells were washed with 3× 300µL of 0.2% PBST before proceeding.

5.3.10. *β-arrestin Recruitment Assay*

The β-Arrestin recruitment activity of CXCL8 variants was measured using CXCR1 and CXCR2 PathHunter® Kits (DiscoverX®). The assay was carried out according to the manufacturer's protocol in collaboration with Professor Krishnan Rajarathnam (University of Texas Medical Branch). In brief, PathHunter® U2OS CXCR1 β-Arrestin cell and PathHunter® HEK293 CXCR2 β-Arrestin cell were cultured using AssayComplete™ cell culture kit. Transfectants were seeded in a 96-well white-walled, clear-bottom plate for 48 hours. Chemokine variants were added to the cells and incubated for 90mins at 37°C. Detection reagents were then added and incubated for 1 hour in the dark. β-galactosidase induced luminescence upon β-arrestin–CXCR1/CXCR2 interaction was then measured using FLUOstar Optima (BMG Labtech).

5.3.11. Immunoprecipitation

BAL samples from patients with confirmed ventilator associated pneumonia were enriched for proteins containing 3-nitrotyrosine using a nitrotyrosine IP kit (Cayman Chemical). In brief, 100µL of BAL was diluted with 100µL of PBS. The nitrotyrosine affinity sorbent was mixed with gentle inversion of the tube and 40µL of the mixture was transferred to the spin columns. The affinity sorbent was washed 3 times, each time, 500µL of wash buffer was added to the spin columns and mixed with gentle pipetting before centrifugation at 1000g for 1 min. The flow through was discarded. 200µL of the diluted BAL samples were added to the column and incubated overnight at 4°C with gentle agitation. Spin columns were subsequently centrifuged at 1000g for 1 min and flow through was retained as unbound fraction. The affinity sorbent was washed 3 times as per mentioned and 20µL of 4× Laemmli buffer was added before heating the spin column at 95°C for 5mins. Finally, the spin columns were centrifuged at 1000g for 1 min and the flow through as well as the unbound fraction were prepared as outlined in Chapter 4.4.3 to 4.4.6 for immunoblotting of CXCL8.

5.3.12. Immunosorbent Sample Preparation and Nano-Scale Liquid Chromatography-Tandem Mass Spectrometry for Proteoform Analysis (ISTAMPA)

The ISTAMPA methodology developed by Professor Paul Proost allowed identification and relative quantification of chemokine proteoform using mass spectrometry (Metzemaekers et al., 2021). Biological samples were analysed in collaboration with Professor Paul Proost.

5.3.12.1. Sample Preparation

5µg of biotinylated polyclonal rabbit anti-human CXCL8 antibody (Peprotech) was immobilised onto 25µL of Dynabeads™ M-280 Streptavidin-coated magnetic beads (ThermoFisher) with constant agitation for 30mins at room temperature. The antibody coupled beads were washed with 4 × 500µL of PBS using a Dynamag 2 magnet (ThermoFisher) and incubated with 100µL of BAL samples for 30mins at room temperature with constant agitation. Subsequently, antigen-antibody bead complex was washed with 4 × 500µL of PBS using a Dynamag 2 magnet (ThermoFisher). Isolated proteins were then eluted with 20µL of 0.1M glycine, pH 2.8 and loaded in a pre-cooled autosampler at 5°C and analysed by nano-LC-MS/MS.

Nitrated CXCL8 was diluted in 0.1% (v/v) trifluoroacetic acid (TFA) prior to mass spectrometry analysis.

5.3.12.2. Mass Spectrometer Settings

5µL of diluted nitrated CXCL8 or eluted fraction from immunosorbent sample preparation were injected on an UltiMate 3000 nano-scale reverse-phase ultra-high performance liquid chromatography (ThermoFisher) equipped with an autosampler. Proteins were separated with a 5 × 0.3mm PepMap 300 C4 pre-column (ThermoFisher) combined with a 50 × 0.15mm Proto 300 C4 column (Higgins Analytical. Inc). Samples were loaded onto the pre-column with 4%(v/v) acetonitrile in 0.1% (v/v) TFA and eluted with an acetonitrile gradient in 0.1% (v/v) formic acid with a flow rate of 0.5µL/min. Eluate was directly injected into an amaZon Speed ETD mass spectrometer (Bruker Daltonics) with captive spray ionisation-ion trap technology. Collision-induced dissociation (CID) was exploited for low energy fragmentation (MS/MS fragmentation amplitude of 1.0) of pre-selected precursor ions with specific m/z values ± 2 in multiple reaction monitoring (MRM) mode. Hystar 3.2 and Trap control 8.0 software (Bruker Daltonics) was used for data collection. Results were analysed with Compass Data Analysis 5.0 software (Bruker Daltonics).

5.4. Results

5.4.1. Generation of Nitrated CXCL8

Previously, the functional alteration of nitrated CXCL8 was assessed by incubating peroxyxynitrite with native CXCL8 *in vitro*. While mass spectrometry confirmed the modification to be only at the Y13 residue and the most abundant protein was nitrated CXCL8, techniques to separate any remnant native CXCL8 from the nitrated CXCL8 are lacking. Hence, to delineate the findings, nitrated CXCL8 was outsourced to a commercial company (Almac) and was chemically synthesised using solid phase peptide synthesis (peptide sequence in Figure 5.1a). As indicated in Figure 5.1b, the reverse-phase high performance liquid chromatography (RP-HPLC) resolved with a single uniform peak at 21.33mins. Furthermore, the deconvoluted mass spectrometry data corresponded to the theoretical mass of nitrated CXCL8 (Figure 5.1c).

5.4.2. Nitration Impedes Neutrophil Chemotaxis

Upon the confirmation that the synthesised nitrated CXCL8 was homogenous, we next assessed its chemotactic capability *in vitro* using a Boyden chamber assay. Using this system, we assessed the capability for nitrated CXCL8 to firstly recruit neutrophils to the inflammatory site using the trans-filter assay. We observed a similar level of migration towards native and nitrated CXCL8 at 10nM. In contrast, when CXCL8 concentrations were increased to 30nM and 50nM, we observed a reduction in the chemotactic index for nitrated CXCL8, but this was not statistically significant (Figure 5.2a).

Following neutrophil localisation, gaining access to the exact site of inflammation requires the transmigration of neutrophils across the vessel endothelium. To model this transmigration, an adapted Boyden chamber assay utilised a layer of pre-activated endothelium seeded on the upper surface of the filter. In this assay, we found that the capability of nitrated CXCL8 to initiate endothelial transmigration was completely abrogated across all concentrations when compared to native CXCL8 (Figure 5.2b). These findings collectively indicated that nitration of CXCL8 induced a lower level of neutrophil recruitment and subsequently impaired their translocation across the endothelium to access the site of inflammation.

a)

A₁VLPRSAK ELRCQCIKTY(NO₂) SKPFHPKFIK ELRVIESGPH CANTEIIVKL SDGRELCLDP KENWVQRRVE KFLKRAENS₇₇

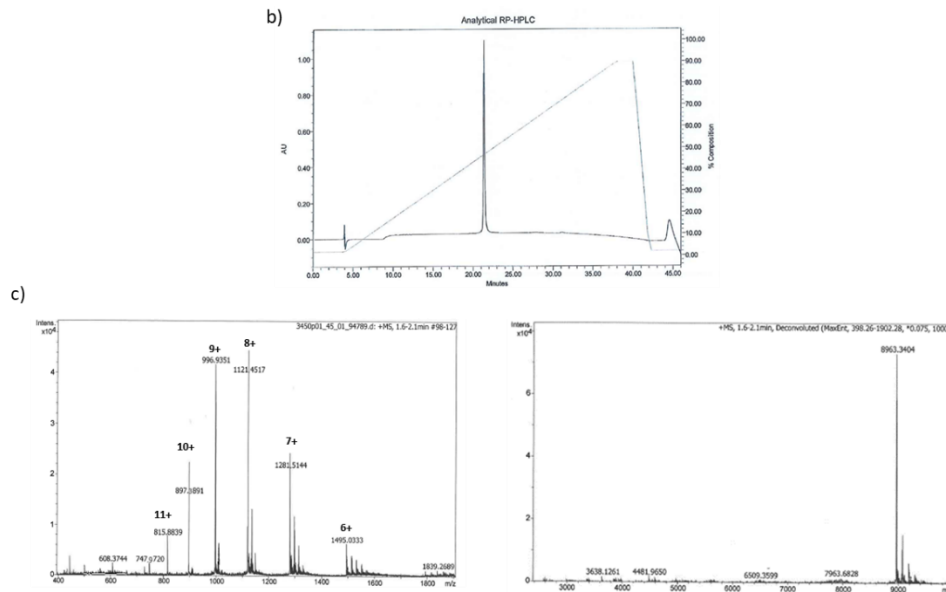


Figure 5.1 HPLC chromatogram and mass spectra of nitrated CXCL8.

Synthesised nitrated CXCL8 was identified as a pure homogenous population free of native CXCL8. a) Sequence of chemically synthesised nitrated CXCL8. b) HPLC chromatogram of the synthesised nitrated CXCL8 resolved as a uniform singular peak. c) The resolved peak from HPLC was subjected to mass spectrometry (ESI-microTOF) analysis with the different ionisation state annotated (left) and the deconvoluted spectra corresponded to nitrated CXCL8 (right).

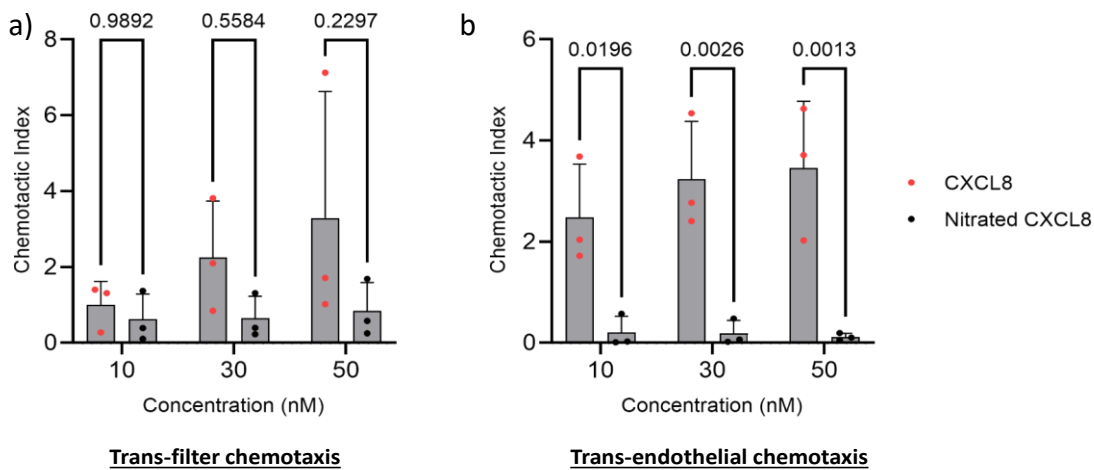


Figure 5.2 Assessment of the migratory potential of nitrated CXCL8 *in vitro*.

a) Trans-filter or b) trans-endothelial was used to assess the capability of CXCL8 variants to induce neutrophil migration across varying concentrations. Nitration of CXCL8 attenuates neutrophil recruitment whilst abrogates transmigration across an endothelium layer. Chemotaxis assays were carried out with 2 technical replicates per conditions with accompanying controls. Experiment was conducted n=3 for both trans-filter and trans-endothelial chemotaxis. Data shown as mean \pm SD of n=3, with each dot representing a biological replicate (different blood donor). Statistical analysis was performed using Two-Way ANOVA with Šídák post-hoc test.

5.4.3. Nitration of CXCL8 Attenuate GAG Binding and Cognate Receptors Signaling

With the migration assays showing alteration to the chemotactic potential of nitrated CXCL8, we set out to investigate the reasons for the observed changes. As mentioned in Chapter 1.3, chemokines including CXCL8 requires interaction with GAGs, which in turn stabilizes a haptotactic concentration gradient. This provides a directional cue for neutrophils. Subsequently, binding of CXCL8 by the CXCR1 and CXCR2 expressed on the neutrophils triggers a signaling cascade and thereby activating downstream mechanisms involved in cellular locomotion. Hence, we first assessed the binding capability of the CXCL8 variants to heparin and heparan sulfate. Results in Figure 5.3 showed that nitration impaired binding to both heparin and heparan sulfate compared to native CXCL8.

We next sought to identify the implication of this for receptor signaling. As outlined in Chapter 5.1, CXCL8 interacts with 2 receptors, namely CXCR1 and CXCR2. While CXCL8 binds both receptors with extremely high affinity (Nasser et al., 2007), marked differences were observed with their downstream signaling and the eventual cellular processes (Nasser et al., 2009, Raghuwanshi et al., 2012). Hence, we attempted to interrogate the signaling potential of the receptors independently using the PathHunter® platform. As shown in Figure 5.4, treatment of PathHunter® CXCR1 transfected U2OS cells resulted in no recruitment of β -arrestin (Figure 5.4a) whereas a mark downregulated was observed in the PathHunter® CXCR2 transfected HEK293 cells (Figure 5.4b). Furthermore, the extent of signaling by native CXCL8 via CXCR1 was to a greater extent compared to CXCR2, which was in line with the published literature (Nasser et al., 2009).

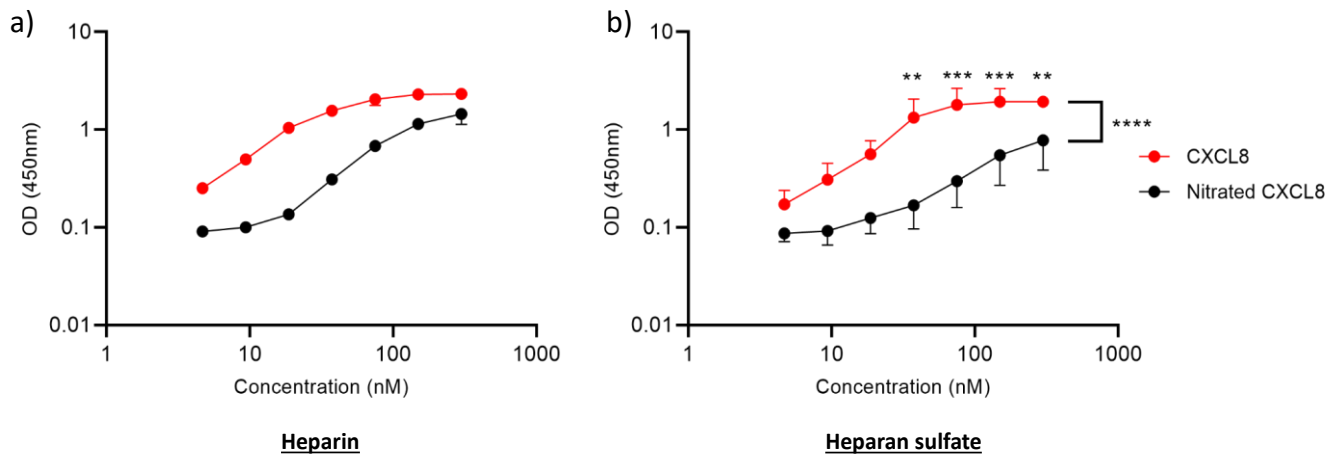


Figure 5.3 Comparisons of CXCL8 variants for glycosaminoglycan binding.

CXCL8 binding to immobilised a) heparin or b) heparan sulfate was assessed using immunodetection against CXCL8 in conjunction with HRP conjugated antibody. The optical density (OD) at 450nm reflects the relative quantity of bound CXCL8 (300nM-4.6875nM) on the immobilised GAG. Binding of nitrated CXCL8 to heparin or heparan sulfate was consistently impaired across all concentrations compared to native CXCL8. GAG binding assays were carried out with 3 technical replicates per concentration. Heparin and heparan sulfate binding were repeated n=2 and n=3 respectively. Data shown as mean \pm SD. Statistical analysis was performed using Two-Way ANOVA with Šídák post-hoc test. ** p< 0.01, ***p<0.001, ****p<0.0001.

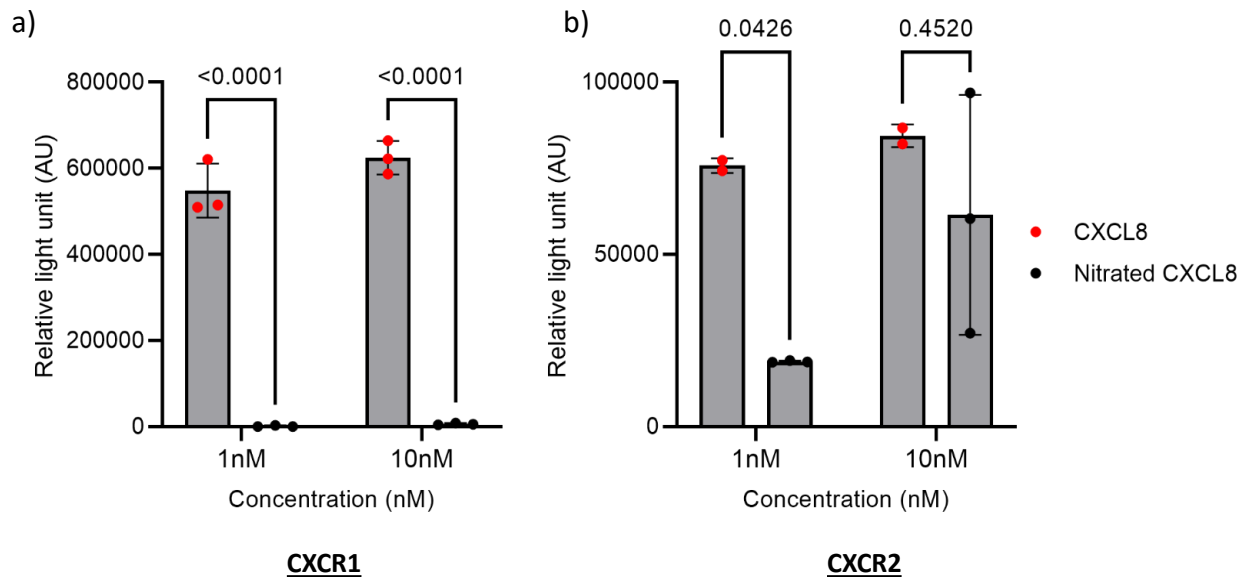


Figure 5.4 Differential signaling between CXCL8 variants with receptors.

Binding of CXCL8 variants to receptors a) CXCR1 and b) CXCR2 induced β -arrestin recruitment was used as a surrogate for receptor downstream signaling. Nitration of CXCL8 completely abrogated CXCR1 downstream signaling whereas CXCR2 signaling was downregulated. CXCR1 and CXCR2 signaling assay were carried out with 3 technical replicates per condition and concentration. CXCR1 and CXCR2 signaling were repeated n=3 and n=2-3 respectively. Data shown as mean \pm SD. Statistical analysis was performed using Two-Way ANOVA with Šídák post-hoc test.

5.4.4. Nitration Did Not Alter CXCL8 Structure

The Y13 residue sits on the unstructured N terminus tail of CXCL8. Therefore, the potential for protein misfolding as a result of tyrosine nitration is considered to be low. To confirm this hypothesis, we assessed the overall structure of nitrated CXCL8 using far UV circular dichroism. It was found that native and nitrated CXCL8 showed similar spectra (Figure 5.5), confirming that tyrosine modification did not impact secondary structure.

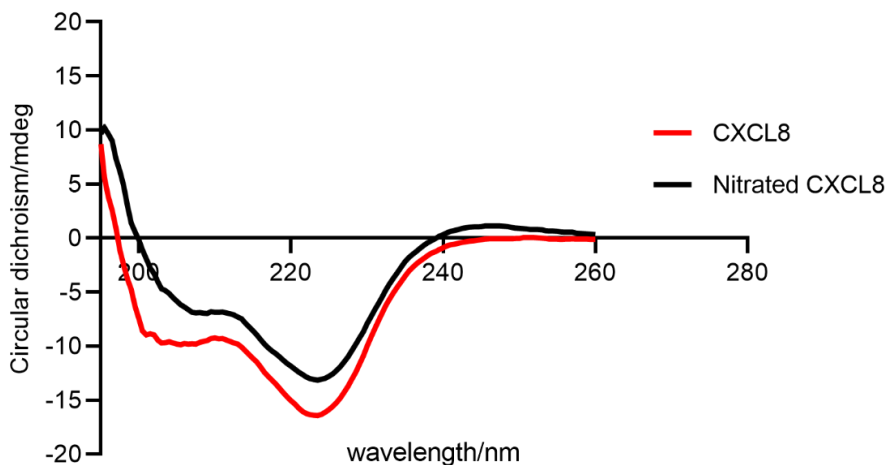


Figure 5.5 Secondary structure assessment of CXCL8 variants.

Protein folding of CXCL8 variants was assessed using far UV circular dichroism. The overlay of the spectra between native CXCL8 (red) with nitrated CXCL8 suggests that the overall secondary structure between variants is the same. All data was collected at room temperature as an accumulation of n=10 measurements, adjusted to the background spectrum (buffer only control).

5.4.5. *In Vitro* Model of CXCL8 Nitration

In concordance with previous work in the group showing that nitration of the Y13 residue in CXCL8 impaired neutrophil recruitment, we sought to develop an *in vitro* model to recapitulate the nitrosative stress in an inflammatory environment, thereby generating nitrated CXCL8. The half-life of peroxynitrite is ~10ms (Szabó et al., 2007) which presents technical difficulty to use as an inducer of nitrosative stress. As an alternative, we utilised 3-morpholinosydnoimine hydrochloride (SIN-1), which spontaneously releases both nitric oxide and superoxide in close proximity. We first set out to show that exposure of CXCL8 to SIN-1 results in tyrosine nitration. As shown in Figure 5b, co-incubation of CXCL8 with increasing concentrations of SIN-1 resulted in an increase in 3-nitrotyrosine signature. Interestingly, we also observed an increase in CXCL8 reactivity at higher molecular weight when incubated with SIN-1 even though the protein was resolved in a reducing condition (Figure 5.6a).

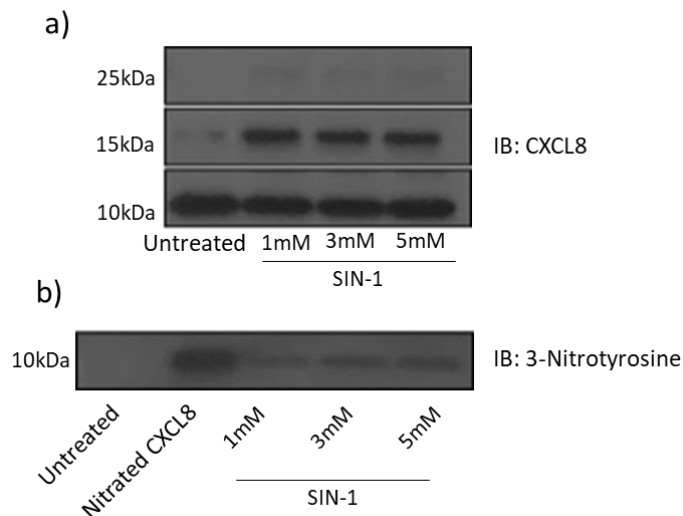


Figure 5.6 SIN-1 nitrates CXCL8 *in vitro*.

Equal amounts of CXCL8 were incubated with varying concentrations of SIN-1 at 37°C for 3 hours. The reaction was terminated with the addition of 4× Laemmli Buffer and heated at 95°C for 10mins before resolving on an 18% SDS-PAGE gel and detected with either a) anti-CXCL8 antibody or b) anti-3 nitrotyrosine antibody using western blot. Nitrated CXCL8 was loaded in b) as a positive control. Western blot shown is representative of n=3.

Upon confirmation that CXCL8 can indeed be nitrated in the presence SIN-1, we proceeded to optimise the concentration of SIN-1 *in vitro*. Using human microvascular endothelial cells (HMEC-1) as the model of inflammation, we first assessed the cell viability post exposure to varying concentrations of SIN-1. Significant increase in cell death was observed when the concentration of SIN-1 exceeded 1mM (Figure 5.7). Furthermore, it was previously reported that SIN-1 showed a lag time of 15mins before eliciting bactericidal activity (Brunelli et al., 1995). Coupled with the experimentally determined rate of degradation of SIN-1 as 1% per min (Brunelli et al., 1995), the treatment duration of 3 hours at 1mM was carried forward.

Pre-formed CXCL8 is stored in the Weibel Palade bodies within endothelial cells to allow rapid release under inflammatory conditions (Utgaard et al., 1998). Hence, pre-stimulation with inflammatory stimuli like TNF- α was necessary to mobilise the release of CXCL8. HMEC-1 was therefore first treated with TNF- α to prime the release of CXCL8 into the culture medium before the addition of SIN-1. Upon treatment, we saw a significant increase in CXCL8 gene expression (Figure 5.8a). The levels of CXCL8 in the harvested media on the other hand showed an almost significant reduction when compared to the control (Figure 5.8b). This finding was however in line with previous work within the group which showed a drop in the detectability and sensitivity of commercial ELISA kits to nitrated CXCL8 compared to the native protein (Dr Sarah Thompson, PhD thesis).

To further confirm the hypothesis that the quantities of CXCL8 released by HMEC-1 in response to SIN-1 was not reduced but was nitrated, we utilised an anti-CXCL8 antibody that was previously screened to detect native and nitrated CXCL8 with equal sensitivity. Total protein in the culture media was precipitated and subjected to detection by western blot. Indeed, we observed equivalent levels of CXCL8 between SIN-1 treated cells and control (Figure 5.8c). While we attempted to detect levels of nitrated CXCL8 within the precipitated protein, we did not observe any reactivity towards 3-nitrotyrosine antibody. We reasoned that this was in part due to the sub-nanogram quantities of CXCL8 released by HMEC-1 cells and the lack of sensitive and specific means for the detection and quantification of nitrated CXCL8.

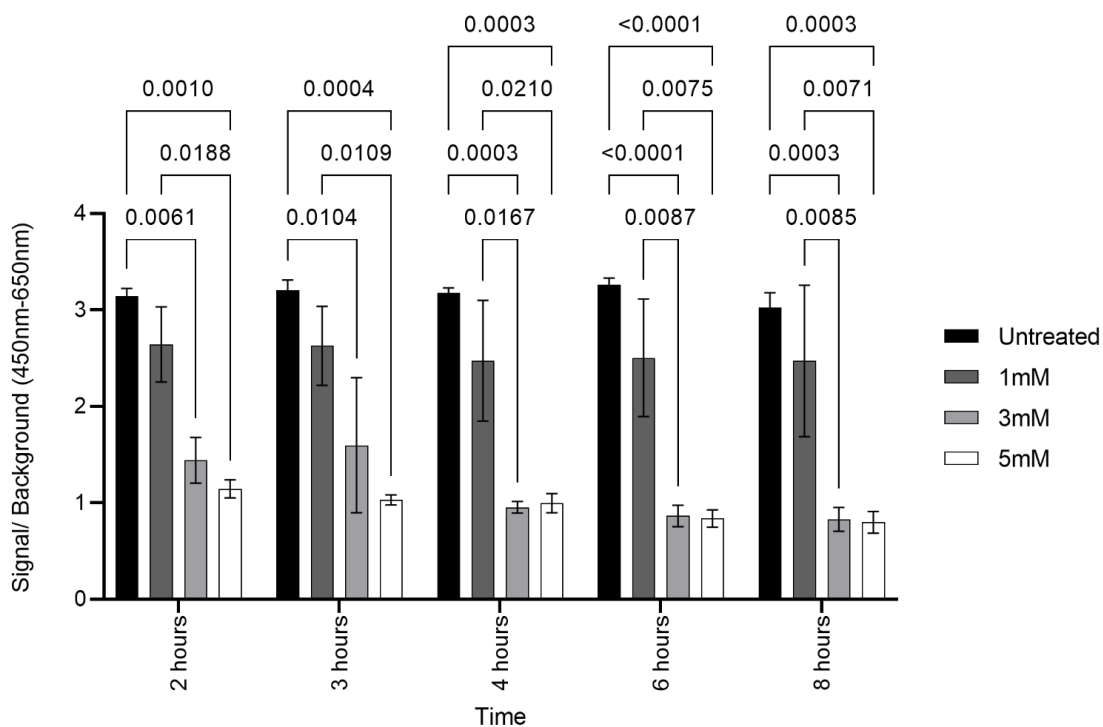


Figure 5.7 HMEC-1 viability in response to SIN-1.

Cells were treated with varying concentrations of peroxyxynitrite donor SIN-1 over time and viability was assessed using XTT assay. A significant reduction in cell viability was observed at 3mM and 5mM SIN-1 whereas 1mM showed no difference in cell viability across all the time points assessed. Treatment and viability assessments were carried out in technical triplicates. Data shown as mean \pm SD of n=3. Statistical analysis was performed using Two-Way ANOVA with Šídák post-hoc test.

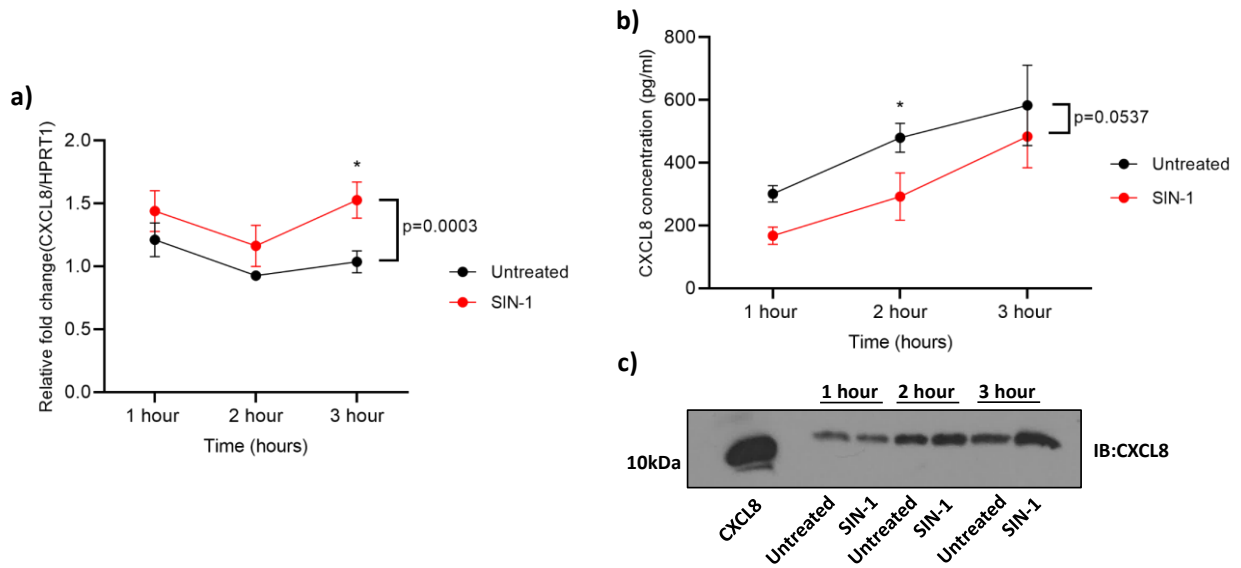


Figure 5.8 CXCL8 gene and protein expression in response to nitrosative stress.

HMEC-1 cells were pre-stimulated with TNF- α before exposing to 1mM SIN-1 over time. SIN-1 treatment of HMEC-1 resulted in an increase in a) CXCL8 gene expression compared to control. This increase in expression was also significant when directly compared between treatments at 3 hours. Levels of CXCL8 quantified by b) commercial ELISA kit indicated a reduction in CXCL8 production when HMEC-1 was exposed to SIN-1. This reduction was also significant when directly compared between treatments at 2 hours. Precipitated HMEC-1 secretome showed comparable levels of CXCL8 between SIN-1 exposure and control when detected using an antibody that showed equivalent detectability across variants. Treatment conditions were carried out in technical triplicates. Gene expression was normalised to HPRT1. Data shown as mean \pm SD of n=3 for a) and b). Western blot shown is representative of n=3. Statistical analysis was performed using Two-Way ANOVA with Šídák post-hoc test. *p < 0.05.

5.4.6. Detection of Nitrated CXCL8 in Lung Ischemia Reperfusion Injury.

Ex vivo normothermic perfusion has been utilised as a platform to assess potential allograft function before transplantation (Andreasson et al., 2017). Moreover, this platform also allows administration of therapeutics in aim to attenuate the inflammation associated with IRI and to further recondition marginal organs before transplantation. The capability to obtain tissue biopsies and biofluid pre- and post-perfusion of the organs also allows for in depth mechanistic study of IRI.

Unpublished work in the group has shown that administration of human amniotic epithelial cells (hAECs) in a split lung *ex vivo* perfusion model improved inflammatory profiles of lungs compared to the control arm (Dr Chelsea Griffith, PhD thesis). To identify the possible presence of nitrated CXCL8 post-perfusion, lung biopsies obtained post-perfusion were stained for both CXCL8 and 3-nitrotyrosine. Lungs perfused with hAEC showed a reduction in double positive cell infiltrates compared to control (Figure 5.9).

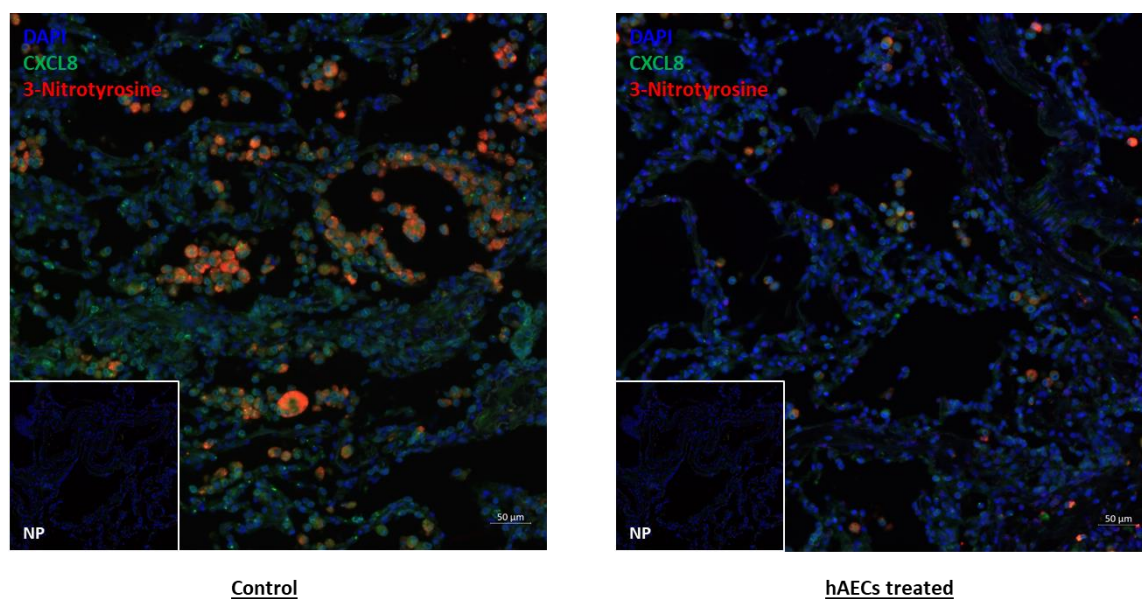


Figure 5.9 Lung immunofluorescence staining for the presence of nitrated CXCL8.

Human lungs were perfused *ex vivo* with human amniotic epithelial cells (hAECs) or control and tissue biopsies were obtained at the end of perfusion. Immunofluorescence staining for CXCL8 (green), 3-nitrotyrosine (red) and nuclei (blue) showed lungs perfused with hAECs have reduced cellular infiltrates that are positive for CXCL8 and 3-nitrotyrosine (orange) compared to control. Images are representative of n=3 pairs of lungs. Scale bar= 50μm.

5.4.7. Detection of Nitrated CXCL8 *In Vivo*

As part of immune surveillance, neutrophils are known to infiltrate tissue under steady state. However, their tissue distribution varies across organs. In particular, lungs have been shown to have extremely high counts of infiltrating neutrophils (Casanova-Acebes et al., 2018). We therefore reasoned that the lungs would be a good starting point for the detection of nitrated CXCL8.

High levels of CXCL8 are associated with many lung pathologies. One such condition is ventilator associated pneumonia. Accurate diagnosis of ventilator-associated pneumonia (VAP) has been particularly challenging due to the lack of clear clinical manifestations (Hellyer et al., 2015). However, it was reported that the levels of CXCL8 in bronchoalveolar lavage (BAL) functions as a good biomarker and assisted with the stewardship of antibiotics administration (Hellyer et al., 2020).

To confirm that the BAL samples from patients have a higher level of CXCL8, we first quantified the CXCL8 concentration using a commercial ELISA kit. Indeed, patients with VAP showed a significantly higher level compared to healthy control samples in which CXCL8 was almost undetectable (Figure 5.10). Following this, BAL samples were subjected to 3-nitrotyrosine immunoprecipitation and probed with anti-CXCL8 antibody to detect the presence of nitrated CXCL8. Within the antibody pulldown, antibody reactivity against CXCL8 was observed, thereby confirming that nitrated CXCL8 can be detected within the BAL samples from patients with VAP (Figure 5.11a). Furthermore, utilising an antibody developed specifically against nitrated CXCL8 generated previously within the group (Figure 5.11b), we went further to confirm the findings from the immunoprecipitations. 9 out of the 12 BAL samples from patients with VAP showed reactivity against the anti-nitrated CXCL8 antibody whereas this reactivity was absent in healthy controls (Figure 5.11c).

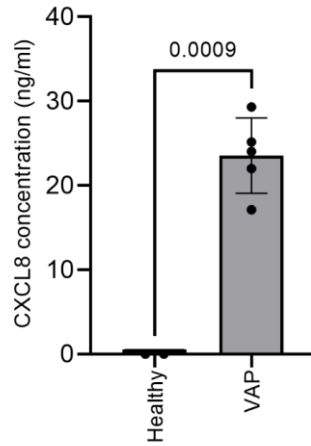


Figure 5.10 CXCL8 levels in bronchoalveolar lavage samples.

CXCL8 levels in bronchoalveolar lavage samples from patients with ventilator-associated pneumonia and healthy controls were quantified using commercial ELISA kit. Patients with confirmed VAP had significantly higher levels of CXCL8 compared to healthy controls. Data shown as mean \pm SD of n=2 for healthy control and n=5 for VAP. Statistical analysis was performed using an unpaired Student's T-test.

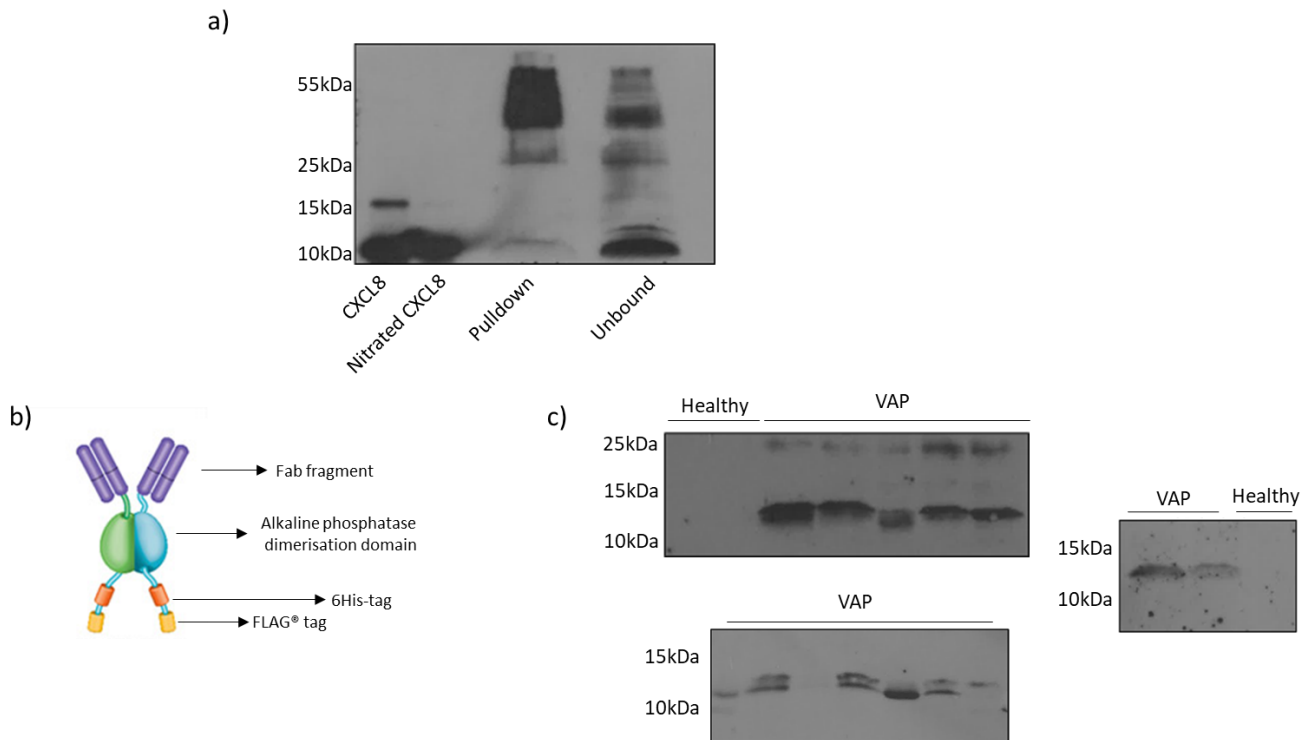


Figure 5.11 Detection of nitrated CXCL8 in Bronchoalveolar lavage samples.

BAL samples from patients with ventilator associated pneumonia were subjected to a) immunoprecipitation and subsequent detection with CXCL8 antibody. CXCL8 was detected in the pulldown fraction. b) An antibody specific for nitrated CXCL8 using phage display technology was developed previously in the group and showed reactivity in c) BAL samples from patients with ventilator associated pneumonia compared to healthy controls. Results shown are representative of a) n=3.

5.4.8. Mass spectrometry detection of nitrated CXCL8

Mass spectrometry detection of cytokines and chemokines are challenging (Nilsson et al., 2010). This is due to the complex matrix within the biological samples coupled with the huge dynamic range of protein abundance within biological fluids. Furthermore, low molecular weight proteins like cytokines and chemokines do not ionise well within the spectrometer which further limits their overall detectability (Nilsson et al., 2010).

Several strategies and workflows have been developed and optimised over the years to overcome such challenges. One such method recently developed for the quantification of CXCL8 within the biological samples is known as Immunosorbent Sample Preparation and Nano-Scale Liquid Chromatography-Tandem Mass Spectrometry for Proteoform Analysis (ISTAMPA) (Metzemaekers et al., 2021).

This involves utilisation of the acidic hydrolysis between the Aspartic acid- Proline (D-P) bond within CXCL8 with an optimised mass spectrometry condition to generate 2 distinct N-terminus and C-terminus fragments (Figure 5.12). Subsequently, utilising MRM mode, fractions were then selected, and relative intensities quantified.

CXCL8(1-77)

AVLPRSAKELRCQCICKTYSKPFHPKFIKELRVIESGPHCANTEIIVKLSDGRELCLDPKENWVQRVVEKFLKRAENS

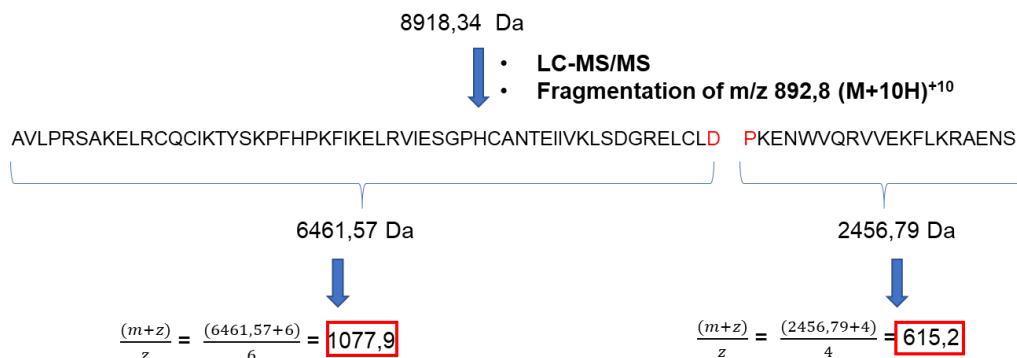


Figure 5.12 Fragmentation of CXCL8 and theoretical mass to charge (m/z) of CXCL8.

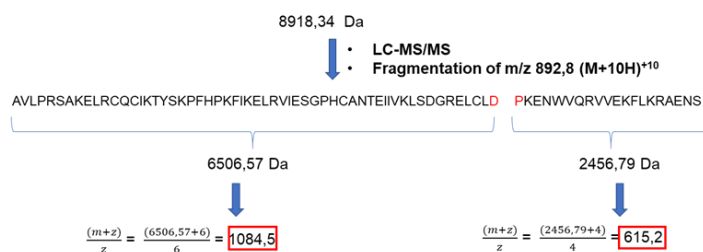
Theoretical calculation of CXCL8 fragmentation and m/z fragments from the N- and C- termini.

To first confirm that Y13 nitration of CXCL8 does not affect the ionisation pattern under the optimised conditions, nitrated CXCL8 was directly injected into the mass spectrometer. As shown in Figure 5.13, the ionisation of nitrated CXCL8 corresponded to the theoretical mass, confirming that nitration did not affect the generation of the ions. Next, nitrated CXCL8 was immunoprecipitation with magnetic beads conjugated to anti-CXCL8 antibody and analysed by mass spectrometry (Figure 5.14). Collectively, these experiments confirmed that nitrated CXCL8 detection is amenable to the ISTAMPA workflow.

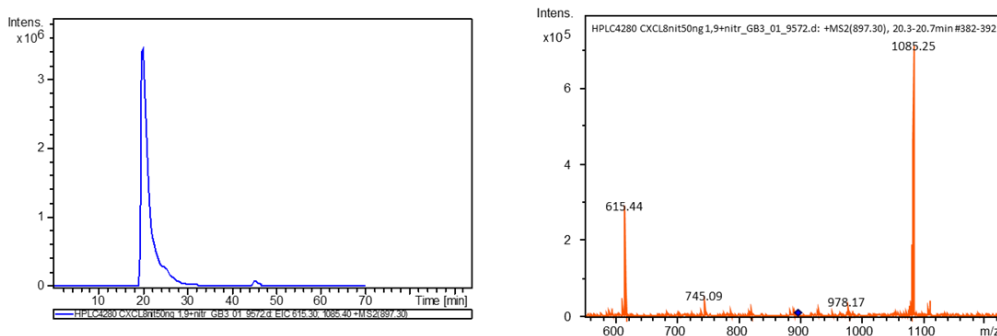
a)

Nitrated CXCL8(1-77)

AVLPRSAKELRCQCIKY(NO₂)SKPFHPKFIKELRVIESGPHCANTEIIVKLSGRELCLDPKENWVQRVVEKFLKRAENS



b)



Proteoform	Selected mother ion for fragmentation	Fragment ions	
CXCL8(1-77)	892.8 (10+)	615.3 (4+)	Without nitration
		1077.7 (6+)	
CXCL8(1-77) nitrated	897.3 (10+)	615.3 (4+)	Nitration on N-terminal fragment
		1085.4 (6+)	
CXCL8(1-77) double nitrated	901.1 (10+)	626.4 (4+)	Nitration on C-terminal fragment
		1077.7 (6+)	
		626.4 (4+)	Double nitration
		1085.4 (6+)	

Figure 5.13 Detection of nitrated CXCL8 using the ISTAMPA workflow.

a) Theoretical calculation of nitrated CXCL8 fragmentation and m/z fragments from the N- and C- termini. Nitrated CXCL8 was directly injected into liquid chromatogram-mass spectrometry (LC-MS) to identify the fragmentation and ionisation pattern. The b) chromatogram (left) and the mass spectra (right) of nitrated CXCL8 and the theoretical m/z of nitrated CXCL8 shown below.

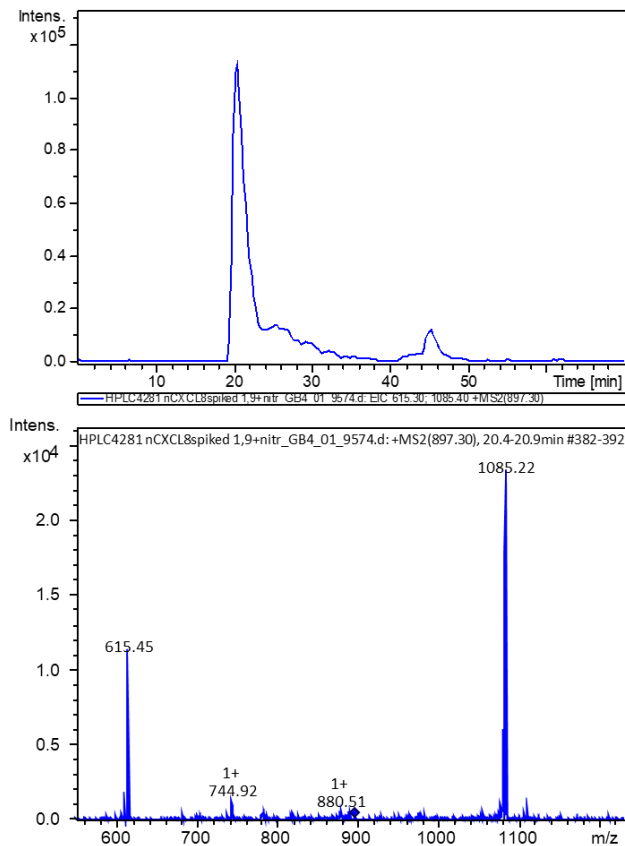


Figure 5.14 Nitrated CXCL8 detection post immuno-isolation.

Nitrated CXCL8 was incubation with a magnetic bead bound anti-CXCL8 antibody to assess antibody recognition and binding. Protein in the pulldown fraction was isolated and subjected to liquid chromatogram-mass spectrometry (LC-MS) detection. The chromatogram (top) and mass spectra (bottom) showed immuno-isolation of nitrated CXCL8.

5.4.9. Detection of CXCL8 proteoforms in bronchoalveolar lavage by mass spectrometry

CXCL8 has been shown to undergo post-translational modification within biological samples (Metzemaekers et al., 2021). Hence to increase the sensitivity of nitrated CXCL8 detection, we expanded the scope to include the possibilities of other nitrated CXCL8 proteoforms. Amongst the 12 VAP BALs, there are indications of 1 sample to carry 2 nitrated CXCL8 proteoforms and another to carry a single nitrated proteoform (Figure 5.15). However, due to the low abundance of these nitrated CXCL8 signals on the mass spectra, it still remains challenging to confidently determine their presence. Alongside the detection of the nitrated CXCL8, we also identified a total of 9 other proteoforms (Figure 5.16), suggesting that CXCL8 within an inflammatory environment is highly heterogenous.

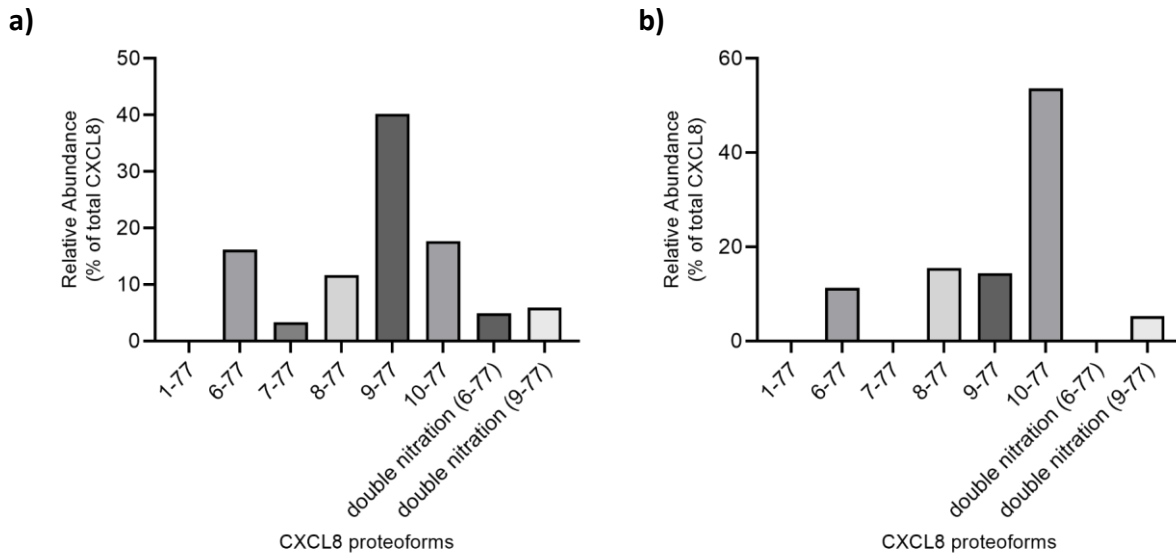


Figure 5.15 Nitrated CXCL8 detection within BAL samples by mass spectrometry.

BAL samples analysed by the ISTAMPA workflow identified 2 samples with nitrated CXCL8 proteoforms. Breakdown of a) patient 1 and b) patient 2 proteoform profile within the sample.

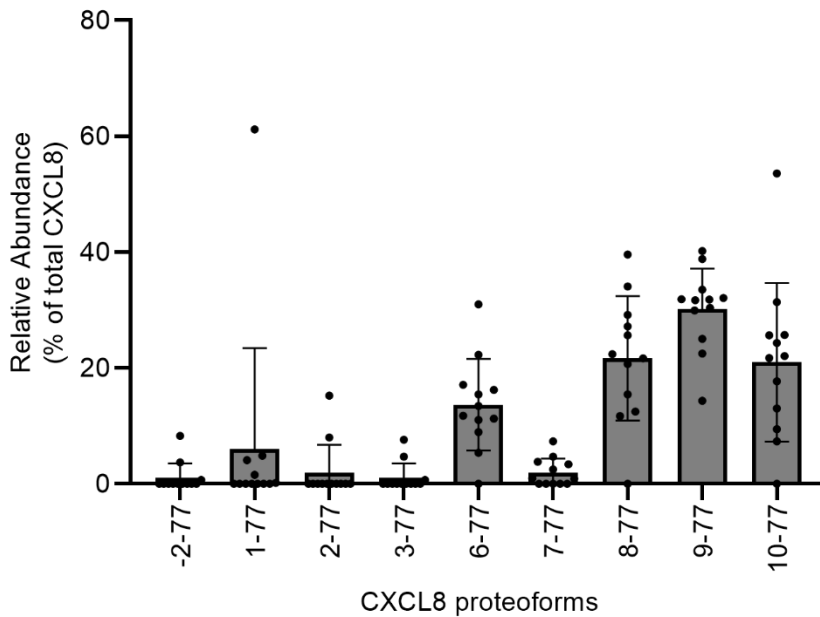


Figure 5.16 Total CXCL8 proteoforms detected within the BAL samples by mass spectrometry.

BAL samples subjected to ISTAMPA workflow and the relative abundance of each CXCL8 proteoforms confidently detected. Data shown as mean \pm SD of n=12.

5.5. Discussion

Effective inflammatory response requires rapid initiation and subsequent resolution upon the removal of stimuli. This often requires a timely orchestration of cellular activities including migration. Amongst these, the release of CXCL8 has immense capabilities to potentiate inflammation by recruiting neutrophils to the vicinity. While the production and spatiotemporal regulation have been well understood, understanding on the clearance of CXCL8 post inflammation remains limited. Erythrocytes express ACKR1, scavenging free CXCL8 and preventing high levels of circulating chemokines (Darbonne et al., 1991). Coupled with the cognate receptor mediated internalisation (Basran et al., 2013), this ensures not only a formation of tight chemokine gradient but also prevents non-specific desensitisation of neutrophils.

To add to the knowledge regarding the turnover of chemokines within an inflammatory milieu, we showed in this chapter that nitration renders CXCL8 non-functional in part due to perturbed interactions with both the GAGs and receptors. Sitting on the unstructured N-terminus loop of CXCL8, the likelihood of functional changes as a result of global structural modification introduced by the nitro-group is unlikely. This was confirmed by our circular dichroism data showing that secondary structure between native and nitrated CXCL8 remains similar.

The addition of the nitro group to tyrosine residues causes the amino acid to exist in an ionised state at physiological pH, resulting in a more polar side chain compared to native tyrosine residues (Filippis et al., 2009). In the context of CXCL8, many amino acids with important functional roles reside on the N-terminus in the periphery of the sole tyrosine residue. These include H18 and K20 as well as K15 (Figure 5.17), which form the core and peripheral binding residues respectively and are essential to interact with the negatively charged GAGs through electrostatic force and hydrogen bonding (Lortat-Jacob et al., 2002, Joseph et al., 2015). Since the tyrosine residue Y13 is in close proximity to these important amino acids that bind to GAGs, it is unsurprising that the introduction of a polar group in turn resulted in lower affinity, as shown by the GAG binding assays.



Figure 5.17 CXCL8 peptide sequence.

The full peptide sequence of CXCL8 was shown and the amino acid contribution to overall structure was indicated below. Cysteine residues contributing to the “CXC” motif are highlighted in red and the “ELR motif” in blue. Numbers above the peptide sequence corresponds to the starting amino acid for the various CXCL8 proteoforms.

We also showed that nitrated CXCL8 downregulated CXCR1 and CXCR2 signaling. Indeed, overlaps in the residues involved in GAG binding and receptor recognition have previously been identified. In fact, GAG bound CXCL8 monomer and dimer were incapable of receptor binding (Joseph et al., 2017). Moreover, many studies used site-specific mutagenesis or chemokine chimeras to show that the binding affinity and activation of the receptors by chemokines are mediated via a two-step, two-site model (Rajagopalan and Rajarathnam, 2009). This model was further supported by the recent molecular dynamics (Sepuru et al., 2020) and Cryo-EM studies (Liu et al., 2020). The differences in the β-arrestin recruitment observed between CXCR1 and CXCR2 in nitrated CXCL8 was also in concordance with a previous mutagenesis study, highlighting a greater importance of Y13 residue in CXCR1 than in CXCR2 (Lowman et al., 1996).

While CXCL8 variants tested *in vitro* are at concentrations far below their dimerisation constant, we posit that the nitration at the tyrosine residue sits far from the dimerisation domains (Figure 3.17, β-1 strand). Hence, there should not be alteration to the binding affinity. Furthermore, the implications to the overall function remains low since dimeric CXCL8 are shown to be the low affinity ligand for both receptors (Nasser et al., 2009).

Alongside the characterisation of nitrated CXCL8, we also attempted to model the inflammatory milieu *in vitro*. Treatment of endothelial cells with SIN-1 induced an upregulation of CXCL8 gene expression which can be attributed to the direct NF-κB activation by peroxynitrite (Zouki et al., 2001, Cooke and Davidge, 2002). When CXCL8 was quantified in the culture media using commercial ELISA, SIN-1 treated cells showed a reduction in detectable levels which is, contrary to what was reported (Zouki et al., 2001). Here, we reasoned that this reduction was due to the loss of epitope recognition as previously reported for CCL2 (Molon et al., 2011).

However, the overall yield of protein nitration is generally low (Souza et al., 2008), therefore the identification of nitrated CXCL8 in this *in vitro* system would be challenging. Hence, we pivoted to biological samples with high levels of CXCL8 to increase the potential detectability of nitrated CXCL8. This also emphasises the physiological relevance of nitrated CXCL8 as the majority of other nitrated chemokines were generated *in vitro* and not identified in *in vivo* settings (Sato et al., 1999, Sato et al., 2000b, Janssens et al., 2016). Utilising immunoprecipitation, nitrated CXCL8 was confirmed in BAL samples from patients with VAP. To further remove any ambiguity of nitrated CXCL8 detection, an antibody was generated specifically against this modified variant of CXCL8 and its presence was confirmed in these samples. Leveraging on the recently ISTAMPA workflow, we also attempted to show the presence of nitrated by mass spectrometry. Due to the low abundance of nitrated CXCL8 within these biological samples, the signature of nitrated CXCL8 was only detected in 2/12 samples.

Instead, we confidently identified a total of 9 CXCL8 proteoforms within the BAL samples from patients with VAP of which 7 are a result of enzymatic truncation. This highlights the heterogeneity of CXCL8 within an inflammatory state as overall susceptibility of CXCL8's N-terminus to enzymatic truncation. The repertoire of CXCL8 proteoforms was also reflected in synovial fluids from patients with arthritis (Metzemaekers et al., 2021), suggesting that this observation is not unique to the lungs.

The removal of the first 9 amino acids on the N-terminus of CXCL8 has been shown to increase the overall activity either by modulating receptor signaling or GAG binding capabilities (Cambier et al., 2023). Moreover, this also supports the notion that the inflammatory environment potentiates CXCL8 activities. What was different in the CXCL8 proteoforms detected in the BAL samples were the high levels of 10-77 amino acid CXCL8 (Figure 3.17). Unlike the other 8 proteoforms, the truncation of the 9th amino acid removes the glutamic acid from the essential important Glu-Leu-Arg (ELR) motif for interaction with CXCR1 and CXCR2 (Hébert et al., 1991, Clark-Lewis et al., 1991, Liu et al., 2020). Removal of this glutamic acid also renders CXCL8 non-functional (Clark-Lewis et al., 1991) and had never been identified *in vivo*.

What remains to be elucidated is the mechanism behind the generation of this highly truncated proteoform. One stark difference is that synovial joints are relatively sterile as compared to the lungs are constantly exposed to the external environment. This constant challenge with inflammatory stimuli might result in site specific adaptations unique to the lungs to resolve local inflammation. Furthermore, pathogens such as *streptococcus pyogenes* (Zinkernagel et al., 2008) and *porphyromonas gingivalis* (Dias et al., 2008) have been previously identified to produce enzymes that can result in truncation of CXCL8. With the difference in disease etiology between VAP and arthritis (bacterial and autoimmune respectively), it may also be possible that truncation to generate this proteoform might be a result of an immune evasion mechanism derived from a pathogen.

In summary, this chapter characterised and identified the mechanism driving the loss of function in nitrated CXCL8. We also identified various post-translational modifications within VAP and showed the heterogeneity of CXCL8 within the inflammatory environment. While we did not identify the mechanism behind the formation of the 10-77 amino acid CXCL8, we reasoned that these post-translational modifications *in vivo* collectively assist in the resolution of inflammation.

6. miRNA Regulation in Glomerular Endothelium

6.1. Introduction

The kidney has a multifaceted role in ensuring normal body functions, resulting in it being one of the most energetically demanding organs. This includes the removal of waste products of protein metabolism, maintenance of fluid and electrolyte homeostasis and also functioning as an endocrine organ. In turn, this makes kidneys highly susceptible to IRI which triggers the onset of acute kidney injury (AKI). In the context of transplantation, AKI results in delayed graft function (DGF), which is associated with poor short- and long-term outcomes in the transplant recipients (Siedlecki et al., 2011).

The proximal tubular epithelial cells are the most abundant cell type present within the kidney and are essential for reabsorption of water and electrolytes (Stewart et al., 2019, Parikh et al., 2022). Besides playing an important function within the kidney, proximal tubule epithelial cells are also the most susceptible to IRI (Balzer et al., 2022). Hence, they have been extensively researched to understand how IRI results in the alteration and perturbation to overall cell function and survival. (Kusaba et al., 2013, Balzer et al., 2022). However, the cellular complexity within the kidney is extremely high and our understanding of some of the other cell types remains relatively limited.

The glomerular endothelium are highly fenestrated endothelial cells that line the inner capillary walls within the glomeruli. Together with the glycocalyx, basement membrane and podocytes, these cells and structures collectively function as a selective filtration barrier for the nephrons. However, there is limited understanding of the impact of IRI on these specialised endothelial cell in part due to the glomerular endothelium representing a small subset of the endothelial cell population present within the kidneys (Stewart et al., 2019, Parikh et al., 2022, Menon et al., 2022, Shan et al., 2023) as highlighted by single-cell RNA-sequencing. Furthermore, the difficulty in maintenance of these cells *in vitro* due to the early onset senescence as well as the alteration in cellular phenotype in culture (Satchell et al., 2006) over a long duration makes it even more challenging.

This chapter aims to understand how the transcriptome of the glomerular endothelium changes in response to hypoxia, a hallmark of IRI, and provide mechanistic insights into how these specialised endothelial cells adapt to cellular stress *in vitro*.

6.2. Specific Aims

- miRNA profiling of glomerular endothelial cells in response to hypoxia.
- Identification of the mRNA targeted by the differentially expressed miRNA.
- Functional implication of the differentially expressed miRNA.

6.3. Specific Materials and Methods

6.3.1. Hypoxia and Re-oxygenation

80,000 cells/well were seeded in 12-well plates and left to grow either overnight (HGENCs and PTECs) or 5 days (ciGenCs) at 37°C in normoxia (21% O₂). Spent culture media was removed and cells were washed with 1mL PBS before replacing with 1ml of complete media. Immediately, cells were transferred to a hypoxic (1% O₂) incubator (Sanyo) and cultured for up to 24 hours. For re-oxygenation experiments, cells were removed from the hypoxic incubator and spent media was removed. Subsequently, cells were washed with 1mL PBS before replacing with 1mL of complete media and cultured for up to further 48 hours.

6.3.2. XTT Assay

A spectrophotometric assay was used to assess HGENC viability as well as nicotinamide adenine dinucleotide (NADH)/nicotinamide adenine dinucleotide phosphate (NADPH) levels post-treatment. In brief, 10,000 cells were seeded per well in 96 well plates and cultured overnight. Cells were treated in hypoxia or transfected with miR-210-3p mimics for 24 hours. Post treatment, media was removed, and cells were washed with PBS before replacing with 100µL of complete media. 50µL of XTT labelling mixture (Roche) consisting of 50 parts XTT labelling reagent: 1 part electron coupling reagent were added to each well (to obtain a final volume of 150µL) and incubated for 24 hours in normoxia. Corrected absorbance corresponding to cell viability was obtained by subtracting background (650nm) signal from 450nm using a plate reader (Synergy™, BioTek).

6.3.3. miRNA-Sequencing

HGEnCs from 3 biological donors were subjected to hypoxia over a time course of 4 hours, 12 hours and 24 hours as outlined in Section 4.3.1. Total RNA was extracted as described in Section 4.3.2. Isolated RNA was submitted to Qiagen for miRNA sequencing.

6.3.3.1. Library Preparation

The library preparation was done using QIAseq miRNA Library Kit (Qiagen). A total of 5µl total RNA was converted into miRNA next generation sequencing (NGS) libraries. Adapters containing UMIs were ligated to the RNA. Then RNA was converted to cDNA. The cDNA was amplified using PCR (16 cycles) and during which the PCR indices were added. After PCR, the samples were purified. Library preparation was quality controlled using capillary electrophoresis. Based on quality of the inserts and the concentration measurements the libraries were pooled in equimolar ratios. The library pool(s) were quantified using qPCR. The library pool(s) were then sequenced on a NextSeq (Illumina® Inc.) with 75 base pair single ended reads. Raw data was de-multiplexed and FASTQ files for each sample were generated using the bcl2fastq software (Illumina® Inc).

6.3.3.2. Read Mapping, Quantification and Gene Expression

All primary analysis is carried out using the Qiagen CLC Genomics Sever 21.0.4. The workflow “QIAseq miRNA Quantification” of CLC Genomics Server with standard parameters is used to map the reads to miRBase version 22. In short, the reads are processed by (1) trimming of the common sequence, UMI and adapters, and (2) filtering of reads with length < 15 nucleotides or length > 55 nucleotides. They are then de-duplicated using their UMI. Reads are grouped into UMI groups when they (1) start at the same position based on the end of the read to which the UMI is ligated, (2) are from the same strand, and (3) have identical UMIs. Groups that contain only one read (singletons) are merged into non-singleton groups if the singleton’s UMI can be converted to a UMI of a non-singleton group by introducing an SNP (the biggest group is chosen).

All reads that do not map to miRBase, either with perfect matches or as isomiRs (maximum 2 mismatches and/or alternative start/end position of 2 nucleotides), are mapped to the human genome GRCh38 with ENSEMBL GRCh38 version 97 annotation. This is carried out using the “RNA-Seq Analysis” workflow of CLC Genomics Server with standard parameters. The ‘Empirical analysis of DGE’ algorithm of the CLC Genomics Workbench 21.0.4 was used for differential expression analysis with default settings which implemented ‘Exact Test’ for two-group comparisons and incorporated in the EdgeR package (Chen et al., 2016). 500 genes with the highest variance were used for the principal component analysis. The variance was calculated agnostically to the pre-defined groups (blind=TRUE). 35 genes with the highest variance across samples were selected for hierarchical clustering. Significantly differentially expressed miRNA are defined as $\text{padj} < 0.05$.

6.3.4.mRNA Sequencing

HGENCs from 3 donors were subjected to hypoxia over a time course of 4 hours, 12 hours and 24 hours as outlined in Section 4.3.1. Total RNA was extracted as described in Section 4.3.2. Isolated RNA was submitted to Newcastle Genomics Services for mRNA sequencing.

6.3.4.1. Library Preparation

The library preparation was done using TruSeq Stranded mRNA Library Kit (Illumina® Inc). mRNA was enriched using oligo-dT magnetic beads and fragmented. Then mRNA was converted to double stranded cDNA before ligating on sequencing adapters and indexing barcodes. The cDNA was amplified using PCR (16 cycles) and subsequently purified. Library preparation was quality controlled using capillary electrophoresis. Based on quality of the inserts and the concentration measurements the libraries were pooled in equimolar ratios. The library pool(s) were then sequenced on a NextSeq (Illumina® Inc.) with 75 base pair single ended reads. Raw data was demultiplexed and FASTQ files for each sample were generated using the bcl2fastq software (Illumina® Inc).

6.3.4.2. Read Mapping, Quantification and Gene Expression

Data analyses were carried out in R. In brief, FASTQ files for each sample were merged with the package Rfastp before assessing read quality. Subsequently, raw FASTQ files were processed by (1) adapter sequence trimming and (2) filtering with minimum nucleotide length ≥ 20 using Trimmomatic. Reads were then mapped to the human genome Gencode GRCh38 V40 using RHISAT2 V3.15, and BAM files were passed to Rsubread V3.16 featurecounts function for reads quantification. Protein-coding genes were filtered before passing on for unsupervised analysis using DESeq2 V3.16 (Love et al., 2014). 200 genes with the highest variance were used for the principal component analysis. 35 genes with the highest variance across samples were selected for hierarchical clustering. Wald test was used for hypothesis testing when comparing between 2 groups. The likelihood ratio test was used for the testing for deviances from the DESeq2 full model from the reduced model. K-means clustering algorithm from base R was utilised to cluster the differential expressed genes (DEGs) from the likelihood ratio test. Significantly differentially expressed genes (DEGs) are defined as $p_{adj} < 0.05$.

6.3.5. Gene-Set Enrichment Analysis (GSEA)

Normalised count matrix from DESeq2 was used as input files for GSEA analysis (Subramanian et al., 2005) using the GSEA software developed by the Broad Institute. Analysis was carried out with the “Hallmark Gene Sets” from the Molecular signature database (MsigDB). Phenotype labels were created for individual comparisons and a continuous phenotype label was also generated for analysis of the time-course.

6.3.6. Over-representation Analysis

Significant genes from each comparison were analysed for pathway enrichment using Gene Ontology Analysis (Ashburner et al., 2000) and the top 15 pathways were plotted using ggplot2.

6.3.7. Transfection

ciGENCs were seeded at 80,000 cells/ well and cultured at 37°C for 5 days. After which, cells were washed and replaced with 1mL antibiotics free EGM™-2MV. Separately, 1µL of Lipofectamine™ RNAiMAX (Invitrogen) was added to 99µL of Opti-MEM™ I Reduced Serum Media (Gibco™) and incubated with 100µL of RNA duplex diluted in Opti-MEM™ I Reduced Serum Media at room

temperature for 15mins. Following incubation, the total mix was added to the ciGENCs and incubated for 24 hours.

6.3.7.1. Efficiency Assessment

Cells were transfected with a final concentration of AlexaFluor647 labelled AllStar Negative control siRNA (Qiagen) ranging from 1nM-50nM. Media containing the transfection mix was removed and cells were washed with PBS. Subsequently, cells were lifted with Accutase® before spinning down at 300g, 5mins. Cells were washed twice with PBS before incubation with Live/Dead™ Fixable Blue Dead Cell Stain (Invitrogen) for 30mins on ice according to manufacturer's protocol. Cells were washed twice with ice-cold PBS before the addition of 100µL 4% PFA and incubated at room temperature for 15mins. PFA was discarded and cells were washed twice with 1mL ice-cold PBS and was resuspended in 2% BSA PBS before data acquisition on Fortessa X20 flow cytometer. Data analysis was then done on FlowJo V9. Figure 6.1 shows the gating strategy for the analysis.

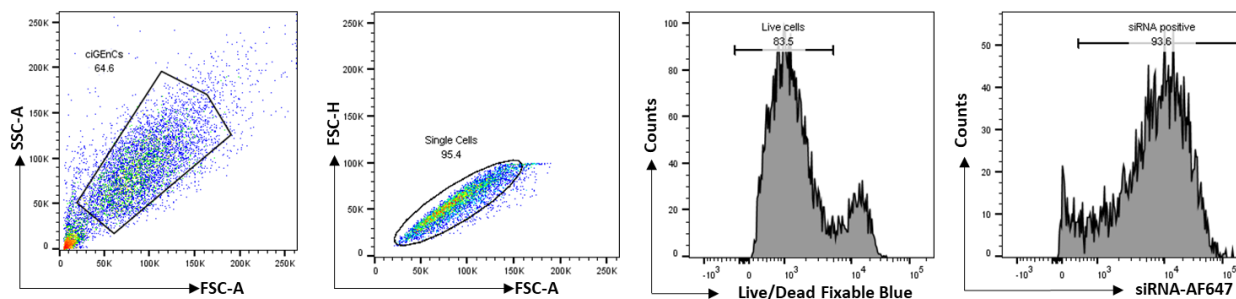


Figure 6.1 Gating strategy for transfection efficiency determination.

The cell population was first gated based off scatter profile before identifying the single cell population. Subsequently, live cells were identified as a Live/Dead™ Fixable Blue negative population and gated for AlexaFluor647 signal.

6.3.7.2. miR-210-3p Transfection

37.5nM of miR-210-3p (Qiagen) or Allstar Negative control siRNA (Qiagen), which gives a final concentration of 3.125nM was carried forward as determined in Section 6.3.7.1. Media containing the transfection mix was removed and cells were washed with PBS. Cells were lysed immediately as outlined in Section 4.3.1 or replaced with fresh media containing antibiotics and rested for an additional 24 hours before lysis. Target validation was carried out using mRNA PCR as outlined in Section 4.3.4 and 4.3.6.

6.3.8. Transferrin Receptor 1 (TfR1) Surface Expression

ciGENCs were transfected with 3.125nM of miR-210-3p or AllStar Negative control siRNA for 24 hours. Cells were stained for surface transferrin receptor (CD71/TfR1) and expression assessed by via flow cytometry as outlined in Section 4.6. Data analysis was then carried out using FlowJo V9. Figure 6.2 shows the gating strategy for the analysis.

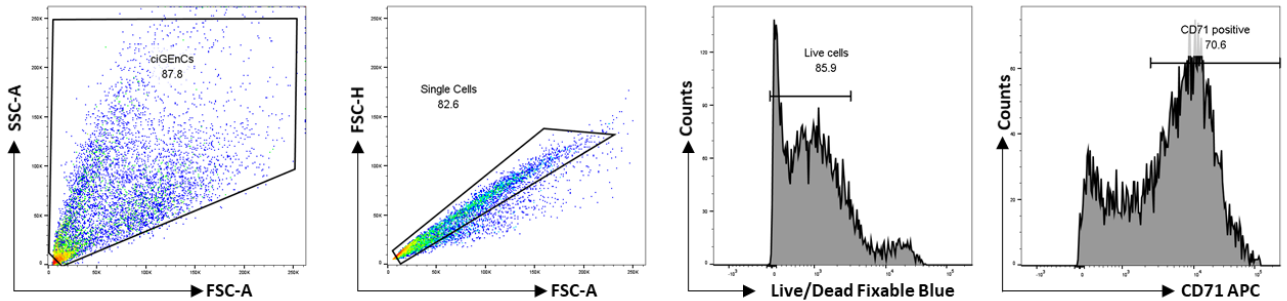


Figure 6.2 Gating strategy for CD71 expression on ciGENCs.

The cell population was first gated based on scatter profile before identifying the single cell population. Subsequently, live cells identified as a Live/Dead™ Fixable Blue negative population was gated for APC signal. Positive gate for CD71 was drawn based on the unstained and isotype control samples.

6.3.9. Mitochondria Ultrastructure Visualisation

ciGENCs were transfected with a final concentration of 3.125nM of miR-210-3p or AllStar Negative control siRNA for 24 hours. Media containing the transfection mix was removed and cells were washed with PBS. Subsequently, cells were lifted with Accutase® before being spun down at 220g, 5mins. Supernatant was decanted and the cell pellet was resuspended in 1mL of 2% glutaraldehyde in 0.1M sodium cacodylate buffer, pH7.4 (supplied by Newcastle Electron Microscopy Research Services). The cell suspension was transferred to a 1.5mL tube and centrifuged at 300g, 5mins using a swing bucket rotor. Supernatant was discarded and cell pellet was resuspended in 1mL 2% glutaraldehyde in 0.1M sodium cacodylate buffer, pH7.4 and submitted to Newcastle Electron Microscopy Research Services.

Briefly, secondary fixation in 1% osmium tetroxide (Agar Scientific) was carried out on the cells before coated in 4% agarose. The cells were then dehydrated in 25%, 50% and 70% acetone for 30mins each before transferring to 100% acetone for 2× 60mins. The dehydrated cells were then placed in 100% epoxy resin (TAAB Laboratories Equipment) for a minimum of 3 changes over 24 hours and finally embedded in 100% resin at 60°C for an additional 24 hours.

Subsequently, 0.5µm semi-thin survey sections were obtained from the epoxy embedded cells and stained with 1% toluidine blue in 1% borax (Leica). Ultrathin sections (70nm) were obtained using a diamond knife on an ultramicrotome (Leica) before stretching with chloroform and mounted on Pioloform-filmed copper grids (Agar Scientific). Finally, a drop of 1% uranyl acetate was added to the grid and stained for 30secs. Excess uranyl acetate was removed, and the grid was dried under a lamp. The grids were then imaged on a 120kV TEM (Hitachi HT7800) attached with a XAROSA CMOS camera (EMSIS).

6.3.10. Real-time Cell Metabolic Assays

10,000 ciGEnCs were seeded into Seahorse XF96 V3 PS cell culture microplates (Agilent) and cultured for 5 days at 37°C. The day before the experiment, cells were transfected with 3.125nM of miR-210-3p mimic or scramble control and left to culture for 24 hours. The sensor cartridge was hydrated with 200µL of Seahorse calibrant (Agilent) overnight in a 37°C non-carbon dioxide (CO₂) incubator.

6.3.10.1. Mitostress Test

On the day of the experiment, the culture media containing transfection mix was removed and cells were washed with PBS. Subsequently, 180µL of Seahorse basal medium (Agilent) containing 1mM pyruvate (Sigma), 2mM L-glutamine (ThermoFisher) and 5.55mM D-glucose, pH 7.4 was added to each well and left for 1 hour in a 37°C non-carbon dioxide (CO₂) incubator. 20µL of 10mM Oligomycin (Sigma), 22µL of 10mM carbonyl cyanide-p-trifluoromethoxyphenylhydrazone (FCCP) and 25µL of 5mM rotenone (Sigma) together with 5mM antimycin A (Sigma) was added to ports A, B and C respectively of the sensor cartridge. Immediately, the sensor cartridge was placed in the Seahorse XF96 extracellular flux analyser (Agilent) for calibration following the Wave software V2.6.3 guide for Mitostress assay. Once calibration was completed, the companion plate was removed and replaced with the cells and the assay was carried out with the standard parameters.

6.3.10.2. Glycolysis Stress Test

On the day of the experiment, the culture media containing transfection mix was removed and cells were washed with PBS. Subsequently, 180µL of Seahorse basal medium (Agilent) containing 2mM L-glutamine (ThermoFisher), pH 7.4 was added to each well and left for 1 hour in a 37°C non-carbon dioxide (CO₂) incubator. 20µL of 200mM D-glucose, 22µL of 10mM Oligomycin (Sigma) and 25µL of 500mM 2-deoxyglucose (Sigma) was added to ports A, B and C respectively of the sensor cartridge. Immediately, the sensor cartridge was placed in the Seahorse XF96 extracellular flux analyser (Agilent) for calibration following the Wave software V2.6.3 guide for Glycolysis stress assay. Once calibration was completed, the companion plate was removed and replaced with the cells and the assay was carried out with the standard parameters.

6.3.10.3. Normalisation

To quantify cell count per well, culture media was removed, and cells were washed with 200 μ L PBS. Subsequently, cells were fixed with 4% PFA for 10mins at room temperature and stained with 1 μ g/mL of DAPI for 20mins at room temperature. The plate was then imaged with CellDiscoverer 7 (Zeiss) high-content imager before segmentation and cell counts on ImageJ (NIH) using a custom script. The cell counts were then imported into the Wave software for normalisation of cells between wells.

6.4. Results

6.4.1. Viability of HGEEnC Remains Unchanged in Hypoxia

Prior to the identification of HGEEnC transcriptomic changes, we first assessed the viability of the cells in a hypoxic environment. As indicated in Figure 6.3, there was no reduction in the viability of the cells post exposure to hypoxia. Instead, we observed a non-significant increase in the signal in the hypoxia treated cells. During hypoxia, the lack of oxygen prevents oxidative phosphorylation, which in turn results in accumulations of NADH and NADPH. Since these are the primary co-factors involved in the reduction of XTT to formazan, an increase in signal from hypoxia treated cells confirmed the induction of a hypoxic response.

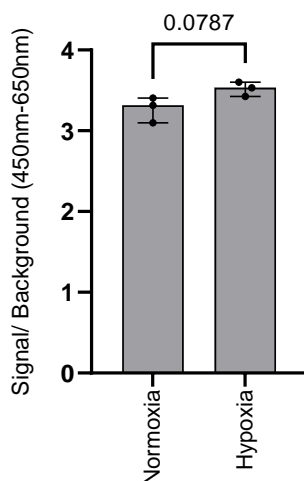


Figure 6.3 Viability assessment of HGEEnC in hypoxia.

Cells were cultured in 1% oxygen and viability was assessed via XTT assay. A non-significant increase in signal was detected in cells cultured in hypoxia compared to control. Treatment and viability assessments were carried out in technical triplicates. Data shown as mean \pm SD of n=3 biological replicates. Statistical analysis was performed using an unpaired student T-test.

6.4.2. miRNA Expression Clustered by Biological Replicates

To assess how hypoxia regulates miRNA expression in HGENC, cells were cultured in 1% oxygen for 4 hours, 12 hours and 24 hours to mimic acute and chronic hypoxia. miRNA sequencing of the HGENC cells showed that the top 10 miRNA transcripts identified accounted for 65% of the total miRNA detected (Figure 6.4a). Amongst them, the most abundant miRNA sequenced was miR-126. This miRNA is known to have its expression restricted to endothelial cells, thereby confirming that the cells were indeed of endothelial origin (Wienholds et al., 2005, Wang et al., 2008). When dimension reduction was applied to the samples, we observed a clustering by biological replicate, suggesting that the hypoxia treatment did not result in extensive perturbation of the miRNA expression (Figure 6.4b). This was further confirmed by hierarchical clustering with no discreet clusters observed (Figure 6.4c).

6.4.3. Hypoxia Induced only miR-210-3p Upregulation

Endothelial cells cultured in hypoxia have previously been reported to show minimal changes to miRNA expression (Voellenkle et al., 2012). In concordance with published literature, only miR-210-3p was significantly upregulated when HGENCs were exposed to hypoxia for 12 hours (Figure 6.5b) and 24 hours (Figure 6.5c) (Voellenkle et al., 2012). Furthermore, short-term exposure (4 hours) to low oxygen did not result in any significant changes to the miRNA expression (Figure 6.5a).

The upregulation of miR-210-3p in response to hypoxia has been previously identified to be a ubiquitous response in all cell types (Fasanaro et al., 2008, Huang et al., 2009, Liu et al., 2017, Virga et al., 2021). This is in part due to the presence of hypoxia response element (HRE) in the promoter region (Huang et al., 2009, Kulshreshtha et al., 2007). The finding by miRNA-seq was confirmed by qPCR of HGENCs cultured under hypoxic conditions (Figure 6.6a). Furthermore, to assess whether other cell types in the kidney have similar responses, PTECs were also subjected to similar culture conditions. As shown in Figure 6.6b, a similar miR-210-3p expression pattern was observed, although variability between biological donors were more apparent compared to HGENCs.

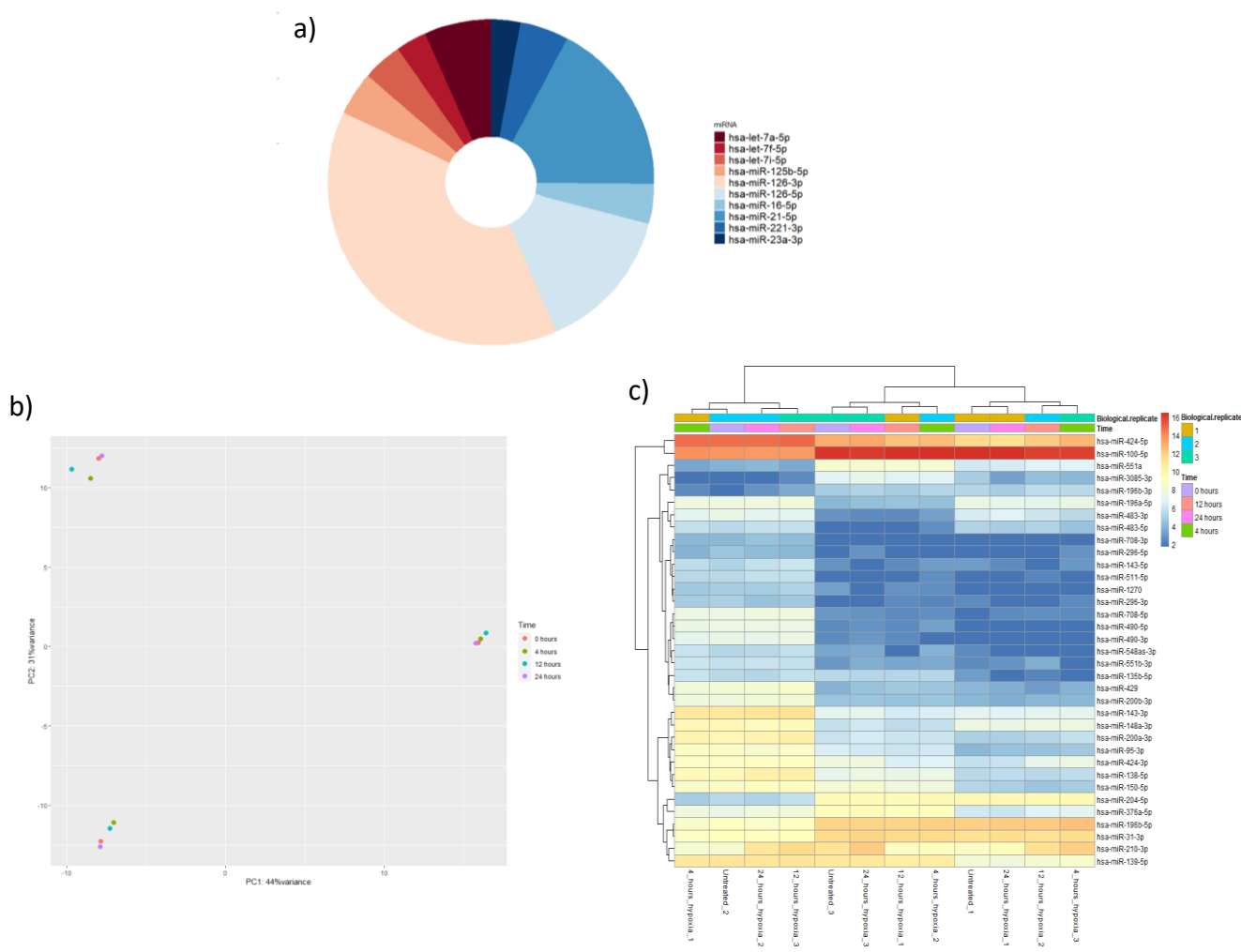


Figure 6.4 miRNA-sequencing of hypoxia treated HGENCs.

Cells were cultured in 1% oxygen for 4, 12 and 24 hours. Isolated RNA was sequenced to profile miRNA changes in response to hypoxia over time. a) The top 10 transcripts across all samples were shown as the donut plot, which accounted for 65% of the total miRNA detected. b) PCA clustering of the miRNA expression of the hypoxia treated HGENCs showed clustering by biological replicate. c) Hierarchical clustering did not show any trend in the clustering of the miRNA expression.

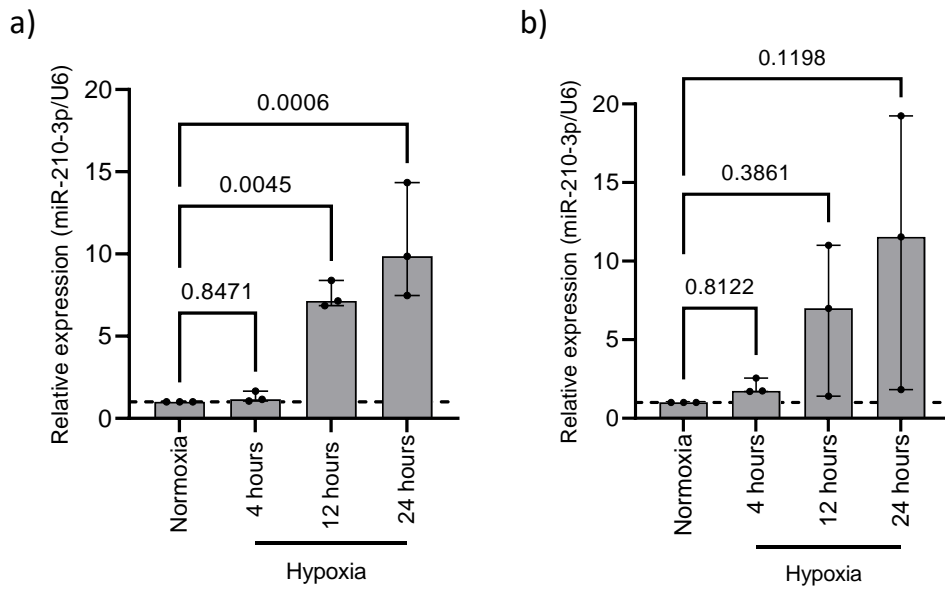


Figure 6.6 miR-210-3p upregulation across HGENCs and PTECs.

Cells were cultured in 1% oxygen for 4 hours, 12 hours and 24 hours before analysing the expression of miR-210-3p. An overall trend of miR-210-3p increase was observed over time in both a) HGENCs and b) PTECs. Statistical significance was observed in HGENCs at 12 hours and 24 hours but not in PTECs. miR-210-3p expression was normalised to U6. Data shown as mean \pm SD of n=3 biological replicates. Statistical analysis was performed using One-way ANOVA with Holm-Šídák post-hoc test.

6.4.4. miR-210-3p Remained Upregulated Post-Hypoxia

The turnover and processing of mature miRNAs are not well understood and highly cell type specific. Various miRNAs have reported half-lives ranging from minutes (Krol et al., 2010, Gantier et al., 2011) to weeks (Rooij et al., 2007, Gantier et al., 2011) after induction and maturation. For miR-210-3p, it was identified to be elevated for 8 hours in endothelial cells post-reoxygenation (Fasanaro et al., 2008). To determine the miR-210-3p turnover rate in HGENCs and PTECs, cells were subjected to 24 hours hypoxia before re-oxygenation. Levels of miR-210-3p remained stable over the course of 48 hours post-reoxygenation in HGENCs (Figure 6.7a) whereas a time dependent decrease was observed in PTECs (Figure 6.7b).

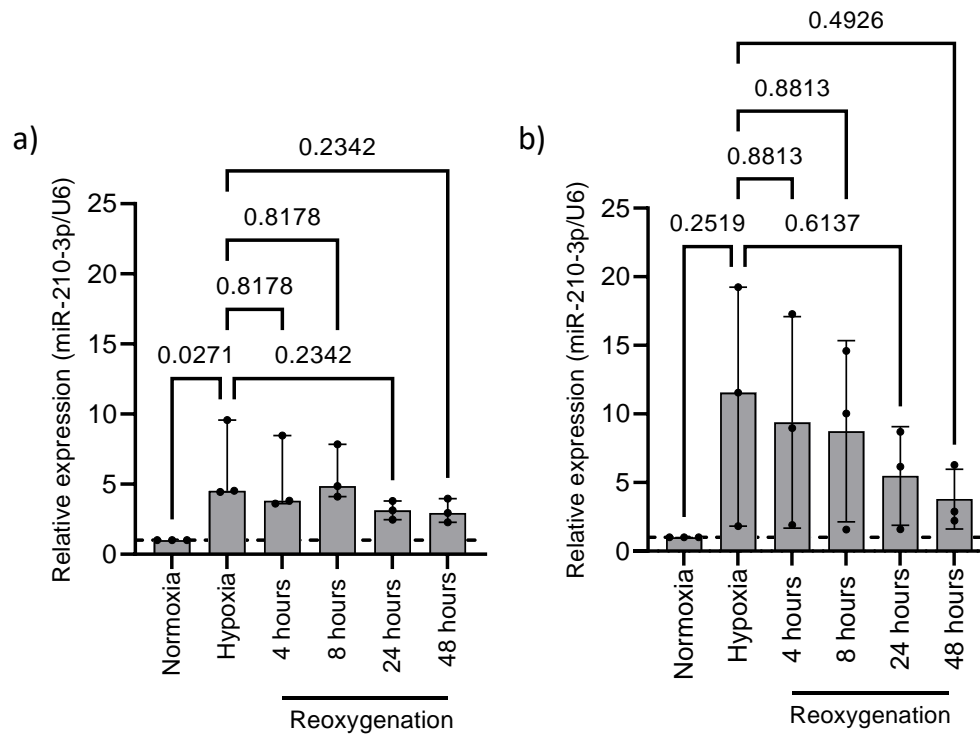


Figure 6.7 Elevated miR-210-3p levels detected post-hypoxia.

a) HGENCs and b) PTECs were cultured in 1% oxygen for 24 hours hypoxia before transferring to culture under normoxic conditions for 4 hours, 8 hours, 24 hours and 48 hours. miR-210-3p expression indicated the upregulation of miR-210-3p in hypoxia and subsequently a sustained upregulation in HGENCs and PTECs compared to untreated cells. Unlike HGENCs, the miR-210-3p expression in PTECs showed a time dependent decrease but not significantly different from the hypoxia treated only cells. miR-210-3p expression was normalised to U6. Data shown as mean \pm SD of n=3 biological replicates. Statistical analysis was performed using One-way ANOVA with Holm-Šídák post-hoc test.

6.4.5. mRNA Expression Clustered by Biological Replicates

miRNA targeting of mRNA has been identified to be cell-type and context specific (Lu et al., 2015, Rogg et al., 2018). While there are existing prediction algorithms (Agarwal et al., 2015) and validated databases (Kehl et al., 2019, Huang et al., 2022) available to identify mRNA targets, empirical testing is still necessary. Therefore, we employed parallel mRNA-sequencing on the samples subjected to hypoxia for target identification. As indicated in Figure 6.8a, the application of dimension reduction to the samples resulted in clustering by biological replicate, suggesting that the hypoxia treatment did not result in extensive perturbation of the mRNA expression. This was further confirmed by hierarchical clustering with clustering by biological replicate (Figure 6.8b).

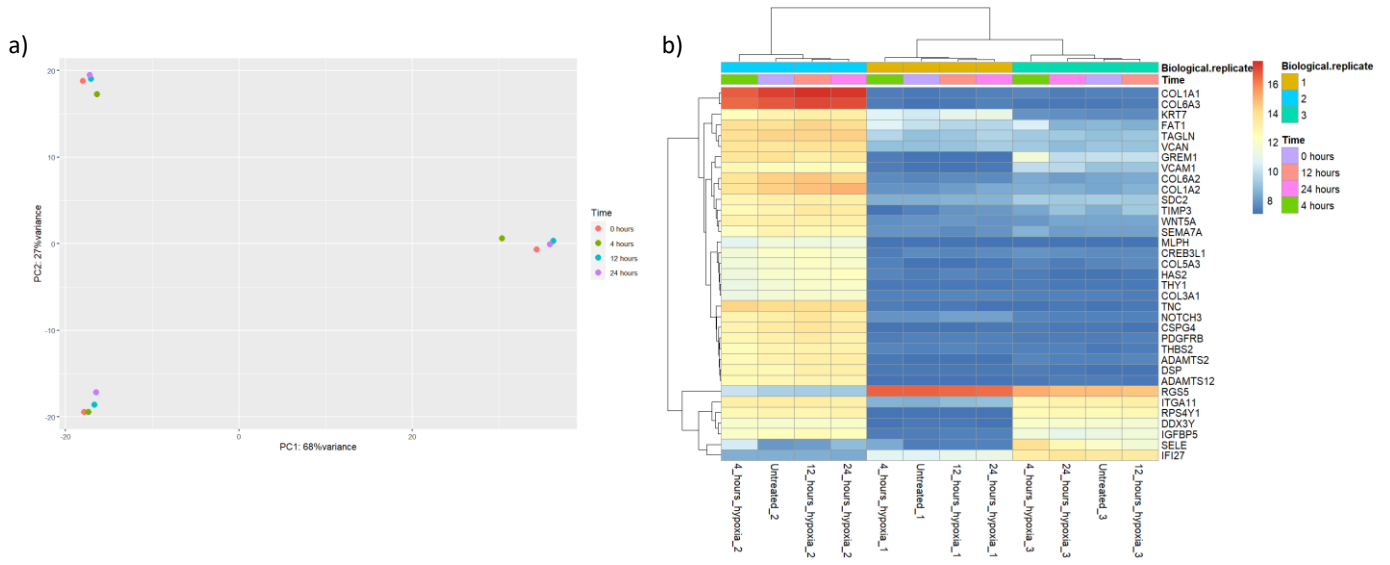


Figure 6.8 mRNA-sequencing of hypoxia treated HGENCs.

Cells were cultured in 1% oxygen for 4, 12 and 24 hours. Isolated RNA was sequenced to profile mRNA changes under hypoxic conditions over time. a) PCA clustering of the mRNA expression of the hypoxia treated HGENCs showed clustering by biological replicates. b) Hierarchical clustering of the mRNA showed the samples clustering by biological replicates.

6.4.6. Hypoxia Exposure Induced Transcriptomic Changes

To assess the transcriptomic changes of the HGENCs over time, we compared the gene expression of the full design model in DESeq2 against a reduced model. This allowed us to identify changes in gene expression as a result of treatment using a likelihood test. A total of 1927 significant DEGs were identified and were further subdivided into 6 clusters based off their normalised z-score (Figure 6.9).

Subsequent analysis of these individual clusters revealed enrichment of biological processes over increasing duration of low oxygen exposure (Figure 6.10). 4 hours hypoxia resulted in increased overall cellular transcription of coding and non-coding RNA (cluster 5), activation of cellular response mechanism towards oxidative stress (cluster 5) and differentiation to mesenchymal phenotype (cluster 6). Increasing the exposure to 12 and 24 hours further initiated cellular responses classically associated with hypoxia such as decrease cell cycle transition (cluster 1), glycolysis (cluster 3) and reduction in overall transcription (cluster 4). Interestingly, enrichment in the NADH regeneration (cluster 3) was validated by the viability assay at 24 hours (Figure 6.3). To cross-validate the over-representation analysis, the unbiased GSEA confirmed positive enrichment of hypoxia and glycolysis pathways as well as negative enrichment of cell cycle and transcription over increasing duration of hypoxia exposure (Figure 6.11).

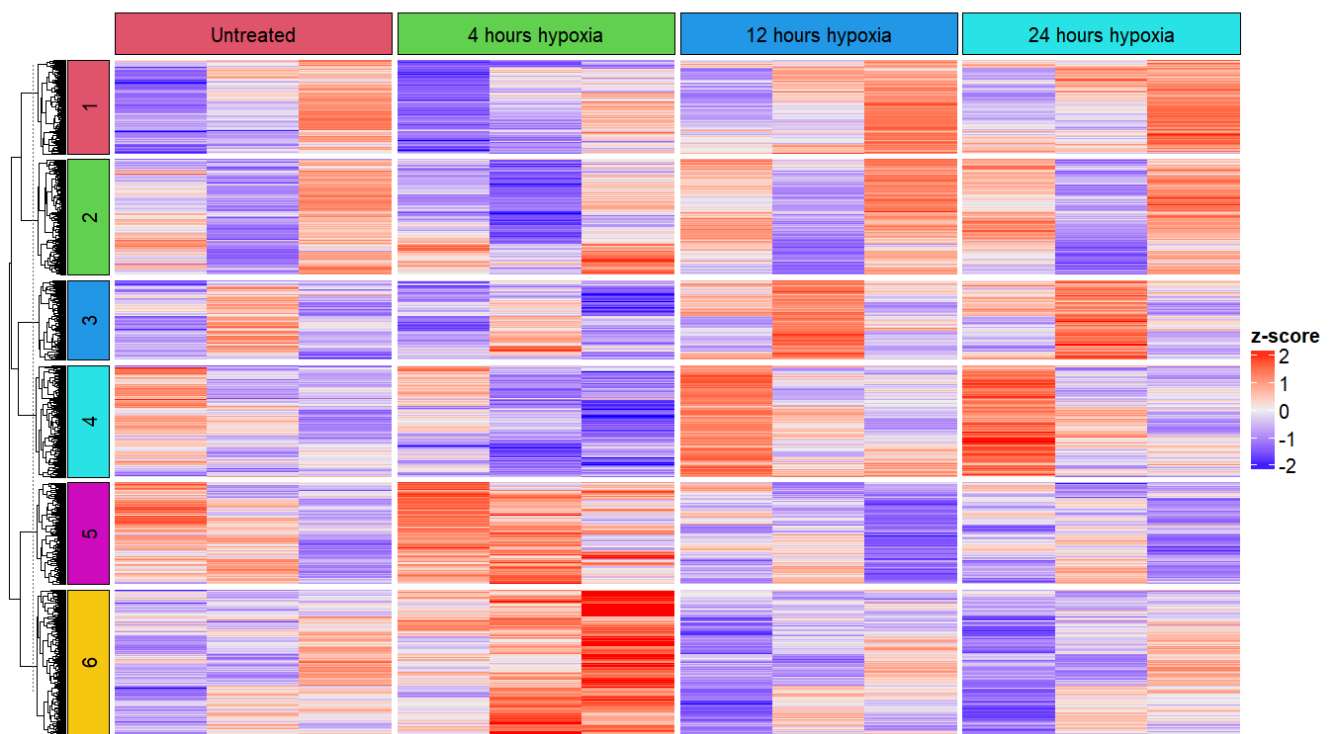


Figure 6.9 Clustering of the DEGs.

Significant genes that are differentially expressed as determined by the likelihood ratio test were clustered using k -means algorithm with $k=6$. Optimum k was determined using the elbow method.

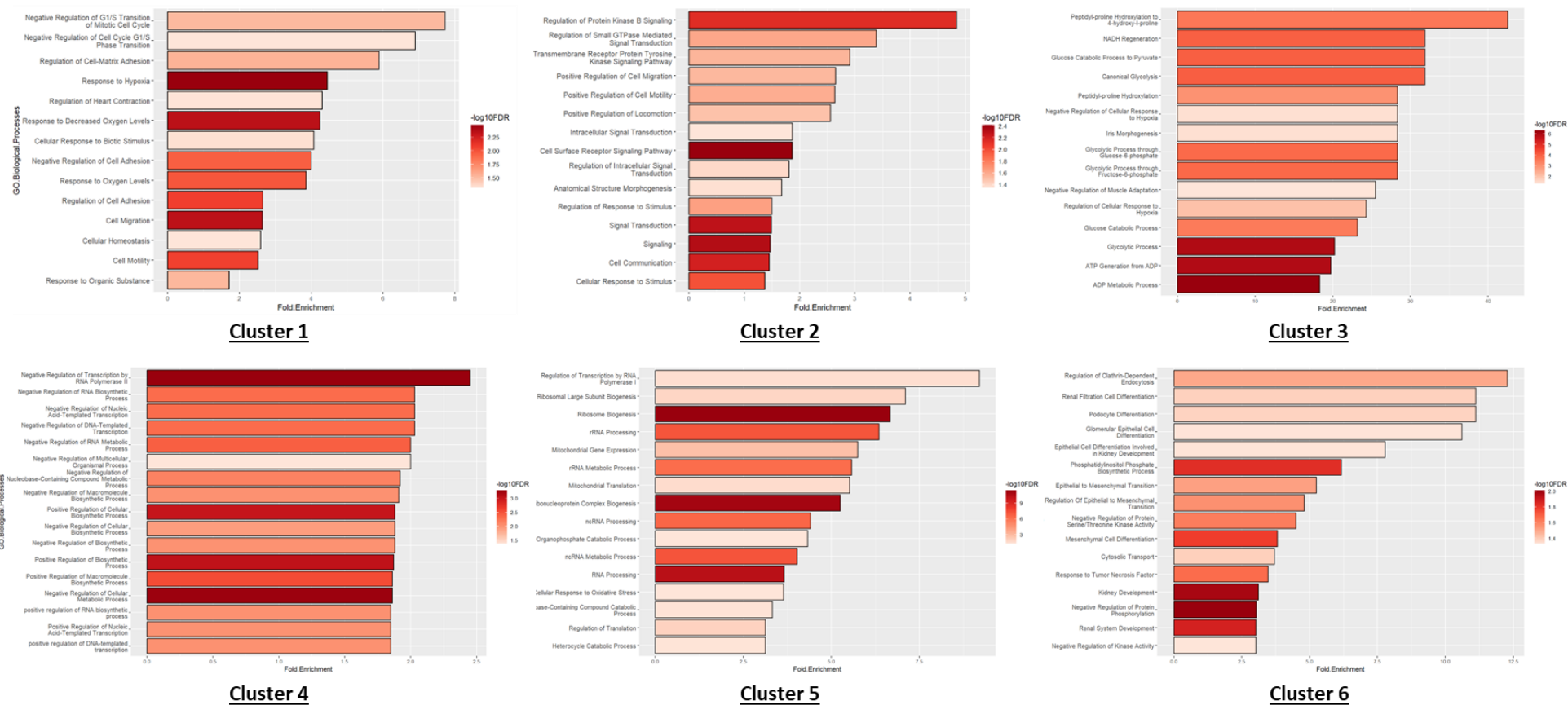


Figure 6.10 Gene ontology analysis for individual clusters.

Top 15 biological processes enriched in each of the 6 clusters were plotted as a bar graph as fold enrichment and the colour representing $-\log_{10}(p\text{-value})$.

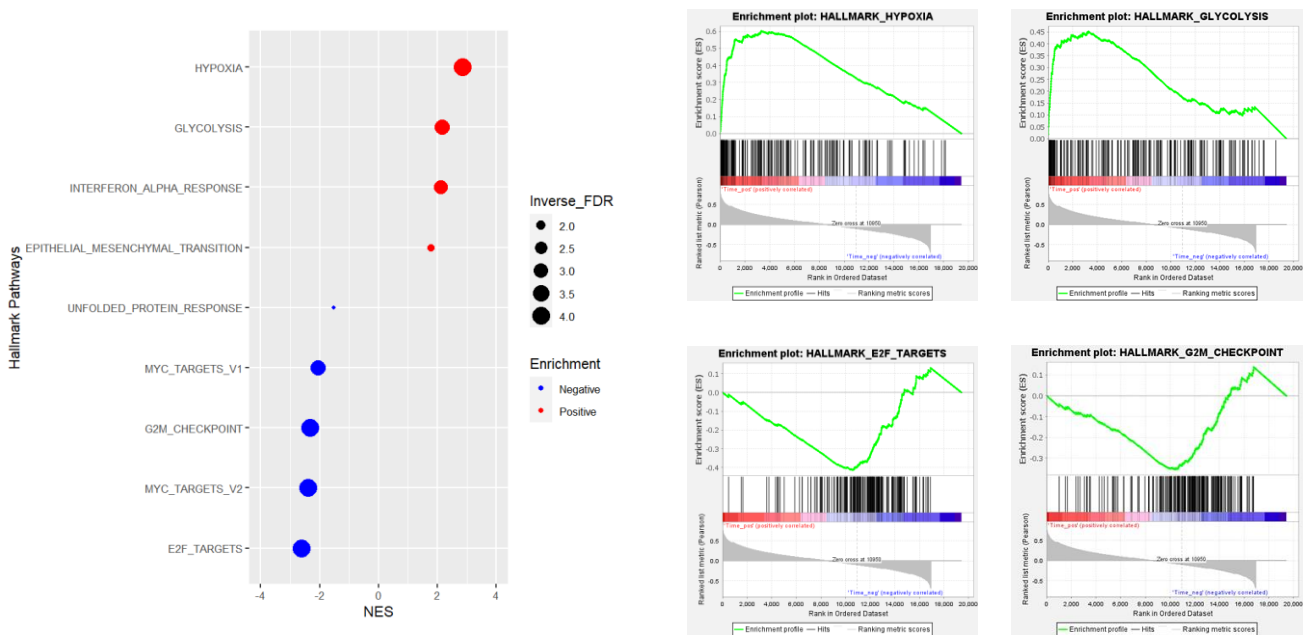


Figure 6.11 GSEA of hypoxia time-course in HGENCs.

Hallmark pathway analysis of cells exposed to 1% oxygen over time showed a positive enrichment of pathways associated with stress response and negatively enriched for pathways associated with cell cycle and transcription. Enrichment plots showing pathway enrichment score as well as gene set ranking.

6.4.7. Gene Expression of HGENC Post 4 Hours Hypoxia

While culturing of HGENCs under hypoxic conditions for 4 hours did not result in any significant changes in the miRNA, it resulted in the differential expression of 623 mRNA (Figure 6.12a). Among these DEGs, *CXCL12*, *EGLN3*, *KDM3A* were upregulated when compared to untreated HGENCs (Figure 6.12a). These genes have been identified to contain HRE upstream in the promoter region and are known to be regulated by hypoxia (Ceradini et al., 2004, Pescador et al., 2005, Osawa et al., 2013). Interestingly, GSEA did not indicate enrichment in hypoxia response in the cells. Instead, transforming growth factor- β (TGF- β), *KRAS* and androgen signaling were positively enriched in the hypoxia treated cells (Figure 6.12b). Similarly, biological processes did not indicate any cellular responses to hypoxia but instead resulted in a proliferative phenotype (Figure 6.12c).

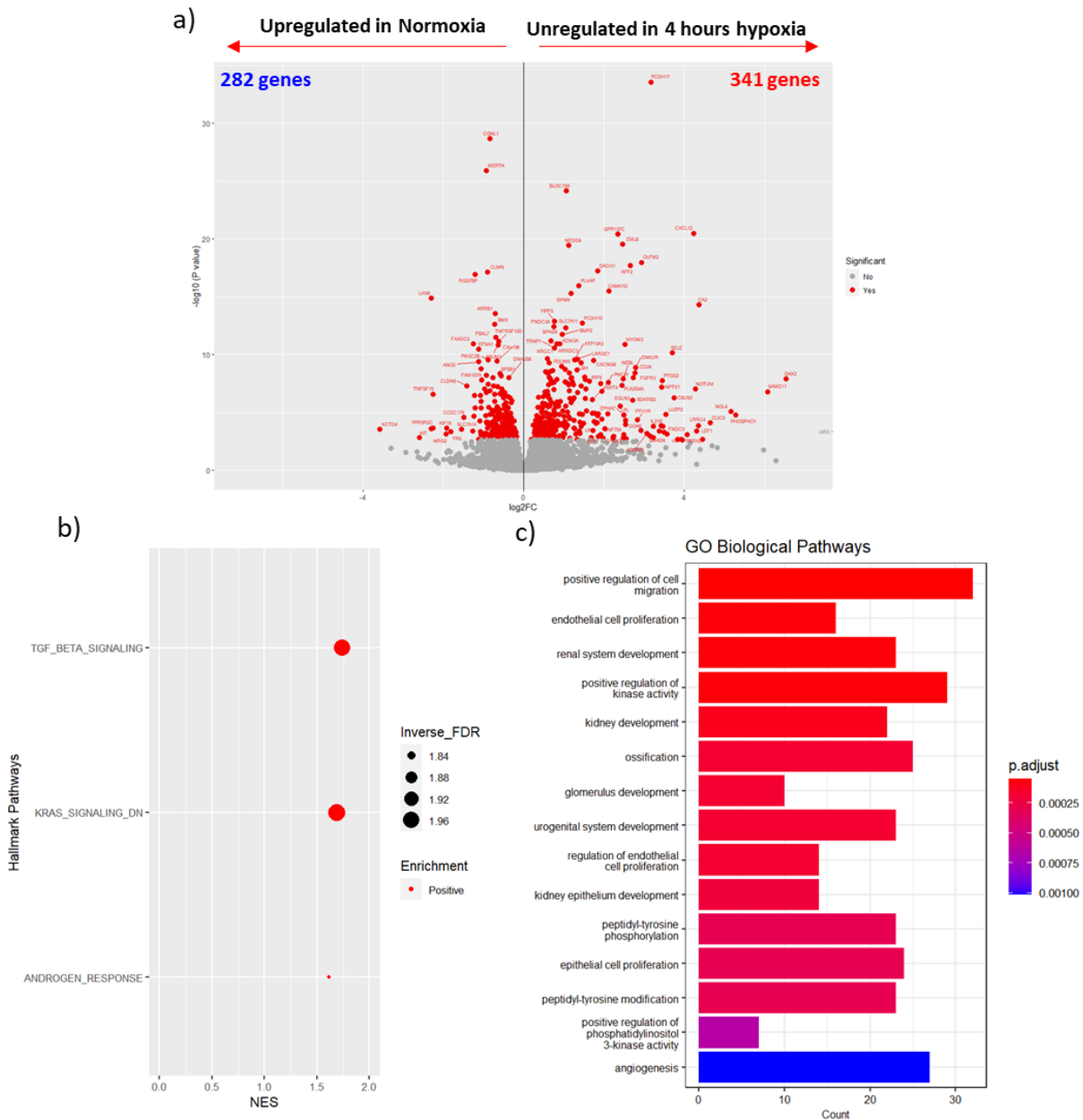


Figure 6.12 mRNA expression of HGENC post 4 hours exposure to hypoxia.

Analysis of mRNA expression in hypoxia cultured HGENC compared to untreated cells. a) Volcano plots showing the DEGs. In total, 623 genes were differentially regulated. b) GSEA showed only 3 hallmark pathways to be significantly positively enriched in the hypoxia cultured cells compared to controls. c) Top 15 biological processes enriched in the hypoxia treated cells showing an overall proliferative and developmental phenotype relative to the controls.

6.4.8. Gene Expression of HGENC Post 12 Hours Hypoxia

When HGENCs were subjected to 12 hours hypoxia, 164 genes were significantly differentially expressed (Figure 6.13a) when compared to the untreated controls. This decrease in DEG corroborated the cluster analysis (cluster 4) indicating a negative regulation of gene transcription (Figure 6.10). Previously, endothelial cells are reported to downregulate *HIF1A* gene expression in response to chronic hypoxia (Bartoszewski et al., 2019). This was also observed in HGENCs (Figure 6.13a). Furthermore, GSEA indicated positive enrichment in hypoxia and glycolysis (Figure 6.13b) and negative enrichment of cell cycle processes. Gene ontology pathways further highlighted alteration in cellular metabolism (Figure 6.13c).

6.4.9. Gene Expression of HGENC Post 24 Hours Hypoxia

A similar gene expression profile was also observed when the duration of hypoxia increases to 24 hours with 190 significantly DEGs identified when compared to the untreated control group (Figure 6.14a). Apart from the observed downregulation of *HIF1A* expression, *EPAS1*, the gene encoding for HIF-2 α expression was also downregulated (Figure 6.14a). This was in concordance with previous reports of chronic hypoxia regulating *EPAS1* expression in specific subsets of endothelial cells. (Bartoszewski et al., 2019). In addition to similar enrichment for hallmark pathways in the 12 hours treatment group (Figure 6.13b), there was additional positive enrichment for epithelial to mesenchymal transition and negative enrichment for oxidative phosphorylation (Figure 6.14c). Gene ontology analysis showed a similar biological pathway enrichment indicating perturbation in cellular metabolism (Figure 6.14c).

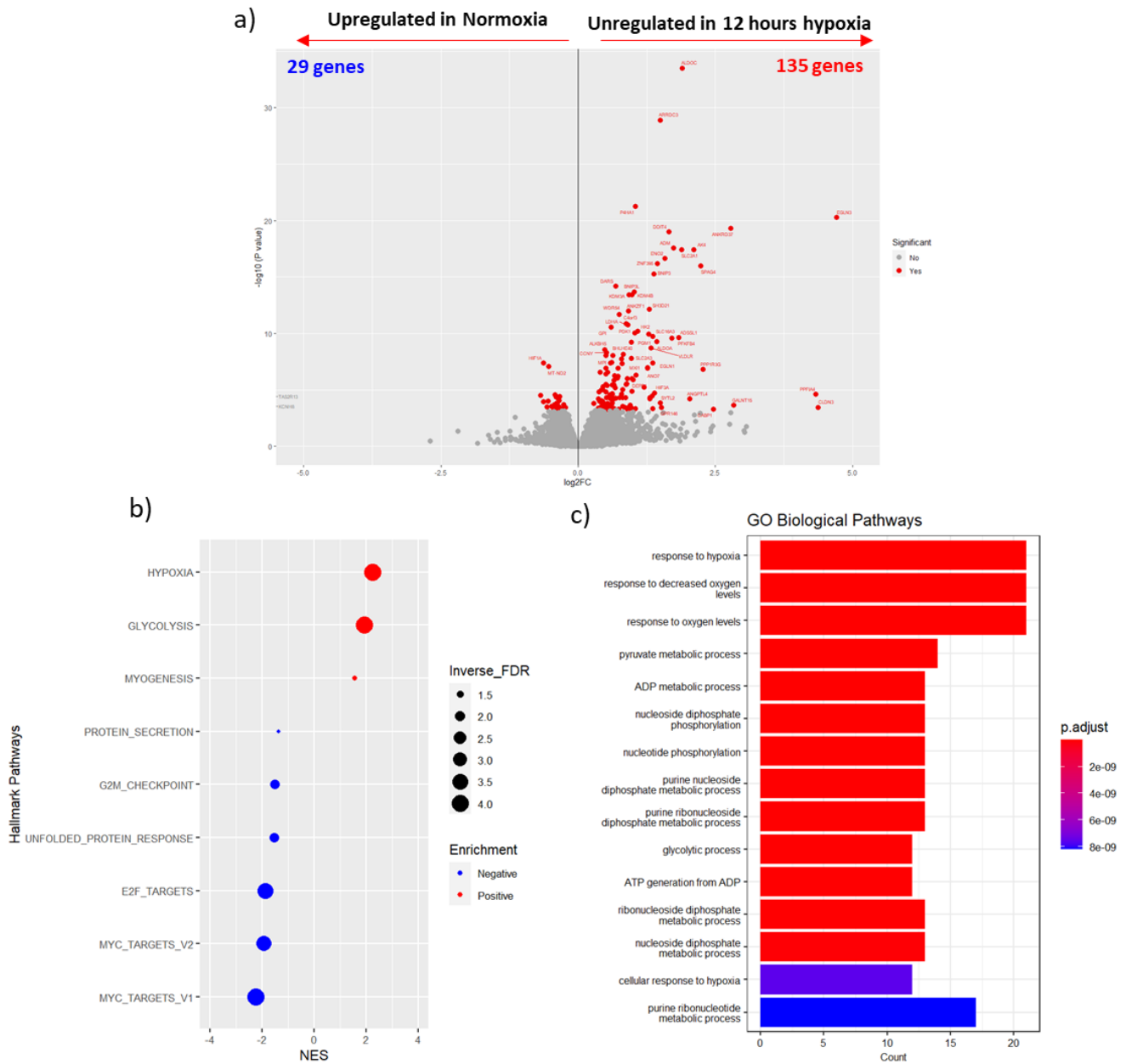


Figure 6.13 mRNA expression of HGENC post 12 hours exposure to hypoxia.

Analysis of mRNA expression in hypoxia cultured HGENC compared to untreated cells. a) Volcano plot showing the DEGs. In total, 164 genes were differentially regulated. b) GSEA showed 3 significantly positively enriched and 6 negatively enriched pathways in the hypoxia cultured cells compared to controls. c) Top 15 biological processes enriched in the hypoxia treated cells showing cellular responses to hypoxia and perturbation to bioenergetic processes.

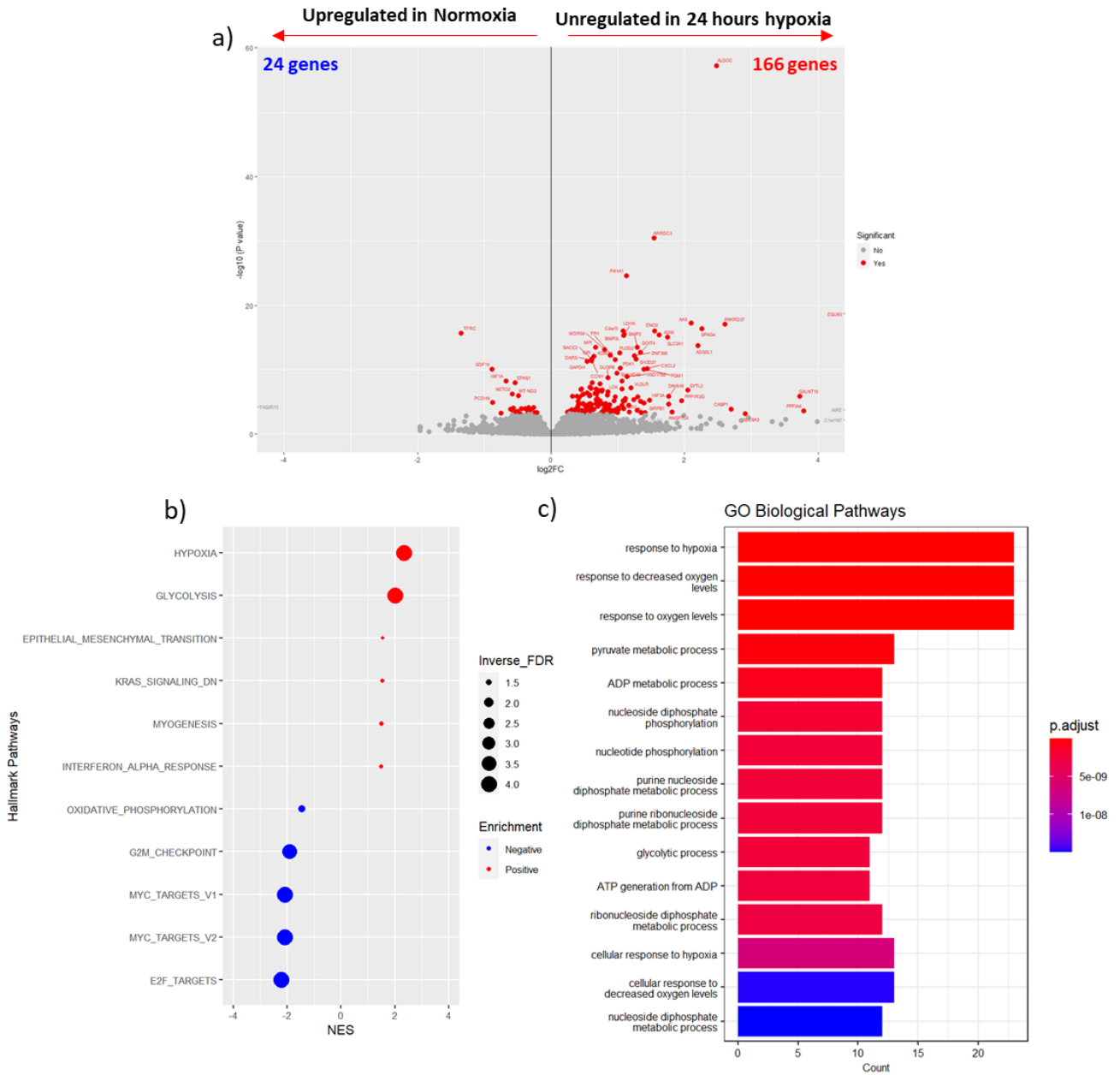


Figure 6.14 mRNA expression of HGENC post 24 hours exposure to hypoxia.

Analysis of mRNA expression in hypoxia cultured HGENC compared to untreated cells. a) Volcano plot showing the DEGs. In total, 190 genes were differentially regulated. b) GSEA showed 6 significantly positively enriched and 5 negatively enriched pathways in the hypoxia cultured cells compared to controls. c) Top 15 biological processes enriched in the hypoxia treated cells showing cellular responses to hypoxia and perturbation to bioenergetic processes.

6.4.10. Validation of Gene Expression

The validation of RNA-seq data was carried out on HGENCs subjected to hypoxia over the time course of 4 hours, 12 hours, and 24 hours. As shown in Figure 6.15, *HIF1A* showed significant downregulation over the course of hypoxia treatment. *VEGFA* is known to be modulated by hypoxia and showed a trend of increased expression although it did not reach significance. In addition, *EPAS1* showed downregulation at 24 hours and *NPTX1* showed upregulation at 4 hours in RNA-seq data but the trends were not observed during validation.

6.4.11. Integrated Analysis Identified 22 miR-210-3p Regulated mRNA Targets

To identify miR-210-3p targeting in HGENCs, DEGs output from the likelihood ratio test was crossed with 2 experimentally validated (Kehl et al., 2019, Huang et al., 2022) and 1 prediction (Agarwal et al., 2015) databases. In total, we identified 11 unique genes that overlapped with 2 databases and another 11 unique genes that overlapped with 3 databases (Figure 6.16a). Among these genes, the downregulation of *HIF1A* and *TFRC* expression were consistent with the upregulation of miR-210-3p at 12 hours and 24 hours hypoxia treatment as indicated by the dot plots (Figure 6.16b).

6.4.12. CiGENCs is a Valid Model of HGENCs

HGENCs attained replicative senescence at relatively low passage as previously described in literature (Satchell et al., 2006). To overcome this issue, we switched over to the utilisation of ciGENC which have been shown to retain phenotypes associated with their primary counterparts. (Satchell et al., 2006). To confirm that the gene expression is similar to HGENCs, cells were subjected to 24 hours hypoxia and assessed their miRNA and mRNA expression. As indicated in Figure 6.17a, a significant increase in miR-210-3p expression was observed. Furthermore, the expression of *ISCU*, a putative miR-210-3p target (Chan et al., 2009) along with *HIF1A* and *TFRC* were in line with HGENCs expression (Figure 6.17b).

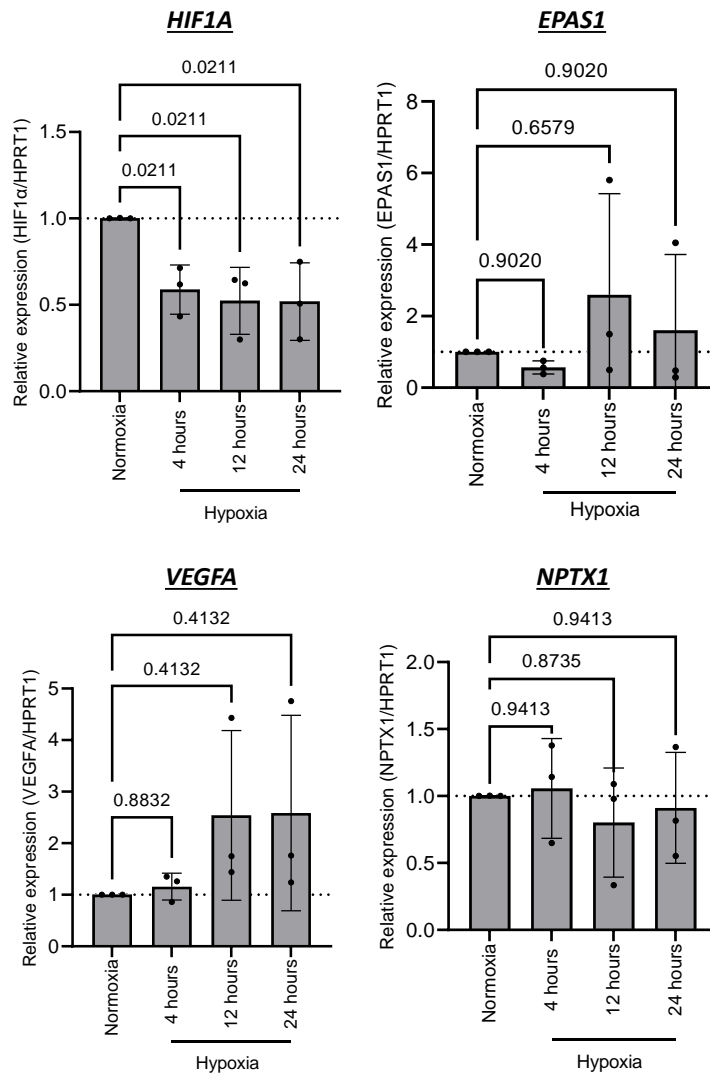
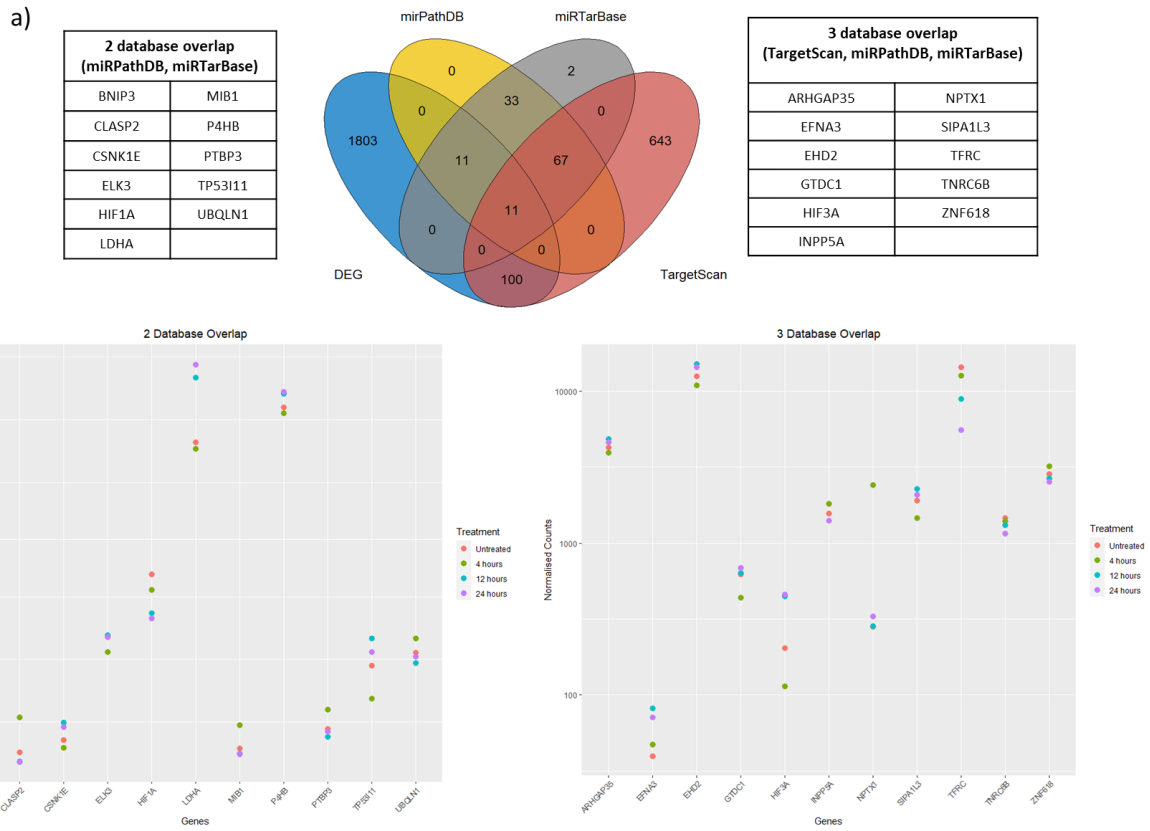


Figure 6.15 RNA-seq validation.

Validation of RNA-seq data was done by qPCR on separate technical replicates of each biological donor. A significant downregulation of HIF1A was observed when cells were cultured in 1% oxygen. VEGFA showed a trend of upregulation, albeit not significant. EPAS1 and NPTX1 expression did not show any observable trend in response to treatment. Gene expression was normalised to HPRT1. Data shown as mean \pm SD of n=3 biological replicates. Statistical analysis was performed using One-way ANOVA with Holm-Šídák post-hoc test.



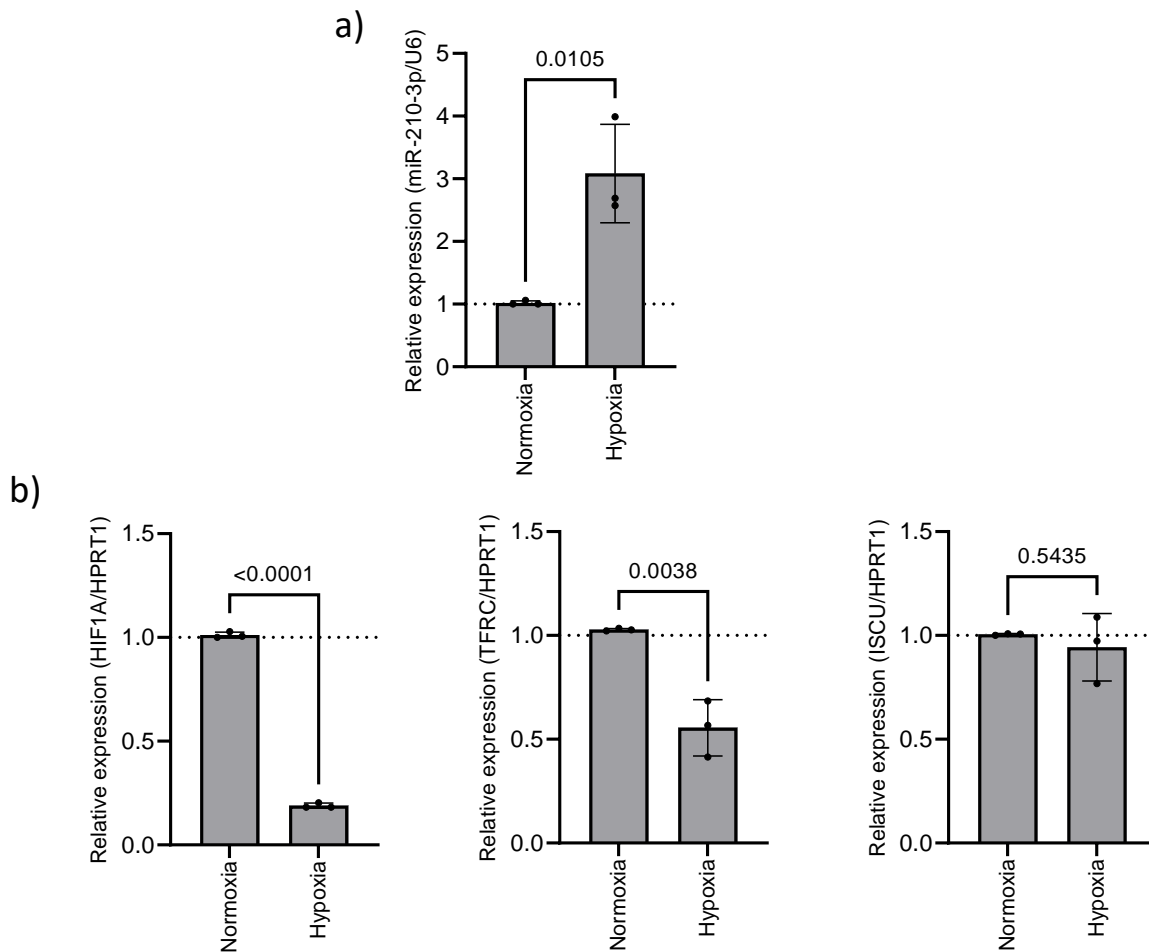


Figure 6.17 miRNA and mRNA expression of ciGENCs in hypoxia.

Cells were cultured for 5 days at 37°C to inactivate the viral transgene before culturing in 1% oxygen for 24 hours. miRNA and mRNA expression were quantified by qPCR. a) miR-210-3p expression was significantly increased in hypoxia cultured cells compared to control. b) *HIF1A*, *TFRC* were significantly downregulated compared to control. *ISCU*, a putative miR-210-3p target did not show any changes in gene expression in response to hypoxia. miR-210-3p expression was normalised to U6 and mRNA expression was normalised to *HPRT1*. Data shown as mean ± SD of n=3 replicates. Statistical analysis was performed using an unpaired student T-test.

6.4.13. Differential Regulation Between ciGENCs and PTECs in Hypoxia

To determine if there are cell specific targeting by miR-210-3p, we sought to compare the mRNA targets that were observed in ciGENCs in PTECs. While both *HIF1A* and *TFRC* showed downregulation in both ciGENCs (Figure 6.17) and PTECs (Figure 6.18), we observed a significant reduction in *ISCU* expression PTECs which was not seen in ciGENCs. While we are unable to fully attribute this difference to miR-210-3p solely, we can confirm a differential response between the two cell types to culture in a hypoxic environment.

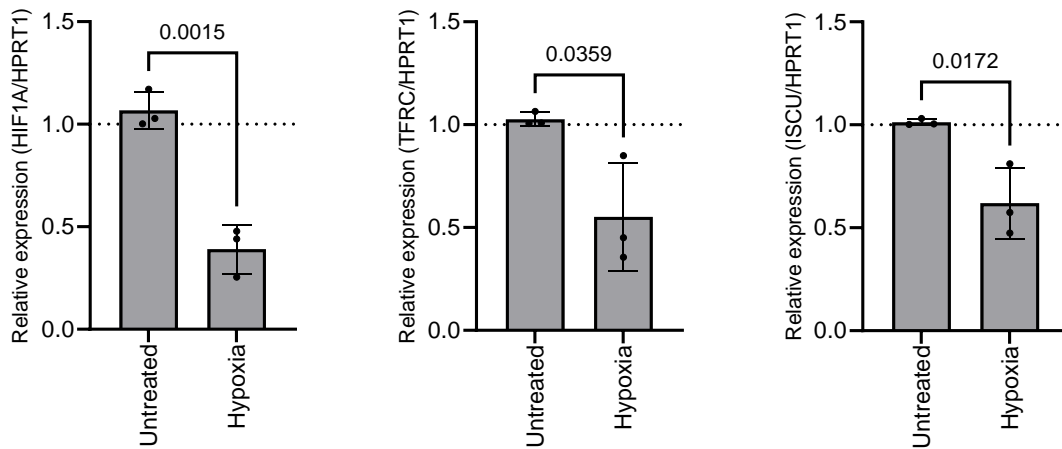


Figure 6.18 PTECs mRNA regulation in hypoxia.

Cells were cultured under 1% oxygen for 24 hours and mRNA expression was quantified by qPCR. *HIF1A*, *TFRC* and *ISCU* were significantly downregulated compared to control. mRNA expression was normalised to *HPRT1*. Data shown as mean \pm SD of n=3 biological replicates. Statistical analysis was performed using an unpaired student T-test.

6.4.14. Transfection Efficiency of ciGENCs

Transient miRNA mimic transfection has been extensively used to study the functions of endogenous miRNA. Previously, it was reported that the common concentrations used in literature can result in the accumulation of high molecular weight RNA species as well the propensity for non-specific targeting (Jin et al., 2015). To determine the lowest possible concentration to achieve efficient transfection, we first determined the uptake efficiency using an AlexaFluor647-labeled siRNA. Transfection of ciGENCs resulted in effective uptake of the labeled siRNA (Figure 6.19a). When the concentration of siRNA was increased from 1nM to 3.125nM, we observed an increase in the overall median fluorescence intensity (MFI) (Figure 6.19b). There was no observable increase in MFI when the concentrations were further increased. Furthermore, when we assessed the number of cells positive for AlexaFluor647, only 1nM showed a significant difference when compared to 25nM and 50nM (Figure 6.19c). Hence, 3.125nM was determined as the minimum concentration of mimics required to efficient transfection.

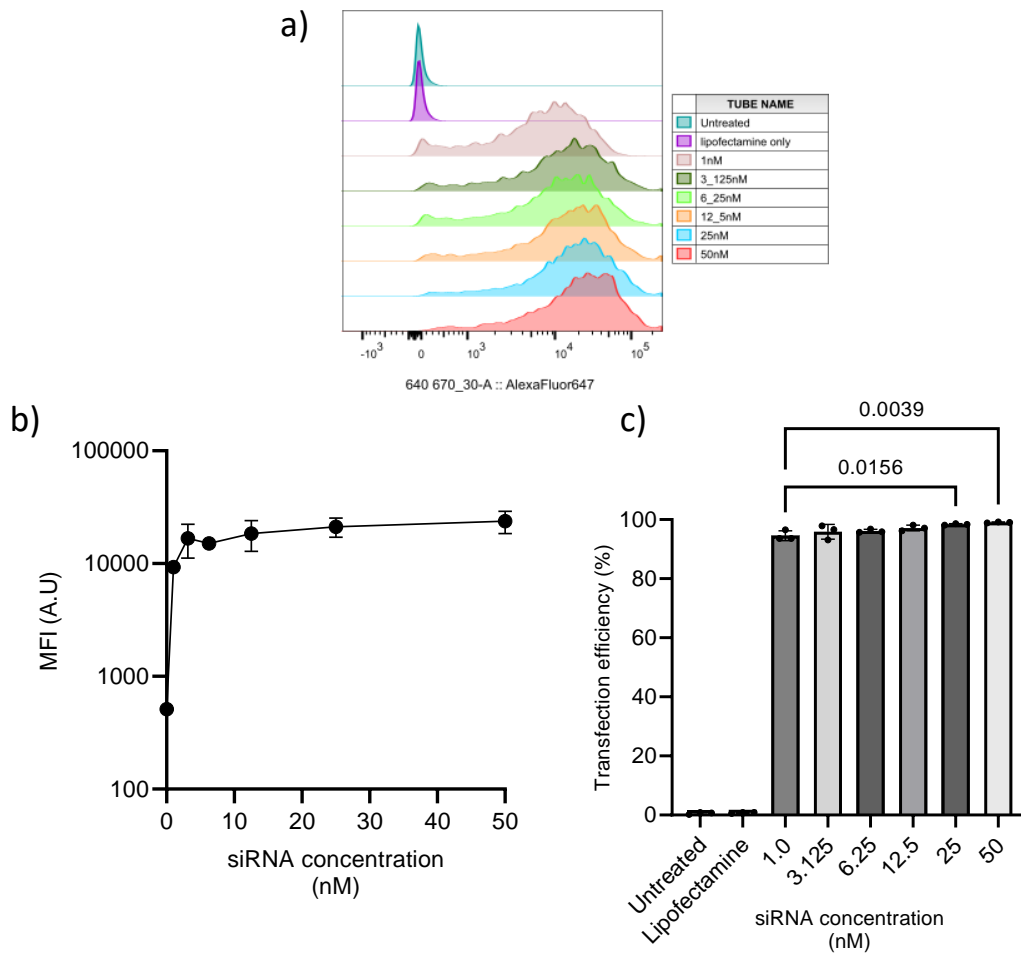


Figure 6.19 Transfection efficiency assessment of ciGenCs for small RNA uptake.

Cells were transfected with 1nM-50nM of Alexafluor647-labeled siRNA and the uptake efficiency was assessed by flow cytometry. a) Overlaid histogram showing transfection with labeled siRNA resulted in Alexafluor647 positive cells population. b) MFI assessment indicated an increase in Alexafluor647 signal from 1nM to 3.125nM before hitting a plateau. c) Overall cell population positive for Alexafluor647 signal post transfection was plotted as percentage transfection efficiency. Data shown as mean \pm SD of n=3 replicates. Statistical analysis was performed using One-Way ANOVA with Tukey's post-hoc test.

6.4.15. mRNA Targeting by miR-210-3p

ciGenCs were transfected with 3.125nM (determined in Section 6.4.14) of miR-210-3p mimics or scramble control to determine the regulation of mRNA targets. As indicated in Figure 6.20, a significant decrease in *HIF1A*, *TFRC* and *ISCU* was observed when the cells were transfected with miR-210-3p mimics. Even though the scramble control resulted in a significant downregulation of *ISCU* expression, the extent of downregulation by miR-210-3p transfected cells was higher. However, this mRNA targeting of *ISCU* was not observed in both HGenCs RNA-seq expression and ciGenCs cultured under hypoxic conditions. This was previously observed in pulmonary vascular endothelial cells where mRNA targeting of *ISCU* was observed at protein levels at 0.2nM and 2nM but regulation at mRNA levels was only observed at the higher concentration (Chan et al., 2009). Moreover, removal of the transfection cocktail and allowing the cells to rest for further 24 hours still resulted in the downregulation of *ISCU* and *TFRC* (Figure 6.21), thereby confirming engagement of miR-210-3p on these 2 genes.

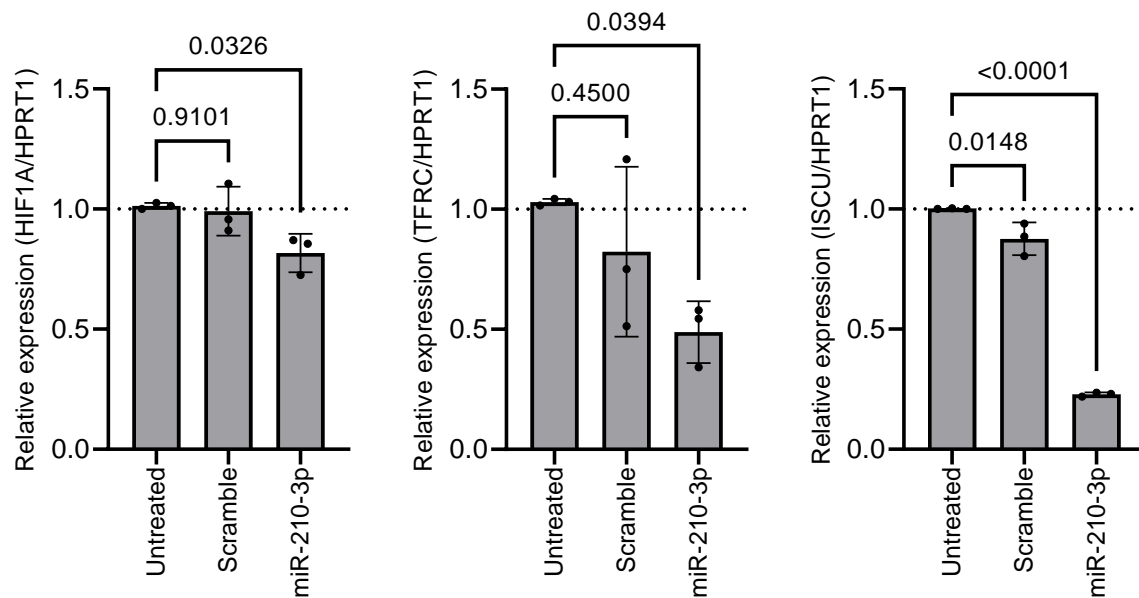


Figure 6.20 miR-210-3p targeting in ciGenCs.

Cells were transfected with scramble or miR-210-3p mimic for 24 hours and gene expression of targets were determined via qPCR. A significant downregulation of *HIF1A*, *TFRC* and *ISCU* was observed compared to the untreated cells. mRNA expression was normalised to *HPRT1*. Data shown as mean \pm SD of n=3 replicates. Statistical analysis was performed using One-Way ANOVA with Dunnett's post-hoc test.

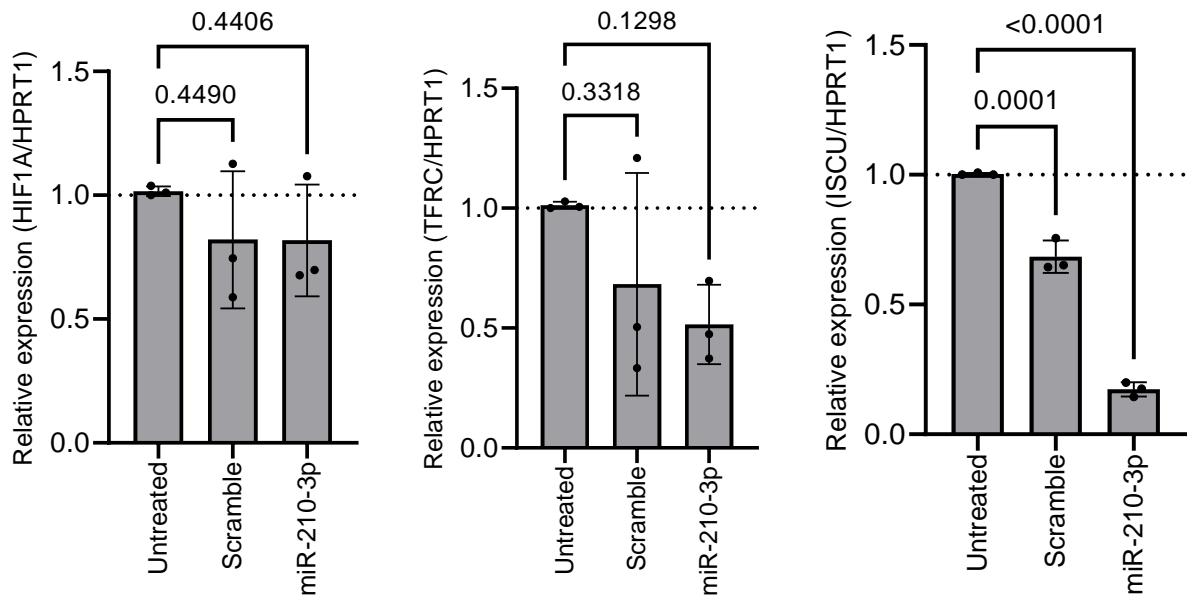


Figure 6.21 miR-210-3p targeting in ciGENCs 24 hours post-transfection.

Cells were transfected with miR-210-3p for 24 hours and replaced with fresh media before culturing for another 24 hours. Gene expression of targets were then determined via qPCR. A significant downregulation of *ISCU* was observed when compared to the untreated cells. *TFRC* expression was also downregulated but not significant and *HIF1A* expression remained unchanged when compared to the controls. mRNA expression was normalised to *HPRT1*. Data shown as mean \pm SD of n=3 replicates. Statistical analysis was performed using One-Way ANOVA with Dunnett's post-hoc test.

6.4.16. *TfR1* is Targeted by miR-210-3p

With the transfection of miR-210-3p downregulating *TFRC* expression, we next sought to determine whether *TfR1*, the protein encoded by *TFRC* was also perturbed by the mimic. As shown in Figure 6.22, ciGENCs transfected with miR-210-3p mimic showed a significant decrease in *TfR1* expression whereas no significant change was observed with the scramble sequence control.

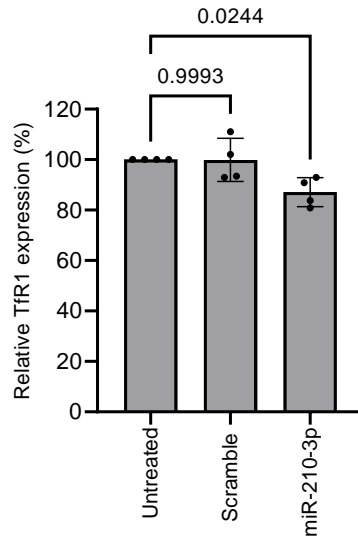


Figure 6.22 TfR1 expression post miR-210-3p transfection.

ciGEnC expression of surface TfR1 was determined using flow cytometry. miR-210-3p transfected cells show a significant decrease in the TfR1 expression compared to untreated control. Relative TfR1 expression was calculated as a percentage MFI of the untreated group. Data shown as mean \pm SD of n=4 replicates. Statistical analysis was performed using One-Way ANOVA with Dunnett's post-hoc test.

6.4.17. Overexpression of miR-210-3p Increased Glycolysis but not Mitochondria Function

Pathway enrichment of the glomerular endothelium at 12 (Figure 6.13) and 24 hours (Figure 6.14) hypoxia showed alterations in the metabolic function. To determine the extent of miR-210-3p contribution to this altered metabolic state, extracellular flux assays were employed to measure the glycolytic and mitochondrial function of ciGEnCs. As shown in Figure 6.23, ciGEnCs transfected with miR-210-3p showed a significantly lower non-glycolytic acidification rate. Upon injection of glucose, the miR-210-3p over-expressing cells showed a higher rate of glycolysis and a higher glycolytic capacity when compared to untreated cells. Interestingly, when mitochondrial function was assessed, we did not observe any significant alterations in any of the measurable parameters (Figure 6.24) as reported in literature with miR-210-3p overexpression in other cell types (Chan et al., 2009, Song et al., 2022).

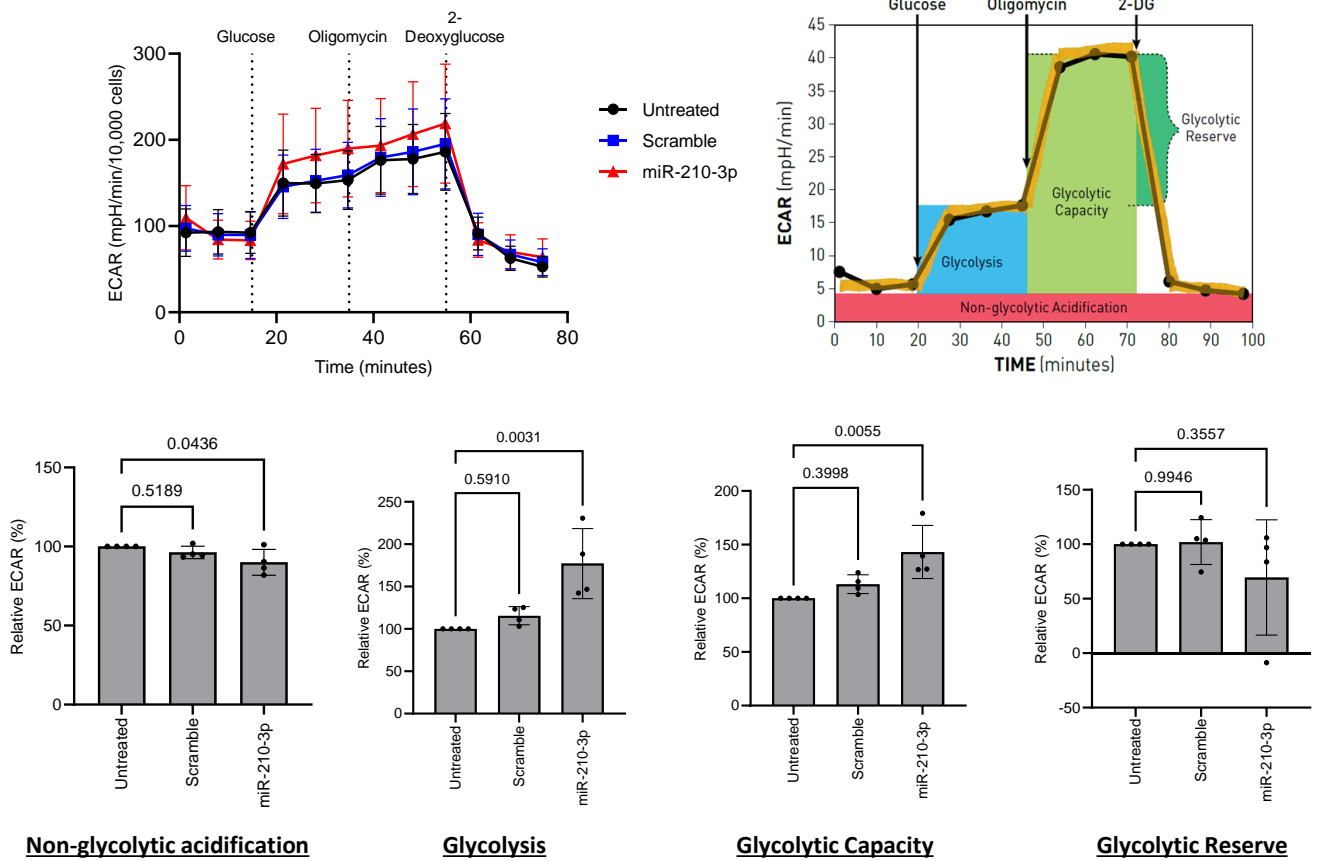


Figure 6.23 Assessment of ciGenCs glycolytic function post miR-210-3p transfection.

ciGenCs cells were transfected with miR-210-3p mimic and glycolysis stress test was performed using Seahorse XF96 analyser. miR-210-3p transfected ciGenC cells showed a significantly lower non-glycolytic acidification whilst having a higher overall glycolysis and glycolytic capacity when compared to untreated control. No significant difference was observed in the glycolytic reserve of ciGenC cells overexpressing miR-210-3p. Data shown as mean \pm SD of n=4 replicates, with 12 technical replicates per run. Statistical analysis was performed using One-Way ANOVA with Dunnett's post-hoc test.

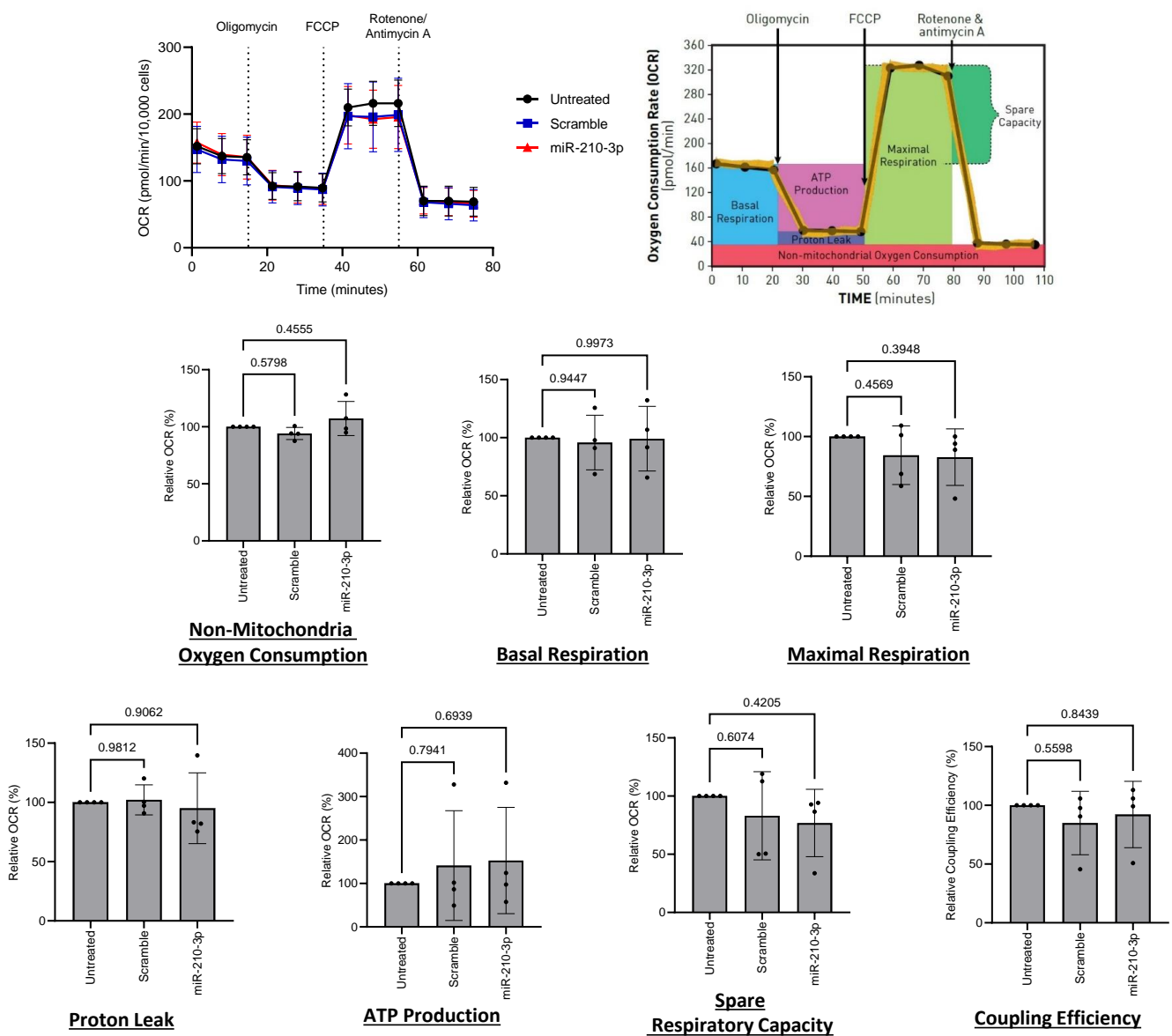


Figure 6.24 Assessment of ciGenCs mitochondria function post miR-210-3p transfection.

ciGenCs cells were transfected with miR-210-3p mimic and mitostress test was performed using Seahorse XF96 analyser. miR-210-3p transfected ciGenC cells did not show any significant changes to the mitochondrial parameters when compared to the controls. Data shown as mean \pm SD of n=4 replicates, with 12 technical replicates per run. Statistical analysis was performed using One-Way ANOVA with Dunnett's post-hoc test.

6.4.18. Mitochondrial Morphology unaltered by miR-210-3p Overexpression

To further confirm that the overexpression of miR-210-3p did not alter mitochondria function, we next assessed the ultrastructure using TEM imaging. Previously, overexpression of miR-210-3p have been reported to result in mitochondria swelling and loss of cristae (Puisségur et al., 2010). While the mitochondria post miR-210-3p transfection showed a more globular structure and the loss of elongated morphology, we did not observe any swelling and loss of cristae in ciGenCs (Figure 6.25).

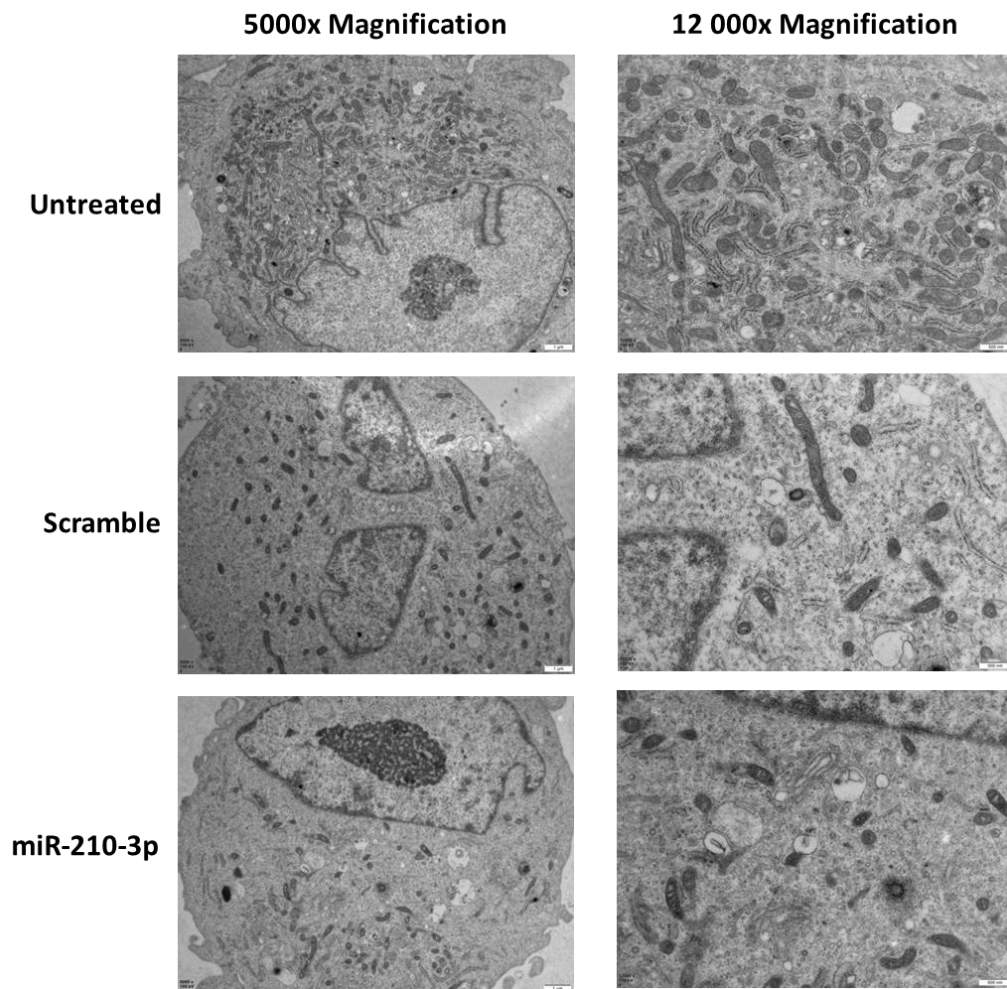


Figure 6.25 Mitochondria ultrastructure of ciGenCs post miR-210-3p transfection.

Electron micrograph of negative stained ciGenCs transfected with miR-210-3p. Mitochondria are shown as electron dense structure and miR-210-3p transfected cells showed more globular mitochondria morphology compared to untreated and scramble controls. Images are representative of n=3. Scale bar= 1 μ m for 5000x magnification and 500nm for 12,000x magnification.

6.5. Discussion

The capacity for oxygen sensing and regulation is key to ensure homeostatic function in living organisms. During the onset of hypoxia, adaptation to the hypoxic environment is predominantly driven by the HIF, the master regulator of hypoxia. However, subtle differences in these adaptations across cells in different organs and tissue have been known to impact the overall survival and outcomes. In kidney ischemia, renal tubular epithelial cells are amongst the most abundant and well-studied cell types. The onset of ischemia has shown miRNA dysregulation, which can result in tissue remodeling (Kuo et al., 2021) and impairing cellular adaptation (Liu et al., 2017). miRNA regulation and cellular adaptation to hypoxia in other less abundant renal cells however is less well understood.

As such, the work from this chapter set out to determine the miRNA expression of glomerular endothelium in response to hypoxia. To identify miRNAs that are differentially regulated in hypoxia, we subjected HGENCs to 4 hours, 12 hours, and 24 hours of culture in 1% oxygen. Importantly, the timepoints chosen for the experiments were set out to mimic short to long ischemic times experienced by renal allografts in the context of transplantation. While culturing of cells under low oxygen tension has been shown to not fully mimic tissue hypoxia *in vivo*, this model was chosen to ensure reproducibility and ease of downstream functional assessment and is currently still the most widely utilised in published literature (Wagner et al., 2011, Pavlacky and Polak, 2020).

Similar to other small RNA libraries, the top 10 most abundant transcripts represented more than 65% of the total miRNA identified within HGENCs with miR-126 being the most abundant in endothelial cells (Voellenkle et al., 2012). The time course data showed that only miR-210-3p is upregulated when HGENCs are cultured under hypoxic conditions from upwards of 12 hours (Figure 6.5 and Figure 6.6a), which was in concordance with the expression kinetics previously reported (Huang et al., 2009). It is however unsurprising to see this upregulation of miR-210-3p as it has been previously reported to be the single miRNA ubiquitously upregulated across all cell types under hypoxic conditions (Huang et al., 2009, Chan et al., 2009) due to the presence of HRE driving the transcription of this miRNA.

This HRE motif allows binding of HIF-1 α and HIF-2 α indiscriminately. However, several mechanisms have been identified to regulate the downstream signaling (Hu et al., 2007, Lau et al., 2007), resulting in HIF isoforms specifically target gene transcription. For miR-210-3p, it was reported to be HIF-1 α dominant (Huang et al., 2009). Hence for endothelial cells like HGENCs, where HIF-2 α is the dominant isoforms (Bartoszewski et al., 2019), the extent of miR-210-3p upregulation would be to a lower extent compared to PTECs (Figure 6.6) in part due to the isoform preferences.

Pathways regulated by miR-210-3p are often associated with cellular metabolism, angiogenesis, apoptosis and differentiation (Chan et al., 2012). In the context of IRI, miR-210-3p has been shown to protect tubular epithelial cells from cell death during the onset of ischemia (Liu et al., 2017) and sustained expression of miR-210-3p in a model of myocardial infarction also attenuated IRI associated injuries (Hu et al., 2010). Hence, to determine the stability of miR-210-3p, both HGENCs and PTECs were subjected to 24 hours hypoxia to induce expression of miR-210-3p before exposing the cells to reoxygenation. We found that miR-210-3p levels remained elevated for up to 48 hours (Figure 6.7), which was longer than the 8 hours reported previously (Fasanaro et al., 2008). Therefore, coupled with the inflammation induced HIF signaling (Virga et al., 2021), miR-210-3p levels would likely remain elevated during reperfusion injury. While this sustained expression protects the heart from injury, the impact in the kidneys likely require experimental validation in part due to cell type and tissue specific mRNA targeting by miRNAs (Rogg et al., 2018, Lu et al., 2015).

Since there is no one-size fit all model to assess the mRNA targeting, we took advantage of the remaining RNA and employed parallel mRNA sequencing to identify downregulated genes that coincided with miR-210-3p elevation. Without artificially inflating the miR-210-3p levels within the cells, we limited the non-specific targeting and regulation by the miRISC (Jin et al., 2015). Furthermore, mRNA sequencing also provided insights into the temporal regulation of the miRNA processing as enrichment of non-coding RNA processing and assembly of ribonuclearprotein biogenesis enriched at 4 hours (6.10, cluster 5) suggest priming of cells to elicit miRNA expression and downstream targeting.

Utilising existing databases that are either predictive (Agarwal et al., 2015) or experimentally validated (Kehl et al., 2019, Huang et al., 2022), we performed an integrated analysis of the sequencing data obtained from hypoxic HGENCs (Figure 6.16). In total, 22 predictive and experimentally validated targets from the databases and temporal expression identified 7 mRNAs (*HIF1A*, *PTBP3*, *UBQLN1*, *TFRC*, *TNRC6B*, *ZNF618*) that downregulated with miR-210-3p upregulation (Figure 6.16). Since the role of *HIF1A* and *TFRC* in hypoxia is well established, we experimentally validated these targets by PCR (Figure 6.17), transfection (Figure 6.19) and protein expression (Figure 6.21).

Functionally, the role of *HIF1A* and *TFRC* are intricately linked as *TFRC* have been shown to be regulated directly by HIF-1 α (Lok and Ponka, 1999). While the importance of TfR1, the protein encoded by *TFRC*, has been shown in erythrocytes (Richard and Verdier, 2020), its role in other organ and tissue remains poorly characterised. However, iron regulation is extremely important for oxidative phosphorylation. In fact, the enzyme aconitase, which is essential for in the tricarboxylic acid (TCA) cycle functions as an iron response protein (Narahari et al., 2000). Together with the targeting of *ISCU*, perturbation to bioenergetics have been shown in cancer cells (Yoshioka et al., 2012). More recently, the increased understanding in cell death pathways also uncovered a new mechanism coined ferroptosis, which is a result in dysregulation of intracellular iron and redox imbalance. Additionally, TfR1 was identified to be a marker of ferroptosis (Feng et al., 2020).

Hence, to explore the impact of downregulating TfR1, ciGENCs were transfected with miR-210-3p and assessed their glycolytic and respiratory capacity. These bioenergetic assays showed an increase in overall capacity to utilise glycolysis (Figure 6.23) for energy while mitochondrial function (Figure 6.24) remains unaltered. While endothelial cells predominantly utilise glycolysis for energy generation (Bock et al., 2013), this unaltered mitochondrial function was surprising as both *TFRC* and *ISCU* have previously been shown to be important for oxidative phosphorylation (Chan et al., 2009, Yoshioka et al., 2012). However, this also highlighted that while *ISCU* downregulation was unintended in ciGENCs, it did not result in supramolecular accumulation of miR-210-3p as it would have resulted in altered mitochondria function (Puisségur et al., 2010). This was also confirmed by the ultrastructure analysis, where we did not observe any mitochondria swelling that is associated with mitochondrial dysregulation (Figure 6.25). This can also suggest the presence of additional regulatory mechanism present to regulate *ISCU* expression or a higher-than-expected levels transfected into the cells even after careful titration (Figure 6.19). However, we can confirm that this did not result in excessive off-targeting effects.

In summary, work from this chapter has shown temporal induction of miR-210-3p in glomerular endothelium in response to hypoxia. Furthermore, we provide insights into the limited alterations in miRNA expression during early onset hypoxia due to the induction of miRNA biogenesis occurring only at the 4 hours mark. Differential *ISCU* regulation was also observed between the renal tubules and the glomerular endothelium, while *TFRC* was actively downregulated in both cell types. We reasoned that this downregulation must be due to miR-210-3p as the HRE upstream of the *TFRC* promoter would result in upregulation by HIF1 signaling and could be a mechanism for the kidneys to avoid the occurrence of ferroptosis. While more work is necessary to characterise the implication of miR-210-3p in the glomerular endothelial, the maintenance of mitochondrial function when this miRNA is overexpressed might provide additional survival advantage over the renal tubules in IRI.

7. Characterisation of Renal Allograft Derived Extracellular Vesicles

7.1. Introduction

The existing dogma states that allorecognition is mediated through two main pathways: direct and indirect. During direct allorecognition, passenger leukocytes within the allograft migrate into the recipient circulation and spleen, where host immune cells identify the mismatched major histocompatibility (MHC) molecules and mount an immune response. This contributes to the development of acute allograft rejection. On the other hand, indirect allorecognition is mediated by cross presentation of donor MHC peptides on recipient antigen presenting cells (APC) class II MHC, resulting in immune activation. Thus, this mechanism is more commonly associated with chronic allograft rejection.

Recent discoveries have however uncovered novel cellular mechanisms mediating intercellular communication, which led to the proposal of semi-direct allorecognition, involving the active transfer of donor MHC molecules released by the allograft to recipient immune cells. The process of donor MHC transfer to recipient immune cells has been shown to be mediated either by recipient dendritic cell trogocytosis of donor MHC molecules (Herrera et al., 2004) or the transfer of intact donor MHC molecules via extracellular vesicles (EVs) (Marino et al., 2016, Ono et al., 2018, Hughes et al., 2019, Prunevieuille et al., 2020, Mastoridis et al., 2020, Zeng et al., 2021). In both instances, the recipient immune cells are “cross-dressed” with the donor MHC molecules allowing direct activation of allospecific recipient immune cells (Section 1.5.3.3).

Beyond MHC molecules, EVs have been shown to transfer other biomolecules including lipids, nucleic acid and metabolites (Niel et al., 2018). This is further complicated by the alteration of EV composition and cargo in response to cellular stresses encountered by the parent cells (Niel et al., 2018). In particular, the enrichment of small RNA species have led to studies identifying how these miRNAs modulate inflammatory states (Zhou et al., 2014, Alexander et al., 2015) and allograft function post transplantation (Franzin et al., 2022).

This chapter aims to show the presence of EVs within the microvasculature of kidney allografts prior to implantation. Subsequently, we also aim to characterise the molecular composition of the cargoes carried by these isolated EVs and identify how these biomolecules work in unison to mediate allorecognition of kidney allografts.

7.2. Specific Aims

- To show the presence of extracellular vesicles within the microvasculature of renal allografts during cold static storage.
- Profiling extracellular vesicles surface proteome and miRNA cargo to identify role their role in pathogenesis of allograft rejection.
- *In vitro* modeling of endothelial cells to generate MHC class II high extracellular vesicles.

7.3. Specific Materials and Methods

7.3.1. Kidney Effluent Collection

University of Washington (UW[®]) solution was instilled into the renal artery during surgical back benching of the kidney at the Freeman Hospital, Newcastle upon Tyne until 20mL was collected from the renal vein into a universal container. Samples were then transferred to Falcon tubes and centrifuged at 800g for 10mins, 4°C before aliquoting and stored at -80°C. In total, 25 samples (8 DCD, 9 DBD and 8 live kidneys) were withdrawn from the Institute of Transplantation Tissue Biobank (17/NE/0022) under study number IOT076.

7.3.2. Cell Culture and Treatment

Confluent HMEC-1 cells were passaged as described in Chapter 2.2. Prior to treatment, cells were seeded at a density of 80,000 cells per well in 12-well plates and cultured overnight unless otherwise stated. Cells were stimulated with interferon gamma (IFN- γ) concentration of 20ng/ml for 72 hours. Post treatment with IFN- γ , cells were prepared for flow cytometry staining for HLA-DQ, HLA-DR, CD31, CD54 and CD105 as outlined in Section 4.6. The gating strategy is shown in Figure 7.1.

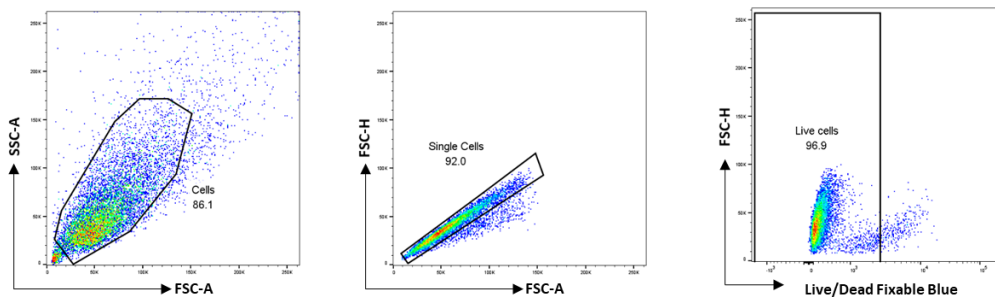


Figure 7.1 Gating strategy for HMEC-1.

Cell population was first gated based on scatter profile before identifying the single cell population. Subsequently, live cells, determined as Live/Dead™ Fixable Blue negative population were gated for other labeled surface markers.

7.3.3. Generation of EVs from In Vitro Culture

Confluent flasks of HMEC-1 or HMEC-1 HLA-DR cultured in T175 was passaged at a ratio of 1: 5. Cells were cultured for 3 days in complete media or in complete media with the addition of 20ng/ml of IFN- γ . After 3 days, spent culture media was removed and cells were washed twice with PBS. Serum free media or serum free media containing 20ng/ml of IFN- γ was added to the cells and cultured for another 3 days for the harvesting of EVs. Conditioned media was harvested from the cells and transferred to Falcon tubes. The media was centrifuged at 300g for 10mins at room temperature before decanting the supernatant into fresh Falcon tubes. The supernatant was then centrifuged at 2000g for 10mins at 4°C. The supernatant was collected and stored at -80°C until isolation of EVs.

7.3.4. Extracellular Vesicle Isolation

7.3.4.1. Differential Centrifugation

Cell and debris depleted kidney effluents were thawed overnight at 4°C. Subsequently, samples were transferred to high-speed centrifuge tubes and spun at 10,000g for 30min at 4°C (Beckman Coulter, Avanti JXN26 equipped with JA25.50 fixed angle rotor) to deplete the microvesicles. Supernatant was collected and subjected to ultracentrifugation at 100,000g (RCF average of 25,000rpm, Beckman Coulter, Optima XE-90 equipped with SW28 swing bucket rotor, k-factor=246) for 2 hours at 4°C. Supernatant was collected before resuspending the pellet with particle-free PBS (Sigma) and centrifuged at 100,000g for 1hour 10mins. Supernatant was carefully removed, and the EV pellet was resuspended in 200 μ L PBS, aliquoted and stored at -80°C.

7.3.4.2. Size Exclusion Chromatography

Conditioned media from cells was thawed overnight at 4°C. Subsequently, samples were transferred to high-speed centrifuge tubes and spun at 10,000g for 30min at 4°C (Beckman Coulter, Avanti JXN26 equipped with JA25.50 fixed angle rotor) to deplete the microvesicles. Supernatant was collected and culture medium was concentrated using a 100kDa Amicon filter (Sigma) down to 150µL. The concentrate was then loaded onto a qEV single 35nm Legacy column (Izon) and samples were fractionated into 20x 200µL fractions. Protein concentration of the fractions were determined using a Nanodrop™ spectrophotometer (ThermoFisher) with the 1 Abs =1mg/ml setting and particle concentration was determined using as outlined in 7.3.5.

7.3.5. Nanoparticle Tracking Analysis (NTA)

Size distribution and total particle estimation of isolated EVs were determined using a Nanosight LM10-HS microscope equipped with a red laser and analysed on NTA software V3.2 (Nanosight). Background extraction was applied and the automatic setting for minimum expected particle size, minimum track length and blur settings were employed. 5 × 60secs recordings at 30 frames per second were taken for each sample which was diluted in particle free PBS (Sigma) at appropriate concentrations. Only measurements with more than 500 completed tracks were analysed.

7.3.6. Electron Microscopy

Negative staining and visualisation under transmission electron microscopy (TEM) was utilised for morphological assessment of EVs. 20µL of isolated EVs was submitted to Newcastle University Electron Microscopy Research Services. In brief, carbon coated copper grids were glow discharged and 10µL of the isolated EVs were adsorbed onto the grid. Excess liquid was removed and a drop of 1% uranyl acetate was added to the grid and stained for 30secs. Excess uranyl acetate was removed, and the grid was dried under a lamp. The grids were then imaged on a 120kV TEM (Hitachi HT7800) attached with a XAROSA CMOS camera (EMSIS).

7.3.7. EV Surface Proteome Analysis

The surface proteome of isolated EVs was analysed using the MACSPlex Human Exosome kit (Miltenyi). In brief, EV isolates were topped up to 120 μ L with MACSPlex buffer in a low bind tube (Sarstedt). Exosome capture beads were vortexed for 30secs and 15 μ L of the capture beads added to each sample. All samples were incubated overnight in the dark at room temperature on a MACSmix™ tube rotator on 12rpm, following which, 500 μ L of MACSPlex buffer was added to each tube and centrifuged at 3000g, 5mins at room temperature. 500 μ L of the supernatant was carefully aspirated and discarded. 15 μ L of antibody cocktail containing equal parts of CD9, CD81, and CD63 was added to each sample and incubated at room temperature for 1 hour on a MACSmix™ tube rotator on 12rpm. Subsequently, 500 μ L of MACSPlex buffer was added to each tube and centrifuged at 3000g, 5mins at room temperature. 500 μ L of the supernatant was carefully aspirated and discarded. Additionally, 500 μ L of MACSPlex buffer was added to each sample and incubated at room temperature for 15mins on a MACSmix™ tube rotator on 12rpm. 500 μ L of the supernatant was removed and the samples were topped up to a final volume of 200 μ L before transferring to flow tubes and data acquisition (Figure 7.2) on the Symphony A5 flow cytometer. Data analysis was then done on FlowJo V9 and a custom Microsoft Excel template generated in-house. Background corrected data was log-transformed and used as inputs into R for data visualisation and clustering of the data was done using base R package.

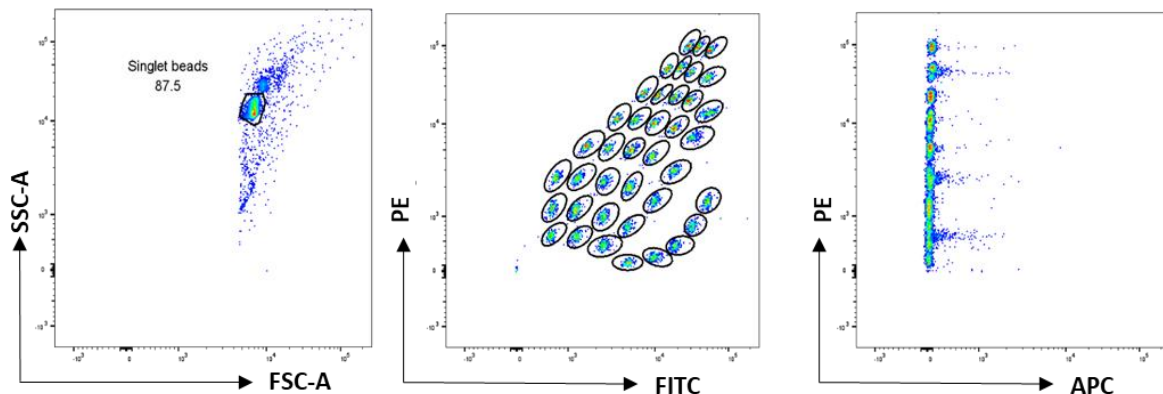


Figure 7.2 Gating strategy for MACSPlex Human Exosome kit.

Singlet bead events were gated off the forward vs side scatter on a log-scale. Subsequently, the individual bead populations were resolved on a FITC vs PE channel before finally looking at the fluorescence intensity of the EV position populations on the PE vs APC channels. Median APC MFI of the individual channels was used for subsequent analysis.

7.3.8. Total RNA Extraction from EVs

RNA from EVs isolated from kidney effluent was isolated using a modified miRNeasy mini kit (Qiagen). The volume of EV isolates used for RNA isolation was standardised at 120µL. Qiazol was added to the EV isolates at 10× the volume (1200µL) and the mixture was vortexed vigorously and left to sit at room temperature for 10mins. Chloroform was added at a 1:5 volume of Qiazol (240 µL) and the mixture was vortexed vigorously for 15 secs. The mixture was incubated at room temperature for 3mins before spinning at 12,000g, 15mins at 4°C. The upper aqueous phase was transferred to a 1.5mL tube and 100% ethanol was added at 1.5× of the aqueous phase volume. Samples were mixed thoroughly before transferring to an RNeasy mini column.

To remove any remaining cellular contaminant, the flow through was discarded before addition of 700µL of Buffer RWT. Subsequently, the RNeasy spin column was centrifuged at 8,000g for 15secs. This was followed by 2× addition of 500µL Buffer RPE and centrifuged at 8,000g for 15secs and 2mins respectively. The spin column was then transferred to a new collection tube and centrifuged at 17,000g, 1 min to dry out the silica and remove any remaining buffer. Lastly, the silica column was transferred to a 1.5mL collection tube followed by the addition of 30µL of RNase free water and left to sit at room temperature for 10mins. The tube was then centrifuged at 8,000g for 15secs to elute the RNA.

7.3.9. RNA Quantification

Total RNA isolated from EVs was quantified using the 2100 BioAnalyzer (Agilent) with the RNA6000 Pico kit (Agilent) following the manufacturer's protocol. Pico gel matrix was prepared as per instructed prior to the assay and all samples and reagents were equilibrated to room temperature prior to commencement of the assay.

In brief, 9µL of gel-dye mix was dispensed into a chip and primed before the addition of 9µL of the gel-dye mix into each of the sampling wells. 9µL of the RNA 6000 Pico conditioning solution was added into the well labeled "CS". Following this, 5µL of RNA 6000 Pico marker was added into all the sampling wells and the well labelled with a ladder symbol. RNA samples were heat denatured at 70°C for 2mins before loading 1µL onto the sampling wells on the chip. Finally, 1µL of the diluted RNA 6000 Pico ladder was added into the well labelled with a ladder symbol. The chip was then placed horizontally into the BioAnalyzer chip adapter mounted MS3 vortex mixer

(IKA) and vortexed for 60secs at 2400 rpm. Finally, the chip was transferred to the Bioanalyzer and ran following the instructions on the Agilent 2100 Expert Software.

7.3.10. Nanostring®

miRNA profiling of the RNA isolated from the EVs was carried out using the nCounter® Human V3 miRNA expression panel. The RNA samples extracted was subjected to a clean-up process by topping the extracted RNA up to 400µL before centrifugation at 14,000g, 90mins at 4°C using a 3kDa Amicon filter (Sigma). Subsequently, these RNA samples were submitted to the Nanostring® facility in the Human Dendritic Cell group and prepared with an alteration to the manufacturer's protocol described by Crossland *et al* (Crossland et al., 2023).

7.3.10.1. Sample preparation

miRNA assay controls were diluted at 1:500. Subsequently, an annealing master mix containing 13µL of annealing buffer, 26µL of nCounter® miRNA Tag reagent and 6.5µL of the diluted miRNA assay controls. 5µL of RNA samples were mixed with 3.5µL of the annealing master mix before running it on a thermocycler with the following conditions: 94°C for 1 min, 65°C for 2mins, 45°C for 10mins and hold at 48°C.

A ligation mix consisting of 22.5µL of polyethylene glycol and 15µL of ligation buffer was prepared and 2.5µL of the ligation mix was added to the samples. The samples containing the ligation mix was returned to the thermocycler and incubated for 5mins at 48°C. 1µL of ligase was added to samples in the thermocycler at 48°C and ran on a thermocycler with the following conditions: 48°C for 3mins, 47°C for 3mins, 46°C for 3mins, 45°C for 5mins, 65°C for 10mins and finally holding the temperature at 4°C. 1µL of the ligation clean-up enzyme was added to the reaction and ran on a thermocycler with the following conditions: 37°C for 1 hour, 70°C for 10mins and holding the final temperature at 4°C. At the end of the run, 40µL of nuclease-free water was added to each sample and proceeded to the next step.

7.3.10.2. Codeset Hybridisation

130µL of miRNA Reporter Codeset was mixed with 130µL of hybridisation buffer to prepare a hybridisation mastermix. 20µL of the mastermix was added to strip tubes. Samples prepared in Section 5.3.10.1 was heat denatured at 85°C for 5mins and cooled quickly on ice and 5µL was transferred to the strip tubes. Subsequently, 5µL of the capture probeset was added to each individual tubes. Immediately sample was placed in a preheated thermocycler at 65°C and left to hybridise for 22 hours.

7.3.10.3. Sample Loading and Data Acquisition

Hybridised samples were immediately removed from the thermocycler and transferred to the nCounter® GEN2 prep station 5s (Nanostring®) for purification and immobilization into the sample cartridge for data collection. Once completed, the cartridge was transferred to the nCounter® Digital Analyzer 5s for imaging with a field of view (FOV) of 550.

7.3.10.4. Data analysis

Data was generated as a custom RCC file and subsequently loaded into the nSolver™ software (Nanostring®). Samples were prepared over 3 different nCounter® Human V3 miRNA expression panels and normalisation were carried out within the software using the geometric means of positive control and the top 100 probe codeset content normalisation. miRNA was determined to be positively detected in each sample lane when the counts exceeds the mean $\pm 2 \times$ standard deviation of 5 out of the 6 negative controls, with the exclusion of Negative control C (Crossland et al., 2023). Post filtering for positively detected miRNA, counts were passed onto DESeq2 V3.16 (Love et al., 2014) for unsupervised analysis. Initial data analysis identified batch effects arising from the profiling, hence batch was subsequently added to the design matrix and passed on to the function “limma:removeBatchEffect” before plotting the heatmaps and PCA plots shown.

7.4. Results

7.4.1. Characterisation of EVs

Following the latest Minimal Information for Studies of Extracellular Vesicles 2018 (MISEV 2018) guidelines (Théry et al., 2018), a combination of methodologies is required to confirm the presence as well as the purity of isolated EVs. Since the EVs derived from the kidney effluent have not been characterised previously, we set out to follow the criteria outlined.

Firstly, TEM micrographs of EVs isolated from DBD, DCD and living donor category (Figure 7.3a, b, c respectively) showed the typical cup shape morphology. The isolated EVs were also identified to have modal sizes less than 200nm (Figure 7.3a, b, c) and NTA analysis of blank UW[®] solution did not detect any particles (data not shown as insufficient particle tracks were detected for the analysis to be valid). Finally, western blot demonstrated that the pooled EV isolates were highly enriched for EV-associated proteins CD9 and TSG101, whilst the endoplasmic reticulum marker calnexin was absent (Figure 7.3f). Collectively, these data confirmed that the isolated particles from kidney effluents are indeed EVs free of cellular contaminants.

Hypoxia as one of the hallmarks of allograft ischemia have been previously shown to alter the number (Bister et al., 2020, Wang et al., 2023) and size (Bister et al., 2020, Ana Muñoz-García, 2022) of EVs. Since these alterations to the released EVs are cell type dependent, we assessed for any observable changes in either quantity or size of the EVs isolated across kidney types. As indicated in Figure 7.3d, the modal size of the isolated EVs did not show any significant changes across all the groups. In contrast, the number of EVs isolated from DCD allograft effluents showed a significant increase when compared to living donor allografts (Figure 7.3e).

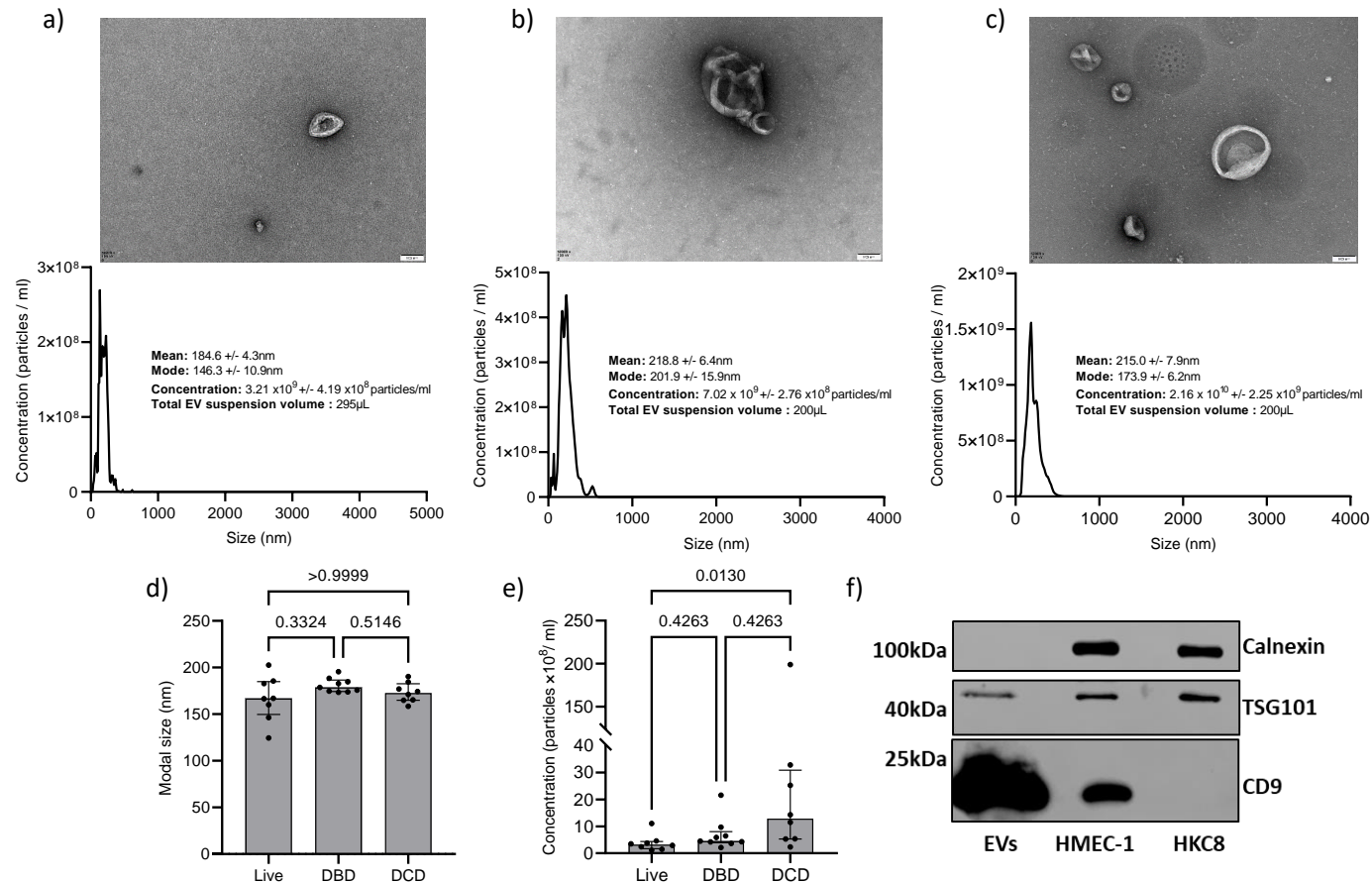


Figure 7.3 Characterisation of EVs isolated from kidney effluents.

EVs isolated from kidney effluent via differential centrifugation was analysed. Representative TEM micrograph and size distribution plot for a) Living donor, b) DBD and c) DCD effluent EVs isolated. d) Average modal size of the isolated EVs did not show any significant difference when compared across allograft groups. e) EVs isolated from DCD allografts showed a significant increase in total particle concentration isolated compared to living donor allograft EVs. f) Western blot of pooled EVs (n=9) identified enrichment in CD9 and TSG101 expression and the absence of calnexin, indicating an isolate free of cellular contaminant. HMEC-1 and HKC8 (renal tubular epithelial cells) cells are loaded as controls. Modal size and particle concentration data shown as mean \pm SD of n=8 for DCD, n=9 for DBD and n=8 for Live kidneys. Statistical analysis was performed using One-Way ANOVA with Tukey's post-hoc test.

Table 7.1 Donor allograft parameters and 1 year kidney function.

	DBD	DCD	Live
Age	53±15	50±21	43±11
CIT (mins)	1136±254	1136±316	223±94
DGF (total)	7 (9)	6 (8)	1(8)
1 year Creatinine (µmol/L)	114±41	212±105	137±87
1 year eGFR (ml/min/1.73 m2)	61±19	42±25	65±26

7.4.2. Total EVs Isolated Correlated with Allograft Cold Ischemic Time (CIT)

Deceased donors tend to have a longer CIT compared to living donor allografts and this was the case in our cohort (Table 7.1). With the significantly increased EVs isolated from DCD allografts compared to the living donors, we set out to identify any correlation between the ischemic times with the total EVs isolated. We found a positive correlation between the allograft CIT and the total EVs isolated (Figure 7.4).

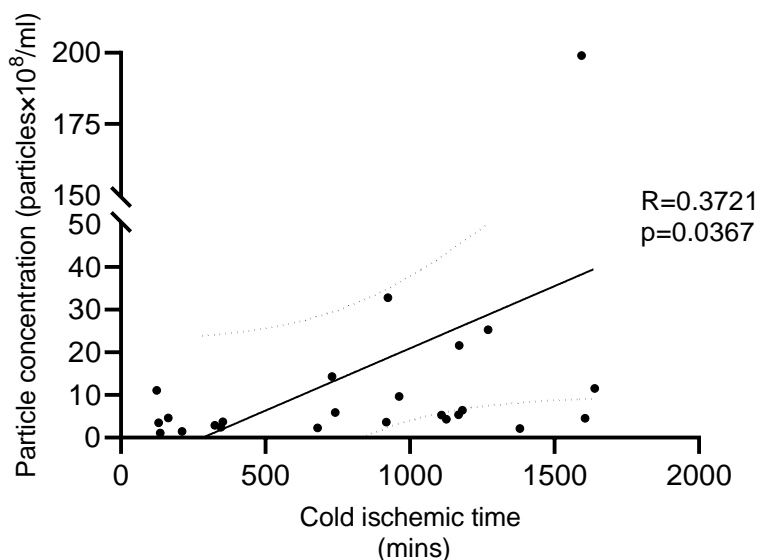


Figure 7.4 Correlation between total particles released with allograft cold ischemic time.

Pearson’s correlation between allograft cold ischemic time and particle concentration showed a significant correlation.

7.4.3. Surface Proteome of Kidney Effluent EVs

Surface marker expression on kidney effluent EVs was analysed with a commercial kit that allows detection of 37 pre-defined markers by flow cytometry (Koliha et al., 2016). Samples within each donation group were pooled to achieve data with high definition. EVs were pooled based on particle concentration in a manner to ensure almost equal contribution from each sample (Table 7.2). These pooled samples were subsequently reassigned with a new sample ID for downstream analysis. As shown in Figure 7.5, kidney effluent EVs showed the expression of all 37 markers to varying degrees. Amongst the high expression markers, EV tetraspanins were highly expressed, further confirming the isolated particles to be EVs.

Table 7.2 Pooled kidney effluent EVs and final particle count.

DBD			DCD			Live		
Sample ID	Combination	Particle count	Sample ID	Combination	Particle count	Sample ID	Combination	Particle count
DBD1	BM48+BM51	3.08x10 ⁸	DCD1	BM29_001+BM30	3.16x10 ⁸	Live 1	BM52+BM56	2.11x10 ⁸
DBD2	BM22+BM047	3.004x10 ⁸	DCD2	BM38+BM41	3.018x10 ⁸	Live 2	BM34+BM17	2.208x10 ⁸
DBD3	BM19+BM50	2.998x10 ⁸	DCD3	BM33+BM39	2.965x10 ⁸	Live 3	BM21+BM23	1.988x10 ⁸
DBD4	BM37+BM42	2.646x10 ⁸	DCD4	BM31+BM40	2.81x10 ⁸	Live 4	BM44+BM54	2.452x10 ⁸

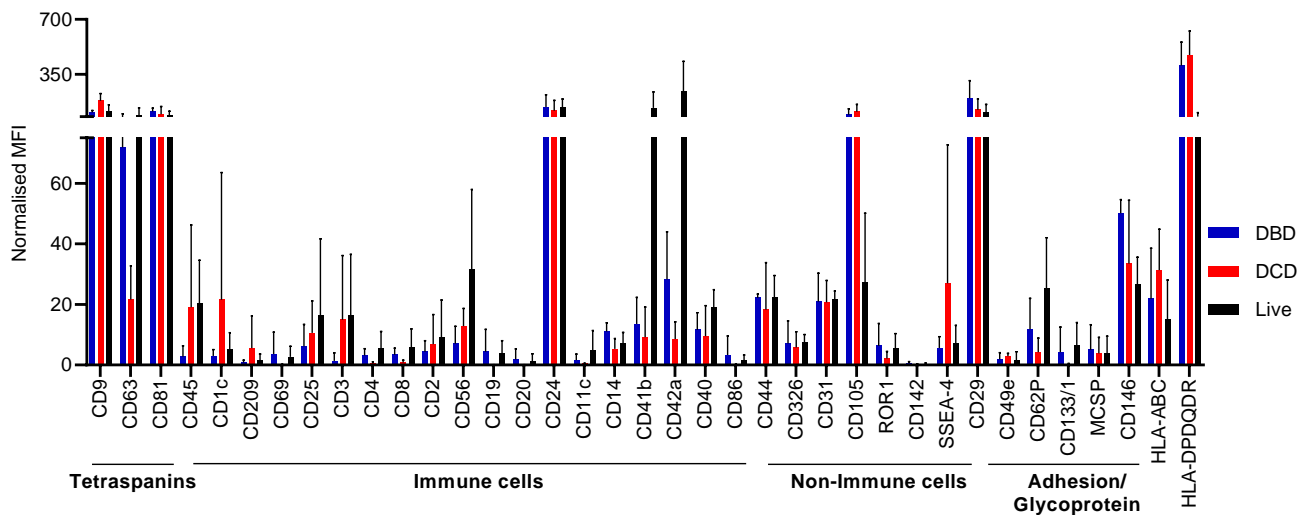


Figure 7.5 Normalised MFI of kidney effluent EVs.

Surface proteome of the kidney effluent EVs were assessed using Miltenyi MACSPlex exosome kit. Expression of surface marker is indicated as MFI normalised to the tetraspanins. Data shown as mean \pm SD of n= 4 per kidney type.

7.4.4. Deceased Donors Associated with Increased EV MHC Class II Expression

Tetraspanin expression on EVs are known to be highly heterogenous (Kugeratski et al., 2021). In fact, knockdown of CD9 (Brzozowski et al., 2018) and CD63 (Hurwitz et al., 2016) in the parent cells have been shown to alter the overall production of EV subpopulations. Within our cohort, we identified significantly higher expression of CD9 in the DCD group compared to both DBD and living donor (Figure 7.5 and Figure 7.6). On the other hand, CD63 expression was significantly higher in living donor group compared to DCD (Figure 7.6). While the implication of these altered tetraspanins within our cohort remains unknown, our findings remain in line with existing literature.

In addition, DBD group showed the highest expression of CD29 whereas the living donor group showed a significantly lowered CD105 expression while expressing the highest levels of CD41b and CD42a (Figure 7.6). The most striking difference in the surface marker expression however was with MHC class II, which was the most highly expressed marker within the panel (Figure 7.5) and highly significantly increased in the deceased donor group compared to the living donor group (Figure 7.6).

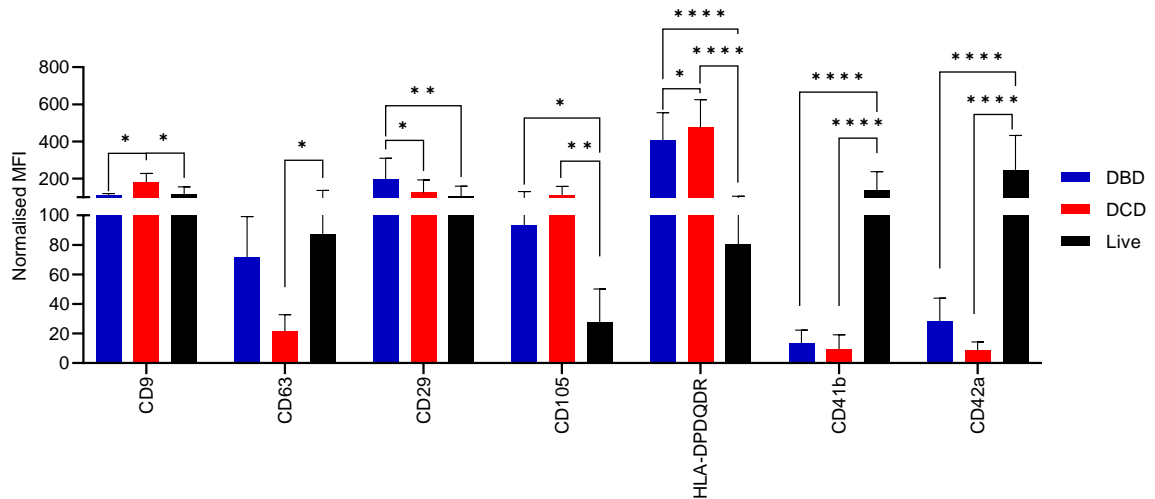


Figure 7.6 Significant differentially expressed surface markers.

Kidney effluent EVs assessed by Miltenyi MACSplex exosome kit and the significant differentially expressed surface markers were plotted separately from the full panel. Expression of surface markers is shown as MFI normalised to the tetraspanins. Data shown as mean \pm SD of n=4 per kidney type. Statistical analysis was carried out with the full panel using Two-Way ANOVA with Tukey's post-hoc test. * p < 0.05, ** p < 0.01, *** p < 0.001, **** p < 0.0001.

7.4.5. Deceased Donors Clustered Independently from Living Donors

To further delineate the implications of these different expressions of surface proteome across all allograft categories, hierarchical clustering was first applied to the data. As highlighted in Figure 7.7a, three main clusters were identified. Of which, the majority of the deceased donor allograft EVs clustered separated from the living donor counterpart. When dimensionality reduction and k-means clustering algorithm was applied to the data, we further observed distinct clustering of the DCD donor (Figure 7.7b).

7.4.6. MHC Class II and CD105 Contributes to Distinct Clustering in DCD samples.

While there was inconsistency with the clustering of the DBD group across the 2 separate unsupervised analysis (Figure 7.7), what was very distinct is the separation of DCD from the living donor group. Analysis on the PCA loading identified MHC class II, CD9 and CD105 to be the main surface markers driving the separation in clusters (Figure 7.8b).

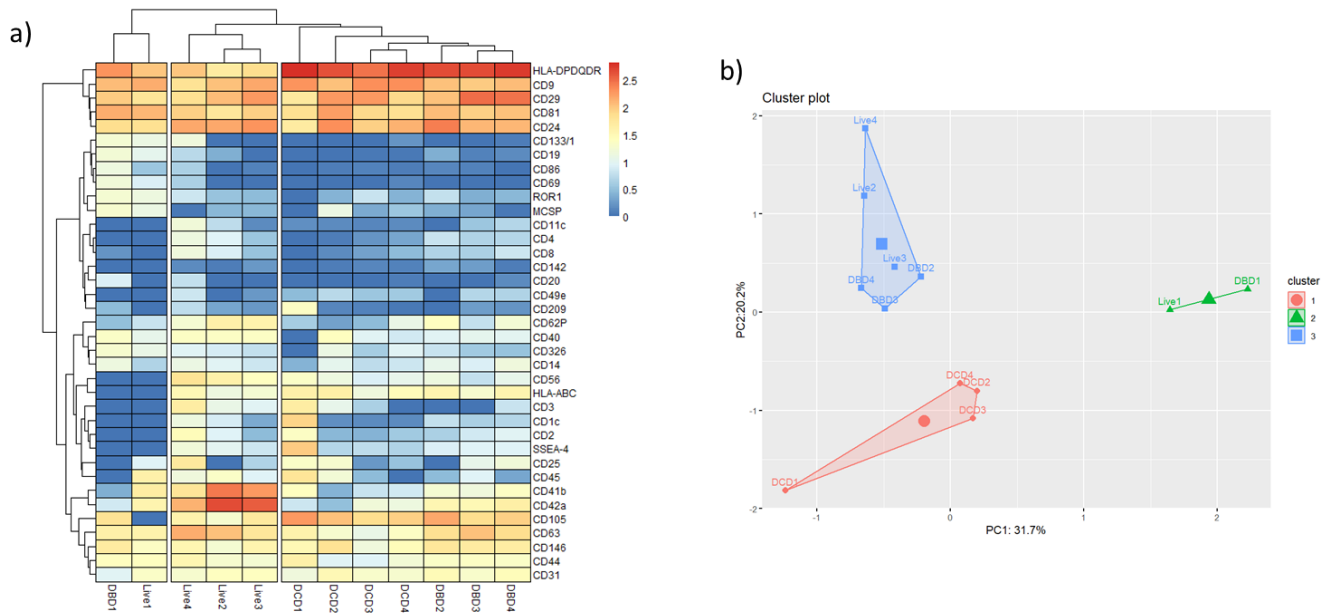


Figure 7.7 Data clustering by surface marker expression on kidney effluent.

Kidney effluent EVs assessed by Miltenyi MACSPlex exosome kit. Normalised MFI was transformed using $\log(\text{Normalised MFI}+1)$ before clustering or dimension reduction. a) Hierarchical clustering showed 3 main clusters identified and distinct separation between living and deceased donor was observed. b) PCA plot and k-means clustering with $k=3$ showed DCD samples clustering away from the rest of the donor category. Optimum k was determined using the silhouette method.

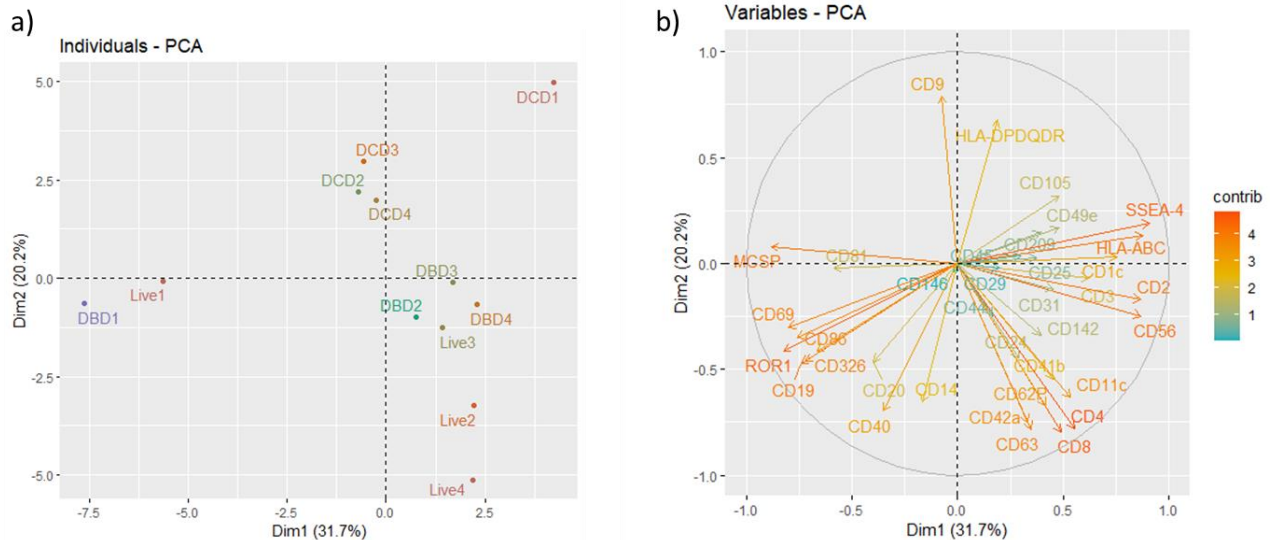


Figure 7.8 PCA loading driving separation of samples.

a) Analysis of the PCA plot showed distinct separation of DCD from other donor groups. b) PCA loading showing the variables that are accounting for the placement of the samples when dimensionality is reduced.

7.4.7. RNA Isolation from Kidney Effluent EVs.

The RNA cargo of EVs has been extensively characterised and shown to alter in response to cellular state (Niel et al., 2018). Total RNA was extracted and analysed using a Bioanalyzer 2100. As indicated in Figure 7.9, the majority of the RNA species isolated across the groups were smaller than 200 nucleotide, which was in line with published work suggesting enrichment of small RNA species within EVs (Garcia-Martin et al., 2021). Furthermore, there was no significant difference between the total RNA isolated from kidney allografts across the categories (Figure 7.9).

7.4.8. No Distinct miRNA Signature was Identified from Kidney Effluent EVs.

With the Bioanalyzer trace showing the majority of the RNA species isolated to be less than 200 nucleotides, we reasoned that these RNA species would be highly enriched in miRNA. The low RNA yield isolated from these EVs presents difficulty for profiling by conventional sequencing. However, successful profiling of EV-derived RNA with a 100 fold lower than the recommended RNA input has been recently shown using the Nanostring® nCounter technology (Crossland et al., 2023). A total of 24 kidney effluent samples were profiled for RNA expression. As indicated in Figure 7.10, dimension reduction did not result in discrete clustering of samples. Furthermore, top 35 expressing miRNA as shown in the heatmap also did not result in meaningful clustering of data (Figure 7.10). In addition, there were no significantly different expressed miRNAs detected across the donor groups.

7.4.9. Induction of Endothelial MHC Class II Expression In Vitro

Endothelial cells lining the microvasculature have been identified to express MHC class II on their surface in response to injury and inflammation (Satchell et al., 2006). Coupled with CD105 being a canonical endothelial cell marker, we reason that the separation we observed in the DCD EV samples can be in part derived from activated endothelium within the allograft microvasculature.

To first show that endothelial cells can be stimulated to express MHC class II, HMEC-1 cells were stimulated with IFN- γ (Taflin et al., 2011, Cross et al., 2021). In order to confirm the activation of the cells, we assessed the adhesion molecule expression of HMEC-1 post stimulation. The treatment resulted in an increase in both CD31 (Figure 7.11a) and ICAM-1 (Figure 7.11b). These activated endothelial cells were found to also increase their HLA-DR expression (Figure 7.12a) whereas only a marginal increase in HLA-DQ (Figure 7.12b) was observed. This was consistent

with a previous report where IFN- γ stimulation alone resulted in minimal HLA-DQ expression and only when stimulated in concert with TNF- α did HMEC-1 increase HLA-DQ expression after three days (Cross et al., 2021).

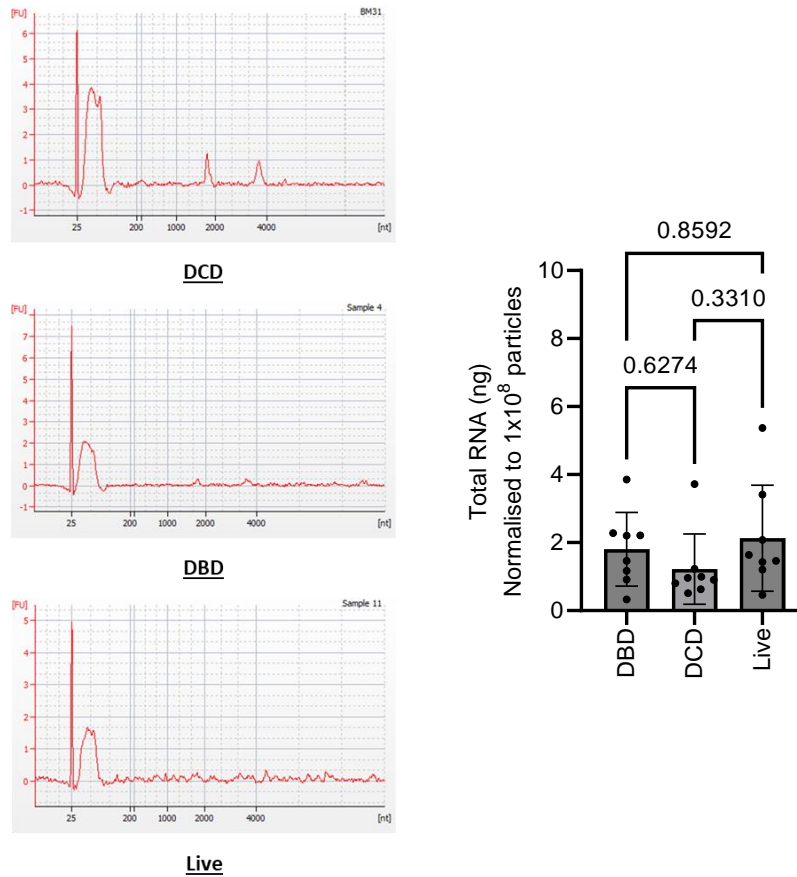


Figure 7.9 RNA quantification from kidney effluent EVs.

Total RNA from EVs were extracted using Qiagen miRNeasy kit and RNA was quantified using a Bioanalyzer RNA6000 PICO kit. The representative RNA trace from each donor category shows the majority of the RNA species isolated are smaller than 200 nucleotides. No significant difference was observed between the total RNA present between allograft categories. Data shown as mean \pm SD of n=24 biological replicates. Statistical analysis was performed using One-Way ANOVA with Tukey's post-hoc test.

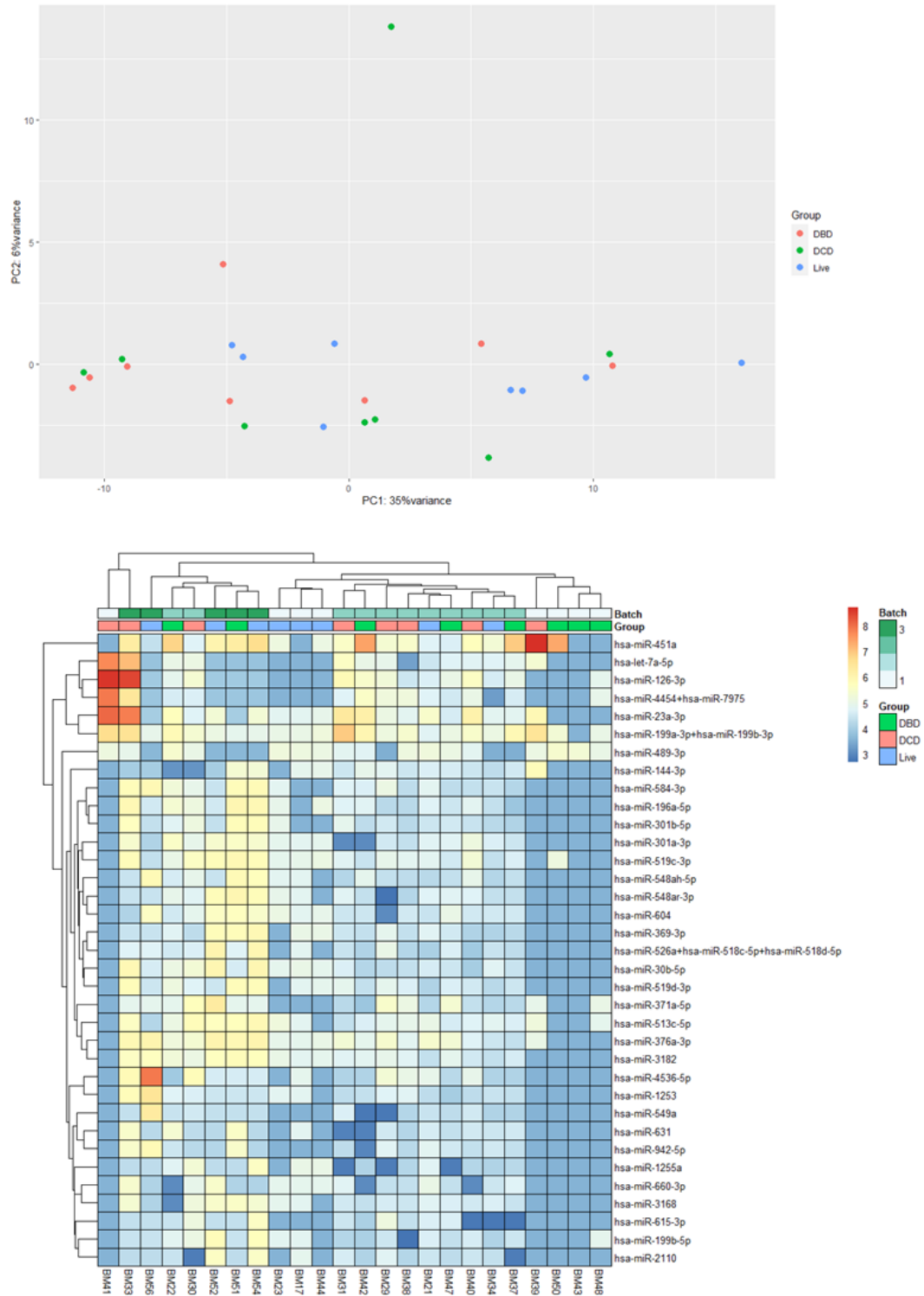


Figure 7.10 miRNA signature in kidney effluent EVs.

miRNA profiling using Nanostring® nCounter Technology showed quantification of miRNA from the kidney effluents. a) Dimension reduction using PCA did not show any discrete clustering of samples. b) Hierarchical clustering on heatmap using the top 35 expressed miRNA did not show any clustering of donor groups.

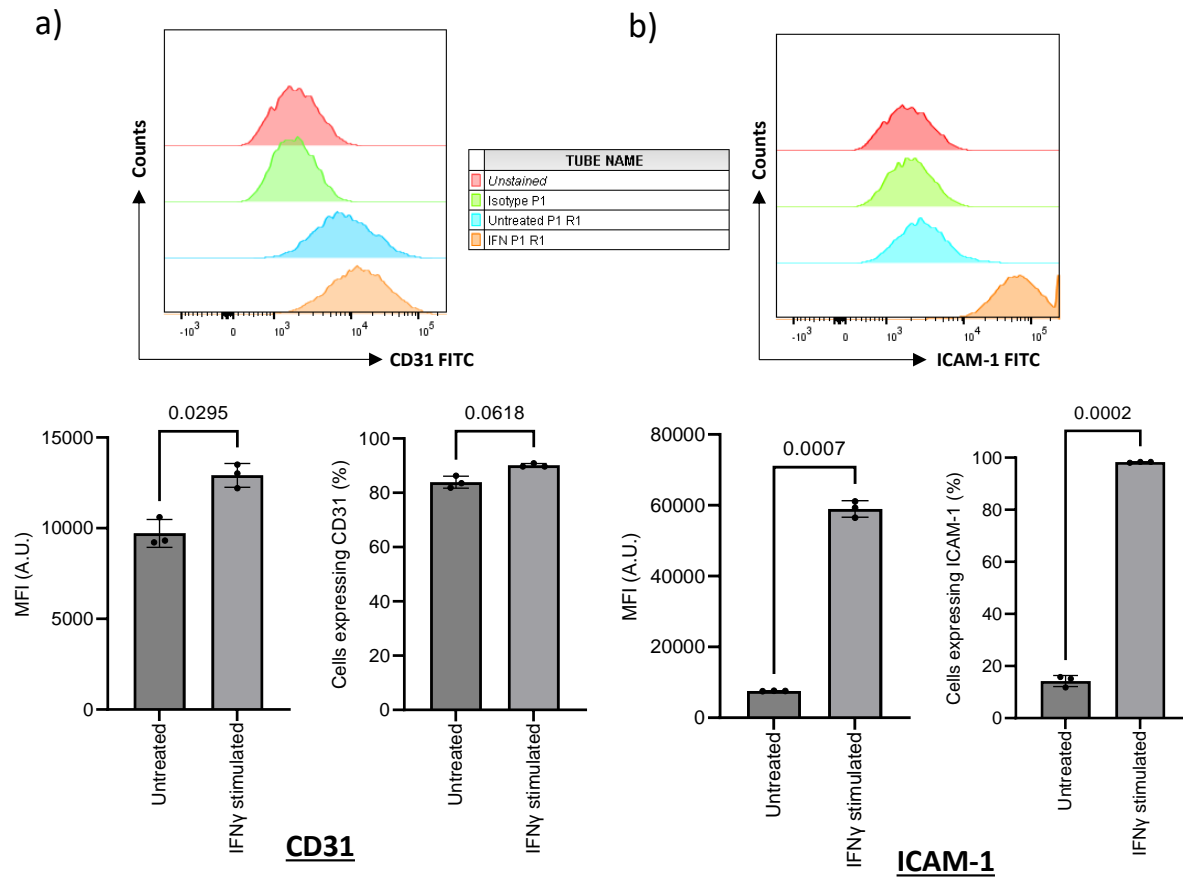


Figure 7.11 Activated endothelial phenotype post-IFN- γ stimulation.

HMEC-1 were treated with 20ng/ml IFN- γ for three days and surface adhesion molecules expression was determined by flow cytometry. a) CD31 and b) ICAM-1 show a significant increase in MFIs. An increase in the total percentage of cells expressing ICAM-1 was also observed. Data shown is representative of n=3 replicates. Statistical analysis was performed using an unpaired Student's T-test.

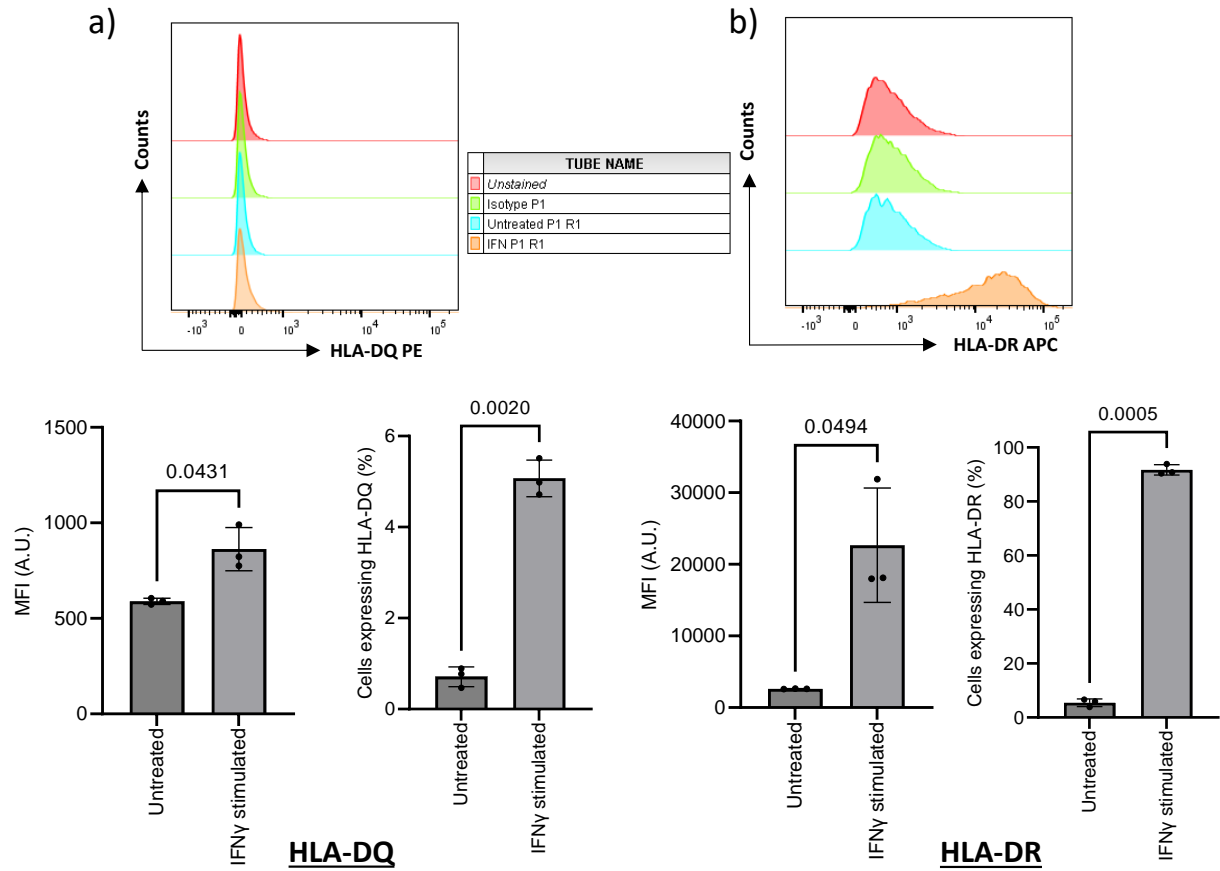


Figure 7.12 MHC class II expression in activated endothelial cells.

HMEC-1 were treated with 20ng/ml IFN- γ for three days and MHC class II expression was determined by flow cytometry. a) HLA-DQ and b) HLA-DR show a significant increase in MFIs as well as an increased in total percentage of cells expressing these MHC class II molecules in response to the treatment. Data shown is representative of n=3 replicates. Statistical analysis was performed using an unpaired Student's T-test.

7.4.10. EV Generation from HMEC-1 In Vitro

Cells cultured *in vitro* have been identified to have different rates of EV production (Kugeratski et al., 2021, Garcia-Martin et al., 2022). Hence, to determine the quantities and properties of EVs derived from HMEC-1 cells, conditioned media from 4×T175 flasks was harvested and EVs were isolated as outlined in Section 7.3.4.2. Enrichment of EVs were identified in Fraction 7 and Fraction 8 of the size exclusion chromatography whilst the majority of the protein within the conditioned media eluted from Fractions 10 onwards (Figure 7.13c). Electron microscopy also showed EVs isolated with the typical cup-shaped morphology (Figure 7.13a) as well as enrichment in EV markers CD9, CD63, TSG101 and HSP70 and the absence of calnexin on western blot (Figure 7.13b). Together with the particle modal size distribution in Fraction 7 and Fraction 8 around 200nm (Figure 7.13d & 7.13e), we confirmed the isolation of EVs with minimal protein contaminants co-isolated.

7.4.11. IFN- γ Stimulation Resulted in Co-isolation of Lipoprotein

With the successful isolation of EVs from HMEC-1 at basal levels, we next sought to characterise EVs isolated under constant IFN- γ stimulation. As indicated in Figure 7.14a, EVs isolated from 4×T175 flasks HMEC-1 under basal conditions showed similar profiles in Figure 7.13c, demonstrating reproducibility of the EV generation *in vitro*. At similar scale however, cells stimulated with IFN- γ showed reduced capacity for EV production (Figure 7.14b) whilst three times higher peak protein eluted at Fraction 15 when compared to the controls. This is in part due to reduced proliferative capability as a result of IFN- γ stimulation (Lee et al., 2021). Next, 10 μ g of total protein from either cell lysates or EV Fraction 7 were resolved to characterise EV purity and enrichment of canonical EV markers. While EVs isolated under basal conditions and stimulation with IFN- γ showed the lack of cellular contaminant as indicated by calnexin, a reduced reactivity in TSG101 was observed in the stimulated cells compared to the controls, confirming the total particle estimation (Figure 7.14c). Furthermore, whilst the electron micrograph from the control HMEC-1 showed typical EV morphology (Figure 7.14d), the IFN- γ stimulated HMEC-1 showed co-isolation of contaminating lipoprotein (Figure 7.14e, red arrows).

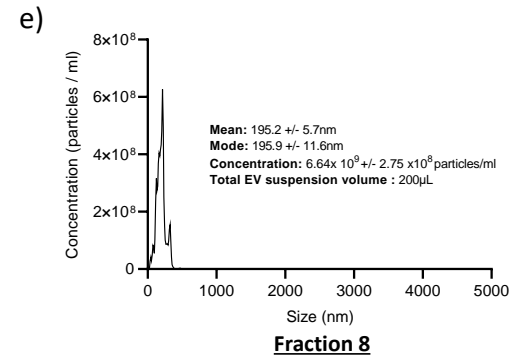
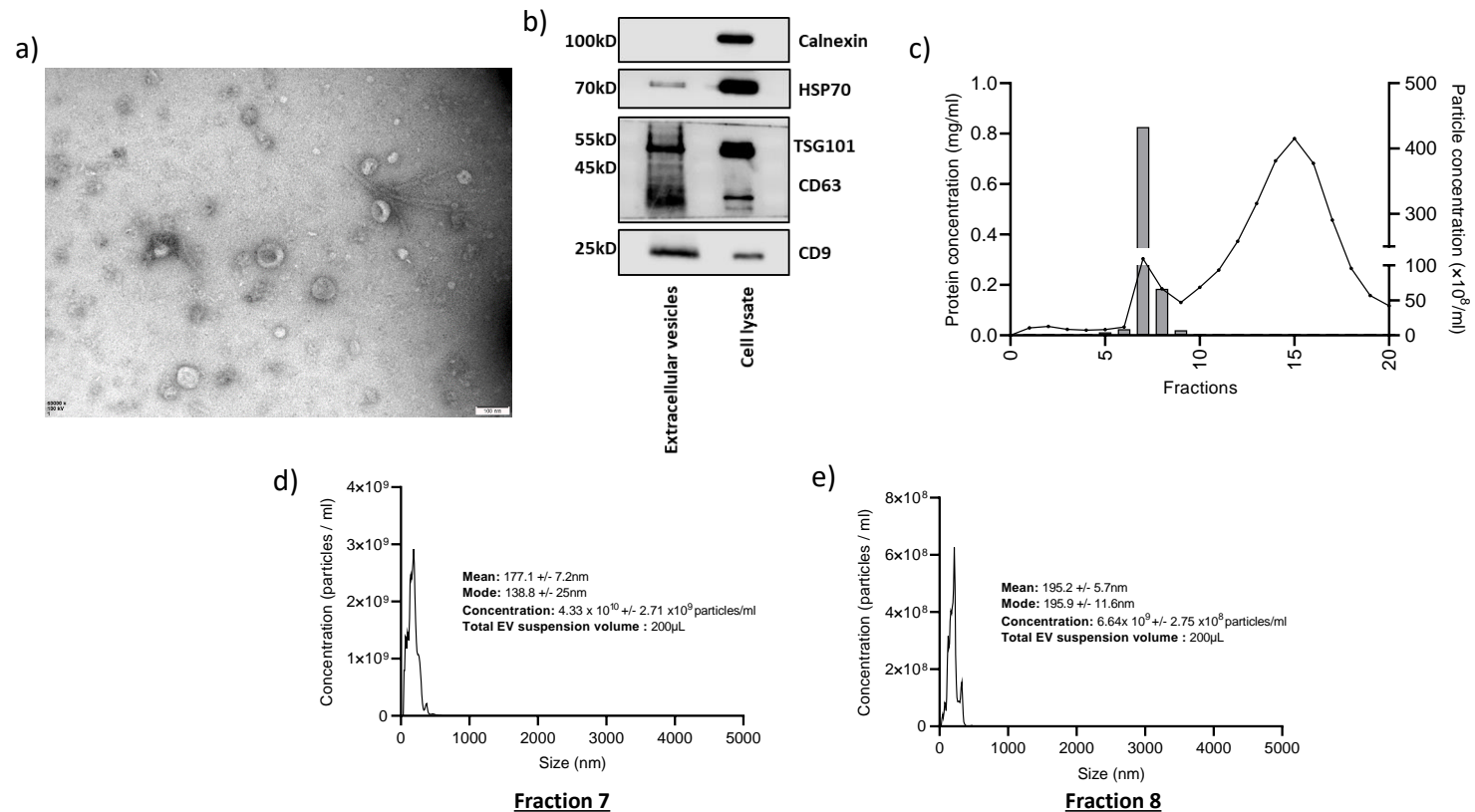


Figure 7.13 Characterisation of HMEC-1 EVs.

Conditioned media from HMEC-1 cultured in serum free condition was harvested and subjected to centrifugation to remove cellular debris and microvesicles. Subsequently, culture media was concentrated on an Amicon filter and purified via size exclusion chromatography. a) Electron micrograph showed typical cup-shape morphology of EVs. b) Western blot analysis of EVs with corresponding cell lysate for EV markers CD9, CD63, TSG101, HSP70 and ER marker calnexin. c) Combined plot showing enrichment of EVs in Fractions 7 and 8 from the size exclusion chromatography with minimal protein contamination co-eluted as determined by Nanodrop™. Particle concentration and modal size of d) fractions 7 and e) 8 indicating majority of the EVs eluting at fraction 7. Data shown represents the pooled EVs from n= 4xT175 flask of cultured HMEC-1. Scale bar = 100nm.

7.4.12. EVs Isolated from HLA-DR Transduced HMEC-1 did not Show Contaminating Lipoprotein

Lipoprotein contaminated EV isolates not only skews particle and total protein quantification but can also negatively impact on the functional studies using isolated EVs (Busatto et al., 2022). Previously, it was reported that HMEC-1 cells transduced with HLA-DR constitutively express MHC class II on cell surface under basal conditions (Taflin et al., 2011). We found 68% of the cell population showed HLA-DR expression under basal condition (Figure 7.15a). To determine if the HLA-DR expression would also be on the surface of the EVs derived from these cells, EVs were isolated from 4× T175 flasks. EVs isolated from the conditioned media were found to be enriched within Fraction 7 and Fraction 8 while maintaining similar protein enrichment profiles from the size exclusion chromatography (Figure 7.15b). Furthermore, electron microscopy showed isolated EVs with typical cup-shaped morphology without the presence of contaminating lipoprotein (Figure 7.15c) and the size distribution in both EVs fraction as less than 200nm (Figure 7.15d and 7.15e). Finally, we confirmed the overall purity of the EV isolates using western blot and showed enrichment in EV markers while being negative for cellular contamination (Figure 7.15e). Surface marker assessment also confirmed the isolates to be enriched for EV markers and negative for cellular contaminant (Figure 7.15f).

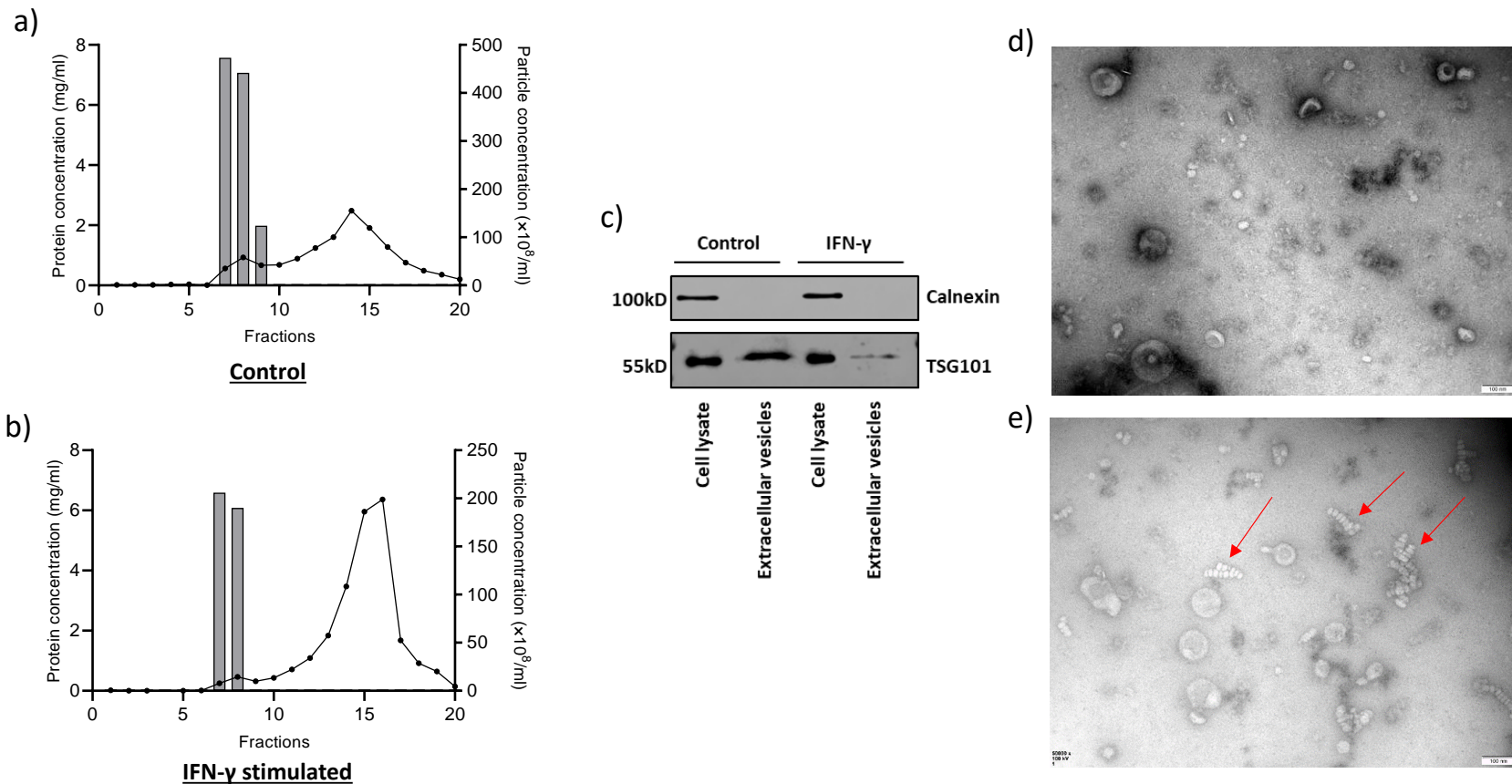


Figure 7.14 Comparisons of EVs isolated under basal or IFN- γ stimulation.

EVs were isolated from conditioned media from HMEC-1 cells cultured under basal or IFN- γ stimulation. Majority of the EVs eluted from fraction 7 and fraction 8 of the size exclusion chromatography in both a) untreated HMEC-1 and b) IFN- γ stimulated HMEC-1 while proteins present within the media eluted from fraction 10 onwards in both conditions. c) 10 μ g of total protein from fraction 7 EV isolates or accompanying cell lysate was loaded onto a western blot and detection for EV marker TSG101 and ER marker calnexin. Reduced TSG101 signature was detected in EVs derived from IFN- γ stimulated HMEC-1 cell. Electron micrograph of EVs from HMEC-1 under d) basal or e) IFN- γ stimulated HMEC-1. Contaminating lipoprotein was highlighted by the red arrows. Data shown represents the pooled EVs from n= 4 \times T175 flask of cultured HMEC-1. Scale bar = 100nm.

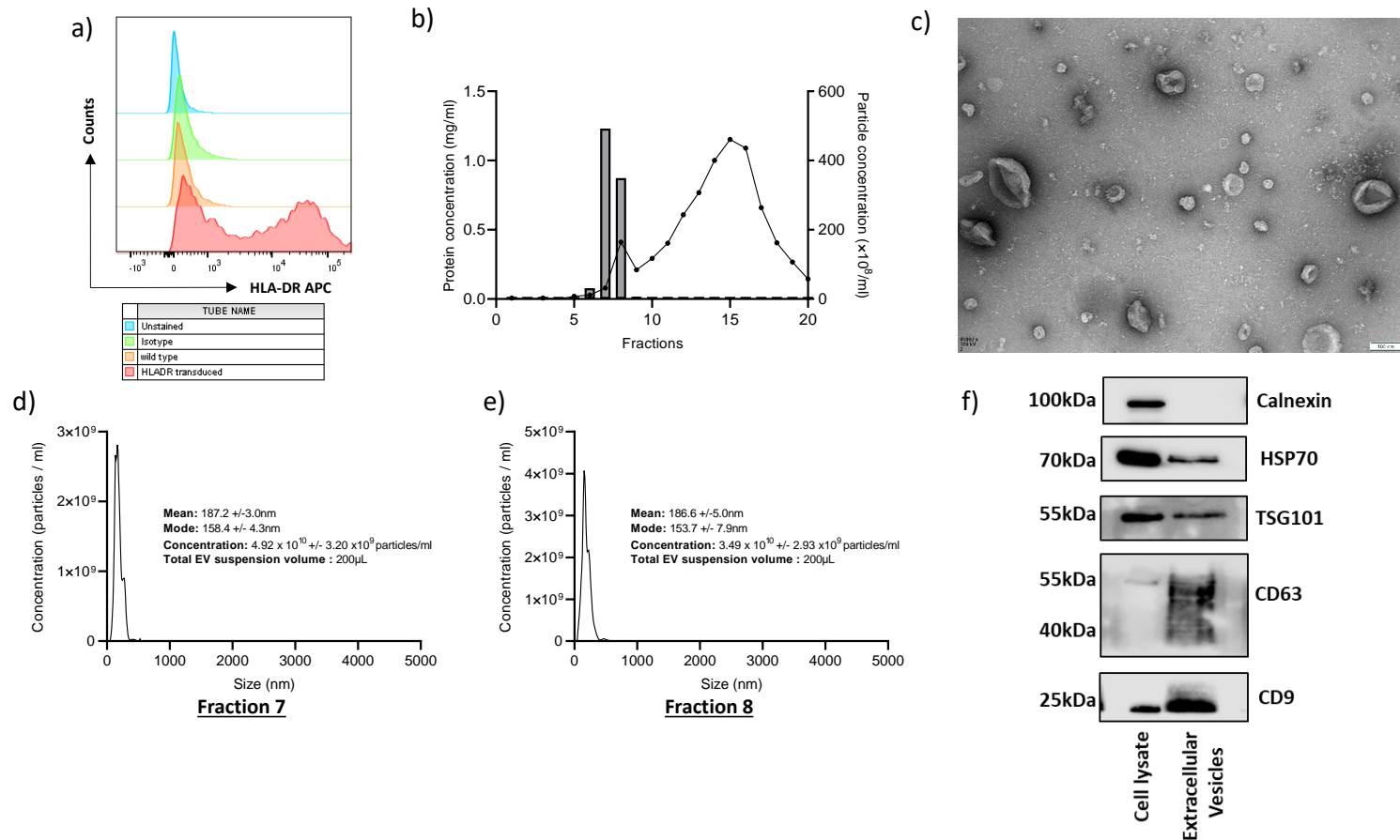


Figure 7.15 Characterisation of EVs isolated from HLA-DR transduced HMEC-1.

EVs were isolated from conditioned media from HLA-DR transduced HMEC-1. a) Flow cytometry analysis of the cells showing high expression of HLA-DR on cell surface under basal conditions. b) EVs were highly enriched in Fraction 7 and Fraction 8 while most of the protein in the conditioned media eluted from Fraction 10. c) Electron micrograph showing EVs isolated with the typical cup-shaped morphology. Modal size distribution of d) Fraction 7 and e) Fraction 8 were less than 200nm, confirming that the isolation was enriched for EVs. f) Western blot analysis of the EVs and cell lysate showing enrichment in EV markers CD9, CD63, TSG101, HSP70 while absence of calnexin confirmed isolation free of cellular contamination. Data shown represents the pooled EVs from n= 4 \times T175 flask of cultured HMEC-1. Flow cytometry data representative of n=3 replicates. Scale bar = 100nm.

7.4.13. HLA-DR is present on EVs derived from HLA-DR transduced HMEC-1

EV surface marker expression was next characterised using the MACSPlex kit (Koliha et al., 2016). Cells transduced with HLA-DR showed a fifteen-fold increase in the normalized MFI expression for MHC class II when compared to the wild-type HMEC-1 derived EVs (Figure 7.16) while maintaining comparable expression profiles of other surface markers. Even though IFN- γ stimulation resulted in co-isolation of lipoprotein with the EVs, the MACSPlex kit utilises tetraspanins enriched in EVs for the signal detection, hence surface marker profiling is still possible. As indicated in Figure 7.16, EVs derived from IFN- γ stimulated HMEC-1 resulted in 100 fold increase in class II MHC expression on the EVs. Furthermore, we also observed increased expression in the endothelial enriched markers CD29 and CD105 as well as co-stimulatory molecules CD40.

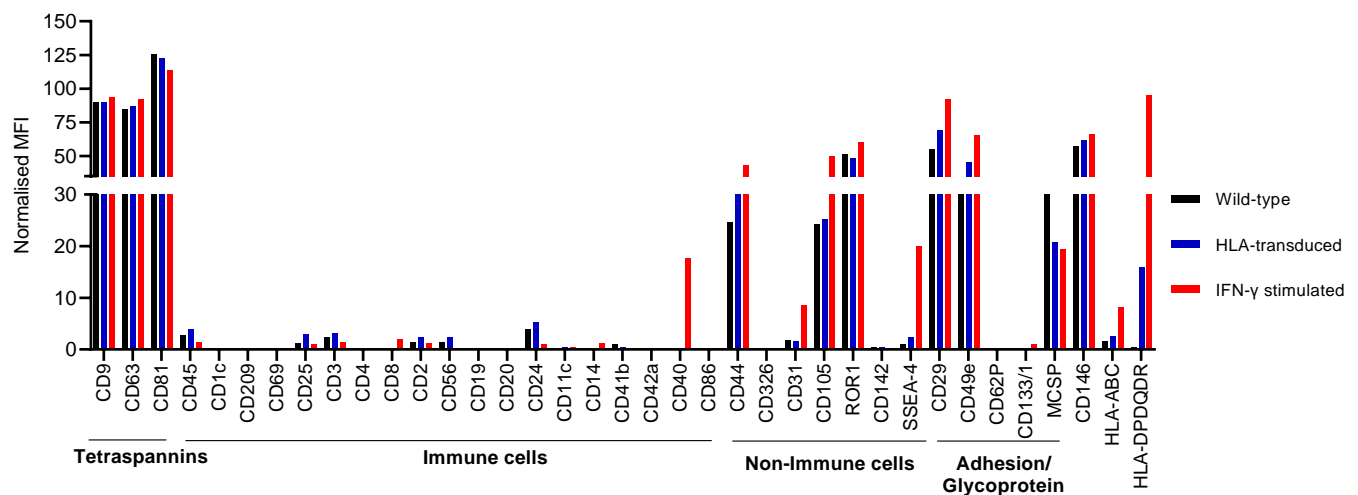


Figure 7.16 Surface marker characterisation of EVs.

EVs derived from wild-type and HLA-DR transduced HMEC-1 cell was characterised using the Miltenyi MACSPlex exosome kit. Surface marker expression on wild-type and HLA-DR transduced HMEC-1 showed similar profiles but only EVs derived from transduced cells show elevated class II MHC expression. IFN- γ stimulation resulted in upregulation of endothelial markers as well as increased class II MHC expression. Expression of surface markers are indicated as MFI normalised to the tetraspanins. Data shown represents n=1 for the characterisation.

7.5. Discussion

EVs have been shown to potentiate allorecognition by decorating recipient dendritic cells with donor MHC molecules and thereby triggering immune cell activation (Marino et al., 2016, Ono et al., 2018, Hughes et al., 2019, Zeng et al., 2021), highlighting a novel function for these extracellular organelles. Understanding the molecular mechanisms and cellular processes underpinning this allorecognition mediated by immune cell cross-dressing could therefore provide a new avenue for clinical intervention to reduce allograft rejection.

The work from this chapter identified an alternative paradigm with regards to semi-direct allorecognition. As opposed to the bulk of the existing literature, we explored the possibility of EVs released by the allograft prior to implantation and how this could provide an initial immune cell priming of the recipient immune system upon transplantation. Firstly, EVs were successfully isolated from renal allograft effluent collected from the microvasculature. Furthermore, we also observed a difference in the total number of EVs isolated from DCD allograft compared to living donor allografts (Figure 7.3).

Deceased donor allografts tend to experience a longer warm and cold ischemic time compared to living donor kidneys. In addition, an initial insult precedes the allograft retrieval from the deceased donor; catecholamine storm in DBD allografts or an extended uncontrolled warm ischemic time in DCD allografts. This damages cells in the kidneys (Kamińska et al., 2016), altering metabolic state (Erp et al., 2018, Erp et al., 2020) and promoting a hyper-inflammatory and hyper-coagulative phenotype (Akhtar et al., 2016). While cold static storage of the allografts reduces cellular metabolism, it is now understood that cells remain bioenergetically active and cellular processes do not come to a complete halt (Ali et al., 2021). Hence the substantially longer CIT from deceased donor allografts can result in the increased EVs isolated. What was not addressed in our work was whether the other confounding factors between allograft categories can contribute to the differences observed within our cohort.

Secondly, we identified enrichment of MHC class II molecules from the isolated kidney effluent EVs (Figure 7.5). In antigen presenting cells (APCs), loading of MHC class II molecules with antigen occurs in the MHC class II-containing compartment (MIIC). The MIIC compartment localise with the multivesicular bodies before trafficking to the cell surface or secreted as vesicles (Raposo et

al., 1996, Roche and Furuta, 2015). Under inflammatory conditions, activated endothelial cells can become semi-professional APCs (Amersfoort et al., 2022). Indeed, our initial hypothesis was that the bulk of EVs we isolate from the microvasculature must come from endothelial cells. However, our current finding identified EVs expressing multiple immune cell markers. These likely would have been released by tissue resident immune cells into the luminal surface of the microvasculature or via a breach in the endothelium layer as a result of the ischemic damage (Kramer et al., 1999). Interestingly, live imaging of zebrafish has provided first evidence of EVs interacting with endothelium and subsequent transmigration across the endothelial cells into the stromal tissue (Verweij et al., 2019).

Several surface markers were also identified to be differentially expressed across the allograft categories. This includes MHC class II, which was increased in deceased donor allografts compared to allografts from living donors. Pre-existing literature on organ transplantation has solely focused on MHC class I cross-dressed dendritic cell activating cytotoxic CD8⁺ T cells and resulting in acute rejection in allografts (Marino et al., 2016, Ono et al., 2018, Hughes et al., 2019, Zeng et al., 2021, Mastoridis et al., 2020). Whether cross-dressing recipient dendritic cells with donor MHC class II could lead to CD4⁺ T cell activation remains to be determined, but work in mice has shown that blockade of endothelial MHC class II expression can indeed mitigate acute rejection (Abrahimi et al., 2016).

In addition, CD29 and CD105 showed significantly higher expression in EVs from deceased donor allografts (Figure 7.6). These surface markers are highly expressed on endothelial cells and thereby supporting the hypothesis that the allograft endothelium from deceased donors is activated to a greater extent compared to that of living donors. Furthermore, when dimension reduction algorithms were applied to the cohort, tight clustering of DCD donors were observed and was identified to be driven in parts by CD105 and MHC class II (Figure 7.8).

To determine whether endothelial cells can indeed produce MHC class II high EVs, we attempted to recapitulate this *in vitro*. However, this proved to be difficult as there is no good endothelial cell model derived from the kidneys. This was also complicated by the heterogeneity within the renal endothelial cell population with their highly specialised roles (Dumas, 2020). Furthermore, cultured endothelial cells express MHC class II in response to interferon- γ stimulation (Figure

7.12). When we attempted to isolate EVs from the stimulated endothelial cells, we observed co-isolation of lipoprotein contaminants, making downstream applications difficult. Instead, utilising HMEC-1 expressing constitutive HLA-DR, we showed the presence of MHC class II expression on their EVs. Yet, this model is unable to fully recapitulate endothelial cells under inflammatory conditions, and hence whether the levels of MHC class II expression would be higher remains undetermined in this study.

CD9 and CD63 were also identified to be differentially expressed between donor allograft categories. These tetraspanins are ubiquitously expressed in EVs from all cell types (Niel et al., 2018). However, the current assay is unable to pinpoint exactly which cells contribute to the altered expression across categories. Therefore, we are unable to draw any concrete conclusions from this observation. Platelets and platelet derived EVs have been shown to express high levels of CD41b and CD42a (Małgorzata S. Małys, 2023). This significantly higher detection within the living donor compared to the deceased donor category could be due to technical limitations as the vasculature of living donors receives reduced flushing relative to the deceased donor allografts.

Finally, alongside the surface proteome profiling, we also attempted to identify differences in the RNA cargo across the allograft categories. Our initial Bioanalyzer trace indicated that the majority of the RNA detected were less than 200 nucleotides. This suggests that the EVs are enriched with small non-coding RNA. The limited quantities of RNA isolated, however, limited our utilisation of conventional sequencing to determine the cargo contents. Instead, we based our methodology on a recent published paper showing high sensitivity of the nCounter® platform from Nanostring for miRNA derived from EVs (Crossland et al., 2023). While we managed to detect miRNAs in all our samples, we did not show enrichment of miRNA across allograft categories. This can be explained in part due to the likely heterogenous origin of the EVs as indicated by the surface marker expression. Coupled with the cell type specific expression of miRNA (Simonas Juzenas, 2017) and selective loading of miRNA into the EVs (Garcia-Martin et al., 2021), the identification of common miRNA profiles proved to be challenging.

In this current study, we focused on the isolation of EVs from the allograft microvasculature prior to transplantation and identified surface markers that can distinguish between donor groups. The

characterisation using the commercial kit however did not account for the co-expression of various surface markers on a single EV. While there is a shift in the paradigm towards high throughput single EV analysis to decipher the heterogeneity present within a bulk EV population (Lersner et al., 2022, Joshua A. Welsh, 2023), the small size still limits the overall number of surface markers one can co-detect without generating excessive noise. Furthermore, EVs have also been shown to play roles in sensitisation of recipients to neoantigens (Dieudé et al., 2015), induction of allograft tolerance (Pêche et al., 2006) and the possibility of non-invasive biomarkers (Vallabhajosyula et al., 2017, Sedej et al., 2022) which are not discussed in our work. Additionally, whether the high MHC class II expressions would be maintained following reperfusion injury remains to be addressed.

What the field is starting to understand is that biomolecules sorting and expression on EVs is a highly regulated process which could confer survival advantage to the parent cells (Sebastian Rühl, 2018, Lamiaa El-Shennawy, 2022) under inflammatory conditions. These MHC high EVs are likely to potentiate a rapid amplification of immune response in order to allow clearance of the trigger. This mechanism, in the context of transplantation, may become a hinderance as we identified the possibility for these EVs to trigger allorecognition.

8. Discussion, Limitations and Future Directions

8.1. General Discussion

Organ transplantation is currently the gold standard of care for patients with end stage organ failure. However, widespread utilisation is currently limited by several factors, including the disparity between donors and recipients, organ quality, organ damage associated with ischemia reperfusion injury (IRI) and management of chronic allograft rejection post-transplantation. While a variety of trials have been tested to circumvent damage brought on by IRI, none have been translated into routine clinical practice (Eltzschig and Eckle, 2011). Therefore, this highlights a knowledge gap in the current understanding of IRI's complex pathophysiology.

The biphasic nature of IRI begins with the initial of ischemia, activating cellular adaptation to the nutrient depleted, hypoxic environment. Extended ischemia however renders the allografts to be highly inflammatory due to the perturbed redox balance, damaging the stromal cells and resulting in the release of cytokines and chemokines. This prolonged ischemia induces a highly inflammatory environment and in turn, primes and exacerbates the inflammatory responses during reperfusion.

CXCL8 is one such chemokine released during ischemia (Fisher et al., 2000), which drives the rapid recruitment and localisation of neutrophils during inflammation. While several mechanisms have been shown to regulate this chemokine (Darbonne et al., 1991, Basran et al., 2013), resolution of CXCL8 in the inflammatory environment have yet to be fully characterised.

Reactive nitrogen species (RNS) modifying chemokines have been previously reported *in vitro* (Sato et al., 2000a, Sato et al., 2000b, Sato et al., 2000c, Janssens et al., 2016) and *in vivo* (Barker et al., 2017, Molon et al., 2011), resulting in altered function to the native protein. Therefore, we hypothesised that during inflammation, high levels of CXCL8 and RNS would result in CXCL8 nitration. Firstly, we showed that exposure of CXCL8 to peroxynitrite donor *in vitro* resulted in nitration of the single tyrosine residue albeit with a relatively low yield. However, using peptide synthesis, we generated nitrated CXCL8 for functional testing. Neutrophil migration was found to be impaired by nitration due to the reduced glycosaminoglycan binding and impaired signaling through cognate receptors CXCR1 and CXCR2.

To confirm that this modification is biologically relevant, we utilise bronchoalveolar lavage samples (BAL) from patients with ventilation associated pneumonia (VAP), which was reported to have high levels of CXCL8 (Hellyer et al., 2015, Hellyer et al., 2020). Immunoprecipitation indicated the presence of nitrated CXCL8, which was further confirmed with an antibody raised specifically against nitrated CXCL8. Finally, utilising targeted proteomics (Metzemaekers et al., 2021), we identified various modifications of CXCL8, including nitrated CXCL8. Furthermore, a highly truncated form of CXCL8 was identified through the targeted proteomics analysis. Interestingly, this 10-77 amino acid CXCL8 that was the most abundant proteoforms identified and was previously reported to be non-functional. (Clark-Lewis et al., 1991). Collectively, this chapter identified various post-translationally modified CXCL8 within inflammatory milieu and we reason that these is a mechanism to resolve CXCL8 induced inflammation.

Another hallmark of ischemia is the induction of hypoxic response, predominantly driven by hypoxia inducible factor (HIF) signaling. While this oxygen sensing mechanism is ubiquitous across all cell types, there are however divergent responses driven by the preference for HIF isoforms, resulting in cell specific adaptations to hypoxia (Lau et al., 2007, Hu et al., 2007). Within the kidneys, much of the ischemic models and studies have focuses on the genotypic and phenotypic changed in the tubular epithelium (Kuo et al., 2021, Liu et al., 2017). However, the cellular composition of the kidneys is extremely complex, and the response of other cell types to hypoxia is less well-defined. Hence, in Chapter 6, we sought to profile the miRNA and mRNA of the glomerular endothelium in response to hypoxia.

Firstly, glomerular endothelial cells (HGENCs) were cultured in 1% oxygen to mimic hypoxia over the span of 24 hours and profiled the temporal changes to both the miRNA and mRNA expression. We observed upregulation of only miR-210-3p in HGENCs, with expression kinetics congruent with other cells profiled previously (Huang et al., 2009). miR-210-3p was also identified to be the most ubiquitously regulated miRNA by hypoxia due to the presence of hypoxia response element and plays an essential role in hypoxia adaptation (Kulshreshtha et al., 2007). Interesting, we showed a longer miR-210-3p half-life than previously reported (Fasanaro et al., 2008), with stable expression for up to 2 days post re-oxygenation.

The miR-210-3p induction in renal tubular epithelial cells (PTECs) was also higher when we compared to HGENCs, and this difference is driven by endothelial HIF-2 α dependence (Bartoszewski et al., 2019) while miR-210-3p transcription showed a preference for HIF-1 α (Huang et al., 2009). Additionally, differential mRNA targeting was observed between HGENCs and PTECs. *ISCU*, the putative target was downregulated by miR-210-3p in PTECs but not in the conditionally immortalised glomerular endothelial cells (ciGENCs) under hypoxic conditions. Instead, through integrated miRNA-mRNA analysis, we identified and confirmed *HIF1A* and *TFRC* as targets of miR-210-3p in the ciGENCs. The implications to metabolic functions of miR-210-3p overexpressing ciGENCs was also assessed. We identified an increase in overall glycolysis whilst mitochondrial respiration remained unaltered. This was also confirmed by the mitochondria ultrastructure analysis with no gross alteration observed as previously reported in other cell types (Puisségur et al., 2010). Since endothelial cells predominantly utilise glycolysis for energy generation (Bock et al., 2013), we reasoned that this increased glycolysis would account for a disparate response to kidney ischemia and subsequent adaptation to reperfusion.

Finally, extracellular vesicles (EVs) have been identified to be released by cells under all conditions and they are thought to reflect the parental cell state. There has been growing evidence in pre-clinical models suggesting that allograft derived EVs can induce allorecognition through a semi-direct presentation (Marino et al., 2016, Ono et al., 2018, Hughes et al., 2019, Mastoridis et al., 2020, Prunevieuille et al., 2020, Zeng et al., 2021). Whether these EVs are released during ischemia or reperfusion phase of IRI remains undetermined. Hence, in Chapter 7, we sought to determine the presence of EVs in the microvasculature of human renal allografts.

The microvasculature of renal allografts was flushed, and we confirmed the presence of EVs within these effluents. Additionally, we showed that effluents from donation after circulatory death (DCD) donors have higher absolute counts of EVs, and a significant positive correlation was also identified. Upon profiling of these EV surface proteome, we identified a large repertoire of markers expressed on these EVs. Most prominently, major histocompatibility complex (MHC) class II expression was higher in deceased donors compared to living donors. This provided the first indication that some of these EVs that can result in cross-dressing of recipient antigen presenting cells are generated during the allograft ischemic phase. Furthermore, we also attempted to profile the miRNA cargoes of these EVs albeit unsuccessful due to the low quantities

isolated. Finally, we showed the possibility of generating endothelial derived EVs expressing high levels of MHC class II expression, laying the path to uncover the possibility of endothelial EV to driving allorecognition.

In conclusion, the work across the three chapters highlighted the complexity of ischemia, involving multiple cellular processes and adaptations which can lead to desirable or undesirable outcomes post-transplantation. We showed nitration and truncation of CXCL8, which can lead to resolution of inflammation. We also showed a divergent adaptation by glomerular endothelium to hypoxia, which requires additional work to determine the implications. Finally, EVs released by the allograft during ischemia can potentiate allorecognition.

8.2. Limitations of Study and Future Directions

In Chapter 5, we showed the presence of nitrated CXCL8 in the BAL samples from patients with VAP. Initial work set out to develop an in-house ELISA to quantitatively determine the levels of nitrated CXCL8 present within biological samples with high sensitivity. However, we were unable to identify an antibody pair and hence, we adapted to the use of western blot to show the presence or absence of nitrated CXCL8. Within the cohort of samples, only 9 out of 12 samples showed antibody reactivity. Whether this undetectability is a result of the assay sensitivity was not interrogated. In addition, the presence of nitrated CXCL8 within transplant samples remains undetermined, and the implication in IRI remains undetermined.

Furthermore, while we identified a highly truncated variant of CXCL8 that has been shown to be non-functional, we were unable to identify the mechanism behind the generation of this proteoform. Whether the production of this non-functional form of CXCL8 is a result of transcriptional or translational regulation remains to be determined, but previous work profiling CXCL8 proteoforms in synovial fluid did not identify this highly truncated form of CXCL8 (Metzemaekers et al., 2021). Therefore, several key questions remain to be answered:

- Identification of mechanism responsible for the generation of 10-77 amino acid length CXCL8.
- Determine the presence of nitrated CXCL8 in transplant biofluid: perfusate from *ex vivo* perfusion, BAL from lung transplantation.

In chapter 6, we focused on the transcriptomic changes in glomerular endothelium cultured under hypoxic conditions, showing upregulation of a single miRNA, miR-210-3p. The use of a relatively small sample size for the transcriptome study is one potential limiting factor behind the identification of other miRNAs differentially regulated. In particular, the miR-210-3p expression in tubular epithelial cells was highly variable across biological donors. Furthermore, *in vitro* cultured cells do not fully recapitulate the environment *in vivo*, hence, whether these findings are translatable to the conditions *in vivo* remains to be determined. Furthermore, while we showed targeting of transferrin receptor 1 (TfR1) by miR-210-3p, we did not fully understand the overall functional implication in aspects of iron regulation in the cells. Further work can therefore provide insights into the regulation of glomerular endothelium cells in kidney ischemia:

- Inhibit miR-210-3p expression and assess the TfR1 expression.
- Assess the ferroptotic capability between miR-210-3p overexpressing compared to wild-type cells.
- IRI mice model with wild-type and miR-210-3p knockout mice and compare the kidney function and tissue histology.
- Assess TfR1 and miR-210-3p expression in human kidney biopsies.

In chapter 7, we have robustly shown EV release by allografts during ischemia. While the initial hypothesis was to identify the presence of miR-210-3p within the effluents isolated from renal allografts. Nanostring® analysis however did not detect robust signature of this miRNA. Hence, to ensure full utilisation of these EVs isolated from this unique biofluid, a natural extension of the project was to characterise the surface proteome. This eventually led to the identification of EVs from DCD allografts showing a unique protein signature that can possibly allude to semi-direct allorecognition in the transplant process. However, further mechanistic study is necessary, but this chapter also laid the groundwork by showing that *in vitro* modeling of endothelial cells can give rise to EVs with similar expression profiles. Additional work listed below is necessary to comprehensively show semi-direct allorecognition by these endothelial derived EVs:

- Constitutive express class II transactivator (CIITA) in endothelial cells with fluorescently tagged MHC class II and isolate EVs.
- Transfer isolated EVs to PBMCs with mismatched MHC class II.
- Single EV flow cytometry to show co-expression of endothelial marker with MHC class II.

9. References

- A.MILLER, A., J.DUSTING, G., L.ROULSTON, C. & G.SOBEY, C. 2006. NADPH-oxidase activity is elevated in penumbral and non-ischemic cerebral arteries following stroke. *Brain Research*, 111, 111-116.
- ABRAHIMI, P., QIN, L., CHANG, W. G., BOTHWELL, A. L. M., TELLIDES, G., SALTZMAN, W. M. & POBER, J. S. 2016. Blocking MHC Class II on Human Endothelium Mitigates Acute Rejection. *Journal of Clinical Investigation*, 1, e85293.
- ADES, E. W., CANDAL, F. J., SWERLICK, R. A., GEORGE, V. G., SUMMERS, S., BOSSE, D. C. & LAWLEY, T. J. 1992. HMEC-1: establishment of an immortalized human microvascular endothelial cell line. *Journal of Investigative Dermatology*, 99, 683-90.
- AGARWAL, V., BELL, G. W., NAM, J.-W. & BARTEL, D. P. 2015. Predicting Effective microRNA Target Sites in Mammalian mRNAs. *eLife*, 4, e05005.
- AKHTAR, M. Z., HUANG, H., KAISAR, M., FARO, M. L. L., REBOLLEDO, R., MORTEN, K., HEATHER, L. C., DONA, A., LEUVENINK, H. G., FUGGLE, S. V., KESSLER, B. M., PUGH, C. W. & PLOEG, R. J. 2016. Using an Integrated -Omics Approach to Identify Key Cellular Processes That Are Disturbed in the Kidney After Brain Death. *American journal of Transplantation*, 16, 1421-1440.
- ALEXANDER, M., HU, R., RUNTSCH, M. C., KAGELE, D. A., MOSBRUGER, T. L., TOLMACHOVA, T., SEABRA, M. C., ROUND, J. L., WARD, D. M. & O'CONNELL, R. M. 2015. Exosome-delivered microRNAs Modulate the Inflammatory Response to Endotoxin. *Nature Communications*, 6, 7321.
- ALI, A., WANG, A., RIBEIRO, R. V. P., BERONCAL, E. L., BACIU, C., GALASSO, M., GOMES, B., MARISCAL, A., HOUGH, O., BRAMBATE, E., ABDELNOUR-BERCHTOLD, E., MICHAELSEN, V., ZHANG, Y., GAZZALLE, A., FAN, E., BROCHARD, L., YEUNG, J., WADDELL, T., LIU, M., ANDREAZZA, A. C., KESHAVJEE, S. & CYPEL, M. 2021. Static lung storage at 10°C maintains mitochondrial health and preserves donor organ function. *Science Translational Medicine*, 13, eabd7601.
- ALI, S., ROBERTSON, H., WAIN, J. H., ISAACS, J. D., MALIK, G. & KIRBY, J. A. 2005. A Non-Glycosaminoglycan-Binding Variant of CC Chemokine Ligand 7 (Monocyte Chemoattractant Protein-3) Antagonizes Chemokine-Mediated Inflammation. *Journal of Immunology*, 175, 1257-1266.
- ALVAREZ-ERVITI, L., SEOW, Y., YIN, H., BETTS, C., LAKHAL, S. & WOOD, M. J. A. 2011. Delivery of siRNA to the Mouse Brain by Systemic Injection of Targeted Exosomes. *Nature Nanotechnology*, 29, 341-345.
- AMERSFOORT, J., EELEN, G. & CARMELIET, P. 2022. Immunomodulation by Endothelial Cells — Partnering Up with the Immune System? *Nature Reviews Immunology*, 22, 576-588.

- AMIN, M. G., WOLF, M. P., JR., J. A. T., JR., R. B. F., CHENG, S. J., PRATT, D. S. & WONG, J. B. 2004. Expanded Criteria Donor Grafts for Deceased Donor Liver Transplantation Under the MELD System: A Decision Analysis. *Liver Transplantation*, 10, 1468-1475.
- AMROUCHE, L., DESBUISSONS, G., RABANT, M., SAUVAGET, V., NGUYEN, C., BENON, A., BARRE, P., RABATÉ, C., LEBRETON, X., GALLAZZINI, M., LEGENDRE, C., TERZI, F. & ANGLICHEAU, D. 2017. MicroRNA-146a in Human and Experimental Ischemic AKI: CXCL8-Dependent Mechanism of Action. *Journal of the American Society for Nephrology*, 28, 479-493.
- ANA MUÑIZ-GARCÍA, M. R., JUAN MANUEL FALCÓN-PEREZ, PATRICIA MURRAY, ANTONIO ZORZANO & SILVIA MORA 2022. Hypoxia-induced HIF1 α Activation Regulates Small Extracellular Vesicle Release in Human Embryonic Kidney Cells. *Scientific Report*, 12, 1443.
- ANDREASSON, A. S. I., BORTHWICK, L. A., GILLESPIE, C., JIWA, K., SCOTT, J., HENDERSON, P., MAYES, J., ROMANO, R., ROMAN, M., ALI, S., FILDES, J. E., MARCZIN, N., DARK, J. H., FISHER, A. J. & INVESTIGATOR, O. B. O. T. D.-U. 2017. The Role of Interleukin-1 β as a Predictive Biomarker and Potential Therapeutic Target During Clinical ex vivo Lung Perfusion. *Journal of Heart and Lung Transplantation*, 36, P985-995.
- ARNOLD, R. S., SHI, J., MURAD, E., WHALEN, A. M., SUN, C. Q., POLAVARAPU, R., PARTHASARATHY, S., PETROS, J. A. & LAMBETH, J. D. 2001. Hydrogen peroxide mediates the cell growth and transformation caused by the mitogenic oxidase Nox1. *Proceedings of the National Academy of Science*, 98, 5550-5555.
- ARROYO, J. D., CHEVILLET, J. R., KROH, E. M., RUF, I. K., PRITCHARD, C. C., GIBSON, D. F., MITCHELL, P. S., BENNETT, C. F., POGOSOVA-AGADJANYAN, E. L., STIREWALT, D. L., TAIT, J. F. & TEWARI, M. 2011. Argonaute2 Complexes Carry a Population of Circulating microRNAs Independent of Vesicles in Human Plasma. *Proceedings of the National Academy of Science of the United States of America*, 108, 5003-5008.
- ASHBURNER, M., BALL, C. A., BLAKE, J. A., BOTSTEIN, D., BUTLER, H., CHERRY, J. M., DAVIS, A. P., DOLINSKI, K., DWIGHT, S. S., EPPIG, J. T., HARRIS, M. A., HILL, D. P., ISSEL-TARVER, L., KASARSKIS, A., LEWIS, S., MATESE, J. C., RICHARDSON, J. E., RINGWALD, M., RUBIN, G. M. & SHERLOCK, G. 2000. Gene Ontology: A tool for the Unification of Biology. *Nature Genetics*, 25, 25-29.
- ASHCROFT, J., LEIGHTON, P., ELLIOTT, T. R., HOSGOOD, S. A., NICHOLSON, M. L. & KOSMOLIAPTIS, V. 2022. Extracellular vesicles in kidney transplantation: a state-of-the-art review. *Kidney International*, 101, 485-497.
- BABIARZ, J. E., RUBY, J. G., WANG, Y., BARTEL, D. P. & BLELLOCH, R. 2010. Mouse ES cells Express Endogenous shRNAs, siRNAs, and Other Microprocessor-independent, Dicer-dependent Small RNAs. *Genes and Development*, 22, 2773-2785.
- BAEK, D., VILLÉN, J., SHIN, C., CAMARGO, F. D., GYGI, S. P. & BARTEL, D. P. 2008. The Impact of microRNA on Protein Output. *Nature*, 455, 64-71.

- BAEYENS, N., MULLIGAN-KEHOE, M. J., CORTI, F., SIMON, D. D., ROSS, T. D., RHODES, J. M., WANG, T. Z., MEJEAN, C. O., SIMONS, M., HUMPHREY, J. & SCHWARTZ, M. A. 2014. Syndecan 4 is Required for Endothelial Alignment in Flow and Atheroprotective Signaling. *Proceedings of the National Academy of Science of the United States of America*, 111, 17308-17313.
- BAIETTI, M. F., ZHANG, Z., MORTIER, E., MELCHIOR, A., DEGEEST, G., GEERAERTS, A., IVARSSON, Y., DEPOORTERE, F., COOMANS, C., VERMEIREN, E., ZIMMERMANN, P. & DAVID, G. 2012. Syndecan–syntenin–ALIX Regulates the Biogenesis of Exosomes. *Nature Cell Biology*, 14, 677-685.
- BALZER, M. S., DOKE, T., YANG, Y.-W., ALDRIDGE, D. L., HU, H., MAI, H., MUKHI, D., MA, Z., SHRESTHA, R., PALMER, M. B., HUNTER, C. A. & SUSZTAK, K. 2022. Single-cell Analysis Highlights Differences in Druggable Pathways Underlying Adaptive or Fibrotic Kidney Regeneration. *Nature Communications*, 13, 4018.
- BARKER, C. E., THOMPSON, S., O'BOYLE, G., LORTAT-JACOB, H., SHEERIN, N. S., ALI, S. & KIRBY, J. A. 2017. CCL2 Nitration is a Negative Regulator of Chemokine-mediated Inflammation. *Scientific Report*, 7, 44384.
- BARTOSZEWSKI, R., MOSZYŃSKA, A., SEROCKI, M., CABAJ, A., POLTEN, A., OCHOCKA, R., DELL'ITALIA, L., BARTOSZEWSKA, S., KRÓLICZEWSKI, J., DAJBROWSKI, M. & COLLAWN, J. F. 2019. Primary Endothelial Cell–specific Regulation of Hypoxia-inducible Factor (HIF)-1 and HIF-2 and Their Target Gene Expression Profiles During Hypoxia. *FASEB Journal*, 33, 7729-7941.
- BASKERVILLE, S. & BARTEL, D. P. 2005. Microarray Profiling of microRNAs Reveals Frequent Coexpression with Neighboring miRNAs and Host Genes. *RNA*, 11, 241-247.
- BASRAN, A., JABEEN, M., BINGLE, L., STOKES, C. A., DOCKRELL, D. H., WHYTE, M. K. B., WALMSLEY, S. R., HIGGINS, K. R., VOGEL, S. N., WILSON, H. L., PRINCE, L. R., PRESTWICH, E. C., SABROE, R. A., PARKER, L. C. & SABROE, I. 2013. Roles of Neutrophils in the Regulation of the Extent of Human Inflammation through Delivery of IL-1 and Clearance of Chemokines. *Journal of Leukocyte Biology*, 93, 7-19.
- BAZAN, J. F., BACON, K. B., HARDIMAN, G., WANG, W., SOO, K., ROSSI, D., GREAVES, D. R., ZLOTNIK, A. & SCHALL, T. J. 1997. A new class of membrane-bound chemokine with a CX3C motif. *Nature*, 385, 640-644.
- BAZZINI, A. A., LEE, M. T. & GIRALDEZ, A. J. 2012. Ribosome Profiling Shows That miR-430 Reduces Translation Before Causing mRNA Decay in Zebrafish. *Science*, 336, 233-237.
- BEREZIKOV, E., CHUNG, W.-J., WILLIS, J., CUPPEN, E. & LAI, E. C. 2007. Mammalian Mirtron Genes. *Molecular Cell*, 28, 328-336.
- BERNE, R. M. 1963. Cardiac nucleotides in hypoxia: Possible role in regulation of coronary blood flow. *American Journal of Physiology*, 204, 317-322.

- BHATTACHARYYA, S. N., HABERMACHER, R., MARTINE, U., CLOSS, E. I. & FILIPOWICZ, W. 2006. Relief of microRNA-Mediated Translational Repression in Human Cells Subjected to Stress. *Cell*, 125, P1111-1124.
- BISTER, N., PISTONO, C., HUREMAGIC, B., JOLKKONEN, J., GIUGNO, R. & MALM, T. 2020. Hypoxia and Extracellular Vesicles: A Review on Methods, Vesicular Cargo and Functions. *Journal of Extracellular Vesicles*, 10, e12002.
- BOCK, K. D., GEORGIADOU, M., SCHOORS, S., GERHARDT, H., DEWERCHIN, M. & CARMELIET, P. 2013. Role of PFKFB3-Driven Glycolysis in Vessel Sprouting. *Cell*, 154, P651-663.
- BONAUER, A., CARMONA, G., IWASAKI, M., MIONE, M., KOYANAGI, M., FISCHER, A., BURCHFIELD, J., FOX, H., DOEBELE, C., OHTANI, K., CHAVAKIS, E., POTENTE, M., TJWA, M., URBICH, C., ZEIHNER, A. M. & DIMMELER, S. 2009. MicroRNA-92a Controls Angiogenesis and Functional Recovery of Ischemic Tissues in Mice. *Science*, 324, 1710-1713.
- BONVIN, P., GUENEAU, F., BUATOIS, V., CHARRETON-GALBY, M., LASCH, S., MESSMER, M., CHRISTEN, U., LUSTER, A. D., JOHNSON, Z., FERLIN, W., KOSCO-VILBOIS, M., PROUDFOOT, A. & FISCHER, N. 2017. Antibody Neutralization of CXCL10 In Vivo Is Dependent on Binding to Free and Not Endothelial-bound Chemokine: Implication for the Design of a New Generation of Anti-Chemokine Therapeutic Antibodies. *Journal of Biological Chemistry*, 292, 4185-4197.
- BORCHERT, G. M., LANIER, W. & DAVIDSON, B. L. 2006. RNA Polymerase III Transcribes Human microRNAs. *Nature Structural & Molecular Biology*, 13, 1097-1101.
- BOTHA, P., JEYAKANTHAN, M., RAO, J. N., FISHER, A. J., PRABHU, M., DARK, J. H. & CLARK, S. C. 2007. Inhaled nitric oxide for modulation of ischemia–reperfusion injury in lung transplantation. *Journal of Heart and Lung Transplantation*, 26, P1199-1205.
- BOURA, E., RÓŻYCKI, B., CHUNG, H. S., HERRICK, D. Z., CANAGARAJAH, B., CAFISO, D. S., EATON, W. A., HUMMER, G. & HURLEY, J. H. 2012. Solution Structure of the ESCRT-I and -II Supercomplex: Implications for Membrane Budding and Scission. *Structure*, 20, 874-886.
- BRUNELLI, L., CROW, J. P. & BECKMAN, J. S. 1995. The Comparative Toxicity of Nitric Oxide and Peroxynitrite to *Escherichia coli*. *Archives of Biochemistry and Biophysics*, 316, 327-334.
- BRUNNER, F., MAIER, R., ANDREW, P., WÖLKART, G., ZECHNER, R. & MAYER, B. 2003. Attenuation of myocardial ischemia/reperfusion injury in mice with myocyte-specific overexpression of endothelial nitric oxide synthase. *Cardiovascular Research*, 57, 55-62.
- BRZOZOWSKI, J. S., BOND, D. R., JANKOWSKI, H., GOLDIE, B. J., BURCHELL, R., NAUDIN, C., SMITH, N. D., SCARLETT, C. J., LARSEN, M. R., DUN, M. D., SKELDING, K. A. & WEIDENHOFER, J. 2018. Extracellular vesicles with altered tetraspanin CD9 and CD151 levels confer increased prostate cell motility and invasion. *Scientific Report*, 8, 8822.

- BUSATTO, S., YANG, Y., IANNOTTA, D., DAVIDOVICH, I., TALMON, Y. & WOLFRAM, J. 2022. Considerations for Extracellular Vesicle and Lipoprotein Interactions in cell culture assays. *Journal of Extracellular Vesicles*, 11, e12202.
- CALDWELL-KENKEL, J. C., CURRIN, R. T., TANAKA, Y., THURMAN, R. G. & LEMASTERS, J. J. 1990. Kupffer cell activation and endothelial cell damage after storage of rat livers: Effects of reperfusion. *Hepatology*, 13, 83-95.
- CALLERI, A., ROGGIO, D., NAVARRO-TABLEROS, V., STEFANO, N. D., PASQUINO, C., DAVID, E., FRIGATTI, G., RIGO, F., ANTICO, F., CAROPRESO, P., PATRONO, D., BRUNO, S. & ROMAGNOLI, R. 2021. Protective Effects of Human Liver Stem Cell-Derived Extracellular Vesicles in a Mouse Model of Hepatic Ischemia-Reperfusion Injury. *Stem Cell Review and Report*, 17, 459-470.
- CAMBIER, S., GOUWY, M. & PROOST, P. 2023. The Chemokines CXCL8 and CXCL12: Molecular and Functional Properties, Role in Disease and Efforts Towards Pharmacological Intervention. *Cellular and Molecular Immunology*, 20, 217-251.
- CAO, M., SONG, W., LIANG, R., TENG, L., ZHANG, M., ZHANG, J. & ZHU, L. 2021. MicroRNA as a Potential Biomarker and Treatment Strategy for Ischemia-Reperfusion Injury. *International Journal of Genomics*, 2021, 9098145.
- CASANOVA-ACEBES, M., NICOLÁS-ÁVILA, J. A., LI, J. L., GARCÍA-SILVA, S., BALACHANDER, A., RUBIO-PONCE, A., WEISS, L. A., ADROVER, J. M., BURROWS, K., A-GONZÁLEZ, N., BALLESTEROS, I., DEVI, S., QUINTANA, J. A., CRAINICIUC, G., LEIVA, M., GUNZER, M., WEBER, C., NAGASAWA, T., SOEHNLEIN, O., MERAD, M., MORTHA, A., NG, L. G., PEINADO, H. & HIDALGO, A. 2018. Neutrophils instruct homeostatic and pathological states in naive tissues. *Journal of Experimental Medicine*, 215, 2778-2795.
- CERADINI, D. J., KULKARNI, A. R., CALLAGHAN, M. J., TEPPER, O. M., BASTIDAS, N., KLEINMAN, M. E., CAPLA, J. M., GALIANO, R. D., LEVINE, J. P. & GURTNER, G. C. 2004. Progenitor Cell Trafficking is Regulated by Hypoxic Gradients through HIF-1 Induction of SDF-1. *Nature Medicine*, 10, 858-864.
- CHAN, S. Y., ZHANG, Y.-Y., HEMANN, C., MAHONEY, C. E., ZWEIER, J. L. & LOSCALZO, A. J. 2009. MicroRNA-210 Controls Mitochondrial Metabolism and Hypoxic Adaptation in Pulmonary Vascular Endothelium. *Cell Metabolism*, 10, 273-284.
- CHAN, Y. C., BANERJEE, J., CHOI, S. Y. & SEN, C. K. 2012. miR-210: The Master Hypoxamir. *Microcirculation*, 19, 215-223.
- CHANG, W.-T., LIN, Y.-W., HUANG, P.-S., LIN, Y.-C., TSENG, S.-Y., CHAO, T.-H., CHEN, Z.-C., SHIH, J.-Y. & HONG, C.-S. 2022. Deletion of MicroRNA-21 Impairs Neovascularization Following Limb Ischemia: From Bedside to Bench. *Frontiers in Cardiovascular Medicine*, 9.
- CHAU, B. N., XIN, C., HARTNER, J., REN, S., CASTANO, A. P., LINN, G., LI, J., TRAN, P. T., KAIMAL, V., HUANG, X., CHANG, A. N., LI, S., KALRA, A., GRAFALS, M., PORTILLA, D., MACKENNA, D. A.,

- ORKIN, S. H. & DUFFIELD, J. S. 2012. MicroRNA 21 Promotes Fibrosis of the Kidney by Silencing Metabolic Pathways. *Science Translational Medicine*, 4, 121ra18.
- CHEKULAEVA, M., MATHYS, H., ZIPPRICH, J. T., ATTIG, J., COLIC, M., PARKER, R. & FILIPOWICZ, W. 2011. miRNA Repression Involves GW182-mediated Recruitment of CCR4–NOT Through Conserved W-containing Motifs. *Nature Structural & Molecular Biology*, 18, 1218-1226.
- CHELOUFI, S., SANTOS, C. O. D., CHONG, M. M. W. & HANNON, G. J. 2010. A Dicer-independent miRNA Biogenesis Pathway that Requires Ago Catalysis. *Nature*, 465, 584-589.
- CHEN, C.-A., LIN, C.-H., DRUHAN, L. J., WANG, T.-Y., CHEN, Y.-R. & ZWEIER, J. L. 2011. Superoxide induces endothelial nitric-oxide synthase protein thiyl radical formation, a novel mechanism regulating eNOS function and coupling. *Journal of Biological Chemistry*, 286.
- CHEN, C.-A., WANG, T.-Y., VARADHARAJ, S., REYES, L. A., HEMANN, C., TALUKDER, M. A. H., CHEN, Y.-R., DRUHAN, L. J. & ZWEIER, J. L. 2010. S-glutathionylation uncouples eNOS and regulates its cellular and vascular function. *Nature*, 468, 1115-1118.
- CHEN, Y., LUN, A. T. L. & SMYTH, G. K. 2016. From Reads to Genes to Pathways: Differential Expression Analysis of RNA-Seq Experiments Using Rsubread and the edgeR Quasi-likelihood Pipeline. *F1000 Research*, 5.
- CHEVILLET, J. R., KANG, Q., RUF, I. K., BRIGGS, H. A., VOJTECH, L. N., HUGHES, S. M., CHENG, H. H., ARROYO, J. D., MEREDITH, E. K., GALLICHOTTE, E. N., POGOSOVA-AGADJANYAN, E. L., MORRISSEY, C., STIREWALT, D. L., HLADIK, F., YU, E. Y., HIGANO, C. S. & TEWARI, M. 2014. Quantitative and Stoichiometric Analysis of the microRNA Content of Exosomes. *Proceedings of the National Academy of Science of the United States of America*, 111, 14888-14893.
- CHIBA, T., CERQUEIRA, D. M., LI, Y., BODNAR, A. J., MUKHERJEE, E., PFISTER, K., PHUA, Y. L., SHAIKH, K., SANDERS, B. T., HEMKER, S. L., PAGANO, P. J., WU, Y. L., HO, J. & SIMS-LUCAS, S. 2021. Endothelial-Derived miR-17~92 Promotes Angiogenesis to Protect against Renal Ischemia-Reperfusion Injury. *Journal of the American Society for Nephrology*, 32, 553-562.
- CHOUCHANI, E. T., PELL, V. R., GAUDE, E., AKSENTIJEVIĆ, D., SUNDIER, S. Y., ROBB, E. L., LOGAN, A. & SERGIY M. NADTOCHIYEMILY N. J. ORD, A. C. S., FILMON EYASSU, RACHEL SHIRLEY, CHOU-HUI HU, ANNA J. DARE, ANDREW M. JAMES, SEBASTIAN ROGATTI, RICHARD C. HARTLEY, SIMON EATON, ANA S. H. COSTA, PAUL S. BROOKES, SEAN M. DAVIDSON, MICHAEL R. DUCHEN, KOUROSH SAEB-PARSY, MICHAEL J. SHATTOCK, ALAN J. ROBINSON, LORRAINE M. WORK, CHRISTIAN FREZZA, THOMAS KRIEG & MICHAEL P. MURPHY 2014. Ischaemic Accumulation of Succinate Controls Reperfusion Injury Through Mitochondrial ROS. *Nature*, 515, 431-435.
- CLARK-LEWIS, I., SCHUMACHER, C., BAGGIOLINI, M. & MOSER, B. 1991. Structure-activity Relationships of Interleukin-8 Determined Using Chemically Synthesized Analogs. Critical Role of NH2-terminal Residues and Evidence for Uncoupling of Neutrophil Chemotaxis,

Exocytosis, and Receptor Binding Activities. *Journal of Biological Chemistry*, 266, 23128-23134.

COOKE, C.-L. M. & DAVIDGE, S. T. 2002. Peroxynitrite Increases iNOS Through NF- κ B and Decreases Prostacyclin Synthase in Endothelial Cells. *American Journal of Physiology Cell Physiology*, 282, C227-C416.

COSTALES, M. G., HAGA, C. L., VELAGAPUDI, S. P., CHILDS-DISNEY, J. L., PHINNEY, D. G. & DISNEY, M. D. 2017. Small Molecule Inhibition of microRNA-210 Reprograms an Oncogenic Hypoxic Circuit. *Journal of American Chemical Society*, 139, 3446-3455.

CROSS, A. R., LION, J., POUSSIN, K., GLOTZ, D. & MOONEY, N. 2021. Inflammation Determines the Capacity of Allogenic Endothelial Cells to Regulate Human Treg Expansion. *Frontiers in Immunology*, 12, 666531.

CROSSLAND, R. E., ALBIERO, A., SANJURJO-RODRÍGUEZ, C., REIS, M., RESTEU, A., ANDERSON, A. E., DICKINSON, A. M., PRATT, A. G., BIRCH, M., MCCASKIE, A. W., JONES, E. & WANG, X.-N. 2023. MicroRNA Profiling of Low Concentration Extracellular Vesicle RNA Utilizing NanoString nCounter Technology. *Journal of Extracellular Biology*, 2, e72.

D'ANGELO, G., RAPOSO, G., NISHIMURA, T. & SUETSUGU, S. 2022. Protrusion-derived Vesicles: New Subtype of EVs? *Nature Reviews Cell Biology*, 24, 81-82.

DARBONNE, W. C., RICE, G. C., MOHLER, M. A., APPLE, T., HÉBERT, C. A., VALENTE, A. J. & BAKER, J. B. 1991. Red Blood Cells are a Sink for Interleukin 8, a Leukocyte Chemotaxin. *Journal of Clinical Investigation*, 88, 1362-1369.

DARLOT, B., EATON, J. R. O., GEIS-ASTEGGIANTE, L., YAKALA, G. K., KARUPPANAN, K., DAVIES, G., ROBINSON, C. V., KAWAMURA, A. & BHATTACHARYA, S. 2020. Engineered anti-inflammatory peptides inspired by mapping an evasin-chemokine interaction. *Journal of Biological Chemistry*, 295, 10926-10939.

DEVKOTA, S. R., ARYAL, P., POKHREL, R., JIAO, W., PERRY, A., PANJIKAR, S., PAYNE, R. J., WILCE, M. C. J., BHUSAL, R. P. & STONE, M. J. 2023. Engineering Broad-Spectrum Inhibitors of Inflammatory Chemokines from Subclass A3 Tick Evasins. *Nature Communications*, 14, 4204.

DIAS, I. H. K., MARSHALL, L., LAMBERT, P. A., CHAPPLE, I. L. C., MATTHEWS, J. B. & GRIFFITHS, H. R. 2008. Gingipains from *Porphyromonas gingivalis* Increase the Chemotactic and Respiratory Burst-Priming Properties of the 77-Amino-Acid Interleukin-8 Variant. *Infection and Immunity*, 76, 317-323.

DIEUDÉ, M., BELL, C., TURGEON, J., BEILLEVAIRE, D., POMERLEAU, L., YANG, B., HAMELIN, K., QI, S., PALLET, N., BÉLAND, C., DHAHRI, W., CAILHIER, J.-F., ROUSSEAU, M., DUCHEZ, A.-C., LÉVESQUE, T., LAU, A., RONDEAU, C., GINGRAS, D., MURUVE, D., RIVARD, A., CARDINAL, H., PERREAULT, C., DESJARDINS, M., BOILARD, É., THIBAUT, P. & HÉBERT, M.-J. 2015. The 20S proteasome core, active within apoptotic exosome-like vesicles, induces

autoantibodyproduction and accelerates rejection. *Science Translational Medicine*, 7, 318ra200.

DILLEMANS, L., YU, K., ZUTTER, A. D., NOPPEN, S., GOUWY, M., BERGHMANS, N., BONDT, M. D., VANBRABANT, L., BRUSSELMANS, S., MARTENS, E., SCHOLS, D., MARQUES, P. E., STRUYF, S. & PROOST, P. 2023. C-terminal truncation of CXCL10 attenuates inflammatory activity but retains angiostatic properties. *BioRxiv*.

DIVITHOTAWELA, C., CYPEL, M., MARTINU, T., SINGER, L. G., BINNIE, M., CHUNG-WAI CHOW, M., CHAPARRO, C., WADDELL, T. K., PERROT, M. D., PIERRE, A., YASUFUKU, K., YEUNG, J. C., DONAHOE, L., KESHAVJEE, S. & TIKKANEN, J. M. 2019. Long-term Outcomes of Lung Transplant With Ex Vivo Lung Perfusion. *JAMA Surgery*, 154, 1143-1150.

DJURANOVIC, S., NAHVI, A. & GREEN, R. 2012. miRNA-Mediated Gene Silencing by Translational Repression Followed by mRNA Deadenylation and Decay. *Science*, 336, 237-240.

DUMAS, S. J. M., ELDA; BORRI, MILA; GOVEIA, JERMAINE; ROHLENOVA, KATERINA; CONCHINHA, NADINE V.; FALKENBERG, KIM; TEUWEN, LAURE-ANNE; DE ROOIJ, LAURA; KALUCKA, JOANNA; CHEN, RONGYUAN; KHAN, SHAWEZ; TAVERNA, FEDERICO; LU, WEISI; PARYS, MAGDALENA; DE LEGHER, CARLA; VINCKIER, STEFAN; KARAKACH, TOBIAS K.; SCHOONJANS, LUC; LIN, LIN; BOLUND, LARS; DEWERCHIN, MIEKE; EELEN, GUY; RABELINK, TON J.; LI, XURI; LUO, YONGLUN; CARMELIET, PETER 2020. Single-Cell RNA Sequencing Reveals Renal Endothelium Heterogeneity and Metabolic Adaptation to Water Deprivation. *Journal of the American Society for Nephrology*, 31, 118-138.

ELDH, M., BAGGE, R. O., LÄSSER, C., SVANVIK, J., SJÖSTRAND, M., MATTSSON, J., LINDNÉR, P., CHOI, D.-S., GHO, Y. S. & LÖTVALL, J. 2014. MicroRNA in Exosomes Isolated Directly from the Liver Circulation in Patients with Metastatic Uveal Melanoma. *BMC Cancer*, 14, 962.

ELTZSCHIG, H. K. & ECKLE, T. 2011. Ischemia and Reperfusion- From Mechanism to Translation. *Naure Medicine*, 17, 1391-1401.

ENDER, C., KREK, A., FRIEDLÄNDER, M. R., BEITZINGER, M., WEINMANN, L., CHEN, W., PFEFFER, S., RAJEWSKY, N. & MEISTER, G. 2008. A Human snoRNA with microRNA-like Functions. *Molecular Cell*, 32, 519-528.

ERP, A. C. V., QI, H., JESPERSEN, N. R., HJORTBAK, M. V., OTTENS, P. J., WIERSEMA-BUIST, J., NØRREGAARD, R., PEDERSEN, M., LAUSTSEN, C., LEUVENINK, H. G. D. & JESPERSEN, B. 2020. Organ-specific Metabolic Profiles of the Liver and Kidney During Brain Death and Afterwards During Normothermic Machine Perfusion of the Kidney. *American journal of Transplantation*, 2020, 2425-2436.

ERP, A. C. V., REBOLLEDO, R. A., HOEKSMAS, D., JESPERSEN, N. R., OTTENS, P. J., NØRREGAARD, R., PEDERSEN, M., LAUSTSEN, C., BURGERHOF, J. G. M., WOLTERS, J. C., J. CIAPAITE, H. E. B., LEUVENINK, H. G. D. & JESPERSEN, B. 2018. Organ-specific Responses During Brain Death: Increased Aerobic Metabolism in the Liver and Anaerobic Metabolism with Decreased Perfusion in the Kidneys. *Scientific Report*, 8, 4405.

- EULALIO, A., HUNTZINGER, E. & IZAURRALDE, E. 2008. GW182 Interaction with Argonaute is Essential for miRNA-mediated Translational Repression and mRNA Decay. *Nature Structural & Molecular Biology*, 15, 346-353.
- EULALIO, A., HUNTZINGER, E., NISHIHARA, T., REHWINKEL, J., FAUSER, M. & IZAURRALDE, E. 2009. Deadenylation is a Widespread Effect of miRNA Regulation *RNA*, 15, 21-32.
- FANUCCHI, S., FOK, E. T., DALLA, E., SHIBAYAMA, Y., BÖRNER, K., CHANG, E. Y., STOYCHEV, S., IMAKAEV, M., GRIMM, D., WANG, K. C., LI, G., SUNG, W.-K. & MHLANGA, M. M. 2019. Immune Genes are Primed for Robust Transcription by Proximal Long Noncoding RNAs Located in Nuclear Compartments. *Nature Genetics*, 51, 138-150.
- FAREH, M., YEOM, K.-H., HAAGSMA, A. C., CHAUHAN, S., HEO, I. & JOO, C. 2016. TRBP Ensures Efficient Dicer Processing of Precursor microRNA in RNA-crowded Environments. *Nature Communications*, 7, 1369.
- FARTHING, D. E., FARTHING, C. A. & XI, L. 2015. Inosine and hypoxanthine as novel biomarkers for cardiac ischemia: From bench to point-of-care. *Experimental Biology and Medicine*, 240, 821-831.
- FASANARO, P., D'ALESSANDRA, Y., STEFANO, V. D., MELCHIONNA, R., ROMANI, S., POMPILIO, G., CAPOGROSSI, M. C. & MARTELLI, F. 2008. MicroRNA-210 Modulates Endothelial Cell Response to Hypoxia and Inhibits the Receptor Tyrosine Kinase Ligand Ephrin-A3. *Journal of Biological Chemistry*, 283, 15878-15883.
- FENG, H., SCHORPP, K., JIN, J., YOZWIAK, C. E., HOFFSTROM, B. G., DECKER, A. M., RAJBHANDARI, P., STOKES, M. E., BENDER, H. G., CSUKA, J. M., UPADHYAYULA, P. S., CANOLL, P., UCHIDA, K., SONI, R. K., HADIAN, K. & STOCKWELL, B. R. 2020. Transferrin Receptor Is a Specific Ferroptosis Marker. *Cell Reports*, 30, 3411-3423.
- FERREIRA, J. V., SOARES, A. D. R., RAMALHO, J., CARVALHO, C. M., CARDOSO, M. H., PINTADO, P., CARVALHO, A. S., BECK, H. C., MATTHIESEN, R., ZUZARTE, M., GIRÃO, H., NIEL, G. V. & PEREIRA, P. 2022. LAMP2A Regulates the Loading of Proteins into Exosomes. *Science Advances*, 8, eabm1140.
- FILIPPIS, V. D., FRASSON, R. & FONTANA, A. 2009. 3-Nitrotyrosine as a Spectroscopic Probe for Investigating Protein-protein Interactions. *Protein Science*, 15, 976-986.
- FISHER, A. J., DONNELLY, S. C., HIRANI, N., HASLETT, C., STRIETER, R. M., DARK, J. H. & CORRIS, P. A. 2000. Elevated Levels of Interleukin-8 in Donor Lungs Is Associated with Early Graft Failure after Lung Transplantation. *American Journal of Respiratory and Critical Care Medicine*, 163, 259-265.
- FITZNER, D., SCHNAARS, M., ROSSUM, D. V., KRISHNAMOORTHY, G., DIBAJ, P., BAKHTI, M., REGEN, T., HANISCH, U.-K. & SIMONS, M. 2011. Selective Transfer of Exosomes from Oligodendrocytes to Microglia by Macropinocytosis. *Journal of Cell Science*, 124, 447-458.

- FRANZIN, R., STASI, A., SALLUSTIO, F., BRUNO, S., MERLOTTI, G., QUAGLIA, M., GRANDALIANO, G., PONTRELLI, P., THURMA, J. M., CAMUSSI, G., STALLONE, G., CANTALUPPI, V., GESUALDO, L. & CASTELLANO, G. 2022. Extracellular Vesicles Derived from Patients with Antibody-Mediated Rejection Induce Tubular Senescence and Endothelial to Mesenchymal Transition in Renal Cells. *American journal of Transplantation*, 22, 2139-2157.
- FRIEDMAN, R. C., FARH, K. K.-H., BURGE, C. B. & BARTEL, D. P. 2009. Most Mammalian mRNAs are Conserved Targets of microRNAs. *Genome Research*, 19, 92-105.
- GANTIER, M. P., MCCOY, C. E., RUSINOVA, I., SAULEP, D., WANG, D., XU, D., IRVING, A. T., BEHLKE, M. A., HERTZOG, P. J., MACKAY, F. & WILLIAMS, B. R. G. 2011. Analysis of microRNA Turnover in Mammalian Cells Following Dicer1 Ablation. *Nucleic Acid Research*, 39, 5692-5703.
- GARCIA-MARTIN, R., BRANDAO, B. B., THOMOU, T., ALTINDIS, E. & KAHN, C. R. 2022. Tissue Differences in the Exosomal/Small Extracellular Vesicle Proteome and their Potential as Indicators of Altered Tissue Metabolism. *Cell Reports*, 38, 110277.
- GARCIA-MARTIN, R., WANG, G., BRANDÃO, B. B., ZANOTTO, T. M., SHAH, S., PATEL, S. K., SCHILLING, B. & KAHN, C. R. 2021. MicroRNA Sequence Codes for Small Extracellular Vesicle Release and Cellular Retention. *Nature*, 601, 446-451.
- GELMAN, A. E., OKAZAKI, M., SUGIMOTO, S., LI, W., KORNFELD, C. G., LAI, J., RICHARDSON, S. B., KREISEL, F. H., HUANG, H. J., TIETJENS, J. R., ZINSELMAYER, B. H., PATTERSON, G. A., MILLER, M. J., KRUPNICK, A. S. & KREISEL, D. 2010. CCR2 Regulates Monocyte Recruitment As Well As CD4+ Th1 Allorecognition After Lung Transplantation. *American journal of Transplantation*, 10, 1189-1199.
- GERARD, C. & ROLLINS, B. J. 2001. Chemokines and Disease. *Nature Immunology*, 2, 108-115.
- GIELIS, E. M., ANHOLTS, J. D. H., BEELEN, E. V., HAASNOOT, G. W., FIJTER, H. W. D., BAJEMA, I., HEIDT, S., VRIE, M. V. D., HILBRANDS, L. B., MALLAT, M. J. K., LEDEGANCK, K. J., CLAAS, F. H. J. & EIKMANS, M. 2021. A Combined microRNA and Chemokine Profile in Urine to Identify Rejection After Kidney Transplantation. *Transplantation Direct*, 7, e711.
- GILL, D. J., TEO, H., SUN, J., PERISIC, O., VEPRINTSEV, D. B., EMR, S. D. & WILLIAMS, R. L. 2007. Structural Insight into the ESCRT-I/-II Link and its Role in MVB Trafficking. *EMBO Journal*, 26, 600-612.
- GODWIN, J. G., GE, X., STEPHAN, K., JURISCH, A., TULLIUS, S. G. & IACOMINIA, J. 2010. Identification of a microRNA Signature of Renal Ischemia Reperfusion Injury. *Proceedings of the National Academy of Science of the United States of America*, 107, 14339-14344.
- GOÑI, F. M. & ALONSO, A. 2009. Effects of Ceramide and Other Simple Sphingolipids on Membrane Lateral Structure. *Biohemica et Biophysica Acta (BBA)- Biomembranes*, 1788, 169-177.

- GRAHAM, G. J., HANDEL, T. M. & PROUDFOOT, A. E. I. 2019. Leukocyte Adhesion: Reconceptualizing Chemokine Presentation by Glycosaminoglycans. *Trends in Immunology*, 40, P472-P481.
- GRAY, A. L., KARLSSON, R., ROBERTS, A. R. E., RIDLEY, A. J. L., PUN, N., KHAN, B., LAWLESS, C., LUÍ'S, R., SZPAKOWSKA, M., ANDY CHEVIGNE´ , HUGHES, C. E., MEDINA-RUIZ, L., BIRCHENOUGH, H. L., MULHOLLAND, I. Z., SALANGA, C. L., YATES, E. A., TURNBULL, J. E., HANDEL, T. M., GRAHAM, G. J., JOWITT, T. A., SCHIESSL, I., RICHTER, R. P., MILLER, R. L. & DYER, D. P. 2023. Chemokine CXCL4 Interactions with Extracellular Matrix Proteoglycans Mediate Widespread Immune Cell Recruitment Independent of Chemokine Receptors. *Cell Reports*, 42, 111930.
- GREGORINI, M., CORRADETTI, V., PATTONIERI, E. F., ROCCA, C., MILANESI, S., PELOSO, A., CANEVARI, S., CECCO, L. D., DUGO, M., AVANZINI, M. A., MANTELLI, M., MAESTRI, M., ESPOSITO, P., BRUNO, S., LIBETTA, C., CANTON, A. D. & RAMPINO, T. 2017. Perfusion of Isolated Rat Kidney with Mesenchymal Stromal Cells/Extracellular Vesicles Prevents Ischaemic Injury. *Journal of Cellular and Molecular Medicine*, 21, 3381-3393.
- GUO, H., INGOLIA, N. T., WEISSMAN, J. S. & BARTEL, D. P. 2010. Mammalian microRNAs Predominantly Act to Decrease Target mRNA Levels. *Nature*, 466, 835-840.
- HA, M. & KIM, V. N. 2014. Regulation of microRNA Biogenesis. *Nature Reviews Molecular Cell Biology*, 15, 509-524.
- HAGIWARA, K., KATSUDA, T., GAILHOUSTE, L., KOSAKA, N. & OCHIYA, T. 2015. Commitment of Annexin A2 in Recruitment of microRNAs into Extracellular Vesicles. *FEBS Letters*, 589, 4071-4078.
- HÉBERT, C. A., VITANGCOL, R. V. & BAKER, J. B. 1991. Scanning Mutagenesis of Interleukin-8 Identifies a Cluster of Residues Required for Receptor Binding. *Journal of Biological Chemistry*, 266, 18989-18994.
- HELLYER, T. P., MCAULEY, D. F., WALSH, T. S., ANDERSON, N., MORRIS, A. C., SINGH, S., DARK, P. P., ROY, A. I., PERKINS, G. D., MCMULLAN, R., EMERSON, L. M., BLACKWOOD, B., WRIGHT, S. E., KEFALA, K., O'KANE, C. M., BAUDOUIN, S. V., PATERSON, R. L., ROSTRON, A. J., AGUS, A., BANNARD-SMITH, J., ROBIN, N. M., WELTERS, I. D., BASSFORD, C., YATES, B., SPENCER, C., LAHA, S. K., HULME, J., BONNER, S., LINNETT, V., SONKSEN, J., BROECK, T. V. D., BOSCHMAN, G., KEENAN, D. J., SCOTT, J., ALLEN, A. J., PHAIR, G., PARKER, J., BOWETT, S. A. & SIMPSON, A. J. 2020. Biomarker-guided Antibiotic Stewardship in Suspected Ventilator-associated Pneumonia (VAPrapid2): A Randomised Controlled Trial and Process Evaluation. *The Lancet Respiratory Medicine*, 8, 182-191.
- HELLYER, T. P., MORRIS, A. C., MCAULEY, D. F., WALSH, T. S., ANDERSON, N. H., SINGH, S., DARK, P., ROY, A. I., BAUDOUIN, S. V., WRIGHT, S. E., PERKINS, G. D., KEFALA, K., JEFFELS, M., MCMULLAN, R., O'KANE, C. M., SPENCER, C., LAHA, S., ROBIN, N., GOSSAIN, S., GOULD, K., RUCHAUD-SPARAGANO, M. H., SCOTT, J., BROWNE, E. M., MACFARLANE, J. G., WISCOMBE, S., WIDDRINGTON, J. D., DIMMICK, I., LAURENSEN, I. F., NAUWELAERS, F. &

- SIMPSON, A. J. 2015. Diagnostic accuracy of pulmonary host inflammatory mediators in the exclusion of ventilator-acquired pneumonia. *Thorax*, 70, 41-7.
- HERRERA, O. B., GOLSHAYAN, D., TIBBOTT, R., OCHOA, F. S., JAMES, M. J., MARELLI-BERG, F. M. & LECHLER, R. I. 2004. A Novel Pathway of Alloantigen Presentation by Dendritic Cells. *Journal of Immunology*, 173, 4828-4837.
- HOFFMANN, F., MÜLLER, W., SCHÜTZ, D., PENFOLD, M. E., WONG, Y. H., SCHULZ, S. & STUMM, R. 2012. Rapid Uptake and Degradation of CXCL12 Depend on CXCR7 Carboxyl-terminal Serine/Threonine Residues. *Journal of Biological Chemistry*, 287, 28362-28377.
- HOSGOOD, S. A., CALLAGHAN, C. J., WILSON, C. H., SMITH, L., MULLINGS, J., MEHEW, J., ONISCU, G. C., PHILLIPS, B. L., BATES, L. & NICHOLSON, M. L. 2023. Normothermic Machine Perfusion Versus Static Cold Storage in Donation After Circulatory Death Kidney Transplantation: A Randomized Controlled Trial. *Nature Medicine*, 29, 1511-1519.
- HU, C.-J., SATAUR, A., WANG, L., CHEN, H. & SIMON, M. C. 2007. The N-Terminal Transactivation Domain Confers Target Gene Specificity of Hypoxia-inducible Factors HIF-1 α and HIF-2 α . *Molecular Biology of the Cell*, 18, 4528-4542.
- HU, S., HUANG, M., LI, Z., JIA, F., GHOSH, Z., LIJKWAN, M. A., FASANARO, P., NING SUN, X. W., MARTELLI, F., ROBBINS, R. C. & WU, J. C. 2010. MicroRNA-210 as a Novel Therapy for Treatment of Ischemic Heart Disease. *Circulation*, 122, S124-S131.
- HUANG, H.-Y., LIN, Y.-C.-D., CUI, S., HUANG, Y., TANG, Y., XU, J., BAO, J., LI, Y., WEN, J., ZUO, H., WANG, W., LI, J., NI, J., RUAN, Y., LI, L., CHEN, Y., XIE, Y., ZHU, Z., CAI, X., CHEN, X., YAO, L., CHEN, Y., LUO, Y., LUXU, S., LUO, M., CHIU, C.-M., MA, K., ZHU, L., CHENG, G.-J., BAI, C., CHIANG, Y.-C., WANG, L., WEI, F., LEE, T.-Y. & HUANG, H.-D. 2022. miRTarBase Update 2022: An Informative Resource for Experimentally Validated miRNA–target Interactions. *Nucleic Acid Research*, 50, D222-D230.
- HUANG, X., DING, L., BENNEWITH, K. L., TONG, R. T., WELFORD, S. M., ANG, K. K., STORY, M., LE, Q.-T. & GIACCIA, A. J. 2009. Hypoxia-Inducible mir-210 Regulates Normoxic Gene Expression Involved in Tumor Initiation. *Molecular Cell*, 35, P856-867.
- HUANG, Y., PAXTON, W. A., WOLINSKY, S. M., NEUMANN, A. U., ZHANG, L., HE, T., KANG, S., CERADINI, D., JIN, Z., YAZDANBAKHS, K., KUNSTMAN, K., ERICKSON, D., DRAGON, E., LANDAU, N. R., PHAIR, J., HO, D. D. & KOUP, R. A. 1996. The Role of a Mutant CCR5 Allele in HIV–1 Transmission and Disease Progression. *Nature Medicine*, 2, 1240-1243.
- HUEBNER, A. R., CHENG, L., SOMPARN, P., KNEPPER, M. A., FENTON, R. A. & PISITKUN, T. 2016. Deubiquitylation of Protein Cargo Is Not an Essential Step in Exosome Formation. *Molecular and Cellular Proteomics*, 15, 1556-1571.
- HUGHES, A. D., ZHAO, D., DAI, H., ABOU-DAYA, K. I., TIEU, R., RAMMAL, R., WILLIAMS, A. L., LANDSITTEL, D. P., SHLOMCHIK, W. D., MORELLI, A. E., OBERBARNSCHEIDT, M. H. &

- LAKKIS, F. G. 2019. Cross-dressed Dendritic Cells Sustain Effector T cell Responses in Islet and Kidney Allografts. *Journal of Clinical Investigation*, 130, 287-294.
- HUGHES, C. E. & NIBBS, R. J. B. 2018. A Guide to Chemokines and Their Receptors. *The FEBS Journal*, 285, 2944-2971.
- HUNDELSHAUSEN, P. V., AGTEN, S. M., ECKARDT, V., BLANCHET, X., SCHMITT, M. M., IPPEL, H., NEIDECK, C., BIDZHEKOV, K., LEBERZAMMER, J., WICHAPONG, K., FAUSSNER, A., DRECHSLER, M., GROMMES, J., GEFFEN, J. P. V., LI, H., ORTEGA-GOMEZ, A., MEGENS, R. T. A., NAUMANN, R., DIJKGRAAF, I., NICOLAES, G. A. F., DÖRING, Y., SOEHNLEIN, O., LUTGENS, E., HEEMSKERK, J. W. M., KOENEN, R. R., MAYO, K. H., HACKENG, T. M. & WEBER, C. 2017. Chemokine Interactome Mapping Enables Tailored Intervention in Acute and Chronic Inflammation. *Science Translational Medicine*, 9, eahh6650.
- HURWITZ, S. N., CONLON, M. M., RIDER, M. A., BROWNSTEIN, N. C. & JR, D. G. M. 2016. Nanoparticle Analysis Sheds Budding Insights into Genetic Drivers of Extracellular Vesicle Biogenesis. *Journal of Extracellular Vesicles*, 5, 31295.
- IAVELLO, A., FRECH, V. S. L., MARIA, C. G., DEREGIBUS, C., QUESENBERRY, P. J. & CAMUSSI, G. 2016. Role of Alix in miRNA packaging during extracellular vesicle biogenesis. *International Journal of Molecular Medicine*, 37, 958-966.
- IRANI, K., XIA, Y., ZWEIER, J. L., SOLLOTT, S. J., DER, C. J., FEARON, E. R., SUNDARESAN, M., FINKEL, T. & GOLDSCHMIDT-CLERMONT, P. J. 1997. Mitogenic signaling mediated by oxidants in Ras-transformed fibroblasts. *Science*, 275, 1649-1652.
- ISCHIROPOULOS, H. 1998. Biological tyrosine nitration: A pathophysiological function of nitric oxide and reactive oxygen species. *Archives of Biochemistry and Biophysics*, 356, 1-11.
- JANSSENS, R., MORTIER, A., BOFF, D., VANHEULE, V., GOUWY, M., FRANCK, C., LARSEN, O., ROSENKILDE, M. M., DAMME, J. V., AMARAL, F. A., TEIXEIRA, M. M., STRUYF, S. & PROOST, P. 2016. Natural Nitration of CXCL12 Reduces its Signaling Capacity and Chemotactic Activity in vitro and Abrogates Intra-articular Lymphocyte Recruitment in vivo. *Oncotarget*, 7, 62439-62459.
- JIN, H. Y., GONZALEZ-MARTIN, A., MILETIC, A. V., LAI, M., KNIGHT, S., SABOURI-GHOMI, M., HEAD, S. R., MACAULEY, M. S., RICKERT, R. C. & XIAO, C. 2015. Transfection of microRNA Mimics Should Be Used with Caution. *Frontiers in Genetics*, 6, 00340.
- JOHN D. LANG, J., TENG, X., CHUMLEY, P., CRAWFORD, J. H., ISBELL, T. S., CHACKO, B. K., LIU, Y., JHALA, N., CROWE, D. R., SMITH, A. B., CROSS, R. C., FRENETTE, L., KELLEY, E. E., WILHITE, D. W., HALL, C. R., PAGE, G. P., FALLON, M. B., BYNON, J. S., ECKHOFF, D. E. & PATEL, R. P. 2007. Inhaled NO accelerates restoration of liver function in adults following orthotopic liver transplantation. *Journal of Clinical Investigation*, 117, 2583-2591.
- JONESON, T. & BAR-SAGI, D. 1998. A Rac1 effector site controlling mitogenesis through superoxide production. *Journal of Biological Chemistry*, 273, 17991-17994.

- JONG, O. G. D., VERHAAR, M. C., CHEN, Y., VADER, P., GREMMELS, H., POSTHUMA, G., SCHIFFELERS, R. M., GUCEK, M. & BALKOM, B. W. M. V. 2012. Cellular Stress Conditions are Reflected in the Protein and RNA content of Endothelial Cell-derived Exosomes. *Journal of Extracellular Vesicles*, 1, 18396.
- JOSEPH, P. R. B., MOSIER, P. D., DESAI, U. R. & RAJARATHNAM, K. 2015. Solution NMR Characterization of Chemokine CXCL8/IL-8 Monomer and Dimer Binding to Glycosaminoglycans: Structural Plasticity Mediates Differential Binding Interactions. *Biochemical Journal*, 472, 121-133.
- JOSEPH, P. R. B., SAWANT, K. V. & RAJARATHNAM, K. 2017. Heparin-bound Chemokine CXCL8 Monomer and Dimer are Impaired for CXCR1 and CXCR2 Activation: Implications for Gradients and Neutrophil Trafficking. *Open Biology*, 7, 170168.
- JOSHUA A. WELSH, G. J. A. A., MICHEL BREMER, MICHAEL CIMORELLI, FRANÇOISE DIGNAT-GEORGE, BERND GIEBEL, ANDRÉ GÖRGENS, AN HENDRIX, MARTINE KUIPER, ROMARIC LACROIX, JOANNE LANNIGAN, TON G. LEEUWEN, ESTEFANÍA LOZANO-ANDRÉS, SHOAB RAO, STÉPHANE ROBERT, LEONIE ROND, VERA A. TANG, TOBIAS TERTEL, XIAOMEI YAN, MARCA H. M. WAUBEN, JOHN P. NOLAN, JENNIFER C. JONES, RIENK NIEUWLAND, EDWIN POL 2023. A compendium of single extracellular vesicle flow cytometry. *Journal of Extracellular Vesicles*, 12, e12299.
- KAJIMOTO, T., OKADA, T., MIYA, S., ZHANG, L. & NAKAMURA, S.-I. 2013. Ongoing Activation of Sphingosine 1-phosphate Receptors Mediates Maturation of Exosomal Multivesicular Endosomes. *Nature Communications*, 4, 2712.
- KAMIŃSKA, D., KOŚCIELSKA-KASPRZAK, K., CHUDOBA, P., HAŁOŃ, A., MAZANOWSKA, O., GOMÓŁKIEWICZ, A., DZIĘGIEL, P., DRULIS-FAJDASZ, D., MYSZKA, M., LEPIESZA, A., POLAK, W., BORATYŃSKA, M. & KLINGER, M. 2016. The Influence of Warm Ischemia Elimination on Kidney Injury During Transplantation – Clinical and Molecular Study. *Scientific Report*, 6, 36118.
- KANNO, S., LEE, P. C., ZHANG, Y., HO, C., GRIFFITH, B. P., II, L. L. S. & BILLIAR, T. R. 2003. Attenuation of myocardial ischemia/reperfusion injury by superinduction of inducible nitric oxide synthase. *Circulation*, 101, 2742-2748.
- KATO, M., ZHANG, J., WANG, M., LANTING, L., YUAN, H., ROSSI, J. J. & NATARAJAN, R. 2007. MicroRNA-192 in Diabetic Kidney Glomeruli and its Function in TGF- β -induced Collagen Expression via Inhibition of E-box Repressors. *Proceedings of the National Academy of Science of the United States of America*, 104, 3432-3437.
- KEHL, T., KERN, F., BACKES, C., FEHLMANN, T., STÖCKEL, D., MEESE, E., LENHOF, H.-P. & KELLER, A. 2019. miRPathDB 2.0: a novel release of the miRNA Pathway Dictionary Database. *Nucleic Acid Research*, 48, D142-D147.

- KIM, J.-W., TCHERNYSHYOV, I., SEMENZA, G. L. & DANG, C. V. 2006. HIF-1-Mediated Expression of Pyruvate Dehydrogenase Kinase: A Metabolic Switch Required for Cellular Adaptation to Hypoxia. *Cell Metabolism*, 3, 177-185.
- KIM, S., LEE, S. A., YOON, H., KIM, M. Y., YOO, J.-K., AHN, S.-H., PARK, C. H., PARK, J., NAM, B. Y., PARK, J. T., HAN, S. H., KANG, S.-W., KIM, N. H., KIM, H. S., HAN, D., YOON, J. I., CHOI, C. & YOO, T.-H. 2021. Exosome-Based Delivery of Super-Repressor I κ B α Ameliorates Kidney Ischemia-Reperfusion Injury. *Kidney International*, 100, 570-584.
- KIM, Y.-K. & KIM, V. N. 2007. Processing of Intronic microRNAs. *EMBO Journal*, 26, 775-783.
- KOEPPEN, M., LEE, J. W., SEO, S.-W., BRODSKY, K. S., KRETH, S., YANG, I. V., BUTTRICK, P. M., ECKLE, T. & ELTZSCHIG, H. K. 2018. Hypoxia-Inducible Factor 2-Alpha-Dependent Induction of Amphiregulin Dampens Myocardial Ischemia-Reperfusion Injury. *Nature Communications*, 9, 816.
- KOLIHA, N., WIENCEK, Y., HEIDER, U., JÜNGST, C., KLADT, N., KRAUTHÄUSER, S., JOHNSTON, I. C. D., BOSIO, A. & ASTRID SCHAUSS, S. W. 2016. A Novel Multiplex Bead-based Platform Highlights the Diversity of Extracellular Vesicles. *Journal of Extracellular Vesicles*, 5, 29975.
- KONG, A. S.-Y., LAI, K.-S., LIM, S.-H. E., SIVALINGAM, S., LOH, J.-Y. & MARAN, S. 2022. miRNA in Ischemic Heart Disease and Its Potential as Biomarkers: A Comprehensive Review. *International Journal of Molecular Sciences*, 23, 9001.
- KOSAKA, N., IGUCHI, H., YOSHIOKA, Y., TAKESHITA, F., MATSUKI, Y. & OCHIYA, T. 2010. Secretory Mechanisms and Intercellular Transfer of MicroRNAs in Living Cells. *Journal of Biological Chemistry*, 285, P17442-17452.
- KOU, M., HUANG, L., YANG, J., CHIANG, Z., CHEN, S., LIU, J., GUO, L., ZHANG, X., ZHOU, X., XU, X., YAN, X., WANG, Y., ZHANG, J., XU, A., TSE, H.-F. & LIAN, Q. 2022. Mesenchymal Stem Cell-Derived Extracellular Vesicles for Immunomodulation and Regeneration: A Next Generation Therapeutic Tool? *Cell Death and Disease*, 13, 580.
- KRAMER, A. A., POSTLER, G., SALHAB, K. F., MENDEZ, C., CAREY, L. C. & RABB, H. 1999. Renal Ischemia/Reperfusion Leads to Macrophage-mediated Increase in Pulmonary Vascular Permeability. *Kidney International*, 55, 2362-2367.
- KROL, J., BUSSKAMP, V., MARKIEWICZ, I., STADLER, M. B., RIBI, S., RICHTER, J., DUEBEL, J., BICKER, S., FEHLING, H. J., SCHÜBELER, D., OERTNER, T. G., SCHRATT, G., BIBEL, M., ROSKA, B. & FILIPOWICZ, W. 2010. Characterizing Light-Regulated Retinal MicroRNAs Reveals Rapid Turnover as a Common Property of Neuronal MicroRNAs. *Cell*, 141, 618-631.
- KUGERATSKI, F. G., HODGE, K., LILLA, S., MCANDREWS, K. M., ZHOU, X., HWANG, R. F., ZANIVAN, S. & KALLURI, R. 2021. Quantitative Proteomics Identifies the Core pPoteome of Exosomes with Syntenin-1 as the Highest Abundant Protein and a Putative Universal Biomarker. *Nature Cell Biology*, 23, 631-641.

- KULSHRESHTHA, R., FERRACIN, M., WOJCIK, S. E., GARZON, R., ALDER, H., AGOSTO-PEREZ, F. J., DAVULURI, R., LIU, C.-G., CROCE, C. M., NEGRINI, M., CALIN, G. A. & IVAN, M. 2007. A microRNA Signature of Hypoxia. *Molecular and Cellular Biology*, 27, 1859-1867.
- KUO, M.-C., CHANG, W.-A., WU, L.-Y., TSAI, Y.-C. & HSU, Y.-L. 2021. Hypoxia-Induced Epithelial-to-Mesenchymal Transition in Proximal Tubular Epithelial Cells through miR-545-3p-TNFSF10. *Biomolecules*, 11, 1032.
- KUO, N.-W., GAO, Y.-G., SCHILL, M. S., ISERN, N., DUPUREUR, C. M. & LIWANG, P. J. 2014. Structural Insights into the Interaction between a Potent Anti-inflammatory Protein, Viral CC Chemokine Inhibitor (vCCI), and the Human CC Chemokine, Eotaxin-1. *Journal of Biological Chemistry*, 289, P6592-6603.
- KUROSE, I., WOLF, R., GRISHAM, M. B. & GRANGER, D. N. 1994. Modulation of ischemia/reperfusion-induced microvascular dysfunction by nitric oxide. *Circulation Research*, 74, 376-382.
- KUSABA, T., LALLI, M., KRAMANN, R., KOBAYASHI, A. & HUMPHREYS, B. D. 2013. Differentiated Kidney Epithelial Cells Repair Injured Proximal Tubule. *Proceedings of the National Academy of Science of the United States of America*, 111, 1527-1532.
- KUZNETSOV, A. V., JAVADOV, S., MARGREITER, R., GRIMM, M., HAGENBUCHNER, J. & AUSSERLECHNER, M. J. 2019. The role of mitochondria in the mechanisms of cardiac ischemia-reperfusion injury. *Antioxidants (Basel)*, 8, 454.
- KWON, S. C., NGUYEN, T. A., CHOI, Y.-G., HOHNG, S., KIM, V. N. & WOO, J.-S. 2016. Structure of Human DROSHA. *Cell*, 164, P81-90.
- LAGOS-QUINTANA, M., RAUHUT, R., LENDECKEL, W. & TUSCHL, T. 2001. Identification of Novel Genes Coding for Small Expressed RNAs. *Science*, 294, 853-858.
- LAI, E. C. & POSANKONY, J. W. 1997. The Bearded Box, A Novel 3' UTR Sequence Motif, Mediates Negative Post-Transcriptional Regulation of Bearded and Enhancer of Split Complex Gene Expression. *Development*, 127, 4847-4856.
- LAI, R. C., ARSLAN, F., LEE, M. M., SZE, N. S. K., CHOO, A., CHEN, T. S., SALTO-TELLEZ, M., TIMMERS, L., LEE, C. N., OAKLEY, R. M. E., PASTERKAMP, G., KLEIJN, D. P. V. D. & LIM, S. K. 2010. Exosome Secreted by MSC Reduces Myocardial Ischemia/Reperfusion Injury. *Stem Cell Research*, 4, 214-222.
- LAMIAA EL-SHENNAWY, A. D. H., NURMAA KHUND DASHZEVEG, KATHLEEN M. MCANDREWS, PAUL J. MEHL, DAPHNE CORNISH, ZIHAO YU, VALERIE L. TOKARS, VLAD NICOLAESCU, ANASTASIA TOMATSIDOU, CHENGSHENG MAO, CHRISTOPHER J. FELICELLI, CHIA-FENG TSAI, CAROLINA OSTIGUIN, YUZHI JIA, LIN LI, KEVIN FURLONG, JAN WYSOCKI, XIN LUO, CAROLINA F. RUIVO, DANIEL BATLLE, THOMAS J. HOPE, YANG SHEN, YOUNG KWANG CHAE, HUI ZHANG, VALERIE S. LEBLEU, TUJIN SHI, SUCHITRA SWAMINATHAN, YUAN LUO, DOMINIQUE MISSIAKAS, GLENN C. RANDALL, ALEXIS R. DEMONBREUN, MICHAEL G. ISON,

- RAGHU KALLURI, DEYU FANG & HUIPING LIU 2022. Circulating ACE2-expressing Extracellular Vesicles Block Broad Strains of SARS-CoV-2. *Nature Communications*, 13, 405.
- LANDSKRONER-EIGER, S., QIU, C., PERROTTA, P., SIRAGUSA, M., LEE, M. Y., ULRICH, V., LUCIANO, A. K., ZHUANG, Z. W., CORTI, F., SIMONS, M., MONTGOMERY, R. L., WU, D., YU, J. & SESSA, W. C. 2015. Endothelial miR-17~92 cluster negatively regulates arteriogenesis via miRNA-19 repression of WNT signaling. *Proceedings of the National Academy of Science of the United States of America*, 112, 12812-12817.
- LANNA, A., VAZ, B., D'AMBRA, C., VALVO, S., VUOTTO, C., CHIURCHIÙ, V., DEVINE, O., SANCHEZ, M., BORSELLINO, G., AKBAR, A. N., BARDI, M. D., GILROY, D. W., DUSTIN, M. L., BLUMER, B. & KARIN, M. 2022. An Intercellular Transfer of Telomeres Rescues T Cells from Senescence and Promotes Long-term Immunological Memory. *Nature Cell Biology*, 25, 1461-1474.
- LÄSSER, C., SHELKE, G. V., YERI, A., KIM, D.-K., CRESCITELLI, R., RAIMONDO, S., SJÖSTRAND, M., GHO, Y. S., JENSEN, K. V. K. & LÖTVALL, J. 2016. Two Distinct Extracellular RNA Signatures Released by a Single Cell Type Identified by Microarray and Next-Generation Sequencing. *RNA Biology*, 14, 58-72.
- LAU, K. W., TIAN, Y.-M., RAVAL, R. R., RATCLIFFE, P. J. & PUGH, C. W. 2007. Target Gene Selectivity of Hypoxia-Inducible Factor- α in Renal Cancer Cells is Conveyed by Post-DNA-Binding Mechanisms. *British Journal of Cancer*, 96, 1284-1292.
- LEE, L. Y.-H., OLDHAM, W. M., HE, H., WANG, R., MULHERN, R., HANDY, D. E. & LOSCALZO, J. 2021. Interferon- γ Impairs Human Coronary Artery Endothelial Glucose Metabolism by Tryptophan Catabolism and Activates Fatty Acid Oxidation. *Circulation*, 144, 1612-1628.
- LEE, R. C., FEINBAUM, R. L. & AMBROS, V. 1993. The *C. elegans* Heterochronic Gene *lin-4* Encodes Small RNAs with Antisense Complementarity to *lin-14* Cell, 75, 843-854.
- LEE, Y.-Y., KIM, H. & KIM, V. N. 2023. Sequence Determinant of Small RNA Production by DICER. *Nature*, 615, 323-330.
- LEE, Y., KIM, M., HAN, J., YEOM, K.-H., LEE, S., BAEK, S. H. & KIM, V. N. 2004. MicroRNA Genes are Transcribed by RNA polymerase II. *EMBO Journal*, 23, 4051-4060.
- LERSNER, A. K. V., FERNANDES, F. C. L., OZAWA, P. M. M., LIMA, S. M., VAGNER, T., SUNG, B. H., WEHBE, M., FRANZE, K., WILSON, J. T., IRISH, J. M., WEAVER, A., VIZIO, D. D. & ZIJLSTRA, A. 2022. EV Fingerprinting: Resolving Extracellular Vesicle Heterogeneity Using Multi-parametric Flow Cytometry. *BioRxiv*.
- LI, X., LI, J.-J., YANG, J.-Y., WANG, D.-S., ZHAO, W., SONG, W.-J., LI, W.-M., WANG, J.-F., HAN, W., ZHANG, Z.-C., YU, Y., CAO, D.-Y. & DOU, K.-F. 2012. Tolerance Induction by Exosomes from Immature Dendritic Cells and Rapamycin in a Mouse Cardiac Allograft Model. *Plos One*, 7, e44045.

- LI, X., PENG, X., ZHOU, X., LI, M., CHEN, G., SHI, W., YU, H., ZHANG, C., LI, Y., FENG, Z., LI, J., LIANG, S., HE, W. & GOU, X. 2023. Small extracellular vesicles delivering lncRNA WAC-AS1 aggravate renal allograft ischemia–reperfusion injury by inducing ferroptosis propagation. *Cell Death and Differentiation*.
- LIU, F., LU, J., MANAENKO, A., TANG, J. & HU, Q. 2018. Mitochondria in ischemic stroke: New insight and implications. *Aging and Disease*, 9, 924-937.
- LIU, K., WU, L., YUAN, S., WU, M., XU, Y., SUN, Q., LI, S., ZHAO, S., HUA, T. & LIU, Z.-J. 2020. Structural Basis of CXC Chemokine Receptor 2 Activation and Signalling. *Nature*, 585, 135-140.
- LIU, L.-L., LI, D., HE, Y.-L., ZHOU, Y.-Z., GONG, S.-H., WU, L.-Y., ZHAO, Y.-Q., HUANG, X., ZHAO, T., XU, L., WU, K.-W., LI, M.-G., ZHU, L.-L. & FAN, M. 2017. miR-210 Protects Renal Cell Against Hypoxia-induced Apoptosis by Targeting HIF-1 Alpha. *Molecular Medicine*, 23, 258-271.
- LIU, X.-M., MA, L. & SCHEKMAN, R. 2021. Selective Sorting of microRNAs into Exosomes by Phase-Separated YBX1 Condensates. *eLife*, 10, e71982.
- LIU, Y., SHAH, S. V., XIANG, X., WANG, J., DENG, Z.-B., LIU, C., ZHANG, L., WU, J., EDMONDS, T., JAMBOR, C., KAPPES, J. C. & ZHANG, H.-G. 2009. COP9-Associated CSN5 Regulates Exosomal Protein Deubiquitination and Sorting. *American Journal of Pathology*, 174, 1415-1425.
- LOK, C. N. & PONKA, P. 1999. Identification of a Hypoxia Response Element in the Transferrin Receptor Gene. *Journal of Biological Chemistry*, 274, P24147-24152.
- LOOS, T., OPDENAKKER, G., DAMME, J. V. & PROOST, P. 2009. Citrullination of CXCL8 Increases this Chemokine's Ability to Mobilize Neutrophils into the Blood Circulation. *Haematologica* 94, 1346-1353.
- LORTAT-JACOB, H., GROSDIDIER, A. & IMBERTY, A. 2002. Structural Diversity of Heparan Sulfate Binding Domains in Chemokines. *Proceedings of the National Academy of Science of the United States of America*, 99, 1229-1234.
- LOVE, M. I., HUBER, W. & ANDERS, S. 2014. Moderated Estimation of Fold Change and Dispersion for RNA-seq data with DESeq2. *Genome Biology*, 15, 550.
- LOWMAN, H. B., SLAGLE, P. H., DEFORGE, L. E., WIRTH, C. M., GILLECE-CASTRO, B. L., BOURELL, J. H. & FAIRBROTHER, W. J. 1996. Exchanging Interleukin-8 and Melanoma Growth-stimulating Activity Receptor Binding Specificities. *Journal of Biological Chemistry*, 271, P14344-14352.
- LU, L.-F., GASTEIGER, G., YU, I.-S., CHAUDHRY, A., HSIN, J.-P., LU, Y., BOS, P. D., LIN, L.-L., ZAWISLAK, C. L., CHO, S., SUN, J. C., LESLIE, C. S., LIN, S.-W. & RUDENSKY, A. Y. 2015. A Single miRNA-mRNA Interaction Affects the Immune Response in a Context- and Cell-Type Specific Manner. *Immunity*, 43, 52-64.

- LUND, L. H., KHUSH, K. K., CHERIKH, W. S., GOLDFARB, S., KUCHERYAVAYA, A. Y., LEVVEY, B. J., MEISER, B., ROSSANO, J. W., CHAMBERS, D. C., YUSEN, R. D., STEHLIK, J. & TRANSPLANTATION, F. T. I. S. F. H. A. L. 2017. The Registry of the International Society for Heart and Lung Transplantation: Thirty-fourth Adult Heart Transplantation Report—2017; Focus Theme: Allograft ischemic time. *The Journal of Heart and Lung Transplantation*, 36, 1037-1046.
- M.KOSIERADZKI & ROWINSKI, W. 2008. Ischemia/Reperfusion injury in kidney transplantation: Mechanisms and prevention. *Transplant Proceedings*, 40, 3279-3288.
- MA, L., LI, Y., PENG, J., WU, D., ZHAO, X., CUI, Y., CHEN, L., YAN, X., DU, Y. & YU, L. 2014. Discovery of the Migrasome, An Organelle Mediating Release of Cytoplasmic Contents During Cell Migration. *Cell Research*, 25, 24-38.
- MACKIE, A. R., KLYACHKO, E., THORNE, T., SCHULTZ, K. M., MILLAY, M., ITO, A., KAMIDE, C. E., LIU, T., GUPTA, R., SAHOO, S., MISENER, S., KISHORE, R. & LOSORDO, D. W. 2012. Sonic Hedgehog-Modified Human CD34+ Cells Preserve Cardiac Function After Acute Myocardial Infarction. *Circulation Research*, 111, 312-321.
- MACRAE, I. J., MA, E., ZHOU, M., ROBINSON, C. V. & DOUDNA, J. A. 2008. In Vitro Reconstitution of the Human RISC-loading Complex. *Proceedings of the National Academy of Science of the United States of America*, 105, 512-517.
- MADU, G. C., MOSHKELGOSHA, S., CYPEL, M. & S. KESHAVJEE, S. J. 2020. Isolation and Characterization of Exosomes from Ex Vivo Perfused Human Lungs. *Journal of Heart and Lung Transplantation*, 39, S198.
- MAHTAL, N., LENOIR, O., TINEL, C., ANGLICHEAU, D. & THARAUX, P.-L. 2022. MicroRNAs in Kidney Injury and Disease. *Nature Reviews Nephrology*, 18, 643-662.
- MAŁGORZATA S. MAŁYS, M. C. K., KRISTIN PAPP, CHRISTOF AIGNER, DAFFODIL DIOSO, PATRICK MUCHER, HELGA SCHACHNER, MICHAEL BONELLI, HELMUTH HASLACHER, ANDREW J. REES, RENATE KAIN 2023. Small extracellular vesicles are released ex vivo from platelets into serum and from residual blood cells into stored plasma. *Journal of Extracellular Biology*, 2, e88.
- MARINO, J., BABIKER-MOHAMED, M. H., CROSBY-BERTORINI, P., PASTER, J. T., LEGUERN, C., GERMANA, S., ABDI, R., UEHARA, M., KIM, J. I., MARKMANN, J. F., TOCCO, G. & BENICHO, G. 2016. Donor Exosomes Rather than Passenger Leukocytes Initiate Alloreactive T cell Responses After Transplantation. *Science Immunology*, 1, aaf8759.
- MARK, L., GAVIN.E, A., OLIVIA.M., S., LARS.O, C., ZHI, Z., RONALD.G, T. & JOHN.J, L. 2003. Dependence of liver injury after hemorrhage/resuscitation in mice on NADPH oxidase-derived superoxide. *Shock*, 19, 345-351.
- MASTORIDIS, S., LONDOÑO, M.-C., KURT, A., KODELA, E., CRESPO, E., MASON, J., BESTARD, O., MARTÍNEZ-LLORDELLA, M. & SÁNCHEZ-FUEYO, A. 2020. Impact of Donor Extracellular

- Vesicle Release on Recipient Cell “cross-dressing” Following Clinical Liver and Kidney Transplantation. *American journal of Transplantation*, 21, 2387-2398.
- MATLOUBIAN, M., DAVID, A., ENGEL, S., RYAN, J. E. & CYSTER, J. G. 2000. A transmembrane CXC chemokine is a ligand for HIV-coreceptor Bonzo. *Nature Immunology*, 1, 298-304.
- MATSUSHIMA, S., TSUTSUI, H. & SADOSHIMA, J. 2015. Physiological and pathological functions of NADPH oxidases during myocardial ischemia-reperfusion. *Trends in Cardiovascular Medicine*, 24, 202-205.
- MAYERS, J. R., FYFE, I., SCHUH, A. L., CHAPMAN, E. R., EDWARDSON, J. M. & AUDHYA, A. 2011. ESCRT-0 Assembles as a Heterotetrameric Complex on Membranes and Binds Multiple Ubiquitylated Cargoes Simultaneously. *Journal of Biological Chemistry*, 286, P9636-9645.
- MCGEARY, S. E., LIN, K. S., SHI, C. Y., PHAM, T. M., BISARIA, N., KELLEY, G. M. & BARTEL, D. P. 2019. The biochemical basis of microRNA targeting efficacy. *Science*, 366, eaav1741.
- MCKENZIE, A. J., HOSHINO, D., HONG, N. H., CHA, D. J., FRANKLIN, J. L., COFFEY, R. J., PATTON, J. G. & WEAVER, A. M. 2016. KRAS-MEK Signaling Controls Ago2 Sorting into Exosomes. *Cell Reports*, 15, P978-987.
- MEISTER, G., LANDTHALER, M., PATKANIOWSKA, A., DORSETT, Y., TENG, G. & TUSCHL, T. 2004. Human Argonaute2 Mediates RNA Cleavage Targeted by miRNAs and siRNAs. *Molecular Cell*, 15, 185-197.
- MENON, R., OTTO, E. A., BERTHIER, C. C., NAIR, V., FARKASH, E. A., HODGIN, J. B., YANG, Y., LUO, J., WOODSIDE, K. J., ZAMANI, H., NORMAN, S. P., WIGGINS, R. C., KRETZLER, M. & NAIK, A. S. 2022. Glomerular Endothelial Cell-Podocyte Stresses and Crosstalk in Structurally Normal Kidney Transplants. *Kidney International*, 101, 779-792.
- MERION, R. M., ASHBY, V. B., WOLFE, R. A., DISTANT, D. A., HULBERT-SHEARON, T. E., METZGER, R. A., OJO, A. O. & PORT, F. K. 2005. Deceased-Donor Characteristics and the Survival Benefit of Kidney Transplantation. *JAMA*, 295, 2726-2733.
- MERRILL, J. P., MURRAY, J. E., HARRISON, J. H. & GUILD, W. R. 1956. Successful Homotransplantation of the Human Kidney between Identical Twins. *Journal of the American Medical Association*, 160, 277-282.
- METZEMAEKERS, M., ABOUELASRAR SALAMA, S., VANDOOREN, J., MORTIER, A., JANSSENS, R., VANDENDRIESSCHE, S., GANSEMAN, E., MARTENS, E., GOUWY, M., NEERINCKX, B., VERSCHUEREN, P., DE SOMER, L., WOUTERS, C., STRUYF, S., OPDENAKKER, G., VAN DAMME, J. & PROOST, P. 2021. From ELISA to Immunosorbent Tandem Mass Spectrometry Proteoform Analysis: The Example of CXCL8/Interleukin-8. *Frontiers in Immunology*, 12.

- METZEMAEKERS, M., DAMME, J. V., MORTIER, A. & PROOST, P. 2016. Regulation of Chemokine Activity – A Focus on the Role of Dipeptidyl Peptidase IV/CD26. *Frontiers in Immunology*, 7, 00483.
- MIYAHARA, N., BENAZZO, A., OBERNDORFER, F., IWASAKI, A., LASZLO, V., DÖME, B., HODA, M. A., JAKSCH, P., KLEPETKO, W. & HOETZENECKER, K. 2022. miR-21 in Lung Transplant Recipients With Chronic Lung Allograft Dysfunction. *Transplant International*, 35, 10184.
- MOLON, B., UGEL, S., POZZO, F. D., SOLDANI, C., ZILIO, S., AVELLA, D., PALMA, A. D., MAURI, P., MONEGAL, A., RESCIGNO, M., SAVINO, B., COLOMBO, P., JONJIC, N., PECANIC, S., LAZZARATO, L., FRUTTERO, R., GASCO, A., BRONTE, V. & VIOLA, A. 2011. Chemokine Nitration Prevents Intratumoral Infiltration of Antigen-Specific T Cells. *Journal of Experimental Medicine*, 208, 1949-1962.
- MONTECLARO, F. S. & CHARO, I. F. 1996. The N-terminal Extracellular Segments of the Chemokine Receptors CCR1 and CCR3 Are Determinants for MIP-1a and Eotaxin Binding, Respectively, but a Second Domain Is Essential for Efficient Receptor Activation. *Journal of Biological Chemistry*, 271, 19084-19092.
- MOREAU, A., VAREY, E., ANEGON, I. & CUTURI, M.-C. 2013. Effector Mechanisms of Rejection. *Cold Spring Harbor Perspectives in Medicine*, 3, a015461.
- MURPHY, M. P. 2009. How mitochondria produce reactive oxygen species. *Biochemical Journal* 417, 1-13.
- MURROW, L., MALHOTRA, R. & DEBNATH, J. 2015. ATG12–ATG3 Interacts with Alix to Promote Basal Autophagic Flux and Late Endosome Function. *Nature Cell Biology*, 17, 300-310.
- N.PANAHIAN, T.YOSHIDA, P.L.HUANG, E.T.HEDLEY-WHYTE, T.DALKARA, M.C.FISHMAN & M.A.MOSKOWITZ 1996. Attenuated hippocampal damage after global cerebral ischemia in mice mutant in neuronal nitric oxide synthase. *Neuroscience*, 72, 343-354.
- NARAHARI, J., MA, R., WANG, M. & WALDEN, W. E. 2000. The Aconitase Function of Iron Regulatory Protein 1. *Journal of Biological Chemistry*, 275, P16227-16234.
- NASSER, M. W., RAGHUWANSHI, S. K., GRANT, D. J., JALA, V. R., RAJARATHNAM, K. & RICHARDSON, R. M. 2009. Differential Activation and Regulation of CXCR1 and CXCR2 by CXCL8 Monomer and Dimer. *Journal of Immunology*, 183, 3425-3432.
- NASSER, M. W., RAGHUWANSHI, S. K., MALLOY, K. M., GANGAVARAPU, P., SHIM, J.-Y., RAJARATHNAM, K. & RICHARDSON, R. M. 2007. CXCR1 and CXCR2 activation and regulation. Role of aspartate 199 of the second extracellular loop of CXCR2 in CXCL8-mediated rapid receptor internalization. *Journal of Biological Chemistry*, 282, 6906-6915.
- NÉMETH, T., SPERANDIO, M. & MÓCSAI, A. 2020. Neutrophils as Emerging Therapeutic Target. *Nature Reviews Drug Discovery*, 19, 253-275.

- NIBBS, R., GRAHAM, G. & ROT, A. 2003. Chemokines on the Move: Control by the Chemokine "Interceptors" Duffy Blood Group Antigen and D6. *Seminars in Immunology*, 15, 287-294.
- NIEL, G. V., CARTER, D. R. F., CLAYTON, A., LAMBERT, D. W., RAPOSO, G. & VADER, P. 2022. Challenges and Directions in Studying Cell–Cell Communication by Extracellular Vesicles. *Nature Reviews Molecular Cell Biology*, 23, 369-382.
- NIEL, G. V., CHARRIN, S., SIMOES, S., ROMAO, M., ROCHIN, L., SAFTIG, P., MARKS, M. S., RUBINSTEIN, E. & RAPOSO, G. 2011. The Tetraspanin CD63 Regulates ESCRT-independent and -dependent Endosomal Sorting during Melanogenesis. *Development Cell*, 21, 708-721.
- NIEL, G. V., D'ANGELO, G. & RAPOSO, G. 2018. Shedding Light on the Cell Biology of Extracellular Vesicles. *Nature Reviews Cell Biology*, 19, 213-228.
- NILSSON, J., JERNRYD, V., QIN, G. & STEEN, A. P. C. M. T. S. S. 2020. A Nonrandomized Open-label Phase 2 Trial of Nonischemic Heart Preservation for Human Heart Transplantation. *Nature Communications*, 11, 2976.
- NILSSON, T., MANN, M., AEBERSOLD, R., III, J. R. Y., BAIROCH, A. & BERGERON, J. J. M. 2010. Mass Spectrometry in High-throughput Proteomics: Ready for the Big Time. *Nature Methods*, 7.
- OKADA, C., YAMASHITA, E., LEE, S. J., SHIBATA, S., KATAHIRA, J., NAKAGAWA, A., YONEDA, Y. & TSUKIHARA, T. 2009. A High-Resolution Structure of the Pre-microRNA Nuclear Export Machinery. *Science*, 326, 1275-1279.
- OKAMOTO, T., MITSUHASHI, M., SOLIMAN, B., ABU-ELMAGD, K. & MCCURRY, K. R. 2016. Detection of Lung-Specific Exosome in Perfusates of Ex Vivo Lung Perfusion System. *Journal of Heart and Lung Transplantation*, 35, S305-S306.
- ONG, S.-G., LEE, W. H., THEODOROU, L., KODO, K., LIM, S. Y., SHUKLA, D. H., BRISTON, T., KIRIAKIDIS, S., ASHCROFT, M., DAVIDSON, S. M., MAXWELL, P. H., YELLON, D. M. & HAUSENLOY, D. J. 2014. HIF-1 Reduces Ischaemia–Reperfusion Injury in the Heart by Targeting the Mitochondrial Permeability Transition Pore. *Cardiovascular Research*, 104, 24-36.
- ONO, Y., PEREZ-GUTIERREZ, A., NAKAO, T., DAI, H., CAMIRAND, G., YOSHIDA, O., YOKOTA, S., STOLZ, D. B., ROSS, M. A., MORELLI, A. E., GELLER, D. A. & THOMSON, A. W. 2018. Graft-infiltrating PD-L1^{hi} Cross-dressed Dendritic Cells Regulate Anti-donor T Cell Responses in Mouse Liver Transplant Tolerance. *Hepatology*, 67, 1499-1515.
- OSAWA, T., TSUCHIDA, R., MURAMATSU, M., SHIMAMURA, T., WANG, F., SUEHIRO, J.-I., KANKI, Y., WADA, Y., YUASA, Y., ABURATANI, H., MIYANO, S., MINAMI, T., KODAMA, T. & SHIBUYA, M. 2013. Inhibition of Histone Demethylase JMJD1A Improves Anti-Angiogenic Therapy and Reduces Tumor-Associated Macrophages. *Cancer Research*, 73, 3019-3028.
- OSTROWSKI, M., CARMO, N. B., KRUMEICH, S., FANGET, I., RAPOSO, G., SAVINA, A., MOITA, C. F., SCHAUER, K., HUME, A. N., FREITAS, R. P., GOUD, B., BENAROCHE, P., HACOEN, N.,

- FUKUDA, M., DESNOS, C., SEABRA, M. C., DARCHEN, F., AMIGORENA, S., MOITA, L. F. & THERY, C. 2009. Rab27a and Rab27b Control Different Steps of the Exosome Secretion Pathway. *Nature Cell Biology*, 12, 19-30.
- PACHER, P., BECKMAN, J. & LIAUDAT, L. 2007. Nitric oxide and peroxynitrite in health and disease. *Physiological Reviews*, 87, 315-424.
- PAN, W.-M., WANG, H., ZHANG, X.-F., XU, P., WANG, G.-L., LI, Y.-J., HUANG, K.-P., ZHANG, Y.-W., ZHAO, H., DU, R.-L., HUANG, H., ZHANG, X.-D. & ZHANG, J.-X. 2020. miR-210 Participates in Hepatic Ischemia Reperfusion Injury by Forming a Negative Feedback Loop With SMAD4. *Hepatology*, 72, 2134-2148.
- PARIKH, S., SIGDEL, T. K., ZHANG, G., VELICKOVIC, D., BARWINSKA, D., ALEXANDROV, T., DOBI, D., RASHMI, P., OTTO, E. A., RIVERA, M., ROSE, M. P., ANDERTON, C. R., SHAPIRO, J. P., PAMREDDY, A., WINFREE, S., XIONG, Y., HE, Y., BOER, I. H. D., HODGIN, J. B., BARISONI, L., NAIK, A. S., SHARMA, K., SARWAL, M. M., ZHANG, K., HIMMELFARB, J., ROVIN, B., EL-ACHKAR, T. M., LASZIK, Z., HE, J. C., DAGHER, P. C., VALERIUS, M. T., JAIN, S., SATLIN, L. M., TROYANSKAYA, O. G., KRETZLER, M., IYENGAR, R., AZELOGLU, E. U. & PROJECT, K. P. M. 2022. A Reference Tissue Atlas for the Human Kidney. *Science Advances*, 8, eabn4965.
- PARK, K. M., BYUN, J.-Y., KRAMERS, C., KIM, J. I., HUANG, P. L. & BONVENTRE, J. V. 2003. Inducible nitric oxide synthase is an important contributor to prolonged protective effects of ischemic pre-conditioning in mouse kidney. *Journal of Biological Chemistry*, 278, 27256-27266.
- PARTIN, A. C., ZHANG, K., JEONG, B.-C., HERRELL, E., LI, S., CHIU, W. & NAM, Y. 2020. Cryo-EM Structures of Human Drosha and DGCR8 in Complex with Primary MicroRNA. *Molecular Cell*, 78, 411-422.
- PASCALI, F. D., HEMANN, C., SAMONS, K., CHEN, C.-A. & ZWEIER, J. L. 2014. Hypoxia and reoxygenation induce endothelial nitric oxide synthase uncoupling in endothelial cells through tetrahydrobiopterin depletion and S-glutathionylation. *Biochemistry*, 53, 3679-3688.
- PAVLACKY, J. & POLAK, J. 2020. Technical Feasibility and Physiological Relevance of Hypoxic Cell Culture Models. *Frontiers in Endocrinology*, 11, 00057.
- PEASE, J. E., WANG, J., PONATH, P. D. & MURPHY, P. M. 1998. The N-terminal Extracellular Segments of the Chemokine Receptors CCR1 and CCR3 Are Determinants for MIP-1a and Eotaxin Binding, Respectively, but a Second Domain Is Essential for Efficient Receptor Activation. *Journal of Biological Chemistry*, 273, 19972-19976.
- PÊCHE, H., RENAUDIN, K., BERIOU, G., MERIEAU, E., AMIGORENA, S. & CUTURI, M. C. 2006. Induction of Tolerance by Exosomes and Short-Term Immunosuppression in a Fully MHC-Mismatched Rat Cardiac Allograft Model. *American journal of Transplantation*, 6, 1541-1550.

- PESCADOR, N., CUEVAS, Y., NARANJO, S., ALCAIDE, M., VILLAR, D., LANDÁZURI, M. O. & PESO, L. D. 2005. Identification of a Functional Hypoxia-responsive Element that Regulates the Expression of the *egl* Nine Homologue 3 (*eglN3/phd3*) Gene. *Biochemical Journal*, 390, 189-197.
- PHILLIPS, L., TOLEDO, A. H., LOPEZ-NEBLINA, F., ANAYA-PRADO, R. & TOLEDO-PEREYRA, L. H. 2009. Nitric oxide mechanism of protection in ischemia and reperfusion injury. *Journal of Investigative Surgery*, 22, 46-55.
- PILLAI, R. S., BHATTACHARYYA, S. N., ARTUS, C. G., ZOLLER, T., COUGOT, N., BASYUK, E., BERTRAND, E. & FILIPOWICZ, W. 2005. Inhibition of Translational Initiation by Let-7 MicroRNA in Human Cells. *Science*, 309, 1573-1576.
- PINLAOR, S., YONGVANIT, P., HIRAKU, Y., MA, N., SEMBA, R., OIKAWA, S., MURATA, M., SRIPA, B., SITHITHAWORN, P. & KAWANISHI, S. 2003. 8-Nitroguanine formation in the liver of hamsters infected with *Opisthorchis viverrini*. *Biochemical and Biophysical Research Communications*, 309, 567-571.
- POMIN, V. H. & MULLOY, B. 2018. Glycosaminoglycan and Proteoglycan. *Pharmaceuticals* 11, 27.
- PROUDFOOT, A. E. I., HANDEL, T. M., JOHNSON, Z., LAU, E. K., WANG, P. L., CLARK-LEWIS, I., BORLAT, F., WELLS, T. N. C. & KOSCO-VILBOIS, M. H. 2003. Glycosaminoglycan Binding and Oligomerization are Essential for the In Vivo Activity of Certain Chemokines. *Proceedings of the National Academy of Science of the United States of America*, 100, 1885-1890.
- PRUNEVIEILLE, A., BABIKER-MOHAMED, M. H., ASLAMI, C., GONZALEZ-NOLASCO, B., MOONEY, N. & BENICHO, G. 2020. T cell Antigenicity and Immunogenicity of Allogeneic Exosomes. *American journal of Transplantation*, 21, 2583-2589.
- PUISSÉGUR, M.-P., MAZURE, N. M., BERTERO, T., PRADELLI, L., GROSSO, S., ROBBE-SERMESANT, K., MAURIN, T., LEBRIGAND, K., CARDINAUD, B., HOFMAN, V., FOURRE, S., MAGNONE, V., RICCI, J. E., POUYSSÉGUR, J., GOUNON, P., HOFMAN, P., BARBRY, P. & MARI, B. 2010. miR-210 is Overexpressed in Late Stages of Lung Cancer and Mediates Mitochondrial Alterations Associated with Modulation of HIF-1 Activity. *Cell Death and Differentiation*, 18, 465-478.
- RAGHUWANSHI, S. K., SU, Y., SINGH, V., HAYNES, K., RICHMOND, A. & RICHARDSON, R. M. 2012. The Chemokine Receptors CXCR1 and CXCR2 Couple to Distinct G Protein-Coupled Receptor Kinases To Mediate and Regulate Leukocyte Functions. *Journal of Immunology*, 189, 2824-2832.
- RAJAGOPAL, S., BASSONI, D. L., CAMPBELL, J. J., GERARD, N. P., GERARD, C. & WEHRMAN, T. S. 2013. Biased Agonism as a Mechanism for Differential Signaling by Chemokine Receptors. *Journal of Biological Chemistry*, 288, 35039-35048.
- RAJAGOPALAN, L. & RAJARATHNAM, K. 2009. Structural Basis of Chemokine Receptor Function—A Model for Binding Affinity and Ligand Selectivity. *Bioscience Report*, 29, 325-339.

- RANADE, S. S., QIU, Z., WOO, S.-H., HUR, S. S., MURTHY, S. E., CAHALAN, S. M., XU, J., MATHUR, J., BANDELL, M., COSTE, B., LI, Y.-S. J., CHIEN, S. & PATAPOUTIAN, A. 2014. Piezo1, A Mechanically Activated Ion Channel, Is Required for Vascular Development in Mice. *Proceedings of the National Academy of Science of the United States of America*, 111, 10347-10352.
- RAPOSO, G., NIJMAN, H. W., STOORVOGEL, W., LEIJENDEKKER, R., HARDING, C., MELIEF, C. J. M. & GEUZE, H. J. 1996. B Lymphocytes Secrete Antigen-presenting Vesicles. *Journal of Experimental Medicine*, 183, 1161-1172.
- REN, X. & HURLEY, J. H. 2011. Structural Basis for Endosomal Recruitment of ESCRT-I by ESCRT-0 in Yeast. *EMBO Journal*, 30, 2130-2139.
- RICHARD, C. & VERDIER, F. 2020. Transferrin Receptors in Erythropoiesis. *International Journal of Molecular Sciences*, 21, 9713.
- RICHARDS, J. A., GAURAV, R., UPPONI, S. S., SWIFT, L., FEAR, C., WEBB, G. J., ALLISON, M. E. D., WATSON, C. J. E. & BUTLER, A. J. 2023. Outcomes of Livers from Donation After Circulatory Death Donors with Extended Agonal Phase and the Adjunct of Normothermic Regional Perfusion. *British Journal of Surgery*, znad099.
- RIGO, F., STEFANO, N. D., NAVARRO-TABLEROS, V., DAVID, E., RIZZA, G., CATALANO, G., GILBO, N., MAIONE, F., GONELLA, F., ROGGIO, D., MARTINI, S., PATRONO, D., SALIZZONI, M., CAMUSSI, G. & ROMAGNOLI, R. 2018. Extracellular Vesicles from Human Liver Stem Cells Reduce Injury in an Ex Vivo Normothermic Hypoxic Rat Liver Perfusion Model. *Transplantation*, 102, e205-e210.
- ROCHE, P. A. & FURUTA, K. 2015. The Ins and Outs of MHC Class II-mediated Antigen Processing and Presentation. *Nature Reviews Immunology*, 15, 203-216.
- RODRIGUEZ, A., GRIFFITHS-JONES, S., ASHURST, J. L. & BRADLEY, A. 2004. Identification of Mammalian microRNA Host Genes and Transcription Units. *Genome Research*, 14, 1902-1910.
- ROGG, E.-M., ABPLANALP, W. T., BISCHOF, C., JOHN, D., SCHULZ, M. H., KRISHNAN, J., FISCHER, A., POLUZZI, C., SCHAEFER, L., BONAUER, A., ZEIHNER, A. M. & DIMMELER, S. 2018. Analysis of Cell Type-Specific Effects of MicroRNA-92a Provides Novel Insights Into Target Regulation and Mechanism of Action. *Circulation*, 138, 2545-2558.
- ROOIJ, E. V., SUTHERLAND, L. B., QI, X., RICHARDSON, J. A., HILL, J. & OLSON, E. N. 2007. Control of Stress-Dependent Cardiac Growth and Gene Expression by a MicroRNA. *Science*, 316, 575-579.
- RUTMAN, A. K., NEGI, S., SABERI, N., KHAN, K., TCHERVENKOV, J. & PARASKEVAS, S. 2022. Extracellular Vesicles From Kidney Allografts Express miR-218-5p and Alter Th17/Treg Ratios. *Frontiers in Immunology*, 13, 784374.

- SALOM, M. G., ARREGUI, B., CARBONELL, L. F., RUIZ, F., GONZÁLEZ-MORA, J. L. & FENOY, F. J. 2005. Renal ischemia induces an increase in nitric oxide levels from tissue stores. *American Journal of Physiology*, 289, R1459-R1466.
- SANTANGELO, L., GIURATO, G., CICCHINI, C., MONTALDO, C., MANCONE, C., TARALLO, R., BATTISTELLI, C., ALONZI, T., WEISZ, A. & TRIPODI, M. 2016. The RNA-Binding Protein SYNCRIP Is a Component of the Hepatocyte Exosomal Machinery Controlling MicroRNA Sorting. *Cell Reports*, 17, 799-808.
- SATCHELL, S. C., TASMAN, C. H., SINGH, A., NI, L., GEELEN, J., VON RUHLAND, C. J., O'HARE, M. J., SALEEM, M. A., VAN DEN HEUVEL, L. P. & MATHIESON, P. W. 2006. Conditionally immortalized human glomerular endothelial cells expressing fenestrations in response to VEGF. *Kidney International*, 69, 1633-40.
- SATO, E., SIMPSON, K. L., GRISHAM, M. B., KOYAMA, S. & ROBBINS, R. A. 1999. Effects of Reactive Oxygen and Nitrogen Metabolites on RANTES- and IL-5-Induced Eosinophil Chemotactic Activity in vitro. *The American Journal of Pathology*, 155, 591-598.
- SATO, E., SIMPSON, K. L., GRISHAM, M. B., KOYAMA, S. & ROBBINS, R. A. 2000a. Effects of Reactive Oxygen and Nitrogen Metabolites on Eotaxin-Induced Eosinophil Chemotactic Activity In Vitro. *American Journal of Respiratory Cell and Molecular Physiology*, 22, 61-67.
- SATO, E., SIMPSON, K. L., GRISHAM, M. B., KOYAMA, S. & ROBBINS, R. A. 2000b. Inhibition of MIP-1 α -induced Human Neutrophil and Monocyte Chemotactic Activity by Reactive Oxygen and Nitrogen Metabolites. *Journal of Laboratory and Clinical Medicine*, 135, 161-169.
- SATO, E., SIMPSON, K. L., GRISHAM, M. B., KOYAMA, S. & ROBBINS, R. A. 2000c. Reactive Nitrogen and Oxygen Species Attenuate Interleukin- 8-induced Neutrophil Chemotactic Activity in Vitro. *Journal of Biological Chemistry*, 275, P10826-10830.
- SCHENK, T., IRTH, H., MARKO-VARGA, G., EDHOLM, L.-E., TJADEN, U. R. & GREEF, J. V. D. 2001. Potential of On-line Micro-LC Immunochemical Detection in the Bioanalysis of Cytokines. *Journal of Pharmaceutical and Biomedical Analysis*, 26, 975-985.
- SCHWARZ, J., BIERBAUM, V., MERRIN, J., FRANK, T., HAUSCHILD, R., BOLLENBACH, T., TAY, S., SIXT, M. & MEHLING, M. 2016. A Microfluidic Device for Measuring Cell Migration Towards Substrate-bound and Soluble Chemokine Gradients. *Scientific Report*, 6, 36440.
- SEBASTIAN RÜHL, K. S., BENJAMIN DEMARCO, ROSALIE HEILIG, JOSÉ CARLOS SANTOS AND PETR BROZ 2018. ESCRT-dependent Membrane Repair Negatively Regulates Pyroptosis Downstream of GSDMD Activation. *Science*, 362, 956-960.
- SEDEJ, I., ŠTALEKAR, M., ŽNIDARIČ, M. T., GORIČAR, K., KOJC, N., KOGOVSŠEK, P., DOLŽAN, V., ARNOL, M. & LENASSI, M. 2022. Extracellular Vesicle-bound DNA in Urine is Indicative of Kidney Allograft Injury. *Journal of Extracellular Vesicles*, 11, e12268.

- SELBACH, M., SCHWANHÄUSSER, B., THIERFELDER, N., FANG, Z., KHANIN, R. & RAJEWSKY, N. 2008. Widespread Changes in Protein Synthesis Induced by microRNAs. *Nature*, 455, 58-63.
- SEPURU, K. M., NAIR, V., PRAKASH, P., GORFE, A. A. & RAJARATHNAM, K. 2020. Long-Range Coupled Motions Underlie Ligand Recognition by a Chemokine Receptor. *iScience*, 23, 101858.
- SHAH, R. J., DIAMOND, J. M., LEDERER, D. J., ARCASOY, S. M., CANTU, E. M., DEMISSIE, E. J., KAWUT, S. M., KOHL, B., LEE, J. C., SONETT, J., CHRISTIE, J. D. & WARE, L. B. 2012. Plasma Monocyte Chemotactic Protein-1 (MCP-1) Levels at 24 hours are a Biomarker of Primary Graft Dysfunction Following Lung Transplantation. *Translational Research*, 160, 435-442.
- SHAN, D., WANG, Y.-Y., CHANG, Y., CUI, H., TAO, M., SHENG, Y., KANG, H., JIA, P. & SONG, J. 2023. Dynamic Cellular Changes in Acute Kidney Injury Caused by Different Ischemia Time. *iScience*, 26, 106646.
- SHAO, Z., SHEN, Q., YAO, B., MAO, C., CHEN, L.-N., ZHANG, H., SHEN, D.-D., ZHANG, C., LI, W., DU, X., LI, F., MA, H., CHEN, Z.-H., XU, H. E., YING, S., ZHANG, Y. & SHEN, H. 2021. Identification and Mechanism of G Protein-Biased Ligands for Chemokine Receptor CCR1. *Nature Chemical Biology*, 18, 264-271.
- SHEN, Y., LI, R., YU, S., ZHAO, Q., WANG, Z., SHENG, H. & YANG, W. 2021. Activation of the ATF6 (Activating Transcription Factor 6) Signaling Pathway in Neurons Improves Outcome After Cardiac Arrest in Mice. *Journal of the American Heart Association*, 10, e020216.
- SHINO, M. Y., TODD, J. L., NEELY, M. L., KIRCHNER, J., FRANKEL, C. W., SNYDER, L. D., PAVLISKO, E. N., FISHBEIN, G. A., SCHAENMAN, J. M., MASON, K., KESLER, K., MARTINU, T., SINGER, L. G., TSUANG, W., BUDEV, M., SHAH, P. D., REYNOLDS, J. M., WILLIAMS, N., ROBIEN, M. A., PALMER, S. M., WEIGT, S. S. & BELPERIO, J. A. 2022. Plasma CXCL9 and CXCL10 at Allograft Injury Predict Chronic Lung Allograft Dysfunction. *American journal of Transplantation*, 22, 2169-2179.
- SIEDLECKI, A., IRISH, W. & BRENNAN, D. C. 2011. Delayed Graft Function in the Kidney Transplant. *American journal of Transplantation*, 11, 2279-2296.
- SIMONAS JUZENAS, G. V., MATTHIAS HÜBENTHAL, MARC P. HOEPPNER, ZHIPEI GRACIE DU, MAREN PAULSEN, PHILIP ROSENSTIEL, PHILIPP SENGER, MARTIN HOFMANN-APITIUS, ANDREAS KELLER, LIMAS KUPCINSKAS, ANDRE FRANKE, GEORG HEMMRICH-STANISAK 2017. A Comprehensive, Cell Specific microRNA Catalogue of Human Peripheral Blood. *Nucleic Acid Research*, 45, 9290-9301.
- SMITH, V. L., JACKSON, L. & SCHOREY, J. S. 2015. Ubiquitination as a Mechanism to Transport Soluble Mycobacterial and Eukaryotic Proteins to Exosomes. *Journal of Immunology*, 195, 2722-2730.

- SONG, N., ZHANG, T., XU, X., LU, Z., YU, X., FANG, Y., HU, J., JIA, P., TENG, J. & DING, X. 2018. miR-21 Protects Against Ischemia/Reperfusion-Induced Acute Kidney Injury by Preventing Epithelial Cell Apoptosis and Inhibiting Dendritic Cell Maturation. *Frontiers in Physiology*, 9, 00790.
- SONG, R., DASGUPTA, C., MULDER, C. & ZHANG, L. 2022. MicroRNA-210 Controls Mitochondrial Metabolism and Protects Heart Function in Myocardial Infarction. *Circulation*, 145, 1140-1153.
- SOUZA, J. M., PELUFFO, G. & RADJ, R. 2008. Protein Tyrosine Nitration—Functional Alteration or Just a Biomarker? *Free Radical Biology and Medicine*, 45, 357-366.
- STEWART, B. A.-O., FERDINAND, J. A.-O., YOUNG, M. A.-O., MITCHELL, T. A.-O., LOUDON, K. A.-O., RIDING, A. A.-O., RICHOS, N., FRAZER, G. L., STANIFORTH, J. A.-O., VIEIRA BRAGA, F. A.-O., BOTTING, R. A.-O., POPESCU, D. M., VENTO-TORMO, R., STEPHENSON, E. A.-O., CAGAN, A. A.-O., FARNDON, S. A.-O., POLANSKI, K. A.-O., EFREMOVA, M., GREEN, K., DEL CASTILLO VELASCO-HERRERA, M. A.-O., GUZZO, C. A.-O., COLLORD, G. A.-O., MAMANOVA, L. A.-O., AHO, T. A.-O., ARMITAGE, J. N., RIDDICK, A. C. P., MUSHTAQ, I. A.-O., FARRELL, S., RAMPLING, D., NICHOLSON, J., FILBY, A., BURGE, J., LISGO, S. A.-O., LINDSAY, S. A.-O., BAJENOFF, M., WARREN, A. Y., STEWART, G. A.-O., SEBIRE, N., COLEMAN, N., HANIFFA, M. A.-O., TEICHMANN, S. A.-O., BEHJATI, S. A.-O. & CLATWORTHY, M. A.-O. 2019. Spatiotemporal immune zonation of the human kidney. *Science*, 365, 1461-1466.
- STONE, M. L., ZHAO, Y., SMITH, J. R., WEISS, M. L., KRON, I. L., LAUBACH, V. E. & SHARMA, A. K. 2017. Mesenchymal Stromal Cell-derived Extracellular Vesicles Attenuate Lung Ischemia-Reperfusion Injury and Enhance Reconditioning of Donor Lungs After Circulatory Death. *Respiratory Research*, 18, 212.
- STRUYF, S., NOPPEN, S., LOOS, T., MORTIER, A., GOUWY, M., VERBEKE, H., HUSKENS, D., LUANGSAY, S., PARMENTIER, M., GEBOES, K., SCHOLS, D., DAMME, J. V. & PROOST, P. 2009. Citrullination of CXCL12 Differentially Reduces CXCR4 and CXCR7 Binding with Loss of Inflammatory and Anti-HIV-1 Activity via CXCR4. *Journal of Immunology*, 182, 666-674.
- STUFFERS, S., WEGNER, C. S., STENMARK, H. & BRECH, A. 2009. Multivesicular Endosome Biogenesis in the Absence of ESCRTs. *Traffic*, 10, 925-937.
- SUBRAMANIAN, A., TAMAYO, P., MOOTHA, V. K., MUKHERJEE, S., EBERT, B. L., GILLETTE, M. A., PAULOVICH, A., POMEROY, S. L., GOLUB, T. R., LANDER, E. S. & MESIROV, J. P. 2005. Gene Set Enrichment Analysis: A Knowledge-based Approach for Interpreting Genome-wide Expression Profiles. *Proceedings of the National Academy of Science of the United States of America*, 102, 15545-15550.
- SVENSSON, K. J., CHRISTIANSON, H. C., WITTRUP, A., BOURSEAU-GUILMAIN, E., LINDQVIST, E., SVENSSON, L. M., MÖRGELIN, M. & BELTING, M. 2013. Exosome Uptake Depends on ERK1/2-Heat Shock Protein 27 Signaling and Lipid Raft-mediated Endocytosis Negatively Regulated by Caveolin-1. *Journal of Biological Chemistry*, 299, P17713-17724.

- SZABÓ, C., ISCHIROPOULOS, H. & RADI, R. 2007. Peroxynitrite: Biochemistry, Pathophysiology and Development of Therapeutics. *Nature Reviews Drug Discovery*, 6, 662-680.
- TAFLIN, C., FAVIER, B., BAUDHUIN, J., SAVENAY, A., HEMON, P., BENSUSSAN, A., CHARRON, D., GLOTZ, D. & MOONEY, N. 2011. Human Endothelial Cells Generate Th17 and Regulatory T cells Under Inflammatory Conditions. *Proceedings of the National Academy of Science of the United States of America*, 108, 2891-2896.
- TANG, T.-T., WANG, B., WU, M., LI, Z.-L., FENG, Y., CAO, J.-Y., YIN, D., LIU, H., TANG, R.-N., CROWLEY, S. D., LV, L.-L. & LIU, B.-C. 2020. Extracellular vesicle-encapsulated IL-10 as novel nanotherapeutics against ischemic AKI. *Science Advances*, 6, eaaz0748.
- TANG, X. N., CAIRNS, B., KIM, J. Y. & YENARI, M. A. 2012. NADPH oxidase in stroke and cerebrovascular disease. *Neurological Research* 34, 338-345.
- TENG, Y., REN, Y., HU, X., MU, J., SAMYKUTTY, A., ZHUANG, X., DENG, Z., KUMAR, A., ZHANG, L., MERCHANT, M. L., YAN, J., MILLER, D. M. & ZHANG, H.-G. 2017. MVP-mediated Exosomal Sorting of miR-193a Promotes Colon Cancer Progression. *Nature Communications*, 8, 14448.
- TERPOLILLI, N. A., KIM, S.-W., THAL, S. C., KATAOKA, H., ZEISIG, V., NITZSCHE, B., KLAESNER, B., ZHU, C., SCHWARZMAIER, S., MEISSNER, L., MAMRAK, U., ENGEL, D. C., PATEL, A. D. R. P., BLOMGREN, K., BARTHEL, H., BOLTZE, J., KUEBLER, W. M. & PLESNILA, N. 2012. Inhalation of nitric oxide prevents ischemic brain damage in experimental stroke by selective dilatation of collateral arterioles. *Circulation Research*, 110, 727-738.
- THÉRY, C., WITWER, K. W., AIKAWA, E., ALCARAZ, M. J., ANDERSON, J. D., ANDRIANTSITOHAINA, R., ANTONIOU, A., ARAB, T., ARCHER, F., ATKIN-SMITH, G. K., AYRE, D. C., BACH, J.-M., BACHURSKI, D., BAHARVAND, H., BALAJ, L., BALDACCHINO, S., BAUER, N. N., BAXTER, A. A., BEBAWY, M., BECKHAM, C., BEDINA ZAVEC, A., BENMOUSSA, A., BERARDI, A. C., BERGESE, P., BIELSKA, E., BLENKIRON, C., BOBIS-WOZOWICZ, S., BOILARD, E., BOIREAU, W., BONGIOVANNI, A., BORRÀS, F. E., BOSCH, S., BOULANGER, C. M., BREAKFIELD, X., BREGLIO, A. M., BRENNAN, M. Á., BRIGSTOCK, D. R., BRISSON, A., BROEKMAN, M. L., BROMBERG, J. F., BRYL-GÓRECKA, P., BUCH, S., BUCK, A. H., BURGER, D., BUSATTO, S., BUSCHMANN, D., BUSSOLATI, B., BUZÁS, E. I., BYRD, J. B., CAMUSSI, G., CARTER, D. R., CARUSO, S., CHAMLEY, L. W., CHANG, Y.-T., CHEN, C., CHEN, S., CHENG, L., CHIN, A. R., CLAYTON, A., CLERICI, S. P., COCKS, A., COCUCCI, E., COFFEY, R. J., CORDEIRO-DA-SILVA, A., COUCH, Y., COUMANS, F. A., COYLE, B., CRESCITELLI, R., CRIADO, M. F., D'SOUZA-SCHOREY, C., DAS, S., DATTA CHAUDHURI, A., DE CANDIA, P., DE SANTANA JUNIOR, E. F., DE WEVER, O., DEL PORTILLO, H. A., DEMARET, T., DEVILLE, S., DEVITT, A., DHONDT, B., DI VIZIO, D., DIETERICH, L. C., DOLO, V., DOMINGUEZ RUBIO, A. P., DOMINICI, M., DOURADO, M. R., DRIEDONKS, T. A., DUARTE, F. V., DUNCAN, H. M., EICHENBERGER, R. M., EKSTRÖM, K., EL ANDALOUSSI, S., ELIE-CAILLE, C., ERDBRÜGGER, U., FALCÓN-PÉREZ, J. M., FATIMA, F., FISH, J. E., FLORES-BELLVER, M., FÖRSÖNITS, A., FRELET-BARRAND, A., et al. 2018. Minimal information for studies of extracellular vesicles 2018 (MISEV2018): a position

statement of the International Society for Extracellular Vesicles and update of the MISEV2014 guidelines. *Journal of Extracellular Vesicles*, 7, 1535750.

THOMPSON, S., MARTÍNEZ-BURGO, B., SEPURU, K. M., RAJARATHNAM, K., KIRBY, J. A., SHEERIN, N. S. & ALI, S. 2017. Regulation of Chemokine Function: The Roles of GAG-Binding and Post-Translational Nitration. *International Journal of Molecular Sciences*, 18, 1692.

THOMPSON, S., PANG, C. Y., SEPURU, K. M., CAMBIER, S., HELLYER, T. P., SCOTT, J., SIMPSON, A. J., PROOST, P., KIRBY, J. A., RAJARATHNAM, K., SHEERIN, N. S. & ALI, S. 2023. Nitration of Chemokine CXCL8 Acts as a Natural Mechanism to Limit Acute Inflammation. *Cellular and Molecular Life Sciences*, 80, 35.

THUM, T., GROSS, C., FIEDLER, J., FISCHER, T., KISSLER, S., BUSSEN, M., GALUPPO, P., JUST, S., ROTTBAUER, W., FRANTZ, S., CASTOLDI, M., SOUTSCHEK, J., KOTELIANSKY, V., ROSENWALD, A., BASSON, M. A., LICHT, J. D., PENA, J. T. R., ROUHANIFARD, S. H., MUCKENTHALER, M. U., TUSCHL, T., MARTIN, G. R., BAUERSACHS, J. & ENGELHARDT, S. 2008. MicroRNA-21 Contributes to Myocardial Disease by Stimulating MAP Kinase Signalling in Fibroblasts. *Nature*, 456, 980-984.

TIAN, Y., SIMANSHU, D. K., MA, J.-B., PARK, J.-E., HEO, I., KIM, V. N. & PATEL, D. J. 2014. A Phosphate-Binding Pocket within the Platform-PAZ-Connector Helix Cassette of Human Dicer. *Molecular Cell*, 53, 606-616.

TRAJKOVIC, K., HSU, C., CHIANTIA, S., RAJENDRAN, L., WENZEL, D., WIELAND, F., SCHWILLE, P., BRÜGGER, B. & SIMONS, M. 2008. Ceramide Triggers Budding of Exosome Vesicles into Multivesicular Endosomes. *Science*, 319, 1244-1247.

TURCHINOVICH, A., WEIZ, L., LANGHEINZ, A. & BURWINKEL, B. 2011. Characterization of extracellular circulating microRNA. *Nucleic Acid Research*, 39, 7223-7233.

USMAN, W. M., PHAM, T. C., KWOK, Y. Y., VU, L. T., MA, V., PENG, B., CHAN, Y. S., WEI, L., CHIN, S. M., AZAD, A., HE, A. B.-L., LEUNG, A. Y. H., YANG, M., SHYH-CHANG, N., CHO, W. C., SHI, J. & LE, M. T. N. 2018. Efficient RNA Drug Delivery Using Red Blood Cell Extracellular Vesicles. *Nature Communications*, 9, 2359.

UTGAARD, J. O., JAHNSEN, F. L., BAKKA, A., BRANDTZAEG, P. & HARALDSEN, G. 1998. Rapid Secretion of Prestored Interleukin 8 from Weibel-Palade Bodies of Microvascular Endothelial Cells. *Journal of Experimental Medicine*, 188, 1751-1756.

VALADI, H., EKSTRÖM, K., BOSSIOS, A., SJÖSTRAND, M., LEE, J. J. & LÖTVALL, J. O. 2007. Exosome-mediated Transfer of mRNAs and microRNAs is a Novel Mechanism of Genetic Exchange between Cells. *Nature Cell Biology*, 9, 654-659.

VALLABHAJOSYULA, P., KORUTLA, L., HABERTHEUER, A., YU, M., ROSTAMI, S., YUAN, C.-X., REDDY, S., LIU, C., KORUTLA, V., KOEBERLEIN, B., TROFE-CLARK, J., RICKELS, M. R. & NAJI, A. 2017. Tissue-specific Exosome Biomarkers for Noninvasively Monitoring Immunologic Rejection of Transplanted Tissue. *Journal of Clinical Investigation*, 127, 1375-1391.

- VÁSQUEZ-VIVAR, J., KALYANARAMAN, B., MARTÁSEK, P., HOGG, N., MASTERS, B. S. S., KAROUI, H., TORDO, P. & KIRKWOOD A. PRITCHARD, J. 1998. Superoxide generation by endothelial nitric oxide synthase: The influence of cofactors. *Proceedings of the National Academy of Science*, 96, 9220-9225.
- VERWEIJ, F. J., REVENU, C., ARRAS, G., DINGLI, F., LOEW, D., PEGTEL, D. M., FOLLAIN, G., ALLIO, G., GOETZ, J. G., ZIMMERMANN, P., HERBOMEL, P., BENE, F. D., RAPOSO, G. & NIEL, G. V. 2019. Live Tracking of Inter-organ Communication by Endogenous Exosomes In Vivo. *Development Cell*, 48, 573-589.e4.
- VILLARROYA-BELTRI, C., GUTIÉRREZ-VÁZQUEZ, C., SÁNCHEZ-CABO, F., PÉREZ-HERNÁNDEZ, D., VÁZQUEZ, J., MARTIN-COFRECES, N., MARTINEZ-HERRERA, D. J., PASCUAL-MONTANO, A., MITTELBRUNN, M. & SÁNCHEZ-MADRID, F. 2013. Sumoylated hnRNPA2B1 Controls the Sorting of miRNAs into Exosomes through Binding to Specific Motifs. *Nature Communications*, 4, 2980.
- VIÑAS, J. L., SPENCE, M., PORTER, C. J., DOUVIRIS, A., GUTSOL, A., ZIMPELMANN, J. A., CAMPBELL, P. A. & BURNS, K. D. 2021. micro-RNA-486-5p Protects Against Kidney Ischemic Injury and Modifies the Apoptotic Transcriptome in Proximal Tubules. *Kidney International*, 100, P597-612.
- VINTEN-JOHANSEN, J. 2004. Involvement of neutrophils in the pathogenesis of lethal myocardial reperfusion injury. *Cardiovascular Research*, 61, 481-497.
- VIRGA, F., CAPPELLESO, F., STIJLEMANS, B., HENZE, A.-T., TROTTA, R., AUDENAERDE, J. V., MIRCHANDANI, A. S., SANCHEZ-GARCIA, M. A., VANDEWALLE, J., ORSO, F., RIERA-DOMINGO, C., GRIFFA, A., IVAN, C., SMITS, E., LAOUI, D., MARTELLI, F., LANGOUCHE, L., BERGHE, G. V. D., FERON, O., GHESQUIÈRE, B., PRENEN, H., LIBERT, C., WALMSLEY, S. R., CORBET, C., GINDERACHTER, J. A. V., IVAN, M., TAVERNA, D. & MAZZONE, M. 2021. Macrophage miR-210 Induction and Metabolic Reprogramming in Response to Pathogen Interaction Boost Life-threatening Inflammation. *Science Advances*, 7, eabf0466.
- VOELLENKLE, C., ROOIJ, J. V., GUFFANTI, A., BRINI, E., FASANARO, P., ISAIA, E., CROFT, L., DAVID, M., CAPOGROSSI, M. C., MOLES, A., FELSANI, A. & MARTELLI, F. 2012. Deep-sequencing of Endothelial Cells Exposed to Hypoxia Reveals the Complexity of Known and Novel microRNAs. *RNA*, 18, 472-484.
- WAGNER, B. A., VENKATARAMAN, S. & BUETTNER, G. R. 2011. The Rate of Oxygen Utilization by Cells. *Free Radical Biology and Medicine*, 51, 700-712.
- WALLERT, T. & HURLEY, J. H. 2010. Molecular Mechanism of Multivesicular Body Biogenesis by ESCRT Complexes. *Nature*, 525, 864-869.
- WANG, S., AURORA, A. B., JOHNSON, B. A., QI, X., MCANALLY, J., HILL, J. A., RICHARDSON, J. A., BASSEL-DUBY, R. & OLSON, E. N. 2008. The Endothelial-Specific MicroRNA miR-126 Governs Vascular Integrity and Angiogenesis. *Development Cell*, 155, 261-271.

- WANG, X., CHEN, Y., ZHAO, Z., MENG, Q., YU, Y., SUN, J., YANG, Z., CHEN, Y., LI, J., MA, T., LIU, H., LI, Z., YANG, J. & SHEN, Z. 2018. Engineered Exosomes With Ischemic Myocardium-Targeting Peptide for Targeted Therapy in Myocardial Infarction. *Journal of the American Heart Association*, 7, e008737.
- WANG, X., WU, R., ZHAI, P., LIU, Z., XIA, R., ZHANG, Z., QIN, X., LI, C., CHEN, W., LI, J. & ZHANG, J. 2023. Hypoxia Promotes EV Secretion by Impairing Lysosomal Homeostasis in HNSCC through Negative Regulation of ATP6V1A by HIF-1 α . *Journal of Extracellular Vesicles*, 12, e12310.
- WANG, Y., LI, G., STANCO, A., LONG, J. E., CRAWFORD, D., POTTER, G. B., PLEASURE, S. J., BEHRENS, T. & RUBENSTEIN, J. L. R. 2011. CXCR4 and CXCR7 Have Distinct Functions in Regulating Interneuron Migration. *Neuron*, 69, 61-76.
- WEI, Z., BATAGOV, A. O., SCHINELLI, S., WANG, J., WANG, Y., FATIMY, R. E., RABINOVSKY, R., BALAJ, L., CHEN, C. C., HOCHBERG, F., CARTER, B., BREAKFIELD, X. O. & KRICHEVSKY, A. M. 2017. Coding and Noncoding Landscape of Extracellular RNA Released by Human Glioma Stem Cells. *Nature Communications*, 8, 1145.
- WIENHOLDS, E., KLOOSTERMAN, W. P., MISKA, E., ALVAREZ-SAAVEDRA, E., BEREZIKOV, E., BRUIJN, E. D., HORVITZ, H. R., KAUPPINEN, S. & PLASTERK, R. H. A. 2005. MicroRNA Expression in Zebrafish Embryonic Development. *Science*, 309, 310-311.
- WINKLER, C., MODI, W., SMITH, M. W., NELSON, G. W., WU, X., CARRINGTON, M., DEAN, M., HONJO, T., TASHIRO, K., YABE, D., BUCHBINDER, S., VITTINGHOFF, E., GOEDERT, J. J., O'BRIEN, T. R., JACOBSON, L. P., DETELS, R., DONFIELD, S., WILLOUGHBY, A., GOMPERS, E., VLAHOV, D., PHAIR, J., STUDY, A., HEMOPHILIA GROWTH AND DEVELOPMENT STUDY (HGDS), MULTICENTER AIDS COHORT STUDY (MACS), MULTICENTER HEMOPHILIA COHORT STUDY (MHCS) & SAN FRANCISCO CITY COHORT (SFCC), S. J. O. B. 1998. Genetic restriction of AIDS pathogenesis by an SDF-1 chemokine gene variant. ALIVE Study, Hemophilia Growth and Development Study (HGDS), Multicenter AIDS Cohort Study (MACS), Multicenter Hemophilia Cohort Study (MHCS), San Francisco City Cohort (SFCC). *Science*, 279, 389-393.
- WOUD, W. W., ARYKBAEVA, A. S., ALWAYS, I. P. J., BAAN, C. C., MINNEE, R. C., HOOGDUIJN, M. J. & BOER, K. 2022. Extracellular Vesicles Released During Normothermic Machine Perfusion Are Associated With Human Donor Kidney Characteristics. *Transplantation*, 106, P2360-2369.
- WU, B., CHIEN, E. Y. T., MOL, C. D., FENALTI, G., LIU, W., KATRITCH, V., ABAGYAN, R., BROOUN, A., WELLS, P., BI, F. C., HAMEL, D. J., KUHN, P., HANDEL, T. M., CHEREZOV, V. & STEVENS, R. C. 2010. Structures of the CXCR4 Chemokine GPCR with Small-Molecule and Cyclic Peptide Antagonists. *Science*, 330, 1066-1071.
- WU, H., CHEN, G., WYBURN, K. R., YIN, J., BERTOLINO, P., ERIS, J. M., ALEXANDER, S. I., SHARLAND, A. F. & CHADBAN, S. J. 2007. TLR4 Activation Mediates Kidney Ischemia/Reperfusion Injury. *Journal of Clinical Investigation*, 117, 2847-2859.

- WU, M., YANG, G., LIAO, W., TSAI, A. P., CHENG, Y., CHENG, P., LI, C. & LI, C. 2018. Current Mechanistic Concepts in Ischemia and Reperfusion Injury. *Cellular Physiology and Biochemistry*, 46, 1650-1667.
- XIAO, F.-J., ZHANG, D., WU, Y., JIA, Q.-H., ZHANG, L., LI, Y.-X., YANG, Y.-F., WANG, H., WU, C.-T. & WANG, L.-S. 2019. miRNA-17-92 Protects Endothelial Cells from Erastin-induced Ferroptosis through Targeting the A20-ACSL4 axis. *Biochemical and Biophysical Research Communications*, 515, 448-454.
- YADID, M., LIND, J. U., ARDOÑA, H. A. M., SEAN P. SHEEHY, L. E. D., EWEJE, F., BASTINGS, M. M. C., POPE, B., O'CONNOR, B. B., STRAUBHAAR, J. R., BUDNIK, B., KLEBER, A. G. & PARKER, K. K. 2020. Endothelial Extracellular Vesicles Contain Protective Proteins and Rescue Ischemia-Reperfusion Injury in a Human Heart-On-Chip. *Science Translational Medicine*, 12, eaax8005.
- YAMAZAWA, R., JIKO, C., CHOI, S., PARK, I. Y., NAKAGAWA, A., EIKI YAMASHITA & LEE, S. J. 2018. Structural Basis for Selective Binding of Export Cargoes by Exportin-5. *Structure*, 26, 1393-1398.
- YAN, H., HUANG, W., RAO, J. & YUAN, J. 2021. miR-21 Regulates Ischemic Neuronal Injury via the p53/Bcl-2/Bax Signaling Pathway. *Aging*, 13, 22242-22255.
- YANAIHARA, N., CAPLEN, N., BOWMAN, E., SEIKE, M., KUMAMOTO, K., YI, M., STEPHENS, R. M., OKAMOTO, A., YOKOTA, J., TANAKA, T., CALIN, G. A., LIU, C.-G., CROCE, C. M. & HARRIS, C. C. 2006. Unique microRNA Molecular Profiles in Lung Cancer Diagnosis and Prognosis. *Cancer Cell*, 9, 189-198.
- YANG, L., WANG, B., ZHOU, Q., WANG, Y., LIU, X., LIU, Z. & ZHAN, Z. 2018. MicroRNA-21 Prevents Excessive Inflammation and Cardiac Dysfunction After Myocardial Infarction through Targeting KBTBD7. *Cell Death and Disease*, 9, 769.
- YANG, X., MENG, S., JIANG, H., ZHU, C. & WU, W. 2011. Exosomes Derived from Immature Bone Marrow Dendritic Cells Induce Tolerogenicity of Intestinal Transplantation in Rats. *Journal of Surgical Research*, 171, 826-832.
- YOSHIOKA, Y., KOSAKA, N., OCHIYA, T. & KATO, T. 2012. Micromanaging Iron Homeostasis Hypoxia-inducible miR-210 Suppresses Iron Homeostasis-related Proteins. *Journal of Biological Chemistry*, 287, 34110-34119.
- YUN, J. J., FISCHBEIN, M. P., LAKS, H., FISCHBEIN, M. C., ESPEJO, M. L., EBRAHIMI, K., IRIE, Y., BERLINER, J. & ARDEHALI, A. 20002. Early and Late Chemokine Production Correlates with Cellular Recruitment in Cardiac Allograft Vasculopathy. *Transplantation*, 69, P2515-2524.
- ZACCAGNINI, G., MAIMONE, B., FUSCHI, P., MASELLI, D., SPINETTI, G., GAETANO, C. & MARTELLI, F. 2017. Overexpression of miR-210 and its Significance in Ischemic Tissue Damage. *Scientific Report*, 7, 9563.

- ZENG, F., CHEN, Z., CHEN, R., SHUFESKY, W. J., BANDYOPADHYAY, M., CAMIRAND, G., OBERBARNSCHEIDT, M. H., SULLIVAN, M. L. G., BATY, C. J., YANG, M.-Q., CALDERON, M., STOLZ, D. B., ERDOS, G., PELANDA, R., BRENNAN, T. V., CATZ, S. D., WATKINS, S. C., LARREGINA, A. T. & MORELLI, A. E. 2021. Graft-derived Extracellular Vesicles Transported Across Subcapsular Sinus Macrophages Elicit B Cell Alloimmunity After Transplantation. *Science Translational Medicine*, 13, eabb0122.
- ZHANG, H., CHEN, K., TAN, Q., SHAO, Q., HAN, S., ZHANG, C., YI, C., CHU, X., ZHU, Y., XU, Y., ZHAO, Q. & WU, B. 2021a. Structural basis for chemokine recognition and receptor activation of chemokine receptor CCR5. *Nature Communications*, 12, 4151.
- ZHANG, H., FREITAS, D., KIM, H. S., FABIJANIC, K., LI, Z., CHEN, H., MARK, M. T., MOLINA, H., MARTIN, A. B., BOJMAR, L., FANG, J., RAMPERSAUD, S., HOSHINO, A., MATEI, I., KENIFIC, C. M., NAKAJIMA, M., MUTVEI, A. P., SANSONE, P., BUEHRING, W., WANG, H., JIMENEZ, J. P., COHEN-GOULD, L., PAKNEJAD, N., BRENDDEL, M., MANOVA-TODOROVA, K., MAGALHÃES, A., FERREIRA, J. A., OSÓRIO, H., SILVA, A. M., MASSEY, A., CUBILLOS-RUIZ, J. R., GALLETI, G., GIANNAKAKOU, P., CUERVO, A. M., BLENIS, J., SCHWARTZ, R., BRADY, M. S., PEINADO, H., BROMBERG, J., MATSUI, H., REIS, C. A. & LYDEN, D. 2018. Identification of Distinct Nanoparticles and Subsets of Extracellular Vesicles by Asymmetric Flow Field-flow Fractionation. *Nature Cell Biology*, 20, 332-343.
- ZHANG, Q., JEPPESEN, D. K., HIGGINBOTHAM, J. N., GRAVES-DEAL, R., TRINH, V. Q., RAMIREZ, M. A., SOHN, Y., NEININGER, A. C., TANEJA, N., MCKINLEY, E. T., NIITSU, H., CAO, Z., EVANS, R., GLASS, S. E., RAY, K. C., FISSELL, W. H., HILL, S., ROSE, K. L., HUH, W. J., WASHINGTON, M. K., AYERS, G. D., BURNETTE, D. T., SHARMA, S., ROME, L. H., FRANKLIN, J. L., LEE, Y. A., LIU, Q. & COFFEY, R. J. 2021b. Supermeres are Functional Extracellular Nanoparticles Replete with Disease Biomarkers and Therapeutic Targets. *Nature Cell Biology*, 23, 1240-1254.
- ZHANG, Z., CHEN, H., ZHOU, L., LI, C., LU, G. & WANG, L. 2022. Macrophage-Derived Exosomal miRNA-155 Promotes Tubular Injury in Ischemia-Induced Acute Kidney Injury. *International Journal of Molecular Medicine*, 50, 116.
- ZHAO, J., FLORENTIN, J., TAI, Y.-Y., TORRINO, S., OHAYON, L., BRZOSKA, T., TANG, Y., YANG, J., NEGI, V., WOODCOCK, C.-S. C., RISBANO, M. G., NOURAI, S. M., SUNDD, P., BERTERO, T., DUTTA, P. & CHAN, S. Y. 2020. Long Range Endocrine Delivery of Circulating miR-210 to Endothelium Promotes Pulmonary Hypertension. *Circulation Research*, 127, 677-692.
- ZHAO, J., LI, X., HU, J., CHEN, F., QIAO, S., SUN, X., GAO, L., XIE, J. & XU, B. 2019. Mesenchymal Stromal Cell-Derived Exosomes Attenuate Myocardial Ischaemia-Reperfusion Injury Through miR-182-Regulated Macrophage Polarization. *Cardiovascular Research*, 115, 1205-1216.
- ZHAO, S.-C., MA, L.-S., CHU, Z.-H., XU, H., WE, W.-Q. & LIU, F. 2017. Regulation of microglial activation in stroke. *Acta Pharmacologica Sinica*, 38, 445-458.

- ZHENG, K., SMITH, J. S., EIGER, D. S., WARMAN, A., CHOI, I., HONEYCUTT, C. C., BOLDIZSAR, N., GUNDRY, J. N., PACK, T. F., INOUE, A., CARON, M. G. & RAJAGOPAL, S. 2022. Biased agonists of the chemokine receptor CXCR3 differentially signal through Gai:β-arrestin complexes. *Science Signaling*, 15, eabg5023.
- ZHOU, L., ZANG, G., ZHANG, G., WANG, H., ZHANG, X., JOHNSTON, N., MIN, W., LUKE, P., JEVIKAR, A., HAIG, A. & ZHENG, X. 2013. MicroRNA and mRNA Signatures in Ischemia Reperfusion Injury in Heart Transplantation. *Plos One*, 8, e79805.
- ZHOU, W., FONG, M. Y., MIN, Y., SOMLO, G., LIU, L., PALOMARES, M. R., YU, Y., CHOW, A., O'CONNOR, S. T. F., CHIN, A. R., YEN, Y., WANG, Y., MARCUSSON, E. G., CHU, P., WU, J., WU, X., LI, A. X., LI, Z., GAO, H., REN, X., BOLDIN, M. P., LIN, P. C. & WANG, S. E. 2014. Cancer-Secreted miR-105 Destroys Vascular Endothelial Barriers to Promote Metastasis. *Cancer Cell*, 25, 501-515.
- ZHOU, X., ZHAO, S., LI, W., RUAN, Y., YUAN, R., NING, J., JIANG, K., XIE, J., YAO, X., LI, H., LI, C., RAO, T., YU, W. & CHENG, F. 2021. Tubular Cell-Derived Exosomal miR-150-5p Contributes to Renal Fibrosis Following Unilateral Ischemia-Reperfusion Injury by Activating Fibroblast in vitro and in vivo. *International Journal of Biological Sciences*, 17, 4021-4033.
- ZINKERNAGEL, A. S., TIMMER, A. M., PENCE, M. A., LOCKE, J. B., T.BUCHANAN, J., TURNER, C. E., MISHALIAN, I., SRISKANDAN, S., HANSKI, E. & NIZET, V. 2008. The IL-8 Protease SpyCEP/ScpC of Group A Streptococcus Promotes Resistance to Neutrophil Killing. *Cell Host and Microbe*, 4, 170-178.
- ZLOTNIK, A. & YOSHIE, O. 2012. The Chemokine Superfamily Revisited. *Immunity*, 36, P705-P716.
- ZOROV, D. B., JUHASZOVA, M. & SOLLOTT, S. J. 2014. Mitochondrial reactive oxygen species (ROS) and ROS-induced ROS release. *Physiological Reviews*, 94, 909-950.
- ZOUKI, C., JÓZSEF, L., OUELLET, S., PAQUETTE, Y. & FILEP, J. G. 2001. Peroxynitrite Mediates Cytokine-induced IL-8 Gene Expression and Production by Human Leukocytes. *Journal of Leukocyte Biology*, 69, 815-824.
- ZWEIER, J. L., WANG, P. & KUPPUSAMY, P. 1995. Direct measurement of nitric oxide generation in the ischemic heart using electron paramagnetic resonance spectroscopy. *Journal of Biological Chemistry*, 270, 304-307.

10. Publications and Presentations

10.1. Publications

Published:

- Thompson, S. *, **Pang, C.Y.***, Sepuru, K.M. et al. Nitration of chemokine CXCL8 acts as a natural mechanism to limit acute inflammation. *Cell. Mol. Life Sci.* 80, 35 (2023).

*Joint first author.

- K. Schell, A. Flinn, L. Cortes, **C.Y. Pang**, A. Gennery, M. Collins, R. Crossland. P1578 Serum extracellular vesicle miRNA profiling to determine extracorporeal photopheresis

treatment response in graft versus host disease patients. *HemaSphere*, 7(Suppl): e5724318.

In progress:

- **C.Y. Pang**, S. Satchell, J.A. Kirby, N.S. Sheerin, S. Ali. miR-210 confers protection to glomerular endothelium in hypoxia.
- **C.Y. Pang**, L. Sture, J. Dobbins, G. Cheemungtoo, S.J. Tingle, B. Mahendran, L. Bates, J.A. Kirby, C. Wilson, N.S. Sheerin, Simi Ali. Endothelial derived extracellular vesicles induce immune response and promotes allorecognition in transplantation.
- C. Griffiths, L. Wang, L. Bates, M. Brown, **CY Pang**, J. Dark, W.E. Scott, S. Ali, A. J. Fisher. Evaluating the immunomodulatory properties of human placenta amniotic epithelial cells as a therapeutic in ex vivo lung reconditioning.
- J. Gilmour, N. Chilvers, **C.Y. Pang**, M. Brown, L. Bates, A.J. Fisher, S. Ali. S1PR1 agonist CYM5442 reduces endothelial permeability during human *ex vivo* lung perfusion.

10.2. Presentations

- Oxidative modification of CXCL8 during inflammation: Implication for neutrophil chemotaxis, 2020, *British Society for Immunology Congress*, Virtual (*Poster*)
- Profiling of extracellular vesicles from renal allograft microvasculature during transplantation, 2022, *UKEV Forum*, Edinburgh, UK (*Poster*)
- Renal allograft microvascular EVs show distinct molecular signature, 2023, *BTS NHSBT Joint Congress*, Edinburgh, UK (*Poster*)
- Oxidative modification of CXCL8 during inflammation. *Regenerative Medicine, Stem Cells, and Transplantation Theme Meeting*, 2021, Newcastle, UK (*Oral presentation*)

- Post-translational modification of CXCL8 in inflammation. *Immunity and Inflammation Theme Meeting, 2022, Newcastle, UK (Oral presentation)*
- CXCL8 in ventilation associated pneumonia bronchoalveolar lavage. *Respiratory and Critical Care Research Group Meeting, 2022, Newcastle, UK (Oral presentation)*
- Nitration of chemokine CXCL8 acts as a natural mechanism to limit acute inflammation, 2022 *NECS Respiratory Inflammation Meeting, Sheffield, UK (Oral presentation)*
- Extracellular vesicles mediating allorecognition in kidney transplantation. *Immunity and Inflammation Theme Meeting, 2023, Newcastle, UK (Oral presentation)*